

**Choline Applied as Counterion –  
A Strategy for the Design of Biocompatible  
Surfactants and Green Ionic Liquids**

**Dissertation**

zur Erlangung des Grades

Doktor der Naturwissenschaften (Dr. rer. nat.)

der Naturwissenschaftlichen Fakultät IV

Chemie und Pharmazie

Universität Regensburg



vorgelegt von

**Regina Klein**

Regensburg 2011



Promotionsgesuch eingereicht am: 15.03.2011

Promotionskolloquium am: 01.04.2011

Die Arbeit wurde angeleitet von Prof. Dr. Werner Kunz

Gutachter: Prof. Dr. Werner Kunz  
Prof. Dr. Hubert Motschmann  
Prof. Dr. Jörg Heilmann

Vorsitzender: Prof. Dr. Dominik Horinek



„So eine Arbeit wird eigentlich nie fertig,  
man muss sie für fertig erklären,  
wenn man nach Zeit und Umständen  
das Möglichste getan hat.“

- Johann Wolfgang von Goethe -



# Preface

This dissertation is based on research carried out between February 2006 and March 2011 at the Institute of Physical and Theoretical Chemistry (Faculty of Natural Sciences IV) of the University of Regensburg. The many experiments performed required a number of cooperations with experts of various fields and involved several stays of the author at departments of different collaborating groups, including the Laboratoire Interdisciplinaire sur l'Organisation Nanométrique et Supramoléculaire (CEA/IRAMIS, CEA Saclay, France), the Institute for Advanced Chemistry of Catalonia (CSIC, Barcelona, Spain), the Department of Chemical Engineering at the University of Manchester, and the Institut de Chimie Séparative de Marcoule (CEA/CNRS, UM2, ENSCM, France).

This work would not have been possible without the help and support of many people to whom I am happy to express my honest gratitude.

First of all, I am sincerely indebted to my supervisor Prof. Dr. Werner Kunz for bestowing me the confidence to work independently, for allocating this fascinating topic, his interest in outcome of the experiments, and the financial support over the years.

Furthermore, I owe a great debt of gratitude to Prof. Dr. Gordon J. T. Tiddy, who gave me the opportunity to work in his laboratory in Manchester and let me benefit from his great expert knowledge in the broad field of surfactants. In particular, I thank him for his excellent support in light microscopy issues and NMR experiments. Moreover, I am grateful to his co-worker Dr. Helen Dutton for performing the NMR relaxation measurements of choline soaps.

In addition, I thank Dr. Jordi Esquena and Prof. Dr. Conxita Solans for their hospitality during my one-week stay at the CSIC Barcelona, for allowing me to use their equipment for X-ray measurements, and for valuable discussions. Likewise, I would like to acknowledge Dr. Olivier Spalla and Olivier Tache (CEA Saclay) for granting me access to their SAXS instrument as well as for their kindness and assistance during my visit. Cordial thanks go to Dr. Olivier Diat (CEA/CNRS Marcoule) for giving me the opportunity to use the X-ray setup at the Institut de Chimie Séparative, and for his genial support during and after my stay at Marcoule.

Further, I am grateful to Gabriele Wienskohl (Max-Planck-Institute Golm) for completing the X-ray experiments. In this context, I would also like to express my sincere thanks to Prof. Dr. Hubert Motschmann for bringing me into contact with the MPI Golm and, apart from that, for his open ears at any time, his permanent assuasive influence on me and his willingness to be examiner of this thesis.

In particular, I appreciate the help of the people who collaborated in the interdisciplinary field of biodegradation and cytotoxicity of soaps. These are Dr. Boris Estrine (Agroindustrie Recherche et Développement, Pomacle, France) as well as Gabi Brunner, Marcel Flemming, Dr. Birgit Krauss and Prof. Dr. Jörg Heilmann (Institute of Pharmaceutical Biology, University of Regensburg). I am especially grateful to Dr. Birgit Krauss and Prof. Dr. Jörg Heilmann for our fruitful discussions and their valuable contributions in the interpretation of the data and development of ideas.

Beyond that, I am pleased to acknowledge Dr. Markus Drechsler (Institute of Macromolecular Chemistry, University of Bayreuth) for performing cryo-transmission electron microscopy studies on distinct series of samples.

Further thanks go to all staff members of the Institute of Physical and Theoretical Chemistry, particularly to Dr. Didier Touraud for his innovative ideas and his continuous interest in the progress of this work, to Dr. Oliver Zech for the fruitful discussions in the field of ionic liquids and his help with conductivity measurements, to Dr. Alexander Stoppa and Dr. Rainer Müller for their support in the handling of technical equipment, to Eva Maurer for carrying out cytotoxicity analyses, and to my lab colleague Doris Rengstl for the great time we had and her patience with me.

This work was partially funded by the Bavarian program “Förderung der Chancengleichheit für Frauen in Forschung und Lehre”, and I acknowledge the granting of a one-year fellowship.

Of course, I wish to thank my whole family for understanding and encouraging me in any respect. Last but not least, I want to offer my heartfelt thanks to my boyfriend Matthias for his permanent mental and practical support, which was essential for the success of this dissertation.

Regina Klein

# Table of Contents

<b>Chapter I</b>	<b>Introduction and Strategy</b> .....	<b>1</b>
I.1.	Motivation .....	1
I.2.	How to Decrease a Surfactant's Krafft Point? .....	2
I.3.	Choline Soaps.....	3
I.4.	Biocompatibility.....	4
I.5.	Aqueous Self-Assembly Behavior .....	5
I.6.	Temperature-Dependent Self-Assembly Behavior of Neat Choline Soaps .....	9
I.7.	Specific Ion Effects and their Consequences .....	10
I.8.	Choline Alkyl Sulfates.....	14
I.9.	Oligoether Carboxylates – Task-Specific Room-Temperature Ionic Liquids .....	15
I.10.	References .....	17
<b>Chapter II</b>	<b>Choline Carboxylate Surfactants: Biocompatible and Highly Soluble in Water</b> .....	<b>21</b>
II.1.	Introduction .....	22
II.2.	Results and Discussion .....	24
II.2.1.	Critical Micellization Concentration ( <i>cmc</i> ).....	24
II.2.2.	Krafft Point .....	25
II.3.	Conclusion .....	27
II.4.	Experimental.....	27
II.4.1.	Soap Synthesis .....	27
II.4.2.	Methods.....	29
II.5.	References .....	31

<b>Chapter III</b>	<b>Biodegradability and Cytotoxicity on Human Cell Lines of Choline Soaps .....</b>	<b>33</b>
<b>III.1.</b>	<b>Introduction .....</b>	<b>34</b>
<b>III.2.</b>	<b>Results and Discussion .....</b>	<b>36</b>
III.2.1.	Biodegradability .....	36
III.2.2.	Cytotoxicity .....	38
III.2.3.	Monitoring of Cellular Uptake and Intracellular Distribution by Fluorescence Microscopy .....	42
<b>III.3.</b>	<b>Conclusion .....</b>	<b>43</b>
<b>III.4.</b>	<b>Experimental.....</b>	<b>44</b>
III.4.1.	Chemicals and Sample Preparation.....	44
III.4.2.	Biodegradability .....	45
III.4.3.	Cytotoxicity Tests .....	46
III.4.4.	Fluorescence Microscopy .....	47
III.4.5.	Statistics .....	47
<b>III.5.</b>	<b>References .....</b>	<b>48</b>
<b>Chapter IV</b>	<b>Aqueous Phase Behavior of Choline Carboxylate Surfactants.....</b>	<b>53</b>
<b>IV.1.</b>	<b>Introduction .....</b>	<b>54</b>
<b>IV.2.</b>	<b>Results and Discussion .....</b>	<b>55</b>
IV.2.1.	Penetration Scans .....	55
IV.2.2.	Binary Phase Diagrams .....	57
IV.2.3.	SAXS Data and Analysis .....	60
<b>IV.3.</b>	<b>Conclusions .....</b>	<b>70</b>
<b>IV.4.</b>	<b>Experimental.....</b>	<b>71</b>
IV.4.1.	Materials and Sample Preparation .....	71
IV.4.2.	Methods.....	72
<b>IV.5.</b>	<b>References .....</b>	<b>75</b>

<b>Chapter V</b>	<b>Thermotropic Phase Behavior of Choline Soaps .....</b>	<b>79</b>
<b>V.1.</b>	<b>Introduction .....</b>	<b>80</b>
<b>V.2.</b>	<b>Results and Discussion .....</b>	<b>81</b>
V.2.1.	Decomposition Temperatures .....	81
V.2.2.	Differential Scanning Calorimetry .....	81
V.2.3.	Polarizing Optical Microscopy .....	85
V.2.4.	NMR Spin-Spin Relaxation Time $T_{2eff}$ .....	87
V.2.5.	X-ray Scattering as a Function of Temperature and Chain Length .....	89
V.2.6.	Transition Enthalpies and Entropies .....	93
V.2.7.	Comparison to Alkali Soaps .....	96
<b>V.3.</b>	<b>Conclusion .....</b>	<b>97</b>
<b>V.4.</b>	<b>Experimental.....</b>	<b>98</b>
V.4.1.	Materials.....	98
V.4.2.	Methods.....	98
<b>V.5.</b>	<b>References .....</b>	<b>100</b>

<b>Chapter VI</b>	<b>Solubilization of Stearic Acid by the Organic Base Choline .....</b>	<b>105</b>
<b>VI.1.</b>	<b>Introduction .....</b>	<b>106</b>
<b>VI.2.</b>	<b>Results and Discussion .....</b>	<b>107</b>
VI.2.1.	Influences of Different Hydroxides on Soap Solubility.....	107
VI.2.2.	Influences of Different Chloride Salts on the Solubility of Choline Stearate.....	109
VI.2.3.	Specific Ion Effects in Aqueous Alkylcarboxylate Surfactant Solutions .....	111
VI.2.4.	Saponification and Solubilization of Butter by Choline Base .....	113
<b>VI.3.</b>	<b>Conclusion .....</b>	<b>115</b>
<b>VI.4.</b>	<b>Experimental.....</b>	<b>115</b>
VI.4.1.	Materials.....	115
VI.4.2.	Methods.....	116
<b>VI.5.</b>	<b>References .....</b>	<b>117</b>

<b>Chapter VII Choline Alkyl Sulfates .....</b>	<b>121</b>
<b>VII.1. Introduction .....</b>	<b>122</b>
<b>VII.2. Results and Discussion .....</b>	<b>124</b>
VII.2.1. Krafft Point and <i>cmc</i> .....	124
VII.2.2. Aqueous Self-Assembly Behavior .....	126
VII.2.3. Cytotoxicity of ChDS .....	129
VII.2.4. Influence of Salts on the Krafft Points of Alkyl Sulfate and Alkyl Carboxylate Surfactants .....	129
<b>VII.3. Conclusion .....</b>	<b>133</b>
<b>VII.4. Experimental.....</b>	<b>133</b>
VII.4.1. Chemicals.....	133
VII.4.2. Synthesis of ChDS and KDS .....	134
VII.4.3. Methods.....	135
<b>VII.5. References .....</b>	<b>140</b>
<b>Chapter VIII Oligoether Carboxylates – Task-Specific Room- Temperature Ionic Liquids.....</b>	<b>143</b>
<b>VIII.1. Introduction .....</b>	<b>144</b>
<b>VIII.2. Results and Discussion .....</b>	<b>146</b>
VIII.2.1. Decomposition and Glass Temperatures.....	146
VIII.2.2. Viscosity and Conductivity Measurements.....	147
VIII.2.3. Walden Plot.....	150
VIII.2.4. Polarity Parameters .....	153
<b>VIII.3. Conclusion.....</b>	<b>158</b>
<b>VIII.4. Experimental.....</b>	<b>159</b>
VIII.4.1. Materials and Syntheses.....	159
VIII.4.2. Methods.....	159
<b>VIII.5. References .....</b>	<b>166</b>
<b>Chapter IX Summary.....</b>	<b>171</b>

**Appendix A: Biodegradability and Cytotoxicity on Human Cell  
Lines of Choline Soaps ..... 175**

<b>A.1</b>	<b>HeLa Dose-Response Curves of ChCm Surfactants for <math>m= 8-16</math> .....175</b>
<b>A.2</b>	<b>SK-Mel-28 Dose-Response Curves of ChCm Surfactants for <math>m= 8-16</math> ....176</b>
<b>A.3</b>	<b>Phase Contrast and Fluorescence Images of HeLa Cells Treated with Pyrene-Substituted Choline and Sodium Soaps over Time.....178</b>

**Appendix B: Aqueous Phase Behavior of Choline Carboxylate  
Surfactants..... 179**

<b>B.1</b>	<b>Density and Determination of the Molar Volume of ChCm Surfactants .....179</b>
<b>B.2</b>	<b>Penetration Scan Images of ChCm Surfactants at Various Temperatures.....181</b>
B.2.1	ChC14 ..... 181
B.2.2	ChC16 ..... 182
B.2.3	ChC18 ..... 182
<b>B.3</b>	<b>SAXS Experimental .....183</b>
<b>B.4</b>	<b>SAXS spectra .....186</b>
B.4.1	ChC12 ..... 186
B.4.2	ChC14 ..... 188
B.4.3	ChC16 ..... 190
B.4.4	ChC18 ..... 192
<b>B.5</b>	<b>X-ray Data and Phase Assignment .....194</b>
B.5.1	Attempt of Assigning $I_1'$ to $P6_3/mmc$ ..... 194
B.5.2	X-ray Data of $I_1''$ ..... 195
B.5.3	X-ray Data of $H_1$ ..... 196
B.5.4	$H_1 - V_1$ Boundary: Intermediate Phase?..... 197
B.5.5	Bicontinuous Cubic Phase $V_1$ ..... 199
<b>B.6</b>	<b>References .....200</b>

<b>Appendix C: Thermotropic Phase Behavior of Choline Soaps .....</b>	<b>201</b>
<b>C.1 Thermogravimetric analyses .....</b>	<b>201</b>
<b>C.2 DSC diagrams .....</b>	<b>201</b>
<b>C.3 Transition Temperatures .....</b>	<b>203</b>
<b>C.4 Transition Enthalpies .....</b>	<b>203</b>
<b>C.5 Optical Polarizing Microscopy .....</b>	<b>205</b>
C.5.1 ChC14 .....	205
C.5.2 ChC16 .....	206
C.5.3 ChC18 .....	207
<b>C.6 NMR Proton Spin-Spin Relaxation Times <math>T_2</math> .....</b>	<b>208</b>
<b>C.7 X-ray Scattering Curves of ChC<math>m</math> Soaps as a Function of Temperature .....</b>	<b>210</b>
C.7.1 ChC12 .....	210
C.7.2 ChC14 .....	211
C.7.3 ChC16 .....	212
C.7.4 $d$ -Spacing of ChC $m$ Surfactants as a Function of Temperature .....	214
C.7.5 $d$ -Spacing of ChC $m$ Surfactants as a Function of $m$ at Low Temperatures ..	215
C.7.6 $d$ -Spacing of ChC $m$ Surfactants as a Function of $m$ at 40°C .....	216
 <b>Appendix D: Oligoether Carboxylates – Task-Specific Room-Temperature Ionic Liquids .....</b>	 <b>217</b>
 <b>List of Figures .....</b>	 <b>219</b>
 <b>List of Tables .....</b>	 <b>225</b>
 <b>List of Publications .....</b>	 <b>227</b>
 <b>List of Patents .....</b>	 <b>231</b>
 <b>List of Oral and Poster Presentations .....</b>	 <b>233</b>

# Chapter I Introduction and Strategy

The main part of this thesis deals with choline carboxylate soaps, in particular with their synthesis and analyses of their cytotoxicity and biodegradability as well as of their self-assembly behavior. In addition, choline alkyl sulfates, recently patented by the University of Regensburg,<sup>1</sup> will be introduced as new promising biocompatible surfactants. Finally, it will be shown that the strategies applied for the development of these surfactants can be conferred to the design of novel green ionic liquids, as documented by a patent claimed in collaboration with BASF SE.<sup>2</sup>

Since this dissertation is concerned with investigations on various fields – ranging from the synthesis of surfactants and ionic liquids over the establishment of phase diagrams, X-ray scattering experiments, and measurements of biodegradability and cytotoxicity to the characterization of ionic liquids in general – each chapter describes a self-contained study and is organized according to the following convention: Abstract, Introduction, Results and Discussion, Conclusion, Experimental Procedures and Bibliography. Individual chapters were thus written to be (part of) a draft for an article (or patent), which is either already published or accepted in a scientific journal, or currently submitted. A complete list of publications, patents, as well as oral and poster presentations at national and international conferences is presented at the end of the thesis.

## I.1. Motivation

First of all, why did we focus our attention on soaps given that they are known already for thousands of years? Surfactants are everyday life products. Besides their primary application as active compounds in washing and cleaning processes (dish-washing agents, washing powders, shampoos, shower gels, etc.), they are further implemented in the fields of textiles, pharmaceuticals, food, metal, paper, and others.<sup>3</sup> Thus, surfactants are fabricated and used on an enormous scale and, therefore, get in a fairly large amount into the environment, which renders the aspect of biocompatibility highly relevant.

Generally, the functionality of surfactants originates from their amphiphilic molecular structure, which is characterized by a polar headgroup and a non-polar chain. Among the different subclasses of surfactants (anionic, cationic, non-ionic, and zwitter-ionic),

the anionic ones are still the most widespread and frequently applied type.<sup>3</sup> This is not only due to their lower toxic impact compared to cationic amphiphiles,<sup>4</sup> but also to their high solubilizing power of hydrophobic substances.

The oldest surfactants known are the classical soaps, the sodium and potassium salts of fatty acids.<sup>5</sup> For thousands of years, they have been prepared by converting tallow and potassium hydroxide.<sup>5</sup> Today, such surfactants are produced by neutralizing fatty acids gained from coconut oil, palm kernel oil and tallow, with caustic soda, soda ash or potash.<sup>5</sup> In this regard, important advantages of classical soaps become evident: their straightforward synthesis and the fact that they can be derived from natural components. The former aspect renders them economically profitable, while the latter implies that they are readily biodegradable.<sup>4</sup> However, an essential drawback of these soaps and in particular the long-chain derivatives is their limited water solubility, which is defined for surfactants by the so-called Krafft point.<sup>3,6</sup> Generally, the Krafft point ( $T_{Kr}$ ) is defined as the temperature at which the solubility of a surfactant equals the critical micellization concentration ( $cmc$ ) and increases sharply.<sup>6</sup>

For both, sodium and potassium carboxylates, the maximum alkyl chain length applicable under ambient conditions is dodecanoate (C12).<sup>7</sup> This is because the Krafft point rises systematically with growing alkyl chain length. For instance,  $T_{Kr}$  is already about 45°C for sodium myristate (NaC14) and even about 60°C for sodium palmitate (NaC16).<sup>7,8</sup> Unfortunately, the longer-chain derivatives are the more desirable surfactants since an increase of the chain length is accompanied with an improvement of properties like surface activity, solubilizing power or washing ability.<sup>9</sup> This shortcoming has in part be circumvented in the past decades by modifying the structure of the alkyl chain or the headgroup, yielding synthetic surfactants of enhanced performance such as linear alkyl benzene sulfonates.<sup>5</sup> However, corresponding modifications often cause problems in view of biodegradation.

On that basis, the initial motivation of this work was to create cost-efficient anionic surfactants of high water solubility, while ensuring at the same time biocompatibility.

## **1.2. How to Decrease a Surfactant's Krafft Point?**

In general, the Krafft point is determined by the interplay of two competing thermodynamic forces, namely by the free energies of the solid crystalline and the solubilized state. If the free energy of the crystalline state is high, the solubilized phase,

i.e. the micellar solution, will be favored. Accordingly, hindering a regular crystalline packing of the surfactant molecules will contribute to a decreased  $T_{Kr}$ . A low free energy of the micellar solution further reduces  $T_{Kr}$ . This can be achieved, for instance, by using salts that exhibit high dissociation. Commonly, the Krafft point is more influenced by the energy content of the solid than of the liquid state.<sup>3</sup>

A regular crystalline packing of the surfactant molecules can be hindered, amongst others, by introducing alkyl chain branching or certain functional groups, or by inserting double bonds in the hydrocarbon chain. The former modifications usually give rise to depressed biodegradability,<sup>4</sup> while the latter render the surfactants sensible to oxidation and “rinsing” effects.<sup>5</sup> Alternatively, the free energy of the crystal lattice can be altered by varying the type of the counterion.<sup>9,10</sup> In 2004, Zana and coworkers showed that bulky tetraalkylammonium ions such as tetrabutylammonium (TBA) are very efficient to increase the water solubility of fatty acid surfactants.<sup>11,12</sup> For example, the Krafft point of TBAC18 was found to be below 0°C,<sup>11</sup> while that of sodium stearate (NaC18) is about 70°C.<sup>7,8</sup> However, simple tetraalkylammonium ions suffer from their inherent toxicity (see Chapter II for details).<sup>13-16</sup> This disadvantage can yet be overcome by applying the benign choline ion ((2-hydroxyethyl)trimethylammonium). Choline as natural metabolite and essential nutrient for mammals is biochemically well investigated (see Chapter II),<sup>17-19</sup> but has for long been neglected concerning its potential as counterion in the design of innovative green materials.

### **I.3. Choline Soaps**

The basic idea of using choline as counterion in fatty acid soaps goes back to the diploma thesis.<sup>20</sup> However, this has only been the starting point for the investigation of choline soaps, or in other words, the proof of concept. For surfactants, the purity of a compound is of pivotal importance since it can substantially affect the phase behavior. Actually, the first major task in the framework of this PhD thesis was to successfully prepare dry and neat powders of choline soaps, which proved to be difficult owing to their high solubility in most organic solvents (and water) and due to their strong hygroscopicity. For achieving reliable physicochemical data, a purified and well-defined batch of surfactant is especially required in the case of long-chain choline soaps, since these are utterly susceptible, for example, to the exact molar ratio of carboxylate anions and choline cations. The latter feature was addressed explicitly in an independent study (Chapter VI), where the effect of excess choline base was investigated and

surprising results – such as the solubilization of butter at room temperature – were obtained.

The synthesis, purification and primary characterization of choline carboxylate soaps (ChC*m*) with alkyl chain lengths ranging from  $m=12$ -18 (see Fig. I.1) are described in Chapter II of the thesis.

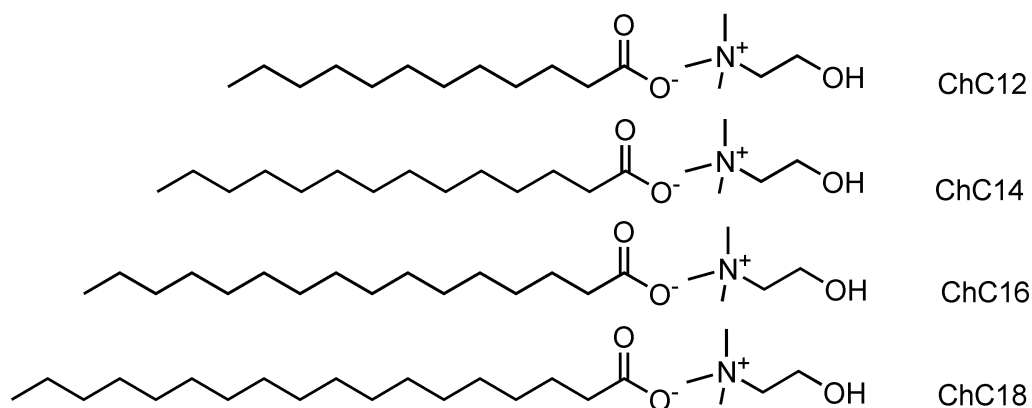


**Fig. I.1** Molecular structure of the studied choline soaps.

In this context, the *cmc* values and Krafft points of ChC*m* surfactants will be presented and related to the sodium, potassium and tetramethylammonium homologues. It will be shown that the *cmc*'s of choline soaps are very similar to those of the alkali derivatives, indicating that the self-assembly behavior at low surfactant concentrations is not noticeably influenced by the nature of the counterion (see below). In turn, the Krafft points are found to be significantly lowered as compared to alkali soaps, which is in agreement with the common tendency of a decreasing Krafft point with increasing counterion size in carboxylate surfactants (reversed trend for alkyl sulfates!). For instance, replacing sodium by choline in a palmitate system ( $m=16$ ) led to a reduction of  $T_{Kr}$  from  $60^{\circ}\text{C}$ <sup>7,8</sup> down to  $12^{\circ}\text{C}$ . Therefore, choline soaps – which consist exclusively of compounds occurring in the human metabolism – can be used under ambient conditions up to a chain length of  $m=16$ .

## I.4. Biocompatibility

Although choline is known to be biodegradable and exhibit no intrinsic toxic impact on the mammalian metabolism (at least up to concentrations on an order similar to for instance sodium chloride),<sup>21-23</sup> its use in cosmetic formulations is curtailed by the European Cosmetic Directive 76/768/EEC (Annex II/168).<sup>24</sup> This restriction is mainly

due to the plain classification of choline as quaternary ammonium ion. In order to facilitate the use of choline soaps in everyday life products and to validate the *a priori* assumption of their high biocompatibility, the biodegradability of ChC $m$  surfactants and their cytotoxicity on two human cell lines (cervix carcinoma cells (HeLa) and keratinocytes (SK-Mel-28)) have been examined (Chapter III). Biodegradability tests were conducted according to the European standard (CE2004/ 648). HeLa cells were selected since they are judged to be a reasonable alternative to the *in vivo* eye-irritancy tests on rabbits (*Draize* test), while keratinocytes were chosen in order to get first information on the skin irritancy power of choline soaps.<sup>25,26,27</sup> The sodium and potassium homologues were also studied so as to allow for comparing the collected data to those of conventional surfactants. Initially, this investigation comprised only the even-numbered carboxylates displayed in Fig. 1. However, to gain more profound insight to structure-activity relationships (SAR),<sup>28</sup> odd-numbered alkyl chains (ranging from  $m=8-15$ ) were later included in the study. In parallel to the mentioned measurements, fluorescence microscopy was conducted on pyrene-substituted soaps to follow the uptake of the surfactants in the cells. This comprehensive investigation took more than two years to be completed, primarily because the cytotoxicity analyses were repeated multiply to confirm the observed uncommon progression of IC<sub>50</sub> values (which represent the toxicity in a manner similar to LD<sub>50</sub> values) with growing alkyl chain length. Detailed results and a possible interpretation of the discerned trends are presented in Chapter III. One of the most important conclusions is that choline soaps were found to be readily biodegradable and, alongside, display IC<sub>50</sub> values which more or less equal those of the widely applied sodium and potassium soaps. Certainly, further tests such as on aquatotoxicity are necessary to complete the ensemble of toxicity studies required for the admission of new substances to the market. Nevertheless, the gathered results clearly support the notion that choline soaps are highly promising candidates for green surfactants in various formulations.

## **I.5. Aqueous Self-Assembly Behavior**

In a further suite of experiments, the aqueous phase behavior of choline soaps has been explored (Chapter IV). To that end, phase diagrams of all compounds shown in Fig. I.1 were established over a temperature interval of 0-100°C by employing diverse techniques like light microscopy and extensive small- and wide-angle X-ray scattering (SAXS and WAXS) measurements. A central criterion to attain a reliable picture of the

occurrence of distinct phases was to ensure that thermodynamic equilibrium was reached. In the present case, this required monitoring of the samples over periods as long as two years or even more. Since this section of the work involves various aspects and highlights many details, only a brief outline of the most important concepts and arguments shall be given here.

The different states of self-organization and structural motifs adopted by choline soaps in water as a function of concentration are depicted in Fig. I.2.

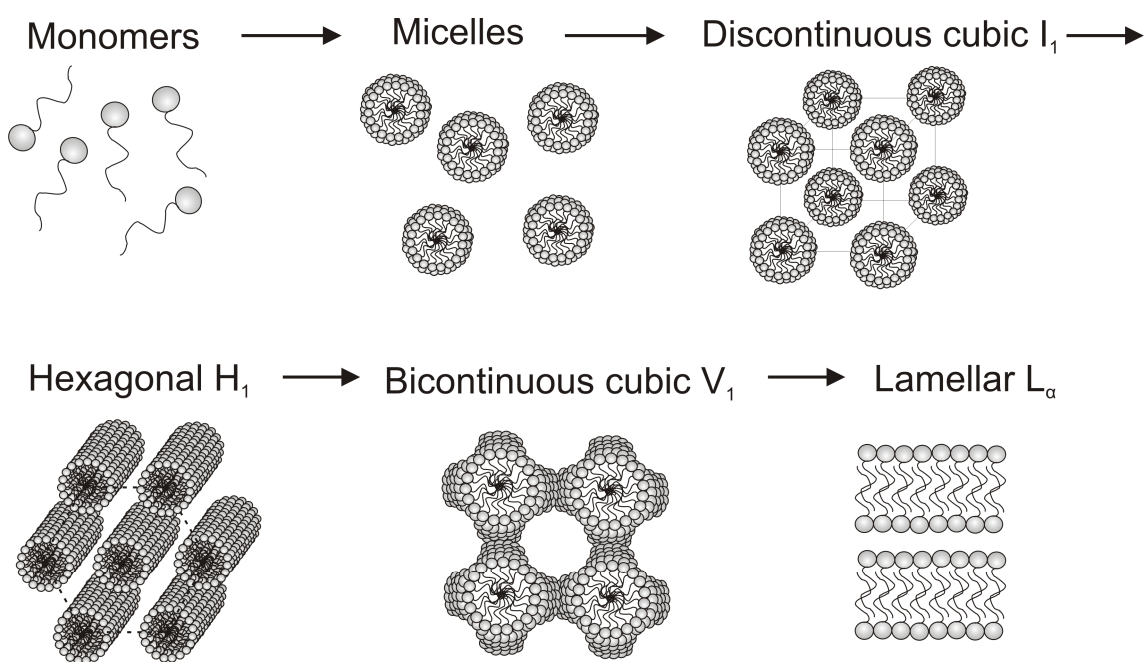


**Fig. I.2** Scheme illustrating the self-assembly behavior of choline soaps in water upon increasing the surfactant concentration. At very low concentrations, only monomers are present. Once the *cmc* is reached, spherical micelles are formed. Their number increases with the surfactant concentration in the following, whereas their size and shape are not affected (i.e. there is no sphere-to-rod transition). The first liquid-crystalline phase observed at a volume fraction of 25-30% is featured by a discontinuous cubic lattice ( $I_1$ ). When further raising the surfactant content, successive transitions into a hexagonal ( $H_1$ ), a bicontinuous cubic ( $V_1$ ) and eventually a lamellar phase ( $L_\alpha$ ) occur.

At very low surfactant content, the soap molecules exist isolated from one another in the solution or, respectively, prevail at the water-air interface. Starting from a certain concentration ( $\approx 10^{-2} - 10^{-3} \text{ mol L}^{-1}$ ) – the critical micellization concentration (*cmc*) – their amphiphilic character causes the soap molecules to self-assemble in aqueous media to form globular micelles, in which the hydrophobic hydrocarbon tails are

imbedded in the interior of the aggregates in order to minimize contact with water. Any further increase of the ChC*m* concentration initially results only in an increment of the number of micelles, whereas their size and shape remain virtually unaltered.<sup>20</sup>

At a distinct level of surfactant content (here 25-30 wt%), the volume fraction of micelles in the system and the interactions between them become large enough to force the micelles to arrange themselves in quasi-crystalline lattices and thus build so-called “liquid-crystalline” phases. Due to the spherical shape of the micelles of choline soaps in dilute solution, the first liquid-crystalline phase formed by the surfactants exhibits a discontinuous cubic structure ( $I_1$ ) which, can have different crystallographic parameters and hence belong to distinct space groups. When the surfactant content is further increased, structural re-ordering occurs and the following sequence of mesophases is observed towards higher concentrations: hexagonal ( $H_1$ ), bicontinuous cubic ( $V_1$ ) and lamellar ( $L_\alpha$ ). This general picture holds for all alkyl chain lengths investigated in ChC*m* surfactants.

In this regard, the basic phase behavior of choline soaps is thus similar to what has been reported for alkali soaps or anionic surfactants in general,<sup>29, 30</sup> with, however, some important differences:

- (1) All other mono-anionic surfactants undergo a sphere-to-rod transition in the micellar solution.<sup>31-36</sup> Consequently, the first liquid-crystalline phase to be formed is usually  $H_1$ . By contrast, choline soaps prefer a cubic  $I_1$  lattice as initial liquid-crystalline phase at comparably low concentrations.
- (2) ChC*m* surfactants exhibit a single cubic  $V_1$  phase up to  $m=18$ . As opposed to that,  $V_1$  is absent in the phase sequence displayed by sodium carboxylates at  $m \geq 12$  and potassium soaps at  $m \geq 14$ .<sup>37</sup>
- (3) The  $L_\alpha$  phase region of ChC*m* surfactants is considerably smaller than what has been found for the alkali homologues.<sup>7,8,29</sup>
- (4) The Krafft boundary of choline soaps is shifted markedly to lower temperatures compared to the alkali counterparts.<sup>7,8,38</sup> For instance, ChC12 shows no Krafft phenomenon down to 0°C for surfactant contents up to 93 wt% in water. By contrast, the Krafft point of a 90 wt% NaC12 solution is 127°C (or 195°C for KC12).<sup>37</sup>

The first three points mentioned above can be interpreted by the notion that choline as counterion in fatty acid soaps promotes phases of higher curvatures as compared to simple alkali cations. In order to understand the reason underlying this behavior, the concept of *packing constraints* must be considered,<sup>39,40</sup> for which Israelachvili and coworkers provided a thermodynamic description.<sup>30,39-41</sup> This model relates the shape of a surfactant molecule to that of the resulting micelles. Thereby, the geometry of a micelle is thought to be determined by the critical surfactant parameter  $N_S$ , which is defined according to:<sup>39, 40</sup>

$$N_s = \frac{v}{a_0 l} \quad (I.1)$$

where  $v$  represents the volume of the hydrophobic part of the surfactant molecule,  $l$  the length of the hydrocarbon chain, and  $a_0$  the effective area per headgroup (see Fig. I.3). At optimum molecular packing,  $N_S$  takes a values of 0.33 for spherical and 0.5 for cylindrical micelles.<sup>6</sup>

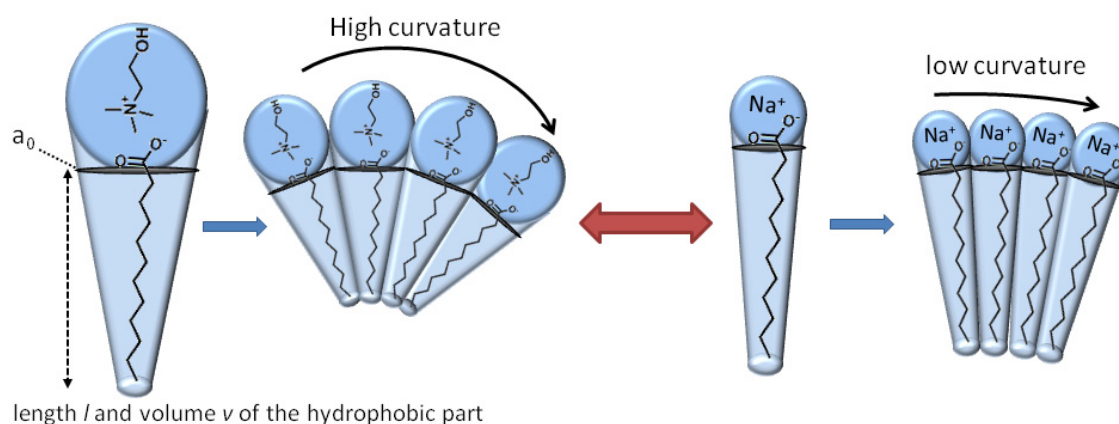


**Fig. I.3** The effect of counterion size and dissociation on the curvature of surfactant aggregates, exemplified for the choline (left) and sodium (right) salts of dodecanoic acid. The bulkiness of the choline cation and its high degree of dissociation cause an increase in the headgroup area  $a_0$  relative to sodium and thus a decrease of the packing parameter  $N_S$ , since the length and volume of the hydrophobic part are the same in both cases. As a consequence, aggregates of higher curvature are promoted when choline is used as counterion (i.e. spherical micelles are for example favored over rod-like ones).

Thus, a large headgroup area provokes aggregates of high curvature. The value of  $a_0$  depends on the size of the headgroups and the electrostatic interactions between them. The latter forces are influenced considerably by the kind of the counterion. For instance,

counterions that are widely dissociated will contribute to high  $a_0$  values. It is well-known that the degree of association between alkali cations and carboxylic headgroups decreases with increasing size of the counterion ( $\text{Li}^+ > \text{Na}^+ > \text{K}^+ > \text{Rb}^+ > \text{Cs}^+$ ).<sup>11,42,57,58</sup> In view of its bulkiness, the choline cation can be considered to continue the reported trend for the alkali ions. Hence, choline soaps are featured by a large area per headgroup  $a_0$ , which induces aggregates of high curvature as illustrated in Fig. I.3. In this regard, liquid-crystalline structures and micellar shapes can in general provide direct information on specific ion effects or, *vice versa*, the mesophase behavior can be tuned by an adequate choice of the counterion.<sup>43</sup>

The above-described considerations also allow for explaining point (4) in the list of differences: the bulky and highly dissociated choline ion effectively impedes a regular crystalline packing of the choline soap molecules and, in doing so, favors the solubilized state and reduces the Krafft boundary to a substantial extent.

## I.6. Temperature-Dependent Self-Assembly Behavior of Neat Choline Soaps

Apart from the concentration-dependent occurrence of different mesophases, also the thermotropic (temperature-dependent) phase behavior of neat choline soaps has been studied in the scope of this work (Chapter V). For this purpose, the surfactants were investigated over a temperature range of  $-20^\circ\text{C}$  to  $100^\circ\text{C}$  by means of polarizing optical microscopy, differential scanning calorimetry (DSC), NMR relaxation experiments, as well as SAXS and WAXS measurements. Usually, surfactants are featured by a rich and complex thermotropic phase behavior.<sup>44-46</sup> For instance, sodium soaps exhibit at least five liquid-crystalline allotropic phases at temperatures between  $100^\circ\text{C}$  and  $320^\circ\text{C}$ .<sup>47-49</sup> Given that choline soaps show various lyotropic (solvent-induced) liquid-crystalline phases, it seems reasonable to expect that they also exhibit thermotropic mesomorphism. Beyond that, regarding the lowering of a salt's melting point, analogous considerations can be put forward as for the reduction of a surfactant's Krafft point (i.e. the hindering of crystalline packing). Coherently, in a very recent study, Petkovic *et al.* found that short- to middle-chain choline carboxylates ( $m= 2-10$ ) are liquid at temperatures below  $100^\circ\text{C}$ .<sup>23</sup>

For the longer-chain derivatives investigated in this work, the experiments outlined in Chapter V show that all choline soaps pass through three different phases in the examined temperature interval. First, at 35-48°C, the crystalline salts are converted into a semi-crystalline lamellar phase before transforming, at temperatures of 68-93°C, into a lamellar liquid-crystalline phase ( $L_\alpha$ ). Thus, also long-chain ChC*m* salts – i.e. choline soaps – have to be considered as ionic liquids and evidently combine low melting points with surfactant properties.

## **I.7. Specific Ion Effects and their Consequences**

As discussed above, counterion-to-headgroup association plays a key role in the phase behavior of surfactants and therefore also in the determination of Krafft and melting points for the surfactants. This feature will be addressed in detail in Chapter VI of this dissertation where, among others, results of investigations on the influence of different chloride salts and of excess choline base on the Krafft temperature of ChC18 solutions are presented. In order to render the drawn conclusion comprehensible, it is necessary to briefly summarize certain fundamental aspects of the very broad field of “salt effects”.

Already in the 1880s, Franz Hofmeister and his coworkers published a series of papers entitled “About the science of the effect of salts”.<sup>50-52</sup> These were among the first studies on the ability of salts to stabilize or destabilize protein solutions (in this case hen egg-white albumin). Based on these experiments, Hofmeister introduced an empirical ordering of salts according to their “salting-in” or “salting-out” impact on proteins. Many years later, this classification has been refined and conveyed to individual ions rather than salts, leading to what is today known as the “Hofmeister series” (see Fig. I.4).<sup>53</sup> Impressively, the Hofmeister series holds for many salt-induced phenomena beyond the behavior of aqueous protein solutions, and is moreover widely applied in areas as diverse as the interpretation of biological scenarios and structures, process optimization in chemical industry, or drug design in pharmaceutical industry.<sup>54</sup>

Several attempts were made to understand the reasons behind such salt effects and to predict the behavior of ions in solution. Nowadays, it is fairly well accepted that the initial paradigm of a salt either “making” or “breaking” the bulk water structure is not valid.<sup>42,55</sup> Instead of long-range electrostatic fields, rather short-range ion-ion interactions appear to be the dominant forces.<sup>56</sup> Accordingly, simple monovalent ions only change the hydrogen bond network of water in their direct vicinity (up to 5 Å or

over a length of  $\sim 2$  H<sub>2</sub>O molecules) and do not affect the bulk of the solution.<sup>56</sup> In the past years, the number of studies devoted to specific ion effects has escalated and thousands of papers exist in the meantime. Recently, the latest approaches and most important results have been reviewed,<sup>53</sup> but a complete overall picture explaining all of the observed phenomena is still missing.

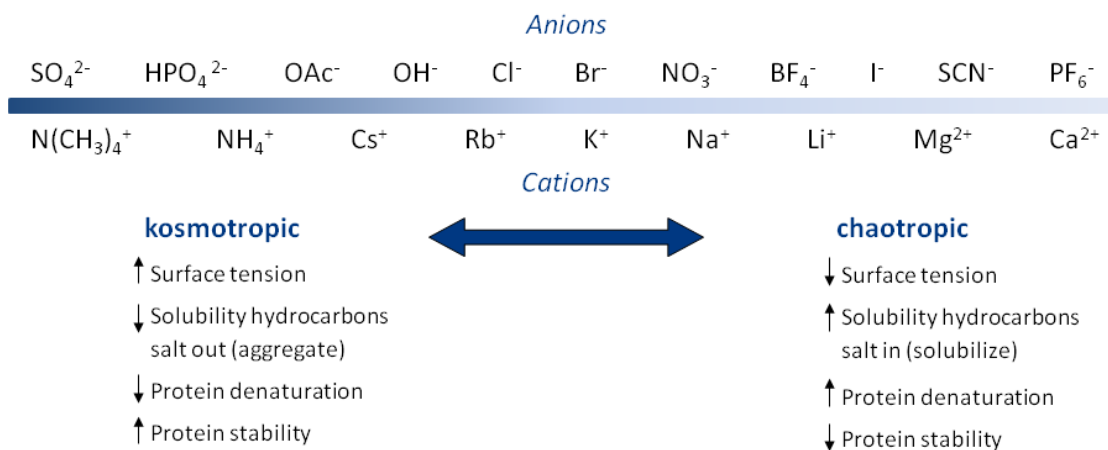


**Fig. I.4** The Hofmeister series – a classification of anions and cations according to their capability of influencing the surface tension of water, solubilizing hydrocarbons and stabilizing protein solutions (drawing based on ref<sup>42</sup>).

One of the milestones towards a rationalization of specific ion effects was the development of Collins' "law of matching water affinities".<sup>54,57,58</sup> This concept provides a useful rule of thumb and applies for many simple systems, often enabling a prediction of their macroscopic properties. Essentially, it assumes that the association of ions or the formation of ion pairs is controlled by hydration-dehydration processes. Basically, ions are divided into two classes with regard to their size compared to the "medium-sized" water molecule (see left-hand panel in Fig. I.5). This ion size-based discrimination relies on the consideration of a simple ion as a hard sphere having a point charge in its center. The larger an ion is, the further away are the surrounding water molecules from the charge. Thus, the hydration water of large ions is expected to be bound only loosely. At a certain distance between the water molecules and the charge, the H<sub>2</sub>O··H<sub>2</sub>O interaction becomes stronger than the ion··H<sub>2</sub>O interaction. In this manner, the size of an ion represents a simple means to estimate its "water affinity". Accordingly, small ions with high charge density, such as Li<sup>+</sup> or F<sup>-</sup>, termed "kosmotropes", are envisaged to be featured by a strong degree of hydration. In turn, large ions with low charge density, such as Cs<sup>+</sup> or I<sup>-</sup>, are weakly hydrated and referred

to as “chaotropes”. In the scope of his model, Collins argues that if congeneric ions are matched in solution (i.e. small + small or big + big), the hydration shells of the ions will break down and an inner-sphere ion pair will be formed (see right-hand panel in Fig. I.5).<sup>57</sup> In the case of two small “kosmotropic” ions, the point charges can approach each other closer than the distance between the charge of one of the ions and the oppositely charged part of a hydrating, medium-sized water molecule. In case of two “chaotropic” ions, the surrounding water molecules will prefer to be bound to one another, as they can come closer together than the point charge of a large ion and the charged part of medium-sized water. If, on the other hand, ions of considerably different sizes and hence distinct water affinities are combined, the hydration shell will persist and the salt will dissociate extensively upon dilution, facilitating its solubility. This behavior may be summarized under the label “like seeks like”.

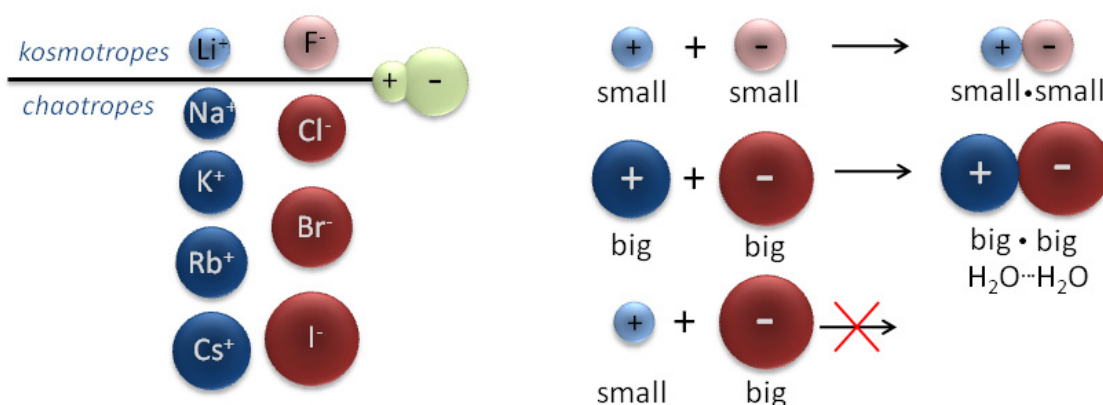


**Fig. I.5** Schematic representation of Collins’ law of matching water affinities (drawing based on ref <sup>57</sup>). Ions are classified concerning their size with respect to to the “medium-sized” water molecule as small “hard” ions of high charge density (kosmotropes) and big “soft” ions of low charge density (chaotropes). Collins’ model states that matching of congeneric ions results in the formation of, an inner-sphere ion pair, whereas the combination of ”unlike” ions will lead to enhanced dissociation as each ion prefers to keep its hydration shell.<sup>54</sup>

Collins’ concept can be applied likewise for surfactants (see Fig. I.6),<sup>59</sup> and in particular also for the soaps studied in this work. Thereby, sodium has to be considered as small hard ion (kosmotrope) and choline as big soft ion (chaotrope). Carboxylate headgroups have been shown to belong to the class of hard anions while alkylsulfates, for instance, are judged to be soft anions.<sup>59</sup> Thus, when combining alkyl carboxylates with sodium, ion-ion association is expected to be strongly pronounced. In turn, choline should be

bound only weakly to the fatty acid anion – in line with the argumentation put forward when outlining the role of choline in lowering the Krafft point and promoting surfactant aggregates of high curvature.

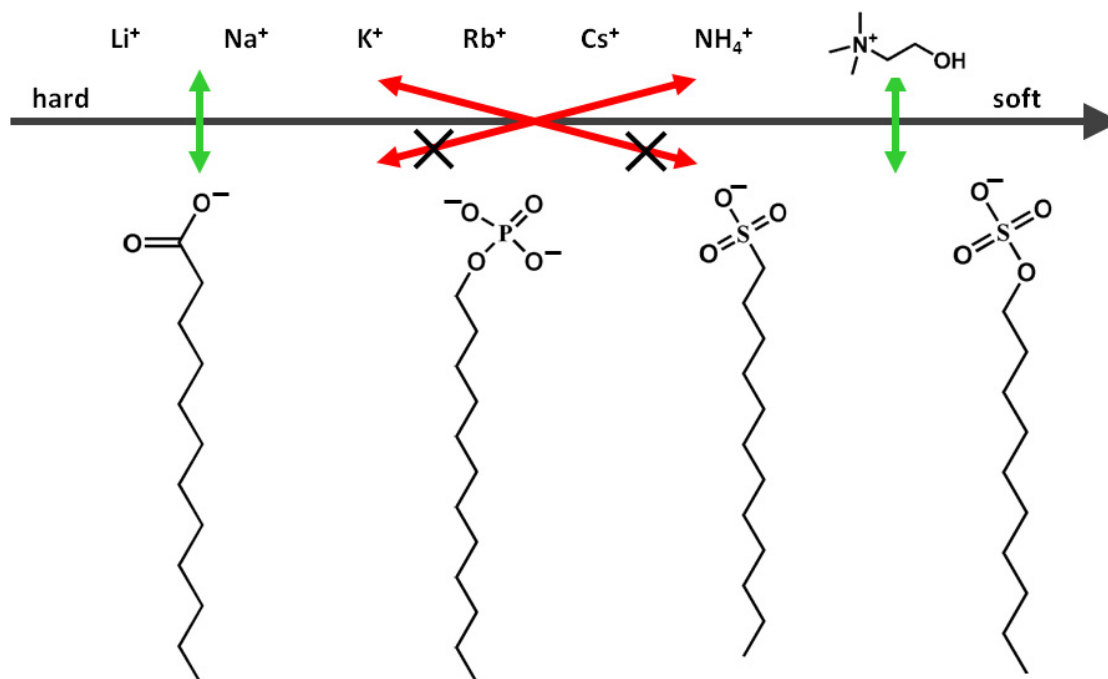


**Fig. I.6** “Like seeks like” for surfactant systems: small “hard” cations preferably interact with congeneric “hard” surfactant headgroups, and *vice versa*. Combining hard and soft ions will in turn yield surfactants of high counterion dissociation.<sup>59</sup>

Another immediate consequence of the above methodology is that adding sodium chloride to a solution of choline soaps should lead to a replacement of choline by sodium as counterion of the surfactant. This assumption is verified by the data compiled in Chapter VI of this thesis. In fact, the presence of NaCl in a 1:1 molar ratio with the choline surfactants is shown to increase the Krafft temperature to levels approaching the value of the pure sodium soaps. This inherent dissociation of choline fatty acid salts certainly contributes to their superior water solubility, but likewise and evidently renders them very sensitive to the addition of alkali (or alkaline-earth) salts. Another advantage of high dissociation will be illustrated in the neutralization curves of the fatty acids. Usually, an excess of for instance sodium hydroxide results in an increase of the Krafft temperature and a gelling of the solution. By contrast, addition of excess choline base was found to be a powerful means to further lower the Krafft point. Following this strategy, even stearate surfactants could be dissolved at room temperature or below, depending on the extra-amount of choline hydroxide applied. This feature is illustrated

by another simple experiment in Chapter VI, in which conventional butter was solubilized by choline base under ambient conditions. Thereby, the ester bridges of the triglycerides in butter are first split by alkaline hydrolysis to release fatty acids, which instantly become water-soluble by the action of choline as a counterion. The generated surfactants finally solubilize other hydrophobic ingredients of the butter, such as cholesterol or vitamin E.

## **I.8. Choline Alkyl Sulfates**

The fact that ChCm surfactants are intimately sensitive to the addition of simple salts is a serious drawback in view of their applicability in formulation products. Another shortcoming arises from the weak acidity of the fatty acid anion which causes a relatively high pH of the surfactant solutions (pH= 10-11). Considering the natural pH of human skin (pH $\approx$  5.5), fatty acid soaps are in general likely to possess undesired skin irritancy potential.

The problem of alkaline pH can be overcome by using a more acidic headgroup such as sulfate. Moreover, with regard to the concept of Collins, the degree of counterion binding to a “soft” alkyl sulfate headgroup should increase according to  $\text{Li}^+ < \text{Na}^+ < \text{K}^+ < \text{Rb}^+ < \text{Cs}^+$ . This notion has been confirmed for example by small-angle neutron scattering measurements (SANS),<sup>60,61</sup> and is reflected also in the reported trends of corresponding Krafft points.<sup>62</sup> Thus, the soft choline cation is supposed to interact strongly with alkyl sulfate anions, and choline alkyl sulfate surfactants should be distinctly less salt sensitive than their carboxylate counterparts – but what about the Krafft temperature?

Choline dodecyl sulfate (ChDS) has been successfully synthesized in this work and characterized concerning its physicochemical properties and cytotoxicity issues, as described in Chapter VII of the thesis. It will be demonstrated that the *cmc* of ChDS is on the order of  $10^{-3}$  mol L<sup>-1</sup>, but yet slightly lower than that of sodium dodecyl sulfate (SDS), thus indicating increased counterion condensation.<sup>63</sup> Nevertheless, the Krafft point of ChDS is about 0°C and hence falls below those of SDS (~14°C) and potassium dodecyl sulfate (KDS, ~37°C).<sup>64</sup> This finding is discussed with respect to the effect of the bulky choline ion on the regular crystalline packing of the surfactant molecules. In addition, a preliminary binary aqueous phase diagram has been established for ChDS, revealing that the Krafft boundary remains constant at around 0°C up to ~65 wt%

surfactant in water and that the first liquid-crystalline phase observed is  $H_1$ . As illustrated in Fig. I.3, the latter feature implies that the effective headgroup area of ChDS is smaller than that of ChC12, again pointing to enhanced counterion-headgroup association in ChDS. Eventually, cytotoxicity analyses, using HeLa and SK-Mel 28 cells, evidence that ChDS is similarly harmless as SDS – which is one of the most intensively studied surfactants and present in various household products. Hence, the introduced choline alkyl sulfates depict a new type of biocompatible anionic surfactants with beneficial properties such as high water solubility or reduced salt sensitivity.

## I.9. Oligoether Carboxylates – Task-Specific Room-Temperature Ionic Liquids

Ionic liquids (ILs) are defined as salts with melting points below 100°C. They have attracted much interest in the past two decades as potential alternative reaction media to common organic solvents. While the latter are typically volatile, ILs possess – due to their salt character – an almost non-detectable vapor pressure and are rarely explosive or flammable. However, recent toxicological studies have elucidated that these characteristics do not allow *per se* a classification of ionic liquids as “green”. Common imidazolium salts with longer alkyl chains were factually confirmed to be toxic.<sup>65-67</sup>

Previous work on ILs has mainly focused on large, preferably non-symmetrical cations of delocalized charged distribution and high conformational flexibility such as imidazolium, pyridinium, or pyrrolidinium.<sup>68</sup> Frequently chosen anions include hexafluorophosphate ( $PF_6^-$ ), tetrafluoroborate ( $BF_4^-$ ) or triflate ( $SO_3CF_3^-$ ).<sup>69</sup> In turn, the possibility of using small cations and large anions for the design of ionic liquids has hardly been considered to date.

The experiments presented in Chapter V of this dissertation show that choline soaps with alkyl chain lengths of  $m=12-18$  melt below 100°C into a lamellar liquid-crystalline phase. There, the hydrocarbon chains exist indeed in a liquid-like state, but the soap molecules are still oriented in bilayers. To further reduce the melting point and prepare true ionic liquids, the methylene groups of the alkyl chain were substituted by ethylene oxide (EO) units, which ought to substantially promote chain flexibility. For this purpose, 2,5,8,11-tetraoxatridecan-13-oate (TOTO) was chosen as anion (see Fig. I.7), as it has proven to form room-temperature ionic liquids (RTILs) even with small cations such as lithium and sodium.<sup>70</sup>

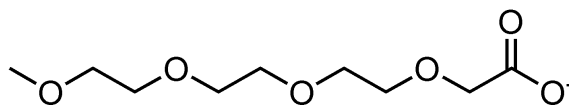


**Fig. I.7** 2,5,8,11-Tetraoxatridecan-13-oate – the TOTO anion.

Though representing a novel class of ionic liquids, these alkali TOTO ILs are restricted in their potential as solvents in practical applications due to their enormous viscosity ( $\eta_{25^\circ\text{C}}$  (Na-TOTO) = 164 000 mPas  $\leftrightarrow$   $\eta_{25^\circ\text{C}}$  (H<sub>2</sub>O) = 1 mPas!) and their relatively low conductivity ( $\kappa_{25^\circ\text{C}}$  (Na-TOTO) = 0.5  $\mu\text{S cm}^{-1}$ ).<sup>70</sup> Dielectric relaxation measurements and solvent polarity investigations revealed that neat Na-TOTO adopts a cross-linked structure with strong  $\text{COO}^- \cdots \text{Na}^+$  interactions.<sup>71</sup> When assuming that strong ion association is responsible for the high viscosity and the low conductivity, these problems might be solved by applying cations that will interact only weakly with the oligoether carboxylate anion. With regard to Figs. I.4-I.6. and the predictions made by theories on specific ion effects, quaternary ammonium ions are obvious candidates for this task.

Therefore, TOTO salts of tetraalkylammonium (TAA) cations as well as of choline (Ch) have been synthesized and investigated in the framework of this thesis. In Chapter VIII, it will be demonstrated that the obtained salts are all liquid at room-temperature and undergo glass transitions at around  $-60^\circ\text{C}$ . As compared to the sodium salt of TOTO, viscosities were found to be drastically decreased and conductivities enhanced by orders of magnitude. To assess ion interactions in the as-prepared ILs, solvent polarities will be evaluated based on the determination of  $E_T^N$ -values<sup>72</sup> and Kamlet-Taft parameters at different temperatures. Corresponding results suggest that TAA-TOTO ILs are dipolar aprotic solvents, whereas Ch-TOTO can be considered as dipolar protic solvent – yet all being more polar than Na-TOTO. The collected data indicate that the strong interactions between “hard” alkali ions and the “hard”  $\text{COO}^-$  group are weakened considerably when using “soft” quaternary ammonium species as cations. This allows for tuning the physicochemical properties of oligoether carboxylates simply by applying different commercially available cations.

## I.10. References

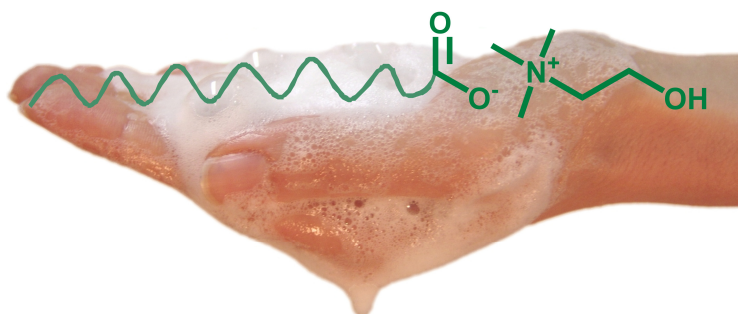
1. W. Kunz, M. Kellermeier, R. Klein, E. Maurer, D. Touraud, *Biologically Acceptable Choline Compounds and their Use as Tensides*, EP 2010-152626 (University of Regensburg, Germany), 2010.
2. W. Kunz, S. Thomaier, E. Maurer, O. Zech, M. Kellermeier, R. Klein, *Onium Salts of Carboxyalkyl-Terminated Polyoxyalkylenes for Use as High-Polar Solvents and Electrolytes*, WO 2008 135 482 (BASF SE, Germany), 2008.
3. B. Lindman, in *Handbook of Applied Surface and Colloid Chemistry*, Ed. K. Holmberg, John Wiley & Sons Ltd., Chichester 2002, pp. 421-443.
4. G. Gloxhuber, *Anionic Surfactants, Surf. Sci. Series*, Vol. 10, Marcel Dekker, New York/Basel, 1980.
5. A. Schmalstieg, G. W. Wasov, in *Handbook of Applied Surface and Colloid Chemistry*, Ed. K. Holmberg, John Wiley & Sons Ltd., 2002, pp. 271-293.
6. D. F. Evans, H. Wennerström, *The Colloidal Domain*, Wiley-VCH, New York, 1999.
7. J. W. McBain, W. W. Lee, *Oil Soap*, 1943, **20**, 17.
8. J. W. McBain, W. C. Sierichs, *J. Am. Oil Chem. Soc.*, 1948, **25**, 221.
9. H. Kunieda, K. Shinoda, *J. Phys. Chem.*, 1976, **80**, 2468.
10. K. Shinoda, M. Hato, T. Hayashi, *J. Phys. Chem.*, 1972, **76**, 909.
11. R. Zana, *Langmuir*, 2004, **20**, 5666.
12. R. Zana, J. Schmidt, Y. Talmon, *Langmuir*, 2005, **21**, 11628.
13. R. Moberg, F. Boekman, O. Bohman, H. O. G. Siegbahn, *J. Am. Chem. Soc.*, 1991, **113**, 3663.
14. E. Kutluay, B. Roux, L. Heginbotham, *Biophys. J.*, 2005, **88**, 1018.
15. M. E. O'Leary, R. Horn, *J. Gen. Physiol.*, 1994, **104**, 507.
16. M. E. O'Leary, R. G. Kallen, R. Horn, *J. Gen. Physiol.*, 1994, **104**, 523.
17. S. H. Zeisel, J. K. Blusztajn, *Annu. Rev. Nutr.*, 1994, **14**, 269.
18. J. K. Blusztajn, R. J. Wurtman, *Science*, 1983, **221**, 614.

19. J. K. Blusztajn, *Science*, 1998, **281**, 794.
20. R. Klein, *Synthesis and Characterisation of Novel Surfactants with Biologically Compatible Ions and Low Krafft Points*, Diploma Thesis, University of Regensburg, Regensburg, 2006.
21. R. S. Boethling, E. Sommer, D. DiFiore, *Chem. Rev.*, 2007, **107**, 2207.
22. G. J. Kortstee, *Arch. Mikrobiol.*, 1970, **71**, 235.
23. M. Petkovic, J. L. Ferguson, H. Q. N. Gunaratne, R. Ferreira, M. C. Leitao, K. R. Seddon, L. P. N. Rebelo, C. S. Pereira, *Green Chem.*, 2010, **12**, 643.
24. Clarification of Annex II, Entry 168 of the Cosmetic Directive: *Choline Salts and their Esters e.g. Choline Chloride* (INN), European Commission, SCCS/1237/09, 2009.
25. K. Chiba, I. Makino, J. Ohuchi, Y. Kasai, H. Kakishima, K. Tsukumo, T. Uchiyama, E. Miyai, J. Akiyama, Y. Okamoto, H. Kojima, H. Okumura, Y. Tsurumi, M. Usami, K. Katoh, S. Sugiura, A. Kurishita, M. Sunouchi, A. Miyajima, M. Hayashi, Y. Ohno, *Toxicol. in Vitro*, 1999, **13**, 189.
26. M. K. Robinson, R. Osborne, M. A. Perkins, *J. Pharmacol. Toxicol.*, 1999, **42**, 1.
27. M. A. Perkins, R. Osborne, F. R. Rana, A. Ghassemi, M. K. Robinson, *Toxicol. Sci.*, 1999, **48**, 218.
28. S. Stolte, J. Arning, U. Bottin-Weber, M. Matzke, F. Stock, K. Thiele, M. Uerdingen, U. Welz-Biermann, B. Jastorff, J. Ranke, *Green Chem.*, 2006, **8**, 621.
29. D. M. Small, *Handbook of Lipid Research 4: The Physical Chemistry of Lipids*, Plenum Press, New York, 1986, pp. 285-343.
30. S. Hassan, W. Rowe, G. J. T. Tiddy, in *Handbook of Applied Surface and Colloid Chemistry*, Ed. K. Holmberg, John Wiley & Sons Ltd., Chichester, 2002, pp. 465-508.
31. F. Reiss-Husson, V. Luzzati, *J. Colloid Interface Sci.*, 1966, **21**, 534.
32. R. M. Clapperton, R. H. Ottewill, A. R. Rennie, B. T. Ingram, *Colloid Polym. Sci.*, 1999, **277**, 15.
33. S. Karlsson, R. Friman, S. Backlund, R. Eriksson, *Tenside Surfact. Det.*, 2004, **41**, 72.

- 
34. M. Jansson, A. Joensson, P. Li, P. Stilbs, *Colloids Surf.*, 1991, **59**, 387.
  35. K. Fontell, *Colloid Polym. Sci.*, 1990, **268**, 264.
  36. G. Lindblom, L. Rilfors, *Biochim. Biophys. Acta, Rev. Biomembr.*, 1989, **988**, 221.
  37. K. Rendall, G. J. T. Tiddy, M. A. Trevethan, *J. Chem. Soc., Faraday Trans. 1*, 1983, **79**, 637.
  38. C. Madelmont, R. Perron, *Colloid Polym. Sci.*, 1976, **254**, 581.
  39. J. N. Israelachvili, D. J. Mitchell, B. W. Ninham, *J. Chem. Soc., Faraday Trans. 2*, 1976, **72**, 1525.
  40. D. J. Mitchell, B. W. Ninham, *J. Chem. Soc., Faraday Trans. 1*, 1981, **77**, 601.
  41. J. N. Israelachvili, *Intermolecular and Surface Forces*, Academic Press, London, 1992.
  42. W. Kunz, *Curr. Opin. Colloid Interface Sci.*, 2010, **15**, 34.
  43. T. Zemb, L. Belloni, M. Dubois, A. Aroti, E. Leontidis, *Curr. Opin. Colloid Interface Sci.*, 2004, **9**, 74.
  44. K. Binnemans, *Chem. Rev.*, 2005, **105**, 4148.
  45. B. Gallot, A. Skoulios, *Compt. Rend.*, 1965, **260**, 3033.
  46. B. Gallot, A. Skoulios, *Kolloid Z. Z. Polym.*, 1966, **210**, 143.
  47. A. Skoulios, V. Luzzati, *Nature*, 1959, **183**, 1310.
  48. R. D. Vold, *J. Am. Chem. Soc.*, 1941, **63**, 2915.
  49. P. Pacor, H. L. Spier, *J. Amer. Oil Chem. Soc.*, 1968, **45**, 338.
  50. S. Lewith, *Arch. Exp. Path. Pharm.*, 1887, **24**, 1.
  51. F. Hofmeister, *Arch. Exp. Path. Pharm.*, 1887, **24**, 247.
  52. F. Hofmeister, *Arch. Exp. Path. Pharm.*, 1888, **25**, 1.
  53. W. Kunz, *Specific Ion Effects*, World Scientific Publishing Co. Pte. Ltd, Singapore, 2010.
  54. K. D. Collins, G. W. Neilson, J. E. Enderby, *Biophys. Chem.*, 2007, **128**, 95.
  55. W. Kunz, J. Henle, B. W. Ninham, *Curr. Opin. Colloid Interface Sci.*, 2004, **9**, 19.

56. Y. Zhang, S. Cremer Paul, *Curr. Opin. Chem. Biol.*, 2006, **10**, 658.
57. K. D. Collins, *Methods*, 2004, **34**, 300.
58. K. D. Collins, *Biophys. Chem.*, 2006, **119**, 271.
59. N. Vlachy, B. Jagoda-Cwiklik, R. Vácha, D. Touraud, P. Jungwirth, W. Kunz, *Adv. Colloid Interface Sci.*, 2009, **146**, 42.
60. J. V. Joshi, V. K. Aswal, P. Bahadur, P. S. Goyal, *Curr. Sci.*, 2002, **83**, 47.
61. J. V. Joshi, V. K. Aswal, P. S. Goyal, *J. Phys. Condens. Matter*, 2007, **19**, 196219/1-196219/9.
62. M. J. Schwuger, *Kolloid-Z. Z. Polym.*, 1969, **233**, 979.
63. H. C. Evans, *J. Chem. Soc.*, 1956, 579.
64. H. Lange, M. J. Schwuger, *Kolloid-Z. Z. Polym.*, 1968, **223**, 145.
65. B. Jastorff, K. Moelter, P. Behrend, U. Bottin-Weber, J. Filser, A. Heimers, B. Ondruschka, J. Ranke, M. Schaefer, H. Schroeder, A. Stark, P. Stepnowski, F. Stock, R. Stoermann, S. Stolte, U. Welz-Biermann, S. Ziegert, J. Thoeming, *Green Chem.*, 2005, **7**, 362.
66. M. Matzke, S. Stolte, K. Thiele, T. Juffernholz, J. Arning, J. Ranke, U. Welz-Biermann, B. Jastorff, *Green Chem.*, 2007, **9**, 1198.
67. X. Wang, C. A. Ohlin, Q. Lu, Z. Fei, J. Hu, P. J. Dyson, *Green Chem.*, 2007, **9**, 1191.
68. I. Krossing, J. M. Slattery, C. Daguinet, P. J. Dyson, A. Oleinikova, H. Weingaertner, *J. Am. Chem. Soc.*, 2006, **128**, 13427.
69. T. L. Greaves, C. J. Drummond, *Chem. Soc. Rev.*, 2008, **37**, 1709.
70. O. Zech, M. Kellermeier, S. Thomaier, E. Maurer, R. Klein, C. Schreiner, W. Kunz, *Chem. Eur. J.*, 2009, **15**, 1341.
71. O. Zech, J. Hunger, J. R. Sangoro, C. Iacob, F. Kremer, W. Kunz, R. Buchner, *Phys. Chem. Chem. Phys.*, 2010, **12**, 14341.
72. C. Reichardt, *Pure Appl. Chem.*, 2008, **80**, 1415.

## Chapter II Choline Carboxylate Surfactants: Biocompatible and Highly Soluble in Water



With choline as a beneficial counterion of biological origin, long-chain carboxylates become water-soluble at room temperature.

## II.1. Introduction

Soaps are known for over 2000 years. The oldest and most common surfactants are sodium or potassium carboxylates due to their simple preparation by neutralization of the fatty acids with the respective hydroxides.<sup>1</sup> None the less, these surfactants are restricted in their applicability by their limited solubility in water. The criterion for a surfactant's solubility is its Krafft point or Krafft temperature. It is the temperature at which the solubility of a surfactant equals the critical micellization concentration (*cmc*) and raises sharply.<sup>2</sup> Furthermore, it is commonly accepted to define the Krafft point of an ionic amphiphile as the clearing temperature of a 1 wt% surfactant solution, since the *cmc* is generally far below 1 wt%.<sup>2</sup>

While the Krafft point is still about 25°C in the case of sodium laurate (NaC12), it is already about 45°C for sodium myristate (NaC14) or even about 60°C for sodium palmitate (NaC16).<sup>3-5</sup> In the same manner as the Krafft point rises systematically with growing length of the hydrophobic chain, the surface activity of an amphiphile, its washing ability and its solubilising power increase.<sup>6</sup> Already in 1972, Shinoda *et al.* pointed out that the type of the counterion markedly affects the Krafft point of a surfactant.<sup>7</sup> Accordingly, Yu *et al.* found in 1990 that a substitution of sodium in alkyl sulfates by tetrabutylammonium (TBA) considerably reduces the Krafft point, e.g. from 50°C to below 23°C in the case of octadecyl sulfate.<sup>8</sup> Furthermore, Jansson *et al.* showed that replacing sodium in NaC12 by tetraalkylammonium (TAA) ions can lower the Krafft temperature ( $T_{Kr}$ ) under 0°C.<sup>9</sup> This general behavior was confirmed by Zana *et al.*, who found, for example, that TBA stearate (C18) is soluble down to 0°C, while sodium stearate (NaC18) has a Krafft point of 71°C.<sup>5,10</sup>

Obviously, substitution of the alkali counterions in soaps by quaternary ammonium ions results in a significantly increased solubility. However, this substitution simultaneously renders the systems toxicologically questionable, since simple TAA ions are potentially harmful. For instance, TAA cations act as phase transfer catalysts and as such they can transport ions across biological membranes.<sup>11,12</sup> Additionally, they can block cellular ion channels even at very low concentrations (500µM of TBA induce a blocking of the cardiac sodium channel), whereby the blocking efficiency increases with the length of the alkyl side chains.<sup>13-16</sup>

A way to benefit from the tendency of quaternary ammonium ions as counterions to reduce the Krafft points of soaps and to avoid their toxicological influence at the same time is to use a quaternary ammonium ion of biological origin, such as choline. Choline chemically refers to the cation (2-hydroxyethyl)trimethylammonium (see Fig. II.1).

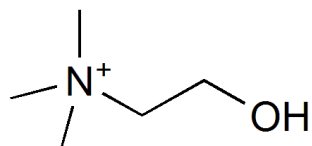


**Fig. II.1** Molecular structure of the choline cation.

Choline, formerly known as vitamin B<sub>4</sub>, is present in most foods.<sup>17,18</sup> In 1998, it was classified as an essential nutrient for humans.<sup>19</sup> Choline is essential for several biological functions of the human body. For instance, it serves as a precursor for phospholipids, the constituents of biological membranes.<sup>17</sup> Furthermore, it is a precursor for the neurotransmitter acetylcholine.<sup>20</sup> Moreover, its derivative betaine provides a source of methyl groups for protein synthesis and transmethylation reactions.<sup>21</sup>

Apparently, the hydroxy group of choline ensures, in contrast to the simple TAA ions, the physiological degradability. Accordingly it was found for example that for rat glioma cells choline chloride is the least toxic amine, 5.5 times less toxic than tetramethylammonium (TMA) chloride and even more than 500 hundred times less toxic than TBA chloride.<sup>22</sup> Due to the hydroxy group, choline can for instance be esterified to give acetylcholine and phosphatidylcholine. Furthermore, choline can also be environmentally decomposed by microorganisms.<sup>23</sup>

Choline carboxylates have already been described in the literature as ingredients of certain formulations, comprising for example cosmetic products or cryoprotectant agents for plants.<sup>24,25</sup> However, there is no physicochemical characterization of these species published to date. In this chapter, the Krafft points and the critical micellar concentrations of choline salts of fatty acids, ranging from dodecanoic acid (C12) to octadecanoic acid (C18), are presented. Furthermore, the obtained values are related to the *cmc*'s and Krafft points of the corresponding sodium, potassium and TMA carboxylates. The whole phase diagrams of these choline surfactants, established by various methods, will be outlined in Chapters IV and V.

## II.2. Results and Discussion

### II.2.1. Critical Micellization Concentration (*cmc*)

In Table II.1, the values of the *cmc*'s for the investigated choline surfactants are compared with those of the related sodium and potassium carboxylates. Apparently, the *cmc*'s of choline carboxylates are in the same order of magnitude as those of the alkali soaps. Moreover, the *cmc* of ChC12 coincides nearly exactly with that of TMAC12 (*cmc* = 25 mM)<sup>9</sup>, indicating that the hydroxy group of choline does not influence noticeably the micelle formation.

**Table II.1** Comparison of the *cmc*'s [mM] of choline, sodium and potassium carboxylates at 25°C.

	Choline	Sodium	Potassium
C12	25.5	24.4 <sup>26</sup>	25.5 <sup>27</sup>
C14	6.4	6.9 <sup>26</sup>	6.6 <sup>27</sup>
C16	1.8		

Furthermore, the *cmc* of ChC*m* salts decreases linearly by a factor of 4 per addition of two CH<sub>2</sub> groups. This feature, typical for ionic amphiphiles, can be illustrated by Equation (II.1), where the logarithm of the *cmc* is a linear function of the alkyl chain length  $n_C$ .<sup>28</sup>

$$\log cmc = A n_C + B \quad (\text{II.1})$$

For mono-ionic surfactants, the constant *A* typically adopts the value 0.3<sup>29</sup>, which is in good agreement with that found for the investigated surfactants (0.29). The parameter *B* (1.9) is a constant for a particular ionic head at a given temperature and corresponds well to that found in the literature for potassium carboxylates (1.9).<sup>29</sup>

From the values of the *cmc*'s, it can be deduced that choline carboxylates at low concentrations generally act in the same manner as the alkali carboxylates in aqueous solutions. Since, for instance, the sodium salts are completely dissociated in dilute solution<sup>26</sup>, the choline salts can also be assumed to reveal no association of the carboxylic headgroup with the counterion choline. In contrast, the TAA salts of sulfates

exhibit a pre-*cmc* ion-pairing.<sup>30</sup> Accordingly, the *cmc* values of TAA sulfates (e.g. *cmc* (TMA dodecyl sulfate) = 5.53 mM) are reduced in comparison to the corresponding alkali sulfates (e.g. *cmc* (Na dodecyl sulfate) = 8.32 mM).<sup>30</sup>

Nonetheless, the most outstanding property of these choline salts is the fact that they are capable of forming micelles at room temperature even with palmitic acid (C16) – in contrast to the homologous alkali soaps, which are restricted in their solubility. As a consequence of the potential use of longer-chain surfactants, a relatively high surface tension reduction down to about 25 mN m<sup>-1</sup> for ChC16 can be obtained.<sup>31</sup>

## II.2.2. Krafft Point

The Krafft point of a surfactant is the result of the interplay between two competing thermodynamic forces. One is the free energy of the solid crystalline state and the other is the free energy of the micellar solution. A strong head group interaction and a good packing in a crystal lattice contribute to the crystal's stability, which is associated with a low free energy. Consequently, the Krafft point is elevated. In turn, a low free energy of the micellar solution, promoted by e.g. the hydrophilicity of a compound, favours the solubilised state. However, the energetic state of the micellar solution varies only slightly when changing for instance the counterion, whereas the free energy of the crystalline state may change considerably from system to system.<sup>32</sup> Hence, the latter contribution can be considered as the main driving force in determining the solubilisation temperature.

In Fig. II.2, the Krafft temperatures for ChC*m*, TMAC*m*, KC*m* and NaC*m* with *m* = 12-18 are shown. The values, which we determined for the potassium carboxylates are generally in good agreement with those found by McBain *et al.*<sup>33</sup> and are in all cases 14-15°C lower than those of the corresponding sodium salts. Concerning the TMA carboxylates, only one value of  $T_{Kr}$  has been reported so far to our knowledge, namely for TMAC12 (< 0°C) by Jansson *et al.*<sup>9</sup> For the other TMA carboxylates we found the same Krafft temperatures as for the choline carboxylates within the experimental error of about 1-2°C. Nevertheless, as can be seen from Fig. II.2, the Krafft points of ChC*m* are substantially lower than those of the corresponding alkali salts. For example,  $T_{Kr}$  of ChC18 takes the value of 40°C, while  $T_{Kr}$  of NaC18 is 71°C<sup>4</sup> and 57°C for KC18. For palmitic acid, a reduction from 60°C in the case of sodium and from 46°C in the case of potassium down to 12°C can be obtained via replacing the alkali ions by choline.<sup>5</sup>

Furthermore, the Krafft temperature of NaC14 and KC14 can be dropped from 45°C and 30°C, respectively, to 0-1°C with choline as counterion.<sup>5</sup> ChC12 is even soluble far below 0°C ( $T_{Kr}(\text{NaC12}) = 25^\circ\text{C}$ ,  $T_{Kr}(\text{KC12}) = 10^\circ\text{C}$ ).<sup>4</sup>

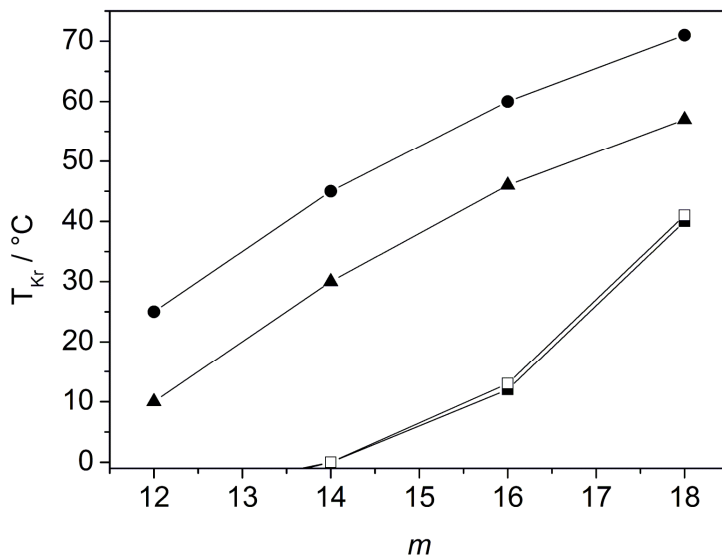


**Fig. II.2** Comparison of the Krafft temperatures  $T_{Kr}$  ( $^\circ\text{C}$ ) of (■) ChCm, (□) TMACm, (▲) KCm and (●) NaCm surfactants with increasing number of carbon atoms  $m$  (values of NaCm with  $m = 12$  taken from [3], with  $m = 14, 16, 18$  from [4]).

Obviously, the Krafft points of carboxylate surfactants decrease with increasing size of the counterion. This fact has already been reported for the homologous series of the alkali ions and can be continued by the implementation of TAA ions.<sup>33</sup> As pointed out above, the micellar state of the ChCm surfactants does not differ a lot from the NaCm and KCm soaps. Thus, the reason for the pronounced  $T_{Kr}$  reduction of choline carboxylates with respect to the alkali soaps must be a high free energy of the crystalline state of ChCm. Taking into account the almost equal  $T_{Kr}$  values of ChCm and TMACm, the alcohol group of choline seems to have no noticeable influence, similar as observed for the micellization process. Very probably, it is mainly the size of the bulky quaternary ammonium headgroup of choline, which hinders the regular packing in a crystal lattice, rendering the solid crystalline state energetically less favourable. Consequently, the Krafft point decreases.

## II.3. Conclusion

Choline carboxylate surfactants have been found to combine the characteristics of common alkali carboxylates in the low concentration regime with a substantially increased water solubility. Accordingly, ChC $m$  surfactants can be used at ambient temperature up to  $m = 16$ . Additionally, the investigated choline salts are featured by a straightforward synthesis with no or few heat requirement. Moreover, choline can be decomposed both in the environment and in the human body. Consequently, choline soaps, consisting exclusively of biogenic material occurring in the human body, are physiologically and environmentally harmless and as such convenient for e.g. drug delivery systems.

## II.4. Experimental

### II.4.1. Soap Synthesis

Dodecanoic acid (Merck, p.a.), tetradecanoic acid (Sigma, puriss.), hexadecanoic acid (Sigma,  $\geq 99\%$ ) and octadecanoic acid (Fluka, puriss.) were used as received. Choline base (ChOH) was purchased from Fluka as methanolic solution (45 wt%, purum). Soaps were prepared by neutralization of the fatty acids with choline hydroxide in ethanol (Baker, p.a.). The resulting choline surfactants (ChC $m$ , with  $m = 12, 14, 16, 18$ ) were recrystallized twice from a 1:100 mixture of ethanol and diethylether (Acros Organics, p.a.). Drying for a minimum of two days yielded the choline carboxylates as shiny, white powders.

All choline salts were found to be highly hygroscopic. Therefore, surfactant solutions were prepared by weighing the appropriate amount of choline carboxylate in nitrogen atmosphere and adding Millipore water afterwards. After 12 hours of stirring at 25°C, the samples were flame-sealed for subsequent temperature studies.

The potassium and tetramethylammonium (TMA) carboxylate solutions, KC $m$  and TMAc $m$  with  $m = 12 - 18$ , were synthesized correspondingly by direct equimolar neutralization of the fatty acids with 1 N titer potassium hydroxide solution and 10 wt% tetramethylammonium hydroxide solution, respectively, both received from Merck. Samples were afterwards treated for the subsequent temperature analysis as described for the choline soaps.

All choline salts were analyzed using  $^1\text{H}$  NMR ( $\text{CDCl}_3$ ),  $^{13}\text{C}$  NMR ( $\text{CDCl}_3$ ) and ES-MS (electro-spray mass spectroscopy) ( $\text{H}_2\text{O}/\text{AcN}$ ):

**ChC12:**

$\delta_{\text{H}}$  (300 MHz;  $\text{CDCl}_3$ ) 0.85 (3 H, t,  $J_{1,2} = 6.31$  Hz,  $J_{2,3} = 7.14$  Hz, Me), 1.22 (16 H, s,  $\text{CH}_2$ ), 1.55 (2 H, quintet,  $J_{1,2} = 7.41$  Hz,  $J_{2,3} = 7.14$  Hz,  $\text{CH}_2$ ), 2.1 (2 H, t,  $J_{1,2} = 7.68$  Hz,  $J_{2,3} = 7.96$  Hz,  $\text{CH}_2$ ), 3.34 (9 H, m,  $\text{NMe}_3$ ), 3.7 (2 H, m,  $\text{NCH}_2$ ), 4.08 (2 H, s,  $\text{CH}_2\text{OH}$ ).

$\delta_{\text{C}}$  (300 MHz;  $\text{CDCl}_3$ ) 14.12, 22.68, 27.17, 29.36 -30.05, 31.91, 39.22, 54.63, 55.99, 68.64, 180.31.

$m/z$  104 ( $\text{M}^+$ , 100%), 148 (10), 207 ( $2\text{M}^+ - \text{H}^+$ , 25), 199 ( $\text{M}^-$ , 100), 502.5 ( $2\text{M}^- + \text{M}^+$ , 17).

**ChC14:**

$\delta_{\text{H}}$  (300 MHz;  $\text{CDCl}_3$ ) 0.86 (3 H, t,  $J_{1,2} = 6.31$  Hz,  $J_{2,3} = 7.14$  Hz, Me), 1.22 (20 H, s,  $\text{CH}_2$ ), 1.56 (2 H, quintet,  $J_{1,2} = 7.41$  Hz,  $J_{2,3} = 7.41$  Hz,  $\text{CH}_2$ ), 2.1 (2 H, t,  $J_{1,2} = 7.41$  Hz,  $J_{2,3} = 7.96$  Hz,  $\text{CH}_2$ ), 3.35 (9 H, m,  $\text{NMe}_3$ ), 3.7 (2 H, m,  $\text{NCH}_2$ ), 4.09 (2 H, s,  $\text{CH}_2\text{OH}$ ).

$\delta_{\text{C}}$  (300 MHz;  $\text{CDCl}_3$ ) 14.12, 22.69, 27.18, 29.36 – 30.06, 31.92, 39.23, 54.66, 55.99, 68.66, 180.36.

$m/z$  104 ( $\text{M}^+$ , 100%), 148 (17), 227 ( $\text{M}^-$ , 100), 558.6 ( $2\text{M}^- + \text{M}^+$ , 3%).

**ChC16:**

$\delta_{\text{H}}$  (300 MHz;  $\text{CDCl}_3$ ) 0.86 (3 H, t,  $J_{1,2} = 6.31$  Hz,  $J_{2,3} = 7.14$  Hz, Me), 1.22 (24 H, s,  $\text{CH}_2$ ), 1.54 (2 H, quintet,  $J_{1,2} = 7.41$  Hz,  $J_{2,3} = 7.14$  Hz,  $\text{CH}_2$ ), 2.1 (2 H, t,  $J_{1,2} = 7.68$  Hz,  $J_{2,3} = 7.96$  Hz,  $\text{CH}_2$ ), 3.35 (9 H, m,  $\text{NMe}_3$ ), 3.7 (2 H, m,  $\text{NCH}_2$ ), 4.11 (2 H, s,  $\text{CH}_2\text{OH}$ ).

$\delta_{\text{C}}$  (300 MHz;  $\text{CDCl}_3$ ) 14.13, 22.69, 27.16, 29.36 – 30.05, 31.93, 39.18, 54.70, 56.04, 68.72, 180.38.

$m/z$  104 ( $\text{M}^+$ , 100%), 148 (43), 255 ( $\text{M}^-$ , 100), 512 ( $2\text{M}^- + \text{H}^+$ , 82), 615 ( $2\text{M}^- + \text{M}^+$ , 10).

**ChC18:**

$\delta_{\text{H}}$  (300 MHz;  $\text{CDCl}_3$ ) 0.86 (3 H, t,  $J_{1,2} = 6.59$  Hz,  $J_{2,3} = 6.86$  Hz, Me), 1.24 (28 H, s,  $\text{CH}_2$ ), 1.57 (2 H, quintet,  $J_{1,2} = 7.41$  Hz,  $J_{2,3} = 7.14$  Hz,  $\text{CH}_2$ ), 2.1 (2 H, t,  $J_{1,2} = 7.41$  Hz,  $J_{2,3} = 8.23$  Hz,  $\text{CH}_2$ ), 3.35 (9 H, m,  $\text{NMe}_3$ ), 3.7 (2 H, m,  $\text{NCH}_2$ ), 4.10 (2 H, s,  $\text{CH}_2\text{OH}$ ).

$\delta_{\text{C}}$  (300 MHz;  $\text{CDCl}_3$ ) 14.13, 22.69, 27.11, 29.36 – 30.04, 31.93, 39.07, 54.70, 56.02, 68.70, 180.32.

$m/z$  104 ( $\text{M}^+$ , 100%), 148 (28), 283 ( $\text{M}^+$ , 100), 568 ( $2\text{M}^+ + \text{H}^+$ , 14), 671 ( $2\text{M}^+ + \text{M}^+$ , 10).

## II.4.2. Methods

The Krafft temperature  $T_{Kr}$  was determined by direct visual observation, spotting the temperature at which a 1 wt% surfactant solution turned completely clear and isotropic.<sup>2</sup> For this purpose, samples of ChC12, ChC14 and ChC16, all of them being clear at ambient temperature, were cooled down slowly until turbidity was discernible. Thereby, ChC12 and samples remained clear and isotropic throughout the whole temperature range investigated (-3°C to 90°C). The Krafft temperatures of ChC14 and ChC16 were confirmed by reheating the samples with a rate of about 1°C per hour. ChC18 samples were turbid at room temperature, so  $T_{Kr}$  was measured by slow heating.

The TMA carboxylate solutions were analyzed in the same manner as the corresponding choline samples, the determined  $T_{Kr}$  values being approximately the same. Regarding the potassium soaps, only KC12 had to be cooled down from room temperature until precipitation occurred. All other  $\text{KC}_m$  samples were turbid at room temperature. The values of  $T_{Kr}$  for potassium carboxylates were determined as described above by heating the samples with about 1°C per hour until a completely clear and isotropic solution was obtained.

The critical micellization concentrations ( $cmc$ ) of the choline surfactants were determined by conductivity measurements.  $cmc$ 's can be obtained from the breakpoint in the plot of the conductivity versus the concentration. Experiments were conducted at 25°C using an autobalance conductivity bridge (Konduktometer 702, Knick) equipped with a Consort SK41T electrode cell. In order to obtain specific conductivities, the cell constant was determined by measuring known conductivities of 0.01 m, 0.1 m and 1 m potassium chloride solutions at 25°C.<sup>34</sup> The  $cmc$  values were determined to within  $\pm 4\%$ .

The values of the micelle ionization degree  $\alpha$  at the *cmc* were calculated from the obtained conductivity data using Equation (II.2) derived by Evans.<sup>35</sup>

$$1000S_2 = N^{2/3} \alpha^2 (1000S_1 - A_{Ch}) + \alpha A_{Ch} \quad (\text{II.2})$$

In Equation (II.2),  $S_1$  and  $S_2$  denote the slopes of the plot of the specific conductivity versus the concentration below and above the *cmc* (see Table II.2).  $A_{Ch}$  is the limiting equivalent conductivity of choline, which is 42.0 S cm<sup>2</sup> according to Fleming.<sup>36</sup>  $N$  terms the aggregation number at the *cmc* and was calculated according to Tanford,<sup>37</sup> assuming the maximal possible aggregation number of a spherical micelle with a fully extended hydrocarbon chain. However, the value of  $\alpha$  (estimated to within  $\pm 3\%$  and shown in Table 1) derived from equation 1 is not very sensitive to the value of  $N$ .

**Table II.2** Values of the Slopes of the Conductivity Plots versus the concentration before ( $S_1$ ) and after ( $S_2$ ) the *cmc* with the resulting  $\alpha$  values

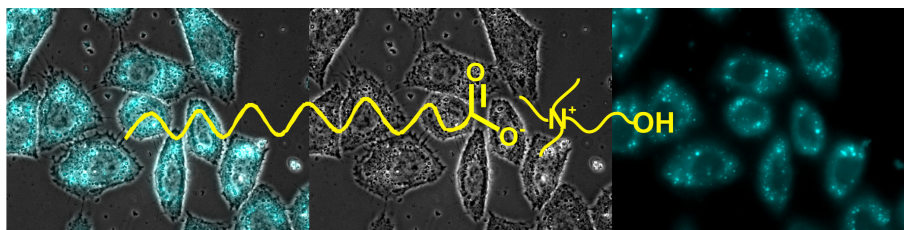
Surfactant	1000· $S_1$ (S cm <sup>2</sup> / mol)	1000· $S_2$ (S cm <sup>2</sup> / mol)	$\alpha$
ChC12	53.87	31.13	0.33
ChC14	58.52	31.68	0.28
ChC16	77.37	30.44	0.18

## II.5. References

73. A. Schmalstieg; G. W. Wasov, in *Handbook of Applied Surface and Colloid Chemistry*, ed. K Holmberg, John Wiley & Sons Ltd, Chichester, 2002, vol. 1, p 271.
74. R. G. Laughlin, *The Aqueous Phase Behavior of Surfactants*, Academic Press, San Diego, 1994, p 108.
75. J. W. McBain, W. W. Lee, *Oil and Soap*, 1943, **20**, 17.
76. C. Madelmont, R. Perron, *Colloid Polym. Sci.*, 1976, **254**, 581.
77. B. Lin, A. V. McCormick, H. T. Davis, R. Strey, *J. Colloid Interface Sci.*, 2005, **291**, 543.
78. W. C. Preston, *J. Phys. Chem.*, 1948, **52**, 84.
79. K. Shinoda, H. Kunieda, *J. Phys. Chem.*, 1976, **80**, 2468.
80. Z.-J. Yu, X. Zhang, G. Xu, *J. Phys. Chem.*, 1990, **94**, 3675.
81. M. Jansson, A. Jönsson, P. Li, P. Stilbs, *Colloids Surf.*, 1991, **59**, 387.
82. R. Zana, *Langmuir*, 2004, **20**, 5666.
83. R. Moberg, F. Bokman, O. Bohman, H. O. G. Siegbahn, *J. Am. Chem. Soc.*, 1991, **113**, 3663.
84. T. Hrobárik, L. Vrbka, P. Jungwirth, *Biophys. Chem.*, 2006, **124**, 238.
85. E. Kutluay, B. Roux, L. Heginbotham, *Biophys. J.*, 2005, **88**, 1018.
86. V. B. Luzhkov, J. Aqvist, *FEBS Letters*, 2001, **495**, 191.
87. M. E. O'Leary, R. G. Kallen, R. Horn, *J. Gen. Physiol.*, 1994, **104**, 523.
88. M. E. O'Leary, R. Horn, *J. Gen. Physiol.*, 1994, **104**, 507.
89. S. H. Zeisel, J. K. Blusztajn, *Annu. Rev. Nutr.*, 1994, **14**, 269.
90. J. C. Howe, J. R. Williams, J. M. Holden, *USDA Database for the Choline Content of Common Foods*, 2004.  
Available at: <http://www.nal.usda.gov/fnic/foodcomp/Data/Choline/Choline.html>

91. Food and Nutrition Board, *Dietary Reference Intakes for Thiamin, Riboflavin, Niacin, Vitamin B<sub>6</sub>, Folate, Vitamin B<sub>12</sub>, Pantothenic Acid, Biotin, and Choline*, National Academic Press, Washington DC, 1998.
92. J. K. Blusztajn, R. J. Wurtman, *Science*, 1983, **221**, 614.
93. J. K. Blusztajn, *Science*, 1998, **281**, 794.
94. L. C. Mokrasch, *Mol. Cell. Biochem.*, 1990, **92**, 85.
95. G. J. J. Kortstee, *Arch. Mikrobiol.*, 1970, **71**, 235.
96. *US Pat.*, 6 120 779, 2000.
97. *US Pat.*, 5 124 061, 1992.
98. A. N. Campbell, G. R. Lakshminarayanan, *Can. J. Chem.*, 1965, **43**, 1729.
99. H. B. Klevens, *J. Colloid Sci.*, 1947, **2**, 301.
100. H. B. Klevens, *J. Am. Oil Chem. Soc.*, 1953, **30**, 74.
101. M. J. Rosen, *Surfactants and Interfacial Phenomena*, John Wiley & Sons Ltd, USA, 2nd Edn., 1989, p 136.
102. P. Mukerjee, *Adv. Colloid Interface Sci.*, 1967, **1**, 241.
103. R. Klein, D. Touraud, W. Kunz, unpublished work.
104. B. Lindman, in *Handbook of Applied Surface and Colloid Chemistry*, ed. K. Holmberg, John Wiley & Sons Ltd, Chichester, 2002, p 428.
105. J. W. McBain, W. C. Sierichs, *J. Am. Oil Chem. Soc.*, 1948, **25**, 221.
106. R. Lide, *The CRC Handbook of Chemistry and Physics*, CRC Press, London/Boca Raton, 82nd Edn., 2001.
107. H. Evans, *J. Chem. Soc.*, 1956, 579.
108. R. Fleming, *J. Chem. Soc.*, 1960, 4914.
109. C. Tanford, *J. Phys. Chem.*, 1972, **76**, 3020.

## Chapter III Biodegradability and Cytotoxicity on Human Cell Lines of Choline Soaps



HeLa cells incubated with pyrene-substituted choline soaps

Using choline as counterion in fatty acid surfactants substantially increases their water solubility as compared to classical sodium and potassium soaps, and thereby enables the application of desirable longer-chain derivatives at ambient temperature. Since choline can be decomposed both, physiologically and environmentally, corresponding fatty acid soaps are considered to be highly biocompatible. Recent toxicity and biodegradability studies of choline ionic liquids, including anions such as short- and middle-chain alkanoates, have verified the expected low toxic impact. However, according to the European Cosmetic Directive 76/768/EEC, all salts of choline are forbidden in cosmetic products mainly just due to its classification as quaternary ammonium ion. In order to facilitate the application of promising choline salts in the future, the biodegradability of choline soaps (ChC $m$ ) with alkyl chain lengths of  $m=12-18$  according to the OCDE 301F standard has been investigated. Further, the cytotoxicity of ChC $m$  surfactants with  $m=8-16$  was determined, both for odd- and even-numbered fatty acids. Studies were carried out using two different human cell lines, namely cervix carcinoma cells (HeLa) and keratinocytes (SK-Mel-28). For a better comparability to common soaps and to shed light on the influence of the cation, sodium and potassium homologues were also investigated. Results reveal a non-linear relationship between the hydrophobic chain length and the IC $_{50}$  value. Most importantly, the presented data show that IC $_{50}$  values of ChC $m$  surfactants coincide with those of the widely applied sodium and potassium soaps and thus support their applicability.

### III.1. Introduction

The Krafft point of surfactants is one of the key factors for their application, since it defines the temperature above which micelles are formed and solubility is drastically enhanced, such that the surfactant can unfold its capabilities. In analogy to the reduced melting points of ionic liquids (salts with m.p. < 100°C), Krafft points of surfactants can be decreased by hindering a regular crystalline packing of the molecules. As shown in Chapter II, the use of the bulky choline cation as counterion in simple fatty acid soaps is very efficient to increase the water solubility of the corresponding surfactants as compared to the sodium and potassium homologues.<sup>1-3</sup> Choline soaps (ChC<sub>m</sub>) can be used up to a chain length of  $m=16$  at ambient temperature, whereas sodium palmitate (NaC<sub>16</sub>) is not soluble below 60°C.<sup>1,4</sup> Choline itself occurs in large amounts in plant, animal and human tissues and is biochemically well characterized.<sup>5-7</sup>

Earlier studies have proven that choline can be decomposed environmentally by certain microorganisms.<sup>8,9</sup> Consequently, choline soaps should be likewise environmentally and physiologically harmless, since they are made up of constituents occurring in considerable quantities in the primary metabolism of mammals. In addition, due to the low Krafft points, the synthesis of choline soaps via saponification of the fatty acids can be conducted at ambient temperature without further energy supply.<sup>1,2</sup> Choline salts such as the chloride are nowadays cost-efficient chemicals, produced on a scale of thousand tons per year. Therefore, choline alkanoates should not only be biocompatible but also bear economical advantages.

Very recently, choline has received much interest in the field of green ionic liquids.<sup>10-17</sup> The cytotoxicity of a family of choline phosphate ionic liquids has been measured for a J774 murine macrophage cell line, revealing that the toxicity essentially depends on the employed anion.<sup>18</sup> Petkovic *et al.* showed that choline salts of short- to middle-chain alkanoates, ranging from ethanoate to decanoate ( $m=2-10$ ), are also ionic liquids.<sup>19</sup> Furthermore, they investigated the toxicity using filamentous fungi as model organisms as well as the biodegradability by *Penicillium corylophilum*, and found that these choline ionic liquids were even less toxic than their sodium counterparts.<sup>19</sup> The capability of choline salts as promising green chemicals appropriate for many applications is not at least reflected by the declaration of several patents in the last two years.<sup>20-22</sup>

However, the European Cosmetic Directive 76/768/EEC (Anex II/ 168) still prohibits the use of choline salts in cosmetic products.<sup>23</sup> This is mainly due to the assignment of choline to the group of quaternary ammonium compounds (QAC), which are known to possess intrinsic irritation potential.

To check whether the *a priori* assumption of a high biocompatibility for choline soaps is valid and to support their use in daily products, the biodegradability of ChC $m$  salts for  $m=12-18$  has been investigated. Further, *in vitro* cytotoxicity analyses with two different human cell lines, namely on cervix carcinoma cells (HeLa) and on keratinocytes (SK-Mel-28), were performed. According to literature, HeLa tests on surfactants generally show good reproducibility and correlation with *in vivo* experiments. Therefore, they are widely accepted as reasonable alternative to the eye irritancy test on rabbits (Draize test).<sup>24-28</sup> A keratinocytic cell line was chosen in order to examine the skin irritancy power. For both cell lines, the influence of the alkyl chain length on the cytotoxicity of fatty acid salts with  $m=8-16$  has been examined. For the sake of a better comparability to previously reported values, the study was completed by measuring the IC<sub>50</sub> values of common sodium and potassium carboxylates in both cell lines under the same assay conditions. Complementarily, cellular fluorescence microscopy analyses were performed using pyrene-substituted C12 carboxylates of both sodium and choline in order to elucidate the mechanism underlying toxicity, that is, to ascertain whether the surfactants act only as unspecific destroyers of the outer cell membrane or if they can penetrate into the cell and affect more specifically cell functions.

It is worth mentioning that hitherto performed studies focused mainly on the cytotoxicity of even numbered soaps as these are most abundant in the natural fatty acid reservoir of mammalian cells. In the present work, also odd-numbered homologues were assessed this way to investigate if these compounds show outlining effects or follow the postulated general trend of increasing cytotoxicity with growing hydrophobic chain length according to structure activity relationships (SAR).<sup>29-31</sup>

## III.2. Results and Discussion

### III.2.1. Biodegradability

The biodegradability of surfactants is important since it expresses their ability to persist in the environment. According to REACH (Registration, Evaluation and Authorisation of Chemicals) legislation, all new chemicals have to pass ultimate biodegradation tests in order to be admitted to the market. Therefore, the biodegradability of choline soaps has been investigated ranging from laurate to stearate, using sodium acetate as standard.

Generally, with regard to the OCDE standard, organic molecules can be considered as biodegradable if 60% of the substance is decomposed within 10 days after the 10% level has been reached, and if globally at least 60% have been consumed after 28 days. Following the European standard CE2004/ 648, surfactants can already be classified as biodegradable if 60% degradation is achieved after 28 days.

Fig. III.1 shows the biodegradation profiles of ChC $m$  soaps with  $m=12-18$  (even numbered) as a function of time. It is obvious that all investigated compounds meet the latter criterion already before 10 days. Moreover, biodegradation is initiated immediately in all cases, indicating that no inhibition effect occurs in the biological medium due to potential toxicity of the choline derivatives.

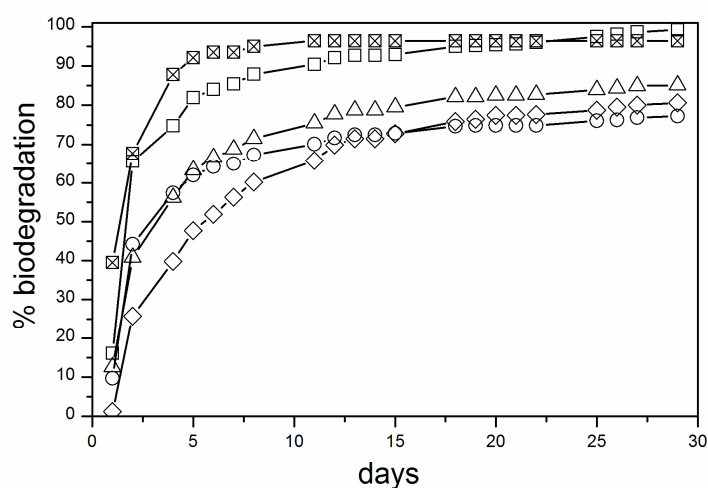


**Fig. III.1** Biodegradation of choline laurate (□), myristate (○), palmitate (Δ) and stearate (◇) as a function of time with sodium acetate (⊠) as standard.

In the OCDE guideline, it is recommended to test products at 100 mg L<sup>-1</sup>. If necessary, the concentration can be decreased afterwards. The presented results are expressed as an average value of tests carried out at 50 and 90 mg L<sup>-1</sup>. Differences between two concentrations of each compound were very small (less than 5%). This confirms a low toxic impact for the studied choline carboxylates. Concerning the influence of the chain length, varying final levels of biodegradability after 28 days were observed, ranging from about 100% for ChC12 over 85% for ChC16 to approximately 80% for ChC14 and ChC18. However, a simple relationship between biodegradability and hydrophobicity cannot be established since the C14 homologue breaks the general trend. Possible reasons for this finding may be related to parameters like Krafft point or unlike aggregation behavior. In fact, among all investigated soaps ChC18 is the only compound with a Krafft point beyond 20°C. At the moment, a reasonable explanation for the unusual ranking of ChC14 cannot be provided. Work addressing this question is underway. Nevertheless, when comparing for instance the level of biodegradation after 5 days of ChC12 (82%) and NaC12 (58%),<sup>32</sup> it is obvious that the choline salt clearly outrivals its sodium analogue.

Classical soaps have been extensively studied and are referred to as readily biodegradable, both under aerobic and anaerobic conditions.<sup>32-37</sup> However, they are susceptible to water hardness. Consequently, poorly water-soluble calcium and magnesium salts are formed, which are less biodegradable.<sup>33,37</sup> Despite their enhanced water solubility relative to the alkali homologues, choline soaps are also very sensitive to the presence of divalent ions and are thus expected to behave similarly.<sup>2</sup> Apart from that, the choline ion itself should not have any additional harmful impact on the environment, since it can be decomposed by microorganisms and no accumulation in soil has been observed.<sup>8,9</sup>

In summary, all studied choline soaps can be regarded as readily biodegradable as they all pass the 10 day window criterion on the one hand, and up to 70% are degraded within 13 days on the other. This agrees well with reports of other groups on choline salts such as short- and middle-chain alkanooates or naphthenic acid derivatives.<sup>15,19</sup>

### III.2.2. Cytotoxicity

A sufficient water solubility of the surfactants is necessary to obtain reliable *in vitro* toxicity results.<sup>38-40</sup> The Krafft temperatures of surfactants are well known to increase towards longer alkyl chain lengths.<sup>41</sup> Thus, with regard to the Krafft points of the investigated soaps which decrease with growing cation size,<sup>1,4,42</sup> the maximum length of the alkyl chain was limited in this study to  $m=12$  for sodium,  $m=13$  for potassium and  $m=16$  for choline. The cytotoxicity (expressed as  $IC_{50}$  values) of choline, sodium and potassium carboxylates in HeLa and SK-Mel-28 cell lines is depicted in Fig. III.2 and Fig. III.3, respectively.

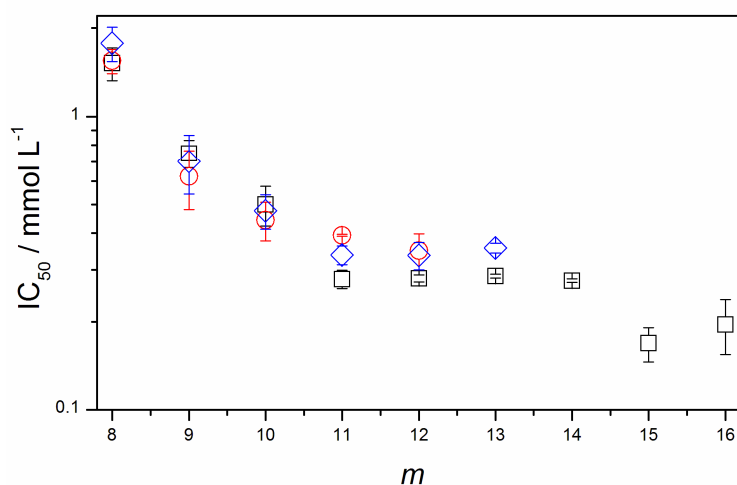


**Fig. III.2**  $IC_{50}$  values of choline ( $\square$ ), sodium ( $\circ$ ) and potassium ( $\diamond$ ) carboxylates obtained on HeLa cells as a function of alkyl chain length  $m$ .

For both cell lines, the cytotoxicity of  $ChCm$  surfactants equals more or less those of sodium or potassium soaps and is, except for  $m=15$  and  $m=16$ , in or near the millimolar range. Thus, it is evident that choline soaps possess low cytotoxicity under the chosen conditions.

In contrast to previous studies, any cation specificity could not be verified. Cytotoxicity tests on anionic surfactants with carboxylate headgroups and varying counterions, including alkali as well as quaternary ammonium ions, pointed out that the toxicity is lower for bigger cations than for small alkali ions.<sup>43,44</sup> Results were interpreted in terms of ion-pair formation. Small alkali ions are known to bind more strongly to the carboxylic headgroup than polarisable large ions. The formation of ion pairs has likewise been found to increase the toxicity of imidazolium and pyridinium ionic

liquids.<sup>31,45</sup> Also, Petkovic *et al.* detected a slightly lower toxic impact for choline ionic liquids than for their sodium counterparts.<sup>19</sup>

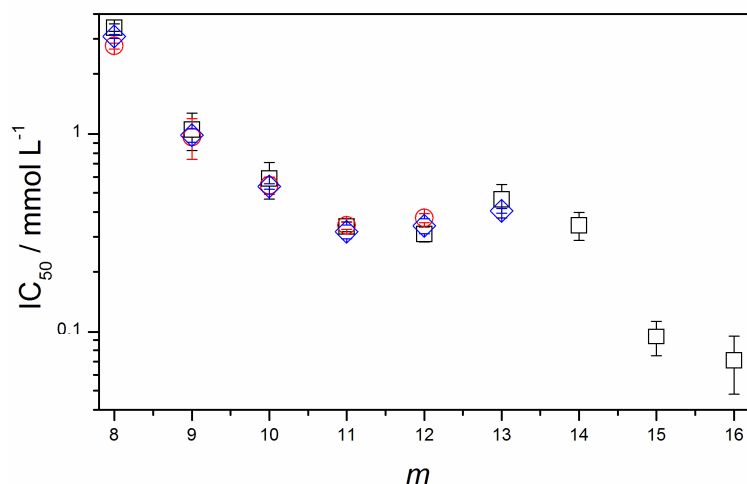


**Fig. III.3** IC<sub>50</sub> values of choline (□), sodium (○) and potassium (◇) carboxylates obtained on SK-Mel-28 cells as a function of alkyl chain length  $m$ .

In view of the cell medium used in this study, which contains diverse salts such as NaCl or CaCl<sub>2</sub>, specific ion effects may not become obvious. The non-specificity of our results with regard to the cations are generally reasonable since sodium, potassium and also choline were shown to exert no intrinsic toxic effect at least at the concerned level of concentration.<sup>19</sup> Thus, the toxicity of the investigated soaps mainly results from the anions.

According to the SAR (structure-activity relationship) concept,<sup>46</sup> the cytotoxicity is expected to scale in a linear fashion with the hydrophobicity.<sup>46-49</sup> This trend was observed for many ionic liquids, mainly for chain lengths of up to  $m=10-12$ .<sup>47,49</sup> The hydrophobicity is usually expressed by the octanol-water coefficient (P) or, for surfactants, alternatively by the critical micellization concentration (*cmc*). Since the *cmc* of surfactants decreases linearly with growing alkyl chain length,<sup>41</sup> plots of the IC<sub>50</sub> values versus  $m$  should basically give same curve progressions.

However, detailed evaluations of the cytotoxicity of odd- and even-numbered choline soaps with  $m=8-16$  demonstrate that, for both cell lines, the linear trend reported in literature is not fully valid (cf. Fig. III.2 and Fig. III.3). Data analysis using the ANOVA routine clearly reveals that the values obtained for  $m=11-14$  show no statistically significant differences among each other. Consequently, instead of a linear trend we observe a plateau between  $m=11-14$ . In turn, values of  $m \leq 11$  fairly well describe a

linear relationship. Equation (III.1), for instance, fits well the experimental results of choline soaps in HeLa cells up to  $m=11$  ( $R=0.995$ ).

$$\log IC_{50} (\text{mmol L}^{-1}) = 2.1_{\pm 0.2} - 0.24_{\pm 0.02} m \quad (\text{III.1})$$

One may assume that odd-numbered carboxylates deviate from the linear trend due to the fact that they are not common in the biosynthesis of fatty acids and are hence not as important for biological functions as their even-numbered counterparts. Likewise, the frequently observed zig-zag behavior of odd- and even-numbered fatty acids concerning their physico-chemical properties such as melting or Krafft temperatures cannot explain the traced progression of the  $IC_{50}$  values with the alkyl chain length.<sup>50</sup>

In fact, such a plateau has not been reported to date to the best of our knowledge. Former studies on soaps or anionic surfactants in general – which were unfortunately performed only on even-numbered paraffinic chains – identified a maximum cytotoxicity for  $m=12-14$ .<sup>39,51-56</sup> This is often referred to as cut-off effect in the literature.<sup>57</sup> Several arguments were put forward to explain this phenomenon, such as insufficient water solubility (i.e. the nominal concentration deviates from real test concentration)<sup>40</sup> or kinetic aspects (uptake is slowed down due to steric effects in the case of higher molecular weight compounds).<sup>57</sup> For surfactants, the found greatest irritant and toxic power of intermediate chain lengths was further ascribed to two contributing factors.<sup>33,51</sup> On the one hand, the *cmc* and therefore also the limiting concentration of available monomers decrease with growing alkyl chain length. On the other, the oil-water partition coefficients and thus the hydrophobicity increase.

In the present study, the argument of insufficient water solubility can be ruled out as an explanation for the observed trends, since only surfactants with Krafft points at ambient temperatures or below have been investigated. Indeed, limited water solubility accounts for the maximum toxic impact of sodium soaps with  $m=12$  reported in literature, given that longer-chain derivatives with sodium as counterion are not soluble in water below 40°C and  $m=11$  has not been investigated.<sup>42</sup> By contrast, the enhanced water solubility of choline soaps enabled the study also of longer alkyl chains. Thereby, the detected  $IC_{50}$  values of choline surfactants render a simple cut-off effect unlikely since, after passing through the plateau, the toxicity increases further with the hydrocarbon chain length.

Also, the formation of micelles should not affect the present  $IC_{50}$  values, as the starting concentrations of all studied compounds were lower than the respective  $cmc$ 's.<sup>1,58</sup> Although the  $cmc$  has not been determined for all of the investigated  $m$  values, the fact that it varies linearly with the chain length allows for an interpolation of the missing values. Further, it was suggested that the toxicity of surfactants is mainly due to monomers and not aggregates.<sup>38,39,51</sup> QSAR (quantitative structure-activity relationship) studies of Roberts *et al.* disclosed that whether a compound is a surfactant or not is irrelevant to its toxicity.<sup>30</sup> Rather, the hydrophobicity is the major determining factor.

Commonly, anionic surfactants are believed to act as polar narcotics.<sup>29,30,59</sup> Roberts *et al.* distinguish between the mechanisms of general and polar narcotics, based on the way in which solutes can partition between water and membranes.<sup>30</sup> They proposed that general narcotics such as alcohols operate via a three-dimensional partition in the membrane, meaning, they are able to move in all directions inside the hydrocarbon interior of the bilayer. In turn, polar narcotics undergo two-dimensional partition, which means that the polar groups of the solute are bound to the phosphatidylcholine head groups at the membrane surface.<sup>30</sup> A closer look at the dose-response curves of choline alkanooates reveals differences in the progressions of the curves for different  $m$  values (see Appendix A.1-2 for further information). Cell viabilities observed in the presence of shorter-chain derivatives increase gradually towards dilution, whereas they rise suddenly between one of the concentration steps in the case of salts with longer alkyl chains. This may indicate that alkanooates up to  $m = 11$  act via a different mechanism than salts with  $m \geq 12$ . A possible scenario is that shorter-chain derivatives behave as general narcotics in the framework of a 3D partition as described by Roberts *et al.*,<sup>30</sup> whereas homologues with  $m \geq 12$  are more efficiently incorporated by the membrane and can thus be considered as a 2D partition solute.<sup>60</sup> Further experiments are necessarily required to sustain this hypothesis and to clarify the uncommon trends of  $IC_{50}$  values with varying alkyl chain length in these fatty acid systems.

### III.2.3. Monitoring of Cellular Uptake and Intracellular Distribution by Fluorescence Microscopy

In order to shed light on the cytotoxic activity of choline soaps as well as of soaps in general, HeLa cells were incubated with 1:2 molar mixtures of pyrene-substituted sodium and choline laurate and corresponding non-functionalized fatty acid salts at concentrations slightly below their respective  $IC_{50}$  values. The ways of the soaps in this cellular context was traced by microscopic imaging of pyrene fluorescence over time. Exemplary series of micrographs are shown in Fig. III.4. The full set of images, recorded in intervals of 10 min up to 60 min, is given for both investigated systems in Appendix A.3.

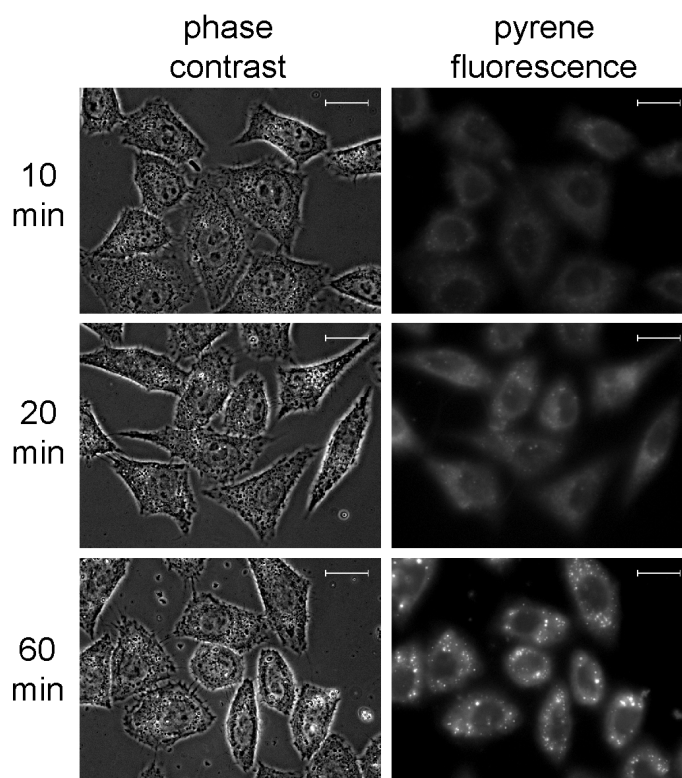


**Fig. III.4** Phase contrast and fluorescence images of HeLa cells incubated with a mixture of ChPC12/ChC12 (molar ratio of 1 : 2), acquired 10, 20 and 60 min after addition of the surfactants. Scale bars: 20  $\mu$ m.

The results obtained by cellular fluorescence microscopy demonstrate that the soaps are not only unspecific destroyers of the cell membrane. Following the fluorescence of pyrene, it can be observed that the surfactants are actually able to penetrate the membrane of the cells and to accumulate inside (cf. Fig. III.4). In this respect, no marked differences between choline and sodium salts could be detected, confirming the

similar  $IC_{50}$  values measured for the distinct cations. Cellular uptake occurred very rapidly. Already after 10 min of incubation, broad pyrene fluorescence was discernable throughout the entire cells. As expected for anionic surfactants, the cell nuclei remained unaffected during the examined time period. Pyrene fluorescence increased with time but showed some kind of saturation already after 30 min. Most notably, besides uniform intracellular fluorescence, there were also fluorescent aggregates inside the cells.

These aggregates likely represent so-called cytoplasmic lipid droplets (CLDs).<sup>61,62</sup> CLDs consist of a neutral lipid core with a surrounding phospholipid monolayer and exist in virtually every mammalian cell type. They form from the endoplasmic reticulum and grow in size by incorporating triacylglycerols.<sup>63</sup> The cellular pyrene fluorescence observed in the experiments (Fig. III.4) closely resembles the typical phenotype of CLDs.<sup>64</sup> As CLDs are known to be deposits for excess lipids and with regard to the neutral pH value of the buffered cell medium, the soaps might be taken up into the cell in the form of protonated fatty acids.<sup>65</sup> Further, an accumulation of pyrene fluorescence in the CLDs is very likely to occur. However, more data are required to understand the exact (co)localization and the fate as well as the composition of the molecules taken up by the cells.

### III.3. Conclusion

Biodegradability studies of choline soaps with chain lengths of  $m= 12-18$  have evidenced that all investigated compounds can be classified as readily biodegradable according to European norm.

Cytotoxicity tests on two human cell lines (HeLa and SK-Mel-28) were carried out for choline, sodium and potassium carboxylates as a function of the alkyl chain length, including odd- and even-numbered fatty acids. Thereby, the corresponding Krafft temperatures limited the length of the hydrocarbon chain useable to  $m= 12$  for sodium,  $m= 13$  for potassium and  $m= 16$  for choline. Both cell lines showed basically same tendencies with similar  $IC_{50}$  values. No cation selectivity could be observed. The  $IC_{50}$  values of choline carboxylates obtained for the different cell lines coincide almost exactly with those of the well-known and widely applied sodium and potassium homologues. Thus, it can be concluded that toxicity mainly originates from the anions.

Considering structure-activity-relationships with regard to variation of the alkyl chain length, the obtained results on odd- and even-numbered hydrocarbon chains indicate a

scheduled cytotoxicity for  $m \leq 11$ . But the simple linear trend of increasing toxicity with increasing hydrophobicity reported in literature was found to be not valid for the longer chain length derivatives. A simple cut-off effect cannot explain the observed progressions of  $IC_{50}$  values versus hydrophobic chain length, since after a plateau identified for  $m=11-14$ , cytotoxicity increases further towards longer alkyl chains. It is proposed that alkanoates up to  $m=11$  act via a different mechanism than salts with  $m \geq 12$ . Most probably, longer alkyl chain length derivatives are more effectively incorporated in the bilayer of the membranes.

Fluorescence microscopy studies on the uptake of pyrene-substituted choline and sodium dodecanoate in HeLa cells disclosed that the surfactants do not simply act as unspecific outer cell membrane destroyers. They actually penetrate relatively fast (within 10 min) inside the cell.

Taken together, the biodegradability and cytotoxicity investigations emphasize the capability of choline soaps of being promising green compounds for the future. Certainly, further investigations, such as measurements of aqua-toxicity, are needed to ascertain whether the simple classification of choline as quaternary ammonium ion justifies an interdiction as ingredient in cosmetic products.

## **III.4. Experimental**

### **III.4.1. Chemicals and Sample Preparation**

Choline dodecanoate (ChC12), tetradecanoate (ChC14), hexadecanoate (ChC16) and octadecanoate (ChC18) were synthesized and purified by twofold recrystallisation as described previously.<sup>1</sup> Sodium octanoate (Min. 99%), decanoate ( $\geq 98\%$ ) and dodecanoate (99-100%) were purchased from Sigma-Aldrich and used as received. The purified powdery choline soaps as well as the commercially available sodium salts served, amongst others, as reference substances in order to check if the neutralization procedure (as described below) is an appropriate method for the preparation of samples for cytotoxicity studies. In fact,  $IC_{50}$  values of assays performed with the above substances and those obtained by neutralization were found to deviate by less than 1-9%. Therefore, the simpler neutralization procedure was chosen to synthesize surfactants for the cytotoxicity measurements, and results were judged to be representative also for purified soaps. Thus, the desired compounds were obtained by

directly converting fatty acids with the corresponding hydroxides. Since carboxylic acids are weak acids and all applied hydroxides are strong bases, the neutralization reaction is expected to be quantitative. The following fatty acids were employed: octanoic acid (Min. 99%, Sigma), nonanoic acid (Min. 97%, Sigma-Aldrich), decanoic acid (99%, Alfa Aesar), undecanoic acid (99%, Aldrich), lauric acid ( $\geq 99\%$ , Merck), tridecanoic acid ( $\geq 98\%$ , Sigma) and pentadecanoic acid (99%, Aldrich). Sodium and potassium hydroxide were applied as titre solutions (0.1 N and 1 N (Merck)). Choline hydroxide was obtained from Taminco as a clear 46 wt% aqueous solution. In order to prevent decomposition of choline base, the stock solution was stored under nitrogen at  $-18^{\circ}\text{C}$  and protected against light. The exact concentration of choline base was determined by a threefold titration with 0.1 M HCl (Merck).

The as-obtained soaps were used as aqueous solutions at concentrations of 1 wt% for C11 and longer chain lengths, 2 wt% for C10, and 5 wt% for both C8 and C9. To allow for a better comparison and ensure uniform representation, Fig. III.2 and Fig. III.3 show data which were collected exclusively with surfactants prepared by direct neutralization.

For fluorescence microscopy, 1-pyrenedodecanoic acid ( $\geq 98\%$ , Sigma) was used as received and subsequently neutralized with either choline base or sodium hydroxide, yielding choline 1-pyrenedodecanoate (ChPC12) and sodium 1-pyrenedodecanoate (NaPC12), respectively. Pyrene-substituted choline and sodium laurate were not soluble below  $60\text{-}80^{\circ}\text{C}$ . Therefore, they were mixed in a 1:2 molar ratio with the corresponding non-functionalized fatty acid soaps, which led to clear solutions at ambient temperature.

### III.4.2. Biodegradability

Biodegradabilities of purified  $\text{ChC}_m$  salts with  $m = 12\text{-}18$  (even-numbered) were studied following the OCDE 301F norm, which requires the biological (BOC) and the theoretical (TOC) oxygen consumption. Sodium acetate was used as reference. With the known molecular structure, the TOC (in mg of oxygen per mg of product) can be calculated according to Equation (III.2). The TOC value reflects the amount of oxygen needed for complete oxidation of a compound.

$$TOC = 16 \times \frac{(2 \times C + 0.5 \times (H - Cl - 3 \times N) + 3 \times S + 2.5 \times P + 0.5 \times Na - O)}{PM} \quad (\text{III.2})$$

The BOC was determined by means of an IBUK respirometer, which detects the oxygen consumption during the degradation process. Experiments were conducted at 20°C over a period of 28 days in a medium containing diverse mineral substances (sodium and potassium phosphates, ammonium, calcium and iron chlorides, magnesium sulfate) and bacteria collected from a local wastewater treatment plant. Finally, biodegradability values are obtained as defined by Equation (III.3):

$$\% \text{ biodegradation} = \text{BOC} / \text{TOC} \times 100 \quad (\text{III.3})$$

Various concentrations of each compound were studied in order to check for a possible harmful effect on bacteria. Several parameters served as criteria for the reliability of the experiments:

- (1) The degradation of sodium acetate has to reach a level higher than 60% after 14 days. In our experiments, it was 96.4%.
- (2) The mineral medium has to exhibit oxygen consumption below 60 mg L<sup>-1</sup> after 28 days. In our case it was only 6 mg L<sup>-1</sup>.
- (3) After 28 days the pH has to be between 6 and 8.5, which proved true in each assay.

### III.4.3. Cytotoxicity Tests

Cytotoxicity tests were performed with the HeLa (cervix carcinoma, ATCC CCL17) and the SK-Mel-28 (keratinocytes, CLS 300337) cell line, using the MTT assay procedure introduced by Mosmann<sup>66</sup> and modified by Vlachy *et al.* in both cases.<sup>67</sup> The IC<sub>50</sub> value (in μmol mL<sup>-1</sup>) was calculated for each substance from a concentration-response curve, which was generated on the basis of 8 different concentrations (see ESI for details). The IC<sub>50</sub> value represents the concentration of test substance, which lowers MTT reduction by 50% relative to the untreated control. For a good comparison, IC<sub>50</sub> values were determined for all substances on the same day (in triplicate). Experiments were repeated three to five times (n= 4-6) over several weeks, and the average IC<sub>50</sub> value and its standard deviation (SD) are reported. The maximum (absolute) standard deviation observed was about 15%.

### III.4.4. Fluorescence Microscopy

HeLa cells were seeded in  $\mu$ -dishes (35 mm, Ibidi GmbH, Martinsried, Germany) at a density of  $1 \times 10^4$  cells per dish and cultured over night. For microscopy analyses, phenolred-free culture medium was used. Imaging was performed with a Carl Zeiss CellObserver system, comprising a computer-controlled inverted fluorescence microscope AxioObserver (Carl Zeiss, Jena, Germany) with AxioVision 4.7 software (Carl Zeiss ISG, Hallbergmoos, Germany) and an AxioCam HRm CCD-Camera at full resolution. Images were acquired with a 63x LCI Plan-Neofluar objective and a set of filters suitable for pyrene fluorescence (HC 340/26, Q380 LP, HQ 420/40).

In order to monitor the cellular uptake of the investigated soaps, mixtures of fluorescent ChPC12 and ChC12 or NaPC12 and NaC12 (both in 1:2 molar ratios) were added to the culture medium. The used concentrations and  $IC_{50}$  values were:

$$IC_{50} (\text{ChPC12} / \text{ChC12}) = (115 \pm 2) \mu\text{M}$$

$$c (\text{ChC12}/\text{ChPC12}) = 81 \mu\text{mol L}^{-1}$$

$$IC_{50} (\text{NaPC12} / \text{NaC12}) = (154 \pm 2) \mu\text{M}$$

$$c (\text{NaC12}/\text{NaPC12}) = 102 \mu\text{mol L}^{-1}$$

Phase contrast and pyrene fluorescence images were taken every 10 min from randomly selected cells.

### III.4.5. Statistics

Statistical differences and consistencies between the  $IC_{50}$  values of the cytotoxicity assay were determined by a oneway ANOVA test and a Posthoc Scheffé Procedure.

### III.5. References

1. R. Klein, D. Touraud, W. Kunz, *Green Chem.*, 2008, **10**, 433.
2. R. Klein, M. Kellermeier, M. Drechsler, D. Touraud, W. Kunz, *Colloids Surf. A*, 2009, **338**, 129.
3. R. Klein, G. J. T. Tiddy, E. Maurer, D. Touraud, J. Esquena, O. Tache, W. Kunz, *Aqueous Phase Behavior of Choline Carboxylate Surfactants - Exceptional Variety and Extent of Cubic Phases*, accepted by *Soft Matter*.
4. J. W. McBain, W. W. Lee, *Oil Soap*, 1943, **20**, 17.
5. J. K. Blusztajn, *Science*, 1998, **281**, 794.
6. J. K. Blusztajn, R. J. Wurtman, *Science*, 1983, **221**, 614.
7. S. H. Zeisel, J. K. Blusztajn, *Annu. Rev. Nutr.*, 1994, **14**, 269.
8. G. J. Kortstee, *Arch. Mikrobiol.*, 1970, **71**, 235.
9. R. S. Boethling, E. Sommer, D. DiFiore, *Chem. Rev.*, 2007, **107**, 2207.
10. D. Constantinescu, K. Schaber, F. Agel, M. H. Klingele and T. J. S. Schubert, *J. Chem. Eng. Data*, 2007, **52**, 1280-1285.
11. Y. Fukaya, Y. Iizuka, K. Sekikawa, H. Ohno, *Green Chem.*, 2007, **9**, 1155.
12. P. Nockemann, B. Thijs, K. Driesen, C. R. Janssen, K. Van Hecke, L. Van Meervelt, S. Kossmann, B. Kirchner, K. Binnemans, *J. Phys. Chem. B*, 2007, **111**, 5254.
13. J. Pernak, A. Syguda, I. Mirska, A. Pernak, J. Nawrot, A. Pradzynska, S. Griffin, R. Rogers, *Chem. Eur. J.*, 2007, **13**, 6817.
14. C. Van Doorslaer, J. Wahlen, P. Mertens, B. Thijs, P. Nockemann, K. Binnemans, D. De Vos, *Chem. Sus. Chem.*, 2008, **1**, 997.
15. Y. Yu, X. Lu, Q. Zhou, K. Dong, H. Yao, S. Zhang, *Chem. Eur. J.*, 2008, **14**, 11174.
16. R. Vijayaraghavan, B. C. Thompson, D. R. MacFarlane, R. Kumar, M. Surianarayanan, S. Aishwarya, P. K. Sehgal, *Chem. Commun.*, 2010, **46**, 294.

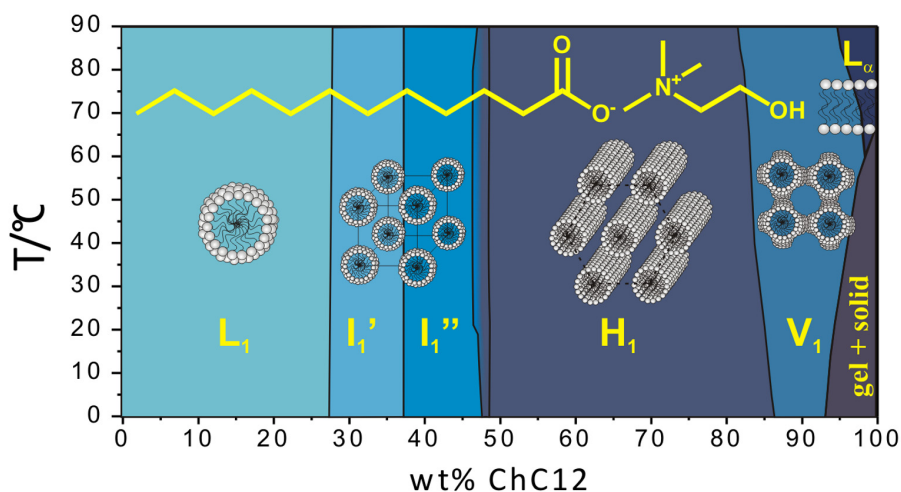
17. M. Petkovic, K. R. Seddon, L. P. N. Rebelo, C. Silva Pereira, *Chem. Soc. Rev.*, doi: 10.1039/C004968A.
18. K. D. Weaver, H. J. Kim, J. Sun, D. R. MacFarlane, G. D. Elliott, *Green Chem.*, 2010, **12**, 507.
19. M. Petkovic, J. L. Ferguson, H. Q. N. Gunaratne, R. Ferreira, M. C. Leitao, K. R. Seddon, L. P. N. Rebelo, C. S. Pereira, *Green Chem.*, 2010, **12**, 643.
20. W. Kunz, M. Kellermeier, R. Klein, E. Maurer, D. Touraud, EP 2010-152626, University of Regensburg, 2010.
21. K. Seddon, N. Gunaratne, M. Earle, M. Gilea, G. Stephens, E. Ivanova, L. Rehmman, E. Green, WO 2010 023490, Enviroways Technologies Limited, 2010.
22. R. D. Rogers, D. T. Daly, G. Gurau, D. MacFarlane, J. Turanjanin, P. M. Dean, J. L. Scott, K. Bica, K. R. Seddon, WO 2010 078300, University of Alabama, USA; Monash University; Queen's University Belfast, 2009.
23. Clarification of Annex II, Entry 168 of the Cosmetic Directive: *Choline Salts and their Esters e.g. Choline Chloride* (INN), European Commission, SCCS/1237/09, 2009.
24. H. Eagle, *J. Exp. Med.*, 1955, **102**, 595.
25. K. Chiba, I. Makino, J. Ohuchi, Y. Kasai, H. Kakishima, K. Tsukumo, T. Uchiyama, E. Miyai, J. Akiyama, Y. Okamoto, H. Kojima, H. Okumura, Y. Tsurumi, M. Usami, K. Katoh, S. Sugiura, A. Kurishita, M. Sunouchi, A. Miyajima, M. Hayashi, Y. Ohno, *Toxicol. in Vitro* 1999, **13**, 189.
26. W. Yang, D. Acosta, *Toxicol. Lett.* , 1994, **70**, 309.
27. M. K. Robinson, R. Osborne, M. A. Perkins, *J. Pharmacol. Toxicol.*, 1999, **42**, 1.
28. M. A. Perkins, R. Osborne, F. R. Rana, A. Ghassemi, M. K. Robinson, *Toxicol. Sci.*, 1999, **48**, 218.
29. D. W. Roberts, J. Costello, *QSAR Comb. Sci.*, 2003, **22**, 220.
30. D. W. Roberts, J. F. Costello, *QSAR Comb. Sci.*, 2003, **22**, 226.
31. S. Stolte, J. Arning, U. Bottin-Weber, M. Matzke, F. Stock, K. Thiele, M. Uerdingen, U. Welz-Biermann, B. Jastorff, J. Ranke, *Green Chem.*, 2006, **8**, 621.

32. R. D. Swisher, *Surfactant Biodegradation*, Surf. Sci. Series, Vol. 3, Marcel Dekker, New York, 1970.
33. M. J. Scott, M. N. Jones, *Biochim. Biophys. Acta, Biomembr.*, 2000, **1508**, 235.
34. P. Varo Galvan, D. Prats Rico, M. Rodriguez Pastor, *Tenside Surfact. Det.*, 2002, **39**, 160.
35. P. Varo Galvan, D. Prats Rico, M. Rodriguez Pastor, *Tenside Surfact. Det.*, 2005, **42**, 40.
36. A. Moreno, J. Bravo, J. Ferrer, C. Bengoechea, *Tenside Surfact. Det.*, 1996, **33**, 479.
37. D. Prats, M. Rodriguez, P. Varo, A. Moreno, J. Ferrer, J. L. Berna, *Water Research*, 1999, **33**, 105.
38. M. C. Scaife, *Int. J. Cosmet. Sci.*, 1982, **4**, 179.
39. H. Schott, *J. Pharm. Sci.*, 1973, **62**, 341.
40. H. Konemann, *Toxicology*, 1981, **19**, 209.
41. B. Lindman, in *Handbook of Applied Surface and Colloid Chemistry*, Ed. K. Holmberg, John Wiley & Sons Ltd., Chichester 2002, pp. 421-443.
42. J. W. McBain, W. C. Sierichs, *J. Am. Oil Chem. Soc.*, 1948, **25**, 221.
43. M. Maugras, M. R. Infante, C. Gerardin, C. Selve, M. P. Vinardell, *Comp. Biochem. Physiol., Part C: Toxicol. Pharmacol.*, 2001, **128C**, 541.
44. L. Sanchez, M. Mitjans, M. R. Infante, M. P. Vinardell, *Pharm. Res.*, 2004, **21**, 1637.
45. S. Stolte, M. Matzke, J. Arning, A. Bösch, W.-R. Pitner, U. Welz-Biermann, B. Jastorff, J. Ranke, *Green Chem.*, 2007, **9**, 1170.
46. B. Jastorff, R. Stoermann, J. Ranke, *Clean: Soil, Air, Water*, 2007, **35**, 399.
47. S. Stolte, J. Arning, U. Bottin-Weber, M. Matzke, F. Stock, K. Thiele, M. Uerdingen, U. Welz-Biermann, B. Jastorff, J. Ranke, *Green Chem.*, 2006, **8**, 621.
48. F. Stock, J. Hoffmann, J. Ranke, R. Stoermann, B. Ondruschka, B. Jastorff, *Green Chem.*, 2004, **6**, 286.

49. J. Ranke, K. Moelter, F. Stock, U. Bottin-Weber, J. Poczobutt, J. Hoffmann, B. Ondruschka, J. Filser, B. Jastorff, *Ecotoxicol. Environ. Saf.*, 2004, **58**, 396.
50. K. Ogino, Y. Ichikawa, *Bull. Chem. Soc. Jpn.*, 1976, **49**, 2683.
51. C. Prottey, T. F. Ferguson, *Food Cosmet. Toxicol.*, 1976, **14**, 425.
52. P. H. Dugard, R. J. Scheuplein, *J. Invest. Dermatol.*, 1973, **60**, 263.
53. I. H. Blank, E. Gould, *J. Invest. Dermatol.*, 1961, **37**, 485.
54. T. F. Ferguson, C. Prottey, *Food Cosmet. Toxicol.*, 1976, **14**, 431.
55. M. Kotani, Y. Masamoto, M. Watanabe, *Toxicol. in Vitro*, 1994, **8**, 229.
56. S. Onitsuka, Y. Kasai, K. Yoshimura, *Chemosphere*, 1989, **18**, 1621.
57. J. Luczak, C. Jungnickel, I. Lacka, S. Stolte, J. Hupka, *Green Chem.*, 2010, **12**, 593.
58. P. Mukerjee, K. J. Mysels, *Critical Micelle Concentrations of Aqueous Surfactant Systems*, NSRDS-NBS 36, 1971.
59. D. W. Roberts, *Sci. Total Environ.*, 1991, **109-110**, 301.
60. C. R. Birnie, D. Malamud, R. L. Schnaare, *Antimicrob. Agents Chemother.*, 2000, **44**, 2514.
61. M. Beller, K. Thiel, P. J. Thul, H. Jaeckle, *FEBS Lett.*, 2010, **584**, 2176.
62. T. Fujimoto, Y. Ohsaki, J. Cheng, M. Suzuki, Y. Shinohara, *Histochem. Cell Biol.*, 2008, **130**, 263.
63. J. Zanghellini, F. Wodlei, H. H. von Grunberg, *J. Theor. Biol.*, **264**, 952.
64. T. Fujimoto, Y. Ohsaki, *Ann. N. Y. Acad. Sci.*, 2006, **1086**, 104.
65. O. Morand, E. Fibach, N. Livni, S. Gatt, *Biochim. Biophys. Acta*, 1984, **793**, 95.
66. T. Mosmann, *J. Immunol. Methods*, 1983, **65**, 55.
67. N. Vlachy, D. Touraud, J. Heilmann, W. Kunz, *Colloids Surf. B*, 2009, **70**, 278.



## Chapter IV Aqueous Phase Behavior of Choline Carboxylate Surfactants



In this chapter, the aqueous binary phase diagrams and a detailed investigation of the lyotropic liquid crystalline phases formed by choline carboxylate surfactants (ChC $m$ ) with chain lengths ranging from  $m=12-18$  and at surfactant concentrations of up to 95-98 wt% are presented. The identification of the lyotropic mesophases and their sequence was achieved by the penetration scan technique. Structural details are elucidated by small-angle X-ray scattering (SAXS). The general sequence of mesophases with increasing soap concentration was found to be as follows: micellar ( $L_1$ ), discontinuous cubic ( $I_1$ ), hexagonal ( $H_1$ ), bicontinuous cubic ( $V_1$ ) and lamellar ( $L_\alpha$ ). The main difference to the phase behavior of alkali soaps or of other mono-anionic surfactants is the appearance and large extent of a discontinuous cubic phase with two or even more different symmetries. The obtained phase diagrams further highlight the extraordinarily high water solubility of ChC $m$  soaps. Finally, structural parameters of ChC $m$  salts such as the cross-sectional area at the polar-nonpolar interface are compared to those of alkali soaps and discussed in the terms of specific counterion binding and packing constraints.

## IV.1. Introduction

The substantial decrease in the Krafft point observed with choline as counterion was explained on the basis of two contributing factors, namely by the hindrance of a regular crystalline packing by the bulky choline ion, which is most probably the main driving force, and by a weak counterion to headgroup binding.<sup>1,2</sup> Regarding their self-assembly behavior, choline soaps were found to behave very akin to alkali soaps in the low concentration region with respect to critical micellization concentrations (*cmc*'s). In fact, measured *cmc* values coincided nearly exactly with those of the corresponding alkali salts.<sup>1</sup> These findings inevitably raise the question in which manner choline carboxylates self-assemble at higher concentrations. This is not only of fundamental interest but also important for industrial applications.<sup>3</sup>

The first binary aqueous phase diagrams of sodium and potassium soaps were established by McBain, Vold and coworkers.<sup>4-6</sup> Later, Madelmont and Perron refined those of sodium laurate (NaC12) and myristate (NaC14) by means of differential thermal analysis.<sup>7</sup> Luzzati, Spegt and Skoulios are just a few further names of authors who investigated in depth the aqueous phase behavior of alkali soaps and resolved the detailed structure of the mesophases by thorough X-ray studies.<sup>8-13</sup> The basic phase behavior is similar for all alkali carboxylate surfactants.<sup>14</sup> The characteristic sequence of mesophases occurring with increasing surfactant concentration is: micellar solution  $L_1$ , normal hexagonal  $H_1$ , bicontinuous cubic  $V_1$  (which may be accompanied or replaced by one or two intermediate phases), and lamellar  $L_\alpha$ . In aqueous micellar solutions, all soaps undergo a transition from spherical to rod-like micelles when their concentration is increased.<sup>15,16</sup> As a consequence, normal hexagonal  $H_1$  is the first liquid crystalline phase to be formed. This has been shown to apply also for carboxylate surfactants with big organic counterions like alkyl amines or quaternary ammonium ions.<sup>17,18</sup> In turn, discontinuous cubic phases ( $I_1$ ), which are typically located between  $L_1$  and  $H_1$  and consist of discrete, mostly spherical micelles arranged in a cubic lattice, have to our knowledge not been reported to date for any binary aqueous mono-anionic surfactant system.<sup>19,20</sup> Such phases are indeed known for divalent anionic,<sup>21</sup> zwitter-ionic,<sup>22</sup> non-ionic<sup>23,24</sup> and even mono-cationic surfactants with highly dissociated counterions (e.g. alkyltrimethylammonium chloride),<sup>22</sup> due to an increased effective area per headgroup  $a_o$ .

In this chapter, the influence of counterion binding on micellar shape and the formation of lyotropic liquid crystals is demonstrated for choline carboxylate systems. To that end, the binary aqueous phase diagrams of choline soaps (ChC $m$ ) are presented for chain lengths of  $m= 12-18$  and a temperature range of 0–90°C. The various mesophases and their sequence were identified first by the penetration scan technique using optical polarizing microscopy. Subsequently, the exact phase boundaries were determined visually between crossed polarizers. Finally, structural details of the lyotropic liquid crystalline phases were elucidated by small-angle X-ray scattering (SAXS) measurements performed for surfactant concentrations up to 95-98 wt%.

## IV.2. Results and Discussion

### IV.2.1. Penetration Scans

The penetration scan method, as described in detail by Lawrence,<sup>25</sup> is a straightforward technique to obtain information on the mesophases formed by a surfactant in water. Thereby, the various liquid crystals with their different characteristic textures are observed in the form of distinct rings along increasing surfactant concentration towards the center of the sample.

Fig. IV.1 shows a penetration scan image of ChC12 at 20°C. When passing to higher surfactant concentrations, the following sequence of mesophases can be identified: micellar ( $L_1$ ), discontinuous cubic ( $I_1'$  and  $I_1''$ ), hexagonal ( $H_1$ ), bicontinuous cubic ( $V_1$ ), and a partially birefringent solid region. A lamellar phase ( $L_\alpha$ ) could not be detected before 62°C. Generally, discontinuous cubic phases can be distinguished in a penetration scan by their high viscosity (obvious when slightly pushing the sample) as well as their isotropy and refractive index discontinuity. The penetration scan of ChC12 clearly indicates the presence of two different discontinuous cubic phases, labeled  $I_1'$  and  $I_1''$ , with almost equal extent. The  $H_1$  phase can be recognized by its characteristic optical texture,<sup>26</sup> while the bicontinuous cubic  $V_1$  phase is isotropic and highly viscous. The solid region was found to be partially birefringent and exhibits, in contrast to a lamellar phase, high viscosity. Therefore, it likely corresponds to a mixture of a gel ( $L_\beta$ ) and a solid phase, as observed previously for potassium and higher alkali soap derivatives.<sup>14, 27</sup> The phase behavior of the gel or coagel region can be rather complex since an equilibrium state is often difficult to attain.<sup>12, 28</sup> Thus, it will be focused in the following on the liquid crystalline phases.

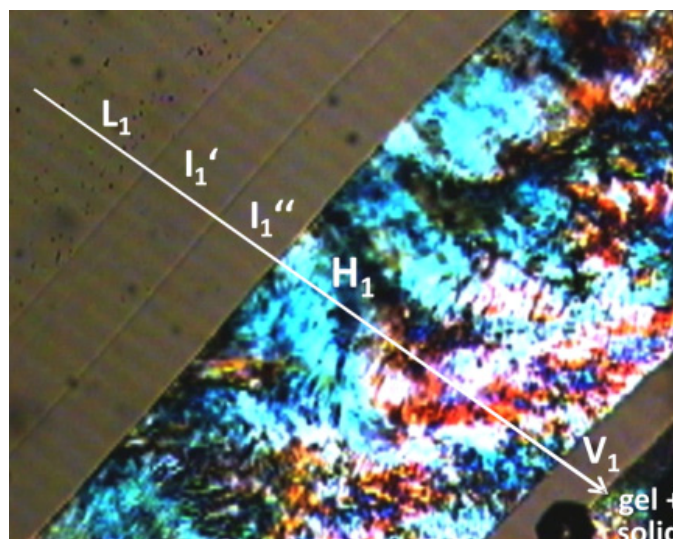


**Fig. IV.1** Penetration scan of ChC12 at 20°C acquired at 100x magnification between half-crossed polarizers, showing the following sequence of the formed mesophases:  $L_1$ ,  $I_1'$  and  $I_1''$ ,  $H_1$ ,  $V_1$  and a gel + solid region. The discontinuous cubic phases  $I_1'$  and  $I_1''$  can be identified by their isotropy, high viscosity and refractive index discontinuities (dark lines).

The general sequence of liquid crystals observed for ChC12 was confirmed also for the longer-chain choline carboxylates, including the existence of two  $I_1$  phases. Only ChC18 differs slightly from the other homologues as the  $I_1''$  phase disappears at around 55°C, while for  $m=12-16$  both cubic phases are present over the entire temperature range investigated.

Fig. IV.2 shows another example of a penetration scan, which illustrates the more concentrated surfactant region of ChC16 at 61°C. The phases occurring towards higher soap concentration are assigned to  $H_1$ ,  $V_1$ ,  $L_\alpha$  and  $L_\beta$ .

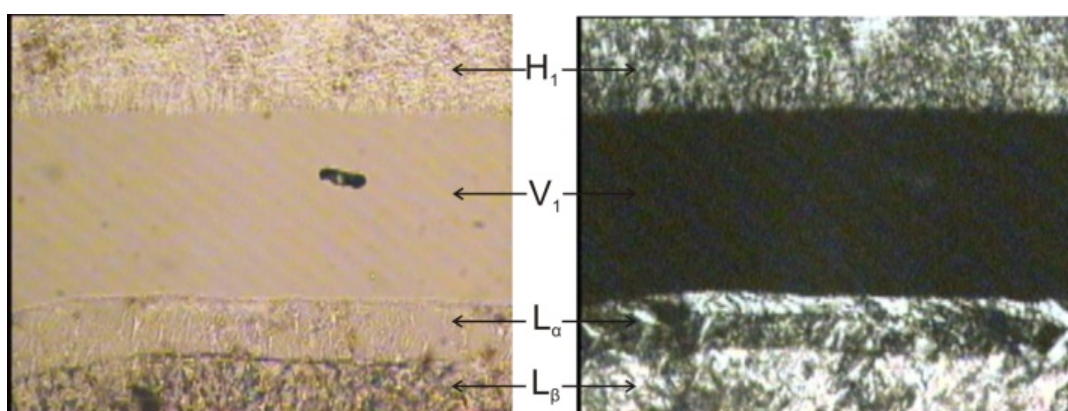


**Fig. IV.2** Penetration scan of ChC16 at 61°C with non-crossed (left) and crossed (right) polarizers at 100x magnification, visualizing the formed mesophases in the more concentrated surfactant region.

Further penetration scan images acquired for the different choline soaps at various temperatures can be found in Appendix B.2.

### IV.2.2. Binary Phase Diagrams

From the penetration scans, it can be deduced that the aqueous phase behavior of choline soaps is characterized by an alternating sequence of isotropic and anisotropic liquid crystals. Consequently, the exact phase boundaries can be identified by inspecting samples with distinct concentrations between crossed polarizers at varying temperature. In turn, the boundary between  $I_1'$  and  $I_1''$  must be estimated based on the penetration scans and SAXS data. The  $T_c$  line, i.e. the boundary between crystalline and “melted” paraffinic chains, was determined visually by detecting the temperature where the samples become transparent and was further confirmed by DSC measurements for selected samples (data not shown). Fig. IV.3 shows the resulting aqueous binary phase diagrams of ChC $m$  surfactants for  $m= 12-18$  and  $T= 0-90^\circ\text{C}$ . The accuracy of the phase boundaries is estimated to be within  $\pm 1$  wt% and  $\pm 1^\circ\text{C}$ . Higher temperatures have not been investigated due to the problem of thermal decomposition. Consisting of organic material only, choline soaps start to become dark when heated over  $90^\circ\text{C}$  for longer periods.

All phase transitions appear to be of first order, as a small two-phase region could be detected in each case, which is distinctly larger in-between  $I_1'' - H_1$  than for the other transitions. Nevertheless, the two-phase regions are in general relatively small and thus suggest high purity of the used surfactants. The Krafft boundary shifts as expected to higher temperatures with growing chain length. At around 95 wt% soap in water all choline surfactants show a pronounced increase in  $T_C$ . However, an unexpected feature concerning the Krafft boundary line is the increase of  $T_C$  at surfactant concentrations lower than 5-10 wt% in the phase diagrams of ChC16 and ChC18. Similar observations have been reported by McBain *et al.* for potassium soaps and were explained by the hydrolysis of the fatty acids, which is more prominent in dilute solutions.<sup>5</sup> Moreover, the degree of hydrolysis also depends strongly on the alkyl chain length. Kanicky *et al.* showed that the apparent  $pK_a$  value increases with the chain length from  $\sim 7.5$  for C12 to 10.15 for C18.<sup>29-31</sup> In this regard, the dilute region of ChC16 and ChC18 does not represent a true binary system. On the other hand, adding an extra amount of choline base to suppress fatty acid hydrolysis would likewise not result in a true binary system, since an excess of choline ions would be present in this case.

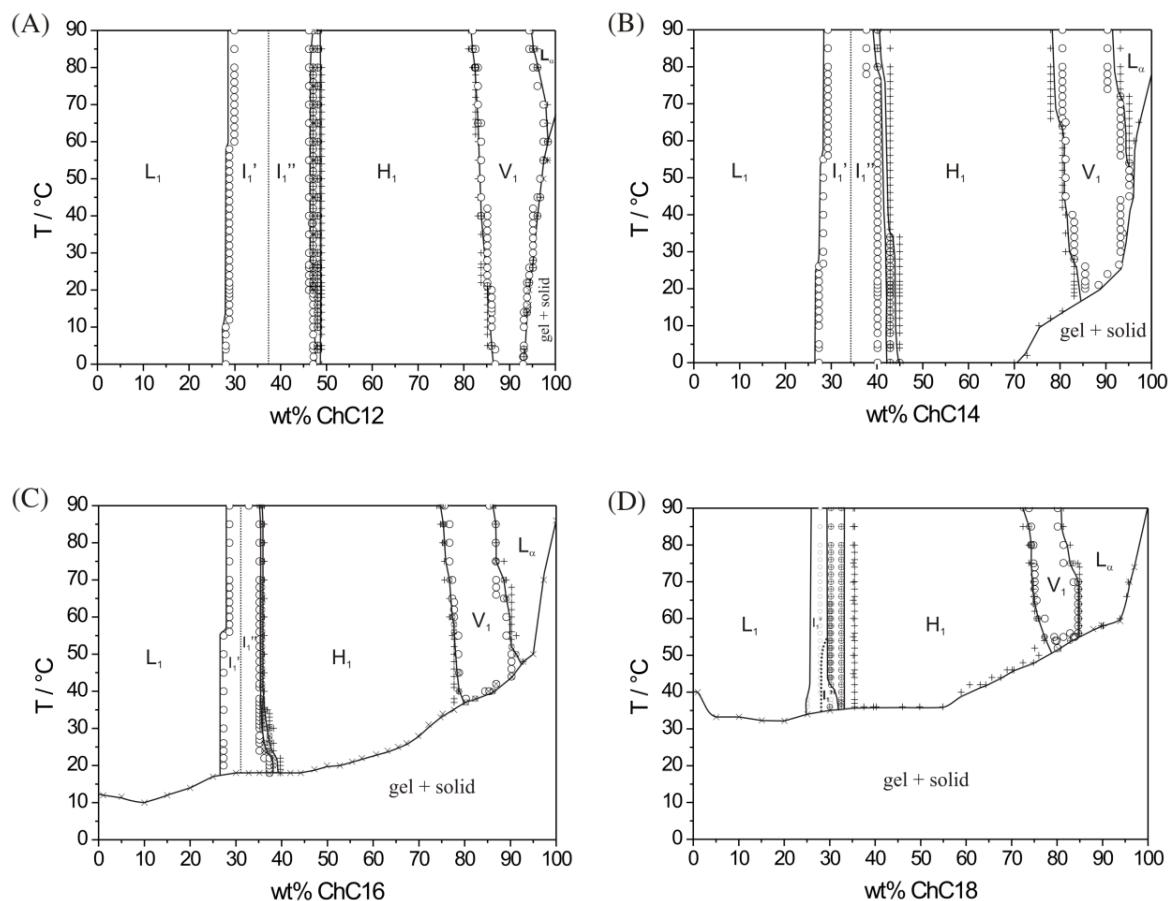


**Fig. IV.3** Binary aqueous phase diagrams of  $\text{ChC}_m$  surfactants between  $0^\circ\text{C}$  and  $90^\circ\text{C}$  for  $m=12$  (A),  $m=14$  (B),  $m=16$  (C) and  $m=18$  (D). Experimental data near the phase boundaries were determined visually between crossed polarizers as isotropic ( $\circ$ ), biphasic ( $\oplus$ ) and anisotropic ( $\times$ ).

Fig. IV.3 further visualizes that choline soaps start forming liquid crystals at around 26-29 wt% surfactant in water. The onset of the  $I_1'$  phase is thereby displaced slightly to lower concentrations with growing chain length. All liquid crystalline phase boundaries shift to lower soap concentrations for longer alkyl chains. This effect is most distinct for  $H_1$ . The  $I_1$  phase region shrinks with increasing  $m$ , extending for  $\text{ChC}_{12}$  over about 18 wt% while for  $\text{ChC}_{18}$  only over roughly 3 wt%. Also, the  $V_1$  region becomes smaller at higher  $m$  values, whereas the  $H_1$  and  $L_\alpha$  phase domains expand simultaneously. Apparently, phases of high curvatures, namely the cubic phases, become less favored the longer the alkyl chain is. This is well in line with literature and the known tendency of longer alkyl chain derivatives to form less curved surfactant aggregates.<sup>28,32,33</sup>

### Comparison to Alkali Soaps

Sodium and potassium soaps form liquid crystals ( $H_1$ ) at comparable concentrations as choline carboxylates (20-30 wt% surfactant in water depending on the chain length).<sup>2,12,14</sup> The found basic phase behaviour of choline soaps is generally also similar to the alkali homologues.<sup>2,12,25</sup> However, there are some important deviations:

- (1) The studied choline soaps exhibit two distinct  $I_1$  phases between  $L_1$  and  $H_1$ .
- (2)  $ChCm$  salts form a single  $V_1$  phase up to  $m=18$  and do not display intermediate phases. By contrast, the  $V_1$  phase is fully replaced by intermediate phase(s) for sodium at  $m=12$  and for potassium soaps at  $m=14$ .<sup>34</sup>
- (3) The  $L_\alpha$  phase region of  $ChCm$  surfactants is considerably smaller than observed for simple soaps, even if compared to large alkali ions such as cesium.<sup>23</sup> Sodium and potassium carboxylates, for instance, typically form a lamellar phase between 60-65 wt%.<sup>2,12</sup>
- (4) The Krafft boundary of choline carboxylates is shifted to considerably lower temperatures relative to alkali soaps.<sup>4,5,7</sup>

When compared to their choline counterparts, alkali carboxylate surfactants prefer phases of lower curvature, to a greater extent the smaller the counterion ( $Li^+ > Na^+ > K^+ > Rb^+ > Cs^+$ ). This trend reflects the known order of counterion binding and becomes further manifest in the Krafft point reduction of carboxylate soaps towards bigger alkali ions.<sup>11,35,57,58</sup> In this context, choline can be regarded as a simple continuation of the alkali series. The bulky, highly dissociated choline counterion induces a large cross-sectional headgroup area  $a_S$  and hence provokes two outstanding characteristics in the aqueous phase behavior: a low Krafft boundary up to very high concentrations and a discontinuous cubic phase which extends over a wide concentration region.<sup>36</sup> For instance,  $ChC12$  shows no Krafft phenomenon down to  $0^\circ C$  up to 93 wt% surfactant in water. As opposed to that, the Krafft temperature of 90 wt%  $NaC12$  is  $127^\circ C$  (or  $195^\circ C$  for  $KC12$ ).<sup>14</sup> Discontinuous cubic phases have to date been observed for example for mono-cationic surfactants like alkyltrimethylammonium chlorides with chain lengths up to  $m=14$ ,<sup>33,59</sup> but not for mono-anionic surfactants in binary mixtures with water. Strikingly, choline soaps even show two distinct  $I_1$  phases in water, which has previously only been reported for non-ionic,<sup>35, 60</sup> zwitter-ionic<sup>33</sup> and divalent surfactants.<sup>32</sup>

### IV.2.3. SAXS Data and Analysis

In the following, SAXS analyses of each liquid crystalline phase (recorded in concentration steps of  $\leq 2.5$ -5.0 wt%) are presented in order to provide further insight into structural details of the phases and confirm their assignment.

#### IV.2.3.1. Discontinuous Cubic $I_1'$

Penetration scans indicate that at least two differently structured  $I_1$  phases occur in the systems. Exemplary two-dimensional X-ray patterns acquired from ChC12 are displayed in Fig. IV.4. These show, with increasing surfactant concentration, a single  $I_1'$  phase (30.0-35.1 wt%), the coexistence of  $I_1'$  and  $I_1''$  (37.9 wt%), a pure  $I_1''$  phase (40.1-45.0 wt%), a biphasic pattern of  $I_1''$  and  $H_1$  (47.2 wt%), and eventually a single  $H_1$  phase (49.7 wt%).

It is well known that cubic phases often grow to large monocrystals, thus effecting rather spotty X-ray patterns instead of rings.<sup>20,37</sup> This applies in particular for the  $I_1'$  phase, while in  $I_1''$  homogeneous rings become more and more established.

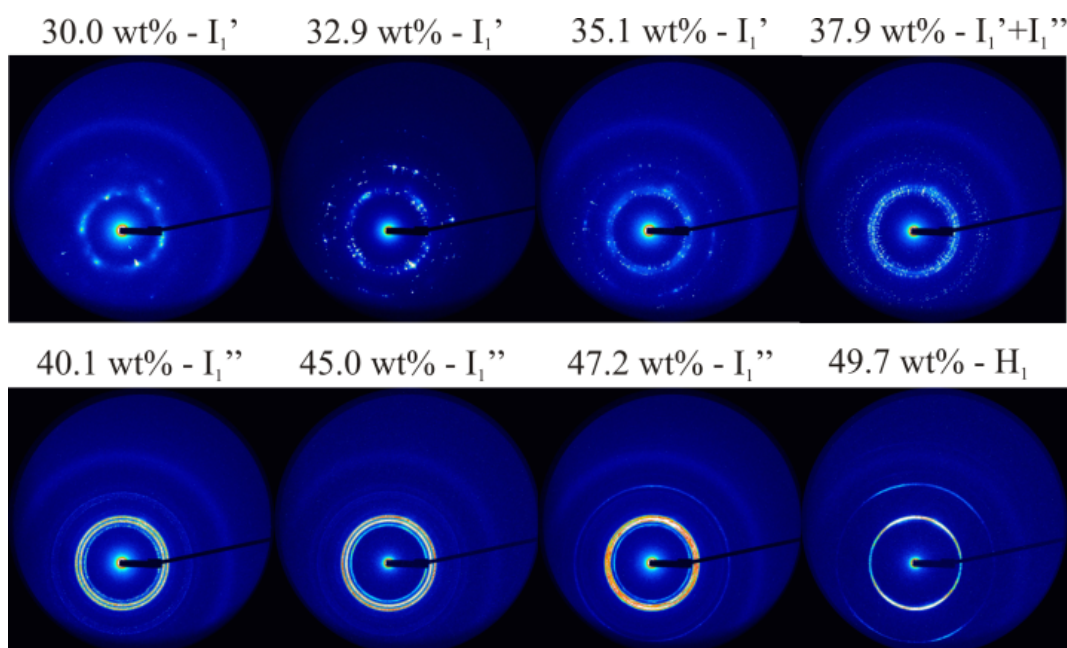


**Fig. IV.4** Two-dimensional X-ray patterns of the system ChC12/H<sub>2</sub>O at 25°C at surfactant concentrations ranging from 30.0-49.7 wt% ChC12, showing single and biphasic patterns of the discontinuous cubic phases  $I_1'$  and  $I_1''$  and the hexagonal phase  $H_1$ .

Fig. IV.5 A shows a radially averaged scattering profile of the  $I_1'$  phase of ChC12 (X-ray spectra of  $I_1'$  for both, different chain lengths and concentrations, are given in

the Appendix B.4). Several attempts were made to solve the structure, but neither a primitive nor a face- (*fcc*) or body-centred (*bcc*) lattice describe the data adequately well. In turn,  $I_1''$  could be clearly assigned to a *Pm3n* structure (see below). Therefore, particular effort was spent trying space groups like *Im3m*, *Fm3m* and *Fd3m*, since they often accompany a *Pm3n* lattice.<sup>19,20,24</sup> Although several reflections match to these space groups, some peaks always remained non-indexed. The best agreement was achieved when using the cubic structure described by Clerc in 1996,<sup>38</sup> which consists of two spherical micelles per unit cell arranged in hexagonal compact structure (*hcp*) with  $P6_3/mmc$  symmetry.<sup>38,39</sup> The dashed lines inserted to the spectrum in Fig. IV.5 A show the attempt to assign  $I_1'$  to this structure (see the Appendix B.5.1 for details on calculations). It is evident that the experimental spectrum is still not properly fitted.

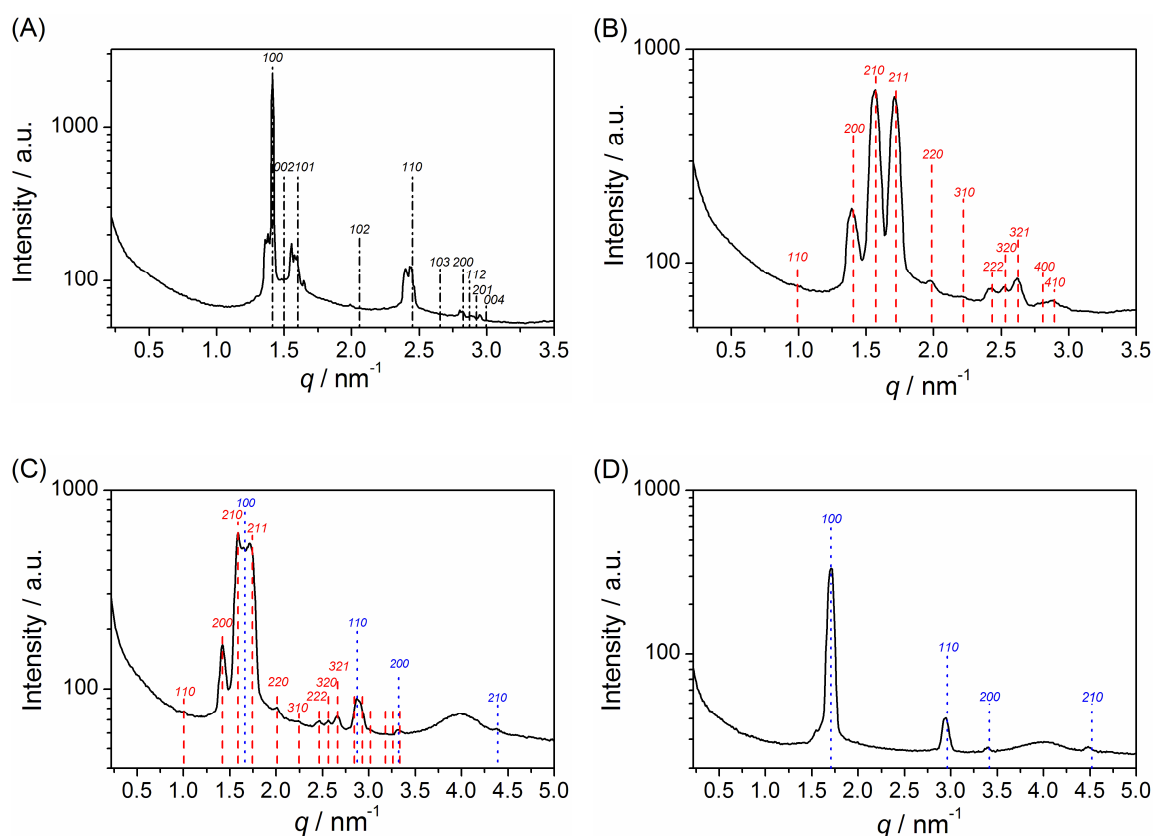


**Fig. IV.5** Radially averaged SAXS profiles of ChC12 at 25°C and surfactant concentrations of (A) 35.1, (B) 40.1, (C) 47.2, and (D) 49.7 wt%. Vertical lines mark the positions and Miller indices of peaks expected for a  $P6_3/mmc$  (---), *Pm3n* (-·-) and  $H_1$  (···) structure. Patterns correspond to (A) a single  $I_1'$  phase tentatively assigned to a  $P6_3/mmc$  structure, (B) a single  $I_1''$  with *Pm3n* symmetry, (C) a biphasic region of  $I_1''$  (*Pm3n*) and  $H_1$ , and (D) a pure  $H_1$  phase. Note that the bump around  $q=4 \text{ nm}^{-1}$  stems from Kapton foil.

A possible reason for the difficulties in finding the right space group could be that the *hcp* and *fcc* packing are energetically closely related.<sup>40</sup> Consequently, the relative stability of these two phases strongly depends on nucleation and growth kinetics.<sup>39</sup> The fact that they are likely to coexist may account for the result that  $I_1'$  cannot be simply assigned to a single structure. However, since samples of different concentrations and chain lengths were measured and no noticeable differences upon ageing for years could be detected, it is assumed that the X-ray pattern of  $I_1'$  reliably represents thermodynamic equilibrium. Another problem in indexing  $I_1'$  may arise due to the formation of large monocrystals. By simple radial averaging over the spots, substantial information on different domains of structures might get lost. Hence, a feasible means to further analyze the system could be to rotate the sample or to measure monodomains, which was unfortunately not possible with the used setups.

#### **IV.2.3.2. Discontinuous Cubic Phase $I_1''$**

As evidenced by Fig. IV.5, the  $I_1''$  phase of ChC12 could be indexed properly by a  $Pm\bar{3}n$  lattice. Equally unambiguous assignments were possible also for the other chain lengths, with up to 12 identified peaks (see the Appendix B.5.2 for further diffraction data). Cubic phases with  $Pm\bar{3}n$  symmetry, located between  $L_1$  and  $H_1$ , have been reported in earlier studies on binary and ternary surfactant systems.<sup>20,37,41,42</sup> However, the detailed structure of  $Pm\bar{3}n$  has in the past been the object of debates.<sup>19,20, 43-46</sup> Eventually, NMR-diffusion measurements<sup>43</sup> as well as detailed X-ray<sup>47</sup> and freeze-fracture electron microscopy studies<sup>48</sup> support the model of Charvolin and Sadoc, who proposed a structure comprising two spherical and six disc-shaped (oblate) micelles per unit cell without any dynamic disorder.<sup>49</sup> Accordingly, structural parameters such as the micellar radius or the effective cross-sectional headgroup area can at this point not be calculated in a straightforward way and would require more efforts such as mapping of the electron density.

The unit cell parameters  $a$  determined for  $I_1''$  range from about 90 Å to 125 Å (Table IV.1) and are reasonable with respect to other systems such as aqueous dodecyltrimethylammonium chloride.<sup>37</sup> The addition of two  $\text{CH}_2$  groups increases  $a$  on average by about 15-20 Å. This cannot be simply explained by the length of two  $\text{CH}_2$  groups (2.5 Å x 4 = 10 Å). The increase of  $a$  with growing chain lengths is most probably also caused by the larger dimensions of oblate micelles.

In a rough approximation, the micelle aggregation number  $N_{agg}$  can be calculated under the assumption of eight spherical micelles in the unit cell according to Equation (IV.1).

$$N_{agg} = (V_{Unitcell} \cdot \Phi_S / V_S) / 8 \quad (IV.1)$$

The resulting values (Table IV.1) vary from 71 for ChC12 up to 139 for ChC16, and are thus on a reasonable order of magnitude. As expected,  $N_{agg}$  increases with the chain length and the concentration.

**Table IV.1** Unit cell parameters  $a$  of the  $Pm3n$  structure detected for the  $I_1''$  phase of ChC*m* salts up to  $m=16$  at 25°C, with corresponding estimated aggregation numbers  $N_{agg}$ . 37.9 wt% ChC12 and 34.9 wt% ChC14 are biphasic samples of  $I_1'$  and  $I_1''$ , while 47.2 wt% ChC12 belongs to the two-phase region of  $I_1''$  and  $H_1$ .

	ChC12				ChC14			ChC16
wt%	37.9	40.1	45.0	47.2	34.9	37.4	40.9	34.8
$a / \text{Å}$	$91.3 \pm 0.5$	$89.9 \pm 0.3$	$88.8 \pm 0.2$	$88.4 \pm 0.4$	$105.8 \pm 1.1$	$106.1 \pm 1.0$	$106.7 \pm 1.2$	$124.9 \pm 0.8$
$N_{agg}$	70.9	71.4	77.4	79.8	92.7	100.1	111.1	139.4

### IV.2.3.3. Hexagonal Phase $H_1$

At around 35-50 wt% (depending on  $m$ ), choline soaps start forming a hexagonal phase, which can be identified by up to 4-5 reflections (see Fig. IV.5 D and Table B.6 in the Appendix). For the  $Pm3n - H_1$  transition, several groups suggested an epitaxial relationship which facilitates the conversion of the  $211$  plane in the cubic phase into the  $100$  plane of the hexagonal lattice.<sup>50, 51</sup> As shown by the biphasic spectrum of 47.2 wt% ChC12 (cf. Fig. IV.5 C), the  $100$  spacing of  $H_1$  is centered exactly in the middle between the  $210$  and  $211$  reflection of  $Pm3n$ . Moreover, no systematic change in the relative intensity of the  $211$  spacing of  $Pm3n$  towards higher soap concentrations could be traced. In this sense, it seems as if choline soaps do not follow the proposed transition mechanism.

The interlayer spacing  $d$  of  $H_1$  decreases linearly with the surfactant concentration (Fig. IV.6 A), which can be interpreted by a closer packing of the micellar cylinders. Corresponding changes in the lipophilic radius  $r_L$  are outlined in Fig. IV.6 B for the different  $m$  values. As expected,  $r_L$  increases in an approximately linear fashion with the concentration. The determined slopes ( $\Delta r_L / \Delta \Phi_L = 4.0-4.8$ ) are within the limits of

experimental error equal for all homologues, indicating that the micellar radii grow in a similar manner. In all cases,  $r_L$  is around 10-20% smaller than the respective fully extended alkyl chain  $l_{max}$  (Table IV.4), which agrees well with literature.<sup>74</sup> Upon addition of two  $\text{CH}_2$  groups,  $r_L$  increases at a given volume fraction by about 1.5-2.4 Å, which complies with reported values.<sup>14, 52</sup>

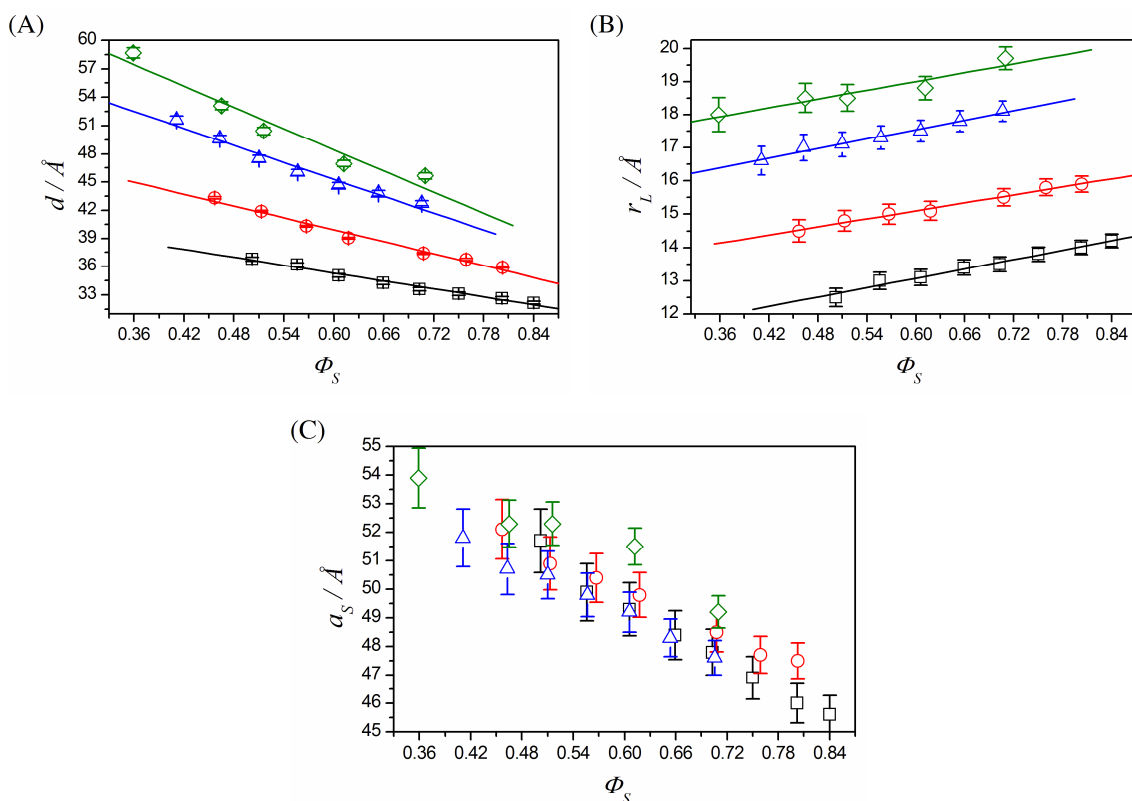


**Fig. IV.6** The interlayer spacing  $d$  (A), the radius of the lipophilic part  $r_L$  (B) and the cross-sectional area at the polar-nonpolar interface  $a_S$  (C) outlined as a function of  $\Phi_S$  for the hexagonal phase of ChCm soaps (ChC12 (□), ChC14 (○), ChC16 (△) and ChC18 (◇)) ( $T=25^\circ\text{C}$  for  $m=12-16$ , and  $T=50-60^\circ\text{C}$  (see SI) for  $m=18$ ). The error bars were calculated assuming uncertainties of  $\Delta q=0.01$  nm and  $\Delta\Phi_L=0.01$ .

The effective cross-sectional area at the polar-nonpolar interface  $a_S$  is reproduced as a function of the surfactant volume fraction for the different  $m$  values in Fig. IV.6 C. Only ChC18 tends to slightly larger  $a_S$  values, while those of  $m=12-16$  are more or less equal. This can probably be attributed to the higher temperatures chosen for measuring the ChC18 data due to its higher Krafft point. With growing surfactant concentration,  $a_S$  decreases from about  $52 \text{ \AA}^2$  to  $46 \text{ \AA}^2$ , finally reaching the limit at which the molecules can be packed in cylinders.

To enable a comparison of the results to data reported for the sodium and potassium homologues, values cited in literature were recalculated in order to obtain the cross-sectional area at the polar-nonpolar instead of the surfactant-water interface.<sup>53</sup> Given the high Krafft temperatures of Na- and K- carboxylates, documented values were determined at 86°C.<sup>53</sup> However, for ionic surfactants the influence of temperature on structural parameters is rather small. When considering similar volume fractions (~50% surfactant), the following tendency of  $a_S$  is obtained for  $m=12$ :

$$\text{NaC12 } (a_S= 46.7 \text{ \AA}^2)^{53} < \text{KC12 } (a_S= 47.3 \text{ \AA}^2)^{53} \ll \text{ChC12 } (a_S= 51.7 \text{ \AA}^2)$$

This is well in line with the increasing size of the counterions and the concurrent decrease of counterion-headgroup association.<sup>2,35</sup> Moreover, it confirms the idea of Zemb *et al.* that ionic micelles are adequate models for quantifying specific ion effects.<sup>36</sup>

#### IV.2.3.4. $H_1 - V_1$ Boundary: Intermediate Phase?

Close to the phase boundary between  $H_1$  and  $V_1$ , additional reflections appear in the X-ray patterns which can be allocated neither to  $H_1$  nor, apparently, to  $V_1$  (which belongs to the  $Ia3d$  space group, see below). These peaks are unlikely to arise from insufficient equilibration, since four months-old samples give the same scattering profiles as those measured after one week.

As already mentioned, several intermediate phases located between  $H_1$  and  $V_1$  or  $H_1$  and  $L_\alpha$  have been identified for alkali soaps or other mono-ionic surfactants. Luzzati *et al.* described an intermediate phase with complex hexagonal structure,<sup>10,12</sup> which is known today as *ribbon* phase with centered rectangular symmetry ( $cmm$ ).<sup>54</sup> This structure exhibits peak ratios typical for a hexagonal lattice, but with much larger lattice dimensions and more irregular peak intensities.<sup>10,12</sup> The additional peaks observed in the  $H_1/V_1$  region match the Bragg spacing ratios of a two-dimensional hexagonal lattice, as shown exemplarily for ChC16 in Fig. IV.7 (see Appendix B.5.4 for further details and X-ray data).

The detected  $d$  spacings are indeed larger than those of  $H_1$ , but by far not to such an extent as reported by Luzzati *et al.*, who observed almost two times higher  $d$  values in the intermediate region than in  $H_1$ .<sup>10</sup> Moreover, common intermediate phases are of anisotropic nature, which is clearly in conflict with the isotropy noticed for the samples

in this concentration regime. And beyond that, the penetration scans gave no evidence of an intermediate phase for any of the investigated choline soaps.

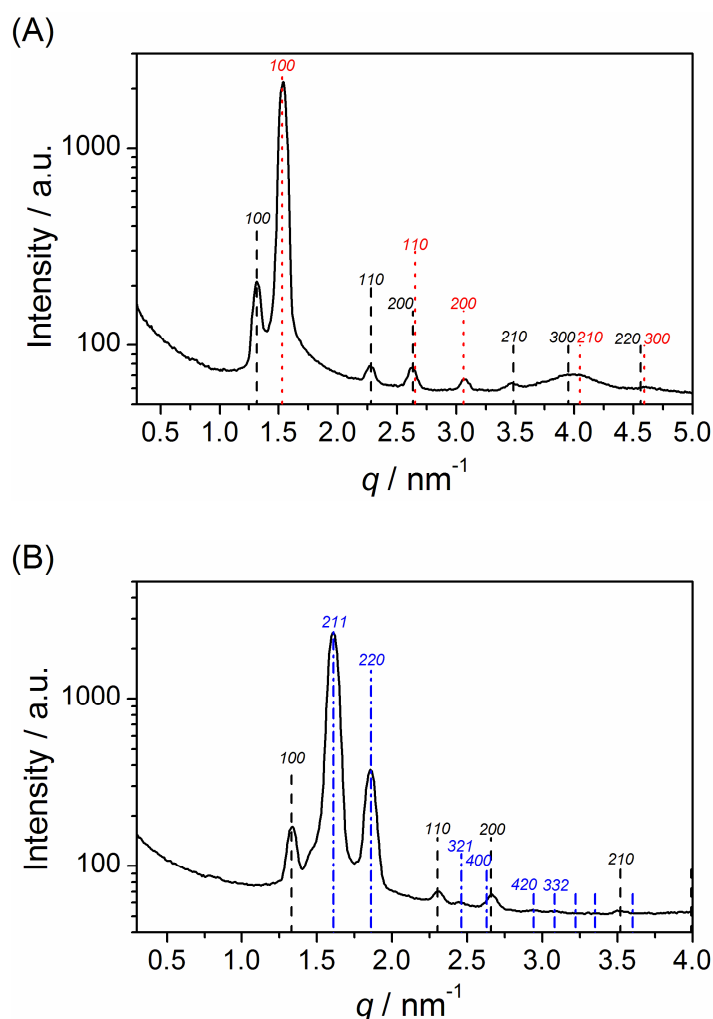


**Fig. IV.7** SAXS spectra of (A) 74.8 wt% ChC16 ( $T= 60^\circ\text{C}$ ) and (B) 79.3 wt% ChC16 ( $T= 50^\circ\text{C}$ ), representing biphasic samples of a potential intermediate phase and  $H_1$  (A) or, respectively,  $V_1$  (B). Theoretical peak positions are indicated by the vertical lines with the corresponding Miller indices outlined above (complex hexagonal (---),  $H_1$  (···) and  $Ia3d$  (---)). The bump around  $q= 4 \text{ nm}^{-1}$  is due to the Kapton foil.

An alternative approach would be to index these additional peaks by another cubic lattice, namely  $I4_132$ ,<sup>55,56</sup> which is a subgroup of  $Ia3d$  (see Appendix B.5.4). However, reflections of fourth and fifth order ( $d_{310}$  and  $d_{222}$ ) are all missing in this case. Consequently, the complex hexagonal structure represents a better fit of the data, since the reflections could be assigned in increasing order without extinctions in-between them.

For the  $H_1$ - $V_1$  transition, Rancon and Charvolin suggested an epitaxial relationship between the  $211$  plane of  $Ia3d$  and the  $100$  plane of the hexagonal lattice.<sup>50</sup> Accordingly,  $2 d_{211} / \sqrt{3}$  of  $Ia3d$  should equal  $d_{100}$  of  $H_1$ ,<sup>50</sup> which however could not be confirmed by the present set of data. This either rules out an epitaxial relationship of  $H_1$  and  $V_1$  or in turn supports the existence of an additional phase between  $H_1$  and  $V_1$ . At the moment, no unambiguous conclusions can be drawn on whether an intermediate phase, an additional cubic phase, or any extra phase at all exists between  $H_1$  and  $V_1$ .

#### IV.2.3.5. Bicontinuous Cubic Phase $V_1$

In a bicontinuous cubic phase, the aggregates form a three-dimensional network extending throughout the sample. The structures formed are well described by *infinite periodic minimal surfaces* (IPMS),<sup>20,57,58</sup> i.e. surfaces whose mean curvature is zero at all points. Most commonly obtained in  $V_1$  phases of lipid-water systems is the  $Ia3d$  group, which corresponds to the “gyroid” (G) type surface, having a negative Gaussian interfacial curvature.<sup>20,58</sup> The  $V_1$  phase of choline soaps also belongs to the  $Ia3d$  symmetry, as confirmed by up to six assigned reflections (see Fig. IV.8).

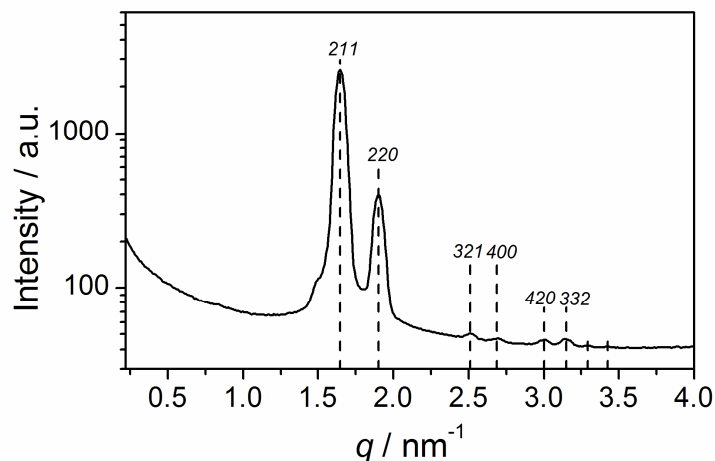


**Fig. IV.8** SAXS spectrum of  $V_1$  of ChC16 (85.5 wt%, 50°C), revealing  $Ia3d$  symmetry. The vertical lines mark the theoretical peak positions with the corresponding Miller indices outlined above.

As observed for  $H_1$ , the peaks are shifted to lower  $d$  values when the surfactant concentration is increased and to higher  $d$  values when longer alkyl chains are used (cf. Table IV.2). In the framework of the IPMS concept, the length of the lipophilic part and the area per surfactant headgroup cannot be calculated in a simple manner. However, the determined unit cell parameters  $a$  (Table IV.2) are generally in the same order of

magnitude as those of other mono-ionic surfactants.<sup>11,19,59</sup> Towards higher soap concentrations,  $a$  decreases as the effective alkyl chain length is increased and the effective headgroup area diminished. Addition of two CH<sub>2</sub> groups enlarges reasonably the unit cell by about 5-10 Å.<sup>14</sup>

**Table IV.2** Results of SAXS analyses for V<sub>1</sub> of ChC $m$  soaps with Ia3d structure, with the volume fraction of surfactant  $\Phi_S$ , the temperature  $T$ , the experimental  $d$ -values of the respective first order reflection and the unit cell parameter  $a$ . Samples of ChC12 up to 89.5 wt% as well as 79.3 wt% ChC16 and 75.7 wt% ChC18 are potentially biphasic as discussed in the text.

	wt%	$\Phi_S$	$T/^\circ\text{C}$	$d_{211}/\text{Å}$	$a/\text{Å}$
<b>ChC12</b>	86.9	0.871	25	31.1	$76.2 \pm 0.1$
	89.5	0.897	25	30.8	$75.6 \pm 0.2$
	91.5	0.916	25	30.4	$74.6 \pm 0.2$
	94.0	0.941	25	30.2	$74.0 \pm 0.2$
	97.5	0.975	60	29.0	$71.1 \pm 0.2$
<b>ChC14</b>	79.8	0.803	60	34.0	$83.1 \pm 0.1$
	83.3	0.837	25	35.1	$86.3 \pm 0.5$
	85.5	0.859	20	34.5	$84.8 \pm 0.3$
	90.4	0.906	25	33.6	$82.6 \pm 0.3$
	93.2	0.934	35	32.9	$80.7 \pm 0.3$
	95.1	0.952	45	32.4	$79.7 \pm 0.4$
<b>ChC16</b>	79.3	0.800	50	39.0	$95.8 \pm 0.4$
	85.5	0.860	50	38.1	$93.4 \pm 0.2$
	89.3	0.897	50	37.6	$92.1 \pm 0.1$
<b>ChC18</b>	75.7	0.766	70	42.2	$103.3 \pm 0.3$
	79.8	0.806	70	41.1	$101.4 \pm 0.4$

#### IV.2.3.6. Lamellar Phase L <sub>$\alpha$</sub>

The lamellar or “neat” phase, in which surfactants are arranged in bilayers, is the most common structure among all liquid crystals. This phase is not only of biological relevance with respect to cellular membranes, but also occurs in daily life products such as hand soaps. However, the region of L <sub>$\alpha$</sub>  formed by choline soaps up to  $m=18$  is rather small. The results of SAXS analyses are summarized in Table IV.3, while

corresponding diagrams are shown in the Appendix B.4. As in the other liquid crystals, reflections shift to lower  $d$  values with increasing surfactant concentrations due to a closer packing of the bilayers, and to larger  $d$  values for longer alkyl chains (Table IV.3).

**Table IV.3** Structural parameters of the lamellar phase formed by ChC $m$  soaps with  $m= 14-18$ , comprising the experimental  $d$ -values, the ratio of the lipophilic bilayer thickness  $d_L$  and the all-*trans* alkyl chain length  $l_{max}$ , the difference of the surfactant length  $r_S$  and the lipophilic half-length  $r_L$  (representing the headgroup-counterion layer), and the thickness of the water layer  $d_w$ .

	wt%	$\Phi_S$	$d_{100}$ /Å	$(d_L / l_{max})$ /Å	$(r_S - r_L)$ /Å	$d_w$ /Å
<b>ChC14</b>	95.1	0.952	29.4	1.03	4.7	1.4
	97.5	0.976	29.0	1.04	4.8	0.7
<b>ChC16</b>	92.0	0.923	32.6	1.01	4.7	2.5
	94.0	0.942	32.2	1.02	4.7	1.9
	95.3	0.955	32.1	1.03	4.7	1.4
	97.5	0.976	31.7	1.04	4.8	0.8
<b>ChC18</b>	85.7	0.863	36.1	0.97	4.5	4.9
	90.2	0.906	35.5	1.00	4.6	3.3
	96.0	0.962	34.9	1.04	4.8	1.3

The half-length of the lipophilic bilayer  $r_L$  increases more or less linearly with the concentration (Fig. IV.9 (A)). Thereby,  $r_L$  is on average around 50% smaller than  $l_{max}$  for all investigated chain lengths. In other words, the total bilayer thickness equals approximately  $1.0 l_{max}$  for all  $m$  values, which indicates high disorder of the paraffinic chains.<sup>46</sup> The water layer  $d_w$  (Table IV.3) is very small due to the high soap concentrations. The headgroup and counterion layer ( $r_S - r_L$ ) covers about 4.7 Å in thickness, irrespective of the concentration and the chain length. This appears quite small when noting that the length of an extended choline ion is about 8 Å. A possible explanation for this finding is that choline is arranged in the layer with its long axis perpendicular to the director plane.

As in H<sub>1</sub>, the effective cross-sectional area  $a_S$  is more or less equal for different  $m$  values and decreases with growing surfactant concentration, from about 44 Å<sup>2</sup> to 40 Å<sup>2</sup> (Fig. IV.9 B). Again, choline surfactants show significantly larger  $a_S$  values than alkali

soaps. For instance, a headgroup area of  $a_S = 34.2 \text{ \AA}^2$  was reported for the lamellar phase of KC18 at 82.3 wt% and  $86^\circ\text{C}$ .<sup>53</sup> For comparison, ChC18 requires  $43.6 \text{ \AA}^2$  at 85.7 wt% and  $70^\circ\text{C}$ . This confirms the reported notion of a low counterion to headgroup association for carboxylate systems with large (or “soft”) counterions.<sup>35,60</sup>

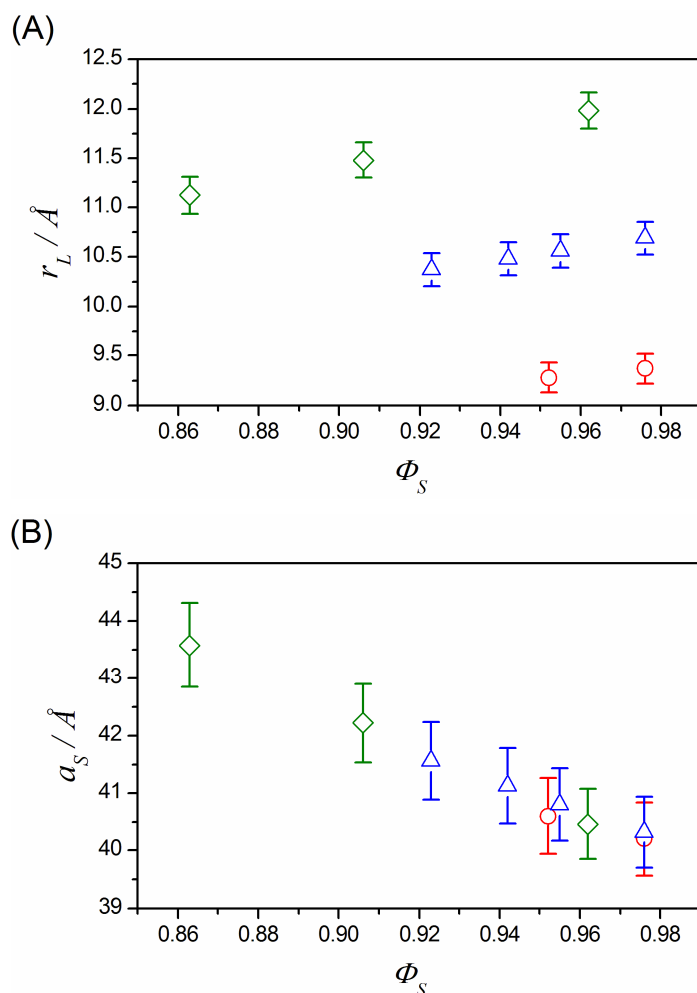


**Fig. IV.9** Half-length of the lipophilic bilayer  $r_L$  (A) and cross-sectional area at the polar-nonpolar interface  $a_S$  (B) in the lamellar phase of ChC*m* surfactants plotted as a function of volume fraction surfactant  $\Phi_S$  (ChC14( $\circ$ ), ChC16( $\Delta$ ) and ChC18( $\diamond$ )). The error bars were calculated assuming uncertainties of  $\Delta q = 0.01 \text{ nm}$  and  $\Delta\Phi_L = 0.01$ .

### IV.3. Conclusions

Aqueous binary phase diagrams of ChC*m* soaps with  $m = 12-18$  have been established over a temperature range of  $0-90^\circ\text{C}$  with the help of polarizing microscopy and small-angle X-ray scattering. In analogy to alkali soaps, choline carboxylates start forming liquid crystals at around 26-29 wt%. Although the basic phase behavior of ChC*m* salts

is similar to that of other mono-anionic surfactants, some outstanding characteristics have been revealed. For instance, with choline as counterion two discontinuous cubic phases extending over large concentration intervals occur up to  $m=18$ . The sequence of the subsequent mesophases towards higher concentrations was confirmed to be  $H_1 - V_1 - L_\alpha$ , although the existence of an intermediate phase between  $H_1$  and  $V_1$  cannot be excluded. In contrast to the alkali soaps, the  $V_1$  phase is formed also by long-chain members of the choline series, while the domain of  $L_\alpha$  is relatively small. The use of choline as counterion in fatty acid soaps apparently promotes mesophases of high curvatures. As evidenced by the presented X-ray data, this behavior can be ascribed to comparatively large headgroup areas originating from the bulky and highly dissociated choline ion. Another essential feature of the obtained phase diagrams is the very low Krafft boundary of  $ChC_m$  surfactants even at high concentrations. For instance,  $ChC_{12}$  shows no Krafft phenomenon down to  $0^\circ\text{C}$  up to 93 wt%  $ChC_{12}$  in water. By contrast, the corresponding sodium and potassium homologues require, at similar concentrations, far more than  $100^\circ\text{C}$  to form liquid crystals.<sup>7</sup>

The reported phase diagrams further emphasize the potential of choline fatty acid soaps as promising alternatives to common anionic surfactants due to their extraordinary water solubility up to high concentrations and their inherent biocompatibility.

## **IV.4. Experimental**

### **IV.4.1. Materials and Sample Preparation**

Choline soaps were synthesized and purified as described previously.<sup>1</sup> The resulting white crystalline powders were dried for at least two days in a desiccator and then stored in a nitrogen glove box.

Lyotropic liquid crystals were obtained by weighing the appropriate surfactant amount into glass ampoules of 1 cm diameter under  $N_2$  atmosphere in order to gain exact concentrations and to prevent water absorption, given that neat choline soaps are hygroscopic. Subsequently, Millipore water was added such that the final total sample mass was about 0.3 g. Afterwards, the ampoules were immediately flame sealed. Adequate mixing was achieved by repeated centrifugation at around 5000 rpm for a minimum of two days at  $40^\circ\text{C}$ . The homogenized samples were kept at  $25^\circ\text{C}$  in a thermostat for at least 48 hours to allow for equilibration. To further ensure that

thermodynamic equilibrium was in fact reached, samples were checked regularly over a period ranging from two days up to two years.

## **IV.4.2. Methods**

### **IV.4.2.1. Penetration scan**

Penetration scan studies were conducted on a Leitz Orthoplan polarizing microscope (Wetzlar, Germany) equipped with a JVC digital camera (TK-C130) and a Linkham hot stage comprising a TMS90 temperature controller ( $\pm 0.5^\circ\text{C}$ ) and a CS196 cooling system. Images were recorded at a magnification of 100x. The heating or cooling rate was in all cases  $10^\circ\text{C min}^{-1}$ . Transition temperatures on cooling were found to be up to  $4^\circ\text{C}$  lower than on heating. Penetration scans were performed by trapping a small amount of dry substance between microscopy slides. Subsequently, a drop of water was added at the border of the sample, which then slowly diffused towards the centre. Distinct rings appeared along the surfactant-water concentration gradient showing the distinct mesophases, which in turn can be identified by their characteristic optical textures.<sup>26,61</sup> In addition, by slightly pushing the sample, relative viscosities can be estimated and used as further evidence for phase identification.

### **IV.4.2.2. Phase Diagrams**

Concentration- and temperature-dependent mappings of the phase diagrams were first done by visual observation between crossed polarizers in steps of 2.5 wt% and  $2\text{-}5^\circ\text{C}$ . Afterwards, steps were refined near the phase boundaries. The temperature of the samples was controlled by placing tubes in a water bath with an accuracy of  $\pm 0.1^\circ\text{C}$ . Specimens were investigated over a temperature range of  $0\text{-}90^\circ\text{C}$  with a heating rate of about  $1\text{-}2^\circ\text{C}$  per hour. Phase changes were detected by direct visual inspection of the samples between crossed polarizers. Cubic phases can be distinguished by their optical isotropy, transparency, and extremely high viscosity, while the hexagonal phase is for example featured by high viscosity, transparency and optical anisotropy. The phase boundary between the micellar solution  $L_1$  and the discontinuous cubic phase  $I_1$  could be easily recognized by a sudden increase of viscosity. Samples were repeatedly checked over extended periods of time (from 2 days up to 2 years). No remarkable changes with time could be discerned except for minor differences within the two-phase regions in some cases. The good agreement over this long time period indicates on the

one hand that an ageing time of about 48-82 hours is already sufficient to achieve thermodynamic equilibrium and, on the other hand, that the samples are long-term stable.

#### **IV.4.2.3. Krafft Points**

The Krafft boundary within the  $L_1$  phase was determined by turbidity measurements using an custom-designed automated setup built in-house.<sup>14,62</sup> Samples were placed in a computer-controlled thermostat and, if necessary, cooled until precipitation occurred. Turbidity was monitored by detecting the transmitted light supplied by a LED with a light-dependent resistor (LDR). The clearing temperature obtained by heating with a rate of 1°C per hour was taken as the Krafft temperature.

#### **IV.4.2.4. Density Measurements**

In order to be able to evaluate the molecular volume of the surfactants, the densities ( $\rho$ ) of aqueous ChC*m* solutions were determined at 25°C for concentrations between 1 and 20 wt% using a vibrating tube densimeter (Anton Paar DMA 60). The instrument was calibrated by measuring purified dry nitrogen and water.

#### **IV.4.2.5. Small-Angle X-ray Scattering**

SAXS measurements were performed on three different setups, due to limited availabilities and distinct specific demands such as the variation of detectable scattering angles, control of temperature, or the recording of two-dimensional X-ray patterns. Detailed information on the utilized SAXS instruments and on which samples were measured on each instrument is given in the Appendix B.4. Spectra were not corrected for the empty cell scattering, since subtraction produced negative data in some instances due to temperature-induced transmission changes. However, absolute intensities are not required, as all SAXS data were analyzed crystallographically. Measured intensities are outlined as a function of the scattering vector  $q$  which is defined as  $q = 4\pi/\lambda \sin(\theta/2)$ , where  $\theta$  is the scattering angle and  $\lambda$  the wavelength of the X-rays.

#### **IV.4.2.6. Calculations**

To calculate the length or radius of the lipophilic part  $r_L$  and the effective cross-sectional area at the polar-nonpolar interface  $a_S$  from the X-ray data, the volume fraction of the surfactant  $\Phi_S$  and of the lipophilic part  $\Phi_L$  are required.  $\Phi_S$  is given by Equation

(IV.2), wherein  $c$  denotes the weight fraction of surfactant and  $\rho_{Surf}$  and  $\rho_W$  are the densities of surfactant and water ( $\rho_W = 997.1 \text{ g L}^{-1}$ ), respectively. Values for  $\rho_{Surf}$  were obtained by extrapolating the densities measured for samples of different concentrations to 100% surfactant (see Table IV.4).

$$\Phi_S = \left( 1 + \frac{\rho_{Surf}(1-c)}{\rho_W c} \right)^{-1} \quad (\text{IV.2})$$

Based thereon,  $\Phi_L$  can be calculated according to Equation (IV.3) where  $V_S$  and  $V_L$  designate the volume of surfactant and the lipophilic part, respectively.

$$\Phi_L = \frac{V_L}{V_S} \Phi_S \quad (\text{IV.3})$$

From the density measurements, the molar volume of surfactant and thus the volume of one surfactant molecule  $V_S$  can be derived (Table IV.4).

**Table IV.4** Density  $\rho_{Surf}$  and volume  $V_S$  of one surfactant molecule of ChC $m$  salts with  $m = 12$ -18 at 25°C. The volume of the lipophilic part  $V_L$  and the length of the fully extended alkyl chains  $l_{max}$  were calculated according to the expression introduced by Tanford.<sup>60</sup>

	$\rho_{Surf} / \text{g L}^{-1}$	$V_S / \text{\AA}^3$	$V_L / \text{\AA}^3$	$l_{max} / \text{\AA}$
<b>ChC12</b>	979.0	515	323	15.4
<b>ChC14</b>	968.9	568	377	17.9
<b>ChC16</b>	956.4	624	431	20.5
<b>ChC18</b>	947.8	679	485	23.0

The volume of the paraffinic chains  $V_L$  can in turn be estimated by using the known densities of corresponding alkanes or via the expression of Tanford.<sup>52</sup> In order to allow for a comparison with the experimentally determined lipophilic radii, Table IV.4 further includes the maximum (fully extended) lengths of the respective alkyl chains, which can also be calculated by the expression of Tanford.<sup>52</sup>

With the interlayer spacing  $d$ , given by the position of the first scattering peak ( $d = 2\pi/q$ ), the radius of the lipophilic part  $r_L$  and, subsequently, the cross-sectional area  $a_S$  at the polar-nonpolar interface in hexagonal phases can be obtained as follows:<sup>10</sup>

$$r_L = d \sqrt{\left(\frac{2\Phi_L}{\sqrt{3}\pi}\right)} \quad (\text{IV.4})$$

$$a_S = \frac{2V_L}{r_L} \quad (\text{IV.5})$$

For lamellar phases, the half-thickness of the lipophilic bilayer  $r_L$  and the cross-sectional area  $a_S$  are defined as expressed by Equations (IV.6) and (IV.7).<sup>10</sup>

$$r_L = d \frac{\Phi_L}{2} \quad (\text{IV.6})$$

$$a_S = \frac{V_L}{r_L} \quad (\text{IV.7})$$

The length of one surfactant molecule  $r_S$  can finally be calculated by exchanging the lipophilic volume fraction for the surfactant volume fraction in Equations (IV.4) and (IV.6).

## IV.5. References

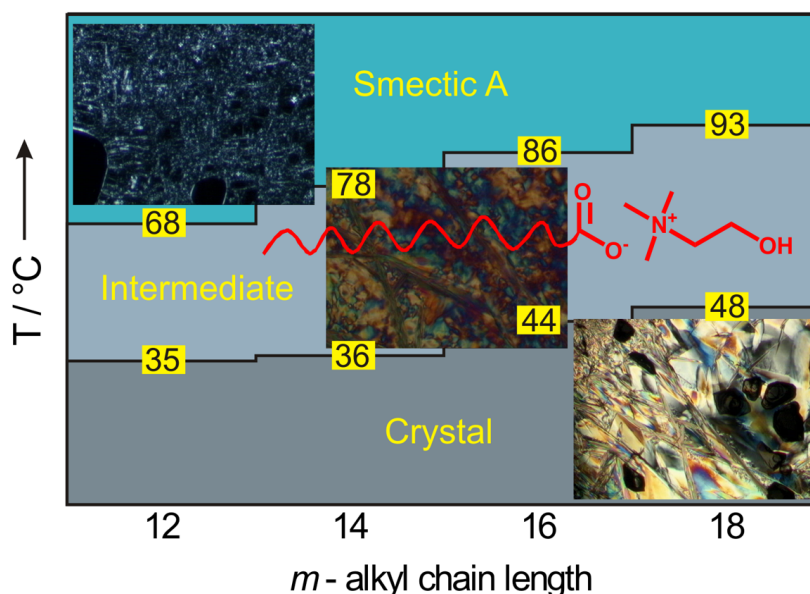
67. R. Klein, D. Touraud, W. Kunz, *Green Chem.*, 2008, **10**, 433.
68. R. Klein, M. Kellermeier, M. Drechsler, D. Touraud, W. Kunz, *Colloids Surf. A*, 2009, **338**, 129.
69. S. T. Hyde, Z. Blum, T. Landh, S. Lidin, B. W. Ninham, S. Andersson, K. Larsson, *The Language of Shape*, Elsevier, Amsterdam, 1996.
70. J. W. McBain, W. W. Lee, *Oil Soap*, 1943, **20**, 17.
71. J. W. McBain, W. C. Sierichs, *J. Am. Oil Chem. Soc.*, 1948, **25**, 221.
72. R. D. Vold, R. Reivere, J. W. McBain, *J. Am. Chem. Soc.*, 1941, **63**, 1293.
73. C. Madelmont, R. Perron, *Colloid Polym. Sci.*, 1976, **254**, 581.
74. V. Luzzati, H. Mustacchi, A. Skoulios, *Nature*, 1957, **180**, 600.
75. V. Luzzati, H. Mustacchi, A. Skoulios, *Meml. Serv. Chim. Etat*, 1957, **41**, 337.

76. V. Luzzati, H. Mustacchi, A. Skoulios, F. Husson, *Acta Crystallogr.*, 1960, **13**, 660.
77. F. Husson, H. Mustacchi, V. Luzzati, *Acta Crystallogr.*, 1960, **13**, 668.
78. V. Luzzati, F. Husson, *J. Cell Biol.*, 1962, **12**, 207.
79. V. Luzzati, A. Tardieu, T. Gulik-Krzywicki, E. Rivas, F. Reiss-Husson, *Nature*, 1968, **220**, 485.
80. D. M. Small, *Handbook of Lipid Research 4: The Physical Chemistry of Lipids*, Plenum Press, New York, 1986, pp. 285-343.
81. F. Reiss-Husson, V. Luzzati, *J. Colloid Interface Sci.*, 1966, **21**, 534.
82. R. M. Clapperton, R. H. Ottewill, A. R. Rennie, B. T. Ingram, *Colloid Polym. Sci.*, 1999, **277**, 15.
83. S. Karlsson, R. Friman, S. Backlund, R. Eriksson, *Tenside Surfact. Det.*, 2004, **41**, 72.
84. M. Jansson, A. Joensson, P. Li, P. Stilbs, *Colloids Surf.*, 1991, **59**, 387.
85. K. Fontell, *Colloid Polym. Sci.*, 1990, **268**, 264.
86. G. Lindblom, L. Rilfors, *Biochim. Biophys. Acta, Rev. Biomembr.*, 1989, **988**, 221.
87. H. Hagslaett, O. Soederman, B. Joensson, *Langmuir*, 1994, **10**, 2177.
88. E. S. Blackmore, G. J. T. Tiddy, *J. Chem. Soc., Faraday Trans. 2*, 1988, **84**, 1115.
89. D. J. Mitchell, G. J. T. Tiddy, L. Waring, T. Bostock, M. P. McDonald, *J. Chem. Soc., Faraday Trans. 1*, 1983, **79**, 975.
90. P. Sakya, J. M. Seddon, R. H. Templer, R. J. Mirkin, G. J. T. Tiddy, *Langmuir*, 1997, **13**, 3706.
91. A. S. C. Lawrence, *Mol. Cryst. Liquid Cryst.*, 1969, **7**, 1.
92. F. B. Rosevear, *J. Am. Oil Chem. Soc.*, 1954, **31**, 628.
93. J. M. Vincent, A. Skoulios, *Compt. Rend.*, 1964, **258**, 1229.
94. S. Hassan, W. Rowe, G. J. T. Tiddy, in *Handbook of Applied Surface and Colloid Chemistry*, Ed. K. Holmberg, John Wiley & Sons Ltd., Chichester 2002, pp. 465-508.

- 
95. J. R. Kanicky, A. F. Poniatowski, N. R. Mehta, D. O. Shah, *Langmuir*, 2000, **16**, 172.
  96. J. R. Kanicky, D. O. Shah, *J. Colloid Interface Sci.*, 2002, **256**, 201.
  97. J. R. Kanicky, D. O. Shah, *Langmuir*, 2003, **19**, 2034.
  98. J. N. Israelachvili, D. J. Mitchell, B. W. Ninham, *J. Chem. Soc., Faraday Trans. 2*, 1976, **72**, 1525.
  99. D. J. Mitchell, B. W. Ninham, *J. Chem. Soc., Faraday Trans. 1*, 1981, **77**, 601.
  100. K. Rendall, G. J. T. Tiddy, M. A. Trevethan, *J. Chem. Soc., Faraday Trans. 1*, 1983, **79**, 637.
  101. W. Kunz, *Curr. Opin. Colloid Interface Sci.*, 2010, **15**, 34.
  102. T. Zemb, L. Belloni, M. Dubois, A. Aroti, E. Leontidis, *Curr. Opin. Colloid Interface Sci.*, 2004, **9**, 74.
  103. R. R. Balmbra, J. S. Clunie, J. F. Goodman, *Nature*, 1969, **222**, 1159.
  104. M. Clerc, *J. Phys. II*, 1996, **6**, 961.
  105. X. Zeng, Y. Liu, M. Imperor-Clerc, *J. Phys. Chem. B*, 2007, **111**, 5174.
  106. S.-C. Mau, D. A. Huse, *Phys. Rev. E: Stat. Phys., Plasmas, Fluids, Relat. Interdiscip. Top.*, 1999, **59**, 4396.
  107. A. Tardieu, V. Luzzati, *Biochim. Biophys. Acta Biomembr.*, 1970, **219**, 11.
  108. P. Mariani, V. Luzzati, H. Delacroix, *J. Mol. Biol.*, 1988, **204**, 165.
  109. P. O. Eriksson, G. Lindblom, G. Arvidson, *J. Phys. Chem.*, 1987, **91**, 846.
  110. G. Arvidson, I. Brentel, A. Khan, G. Lindblom, K. Fontell, *Eur. J. Biochem.*, 1985, **152**, 753.
  111. A. Tardieu, V. Luzzati, F. C. Reman, *J. Mol. Biol.*, 1973, **75**, 711.
  112. K. Fontell, K. K. Fox, E. Hansson, *Mol. Cryst. Liq. Cryst., Lett. Sect.*, 1985, **1**, 9.
  113. R. Vargas, P. Mariani, A. Gulik, V. Luzzati, *J. Mol. Biol.*, 1992, **225**, 137.
  114. H. Delacroix, T. Gulik-Krzywicki, P. Mariani, V. Luzzati, *J. Mol. Biol.*, 1993, **229**, 526.
  115. J. Charvolin, J. F. Sadoc, *J. Phys. Chem.*, 1988, **92**, 5787.

116. Y. Rancon, J. Charvolin, *J. Phys. Chem.*, 1988, **92**, 2646.
117. P. Mariani, L. Q. Amaral, L. Saturni, H. Delacroix, *J. Phys. II* 1994, **4**, 1393.
118. C. Tanford, *J. Phys. Chem.*, 1972, **76**, 3020.
119. B. Gallot, A. Skoulios, *Kolloid Z. Z. Polym.*, 1966, **208**, 37.
120. H. Hagslaett, O. Soederman, B. Joensson, *Liq. Cryst.*, 1992, **12**, 667.
121. P. Saludjian, F. Reiss-Husson, *Proc. Natl. Acad. Sci. U. S. A.*, 1980, **77**, 6991.
122. S. Piotto, *Origins Life Evol. Biosphere*, 2004, **34**, 123.
123. S. Andersson, S. T. Hyde, K. Larsson, S. Lidin, *Chem. Rev.*, 1988, **88**, 221.
124. K. Larsson, F. Tiberg, *Curr. Opin. Colloid Interface Sci.*, 2005, **9**, 365.
125. V. Luzzati, F. R. Husson, *Nature*, 1966, **210**, 1351.
126. O. Söderman, *Curr. Opin. Colloid Interface Sci.*, 2004, **9**, 154.
127. F. B. Rosevear, *J. Soc. Cosmet. Chem.*, 1968, **19**, 581.
128. S. Schroedle, R. Buchner, W. Kunz, *Fluid Phase Equilib.*, 2004, **216**, 175.

## Chapter V Thermotropic Phase Behavior of Choline Soaps



As depicted in chapter IV, choline carboxylates ( $\text{ChC}_m$  with  $m=12-18$ ) show a rich self-assembly behavior in water. In the following, the thermotropic mesomorphism of anhydrous  $\text{ChC}_m$  salts for  $m=12-18$  is presented. Transition temperatures and enthalpies determined by differential scanning calorimetry reveal that all investigated compounds exhibit three different phases between  $-20^\circ\text{C}$  and  $95^\circ\text{C}$ . The phases were further characterized by optical polarizing microscopy, NMR spin-spin relaxation and X-ray scattering measurements. The nature of the phases was identified with increasing temperature as crystalline, semi-crystalline and liquid-crystalline lamellar. Even long-chain choline carboxylates ( $m=18$ ) were found to melt into a lamellar liquid-crystalline phase below  $100^\circ\text{C}$ . Accordingly, with choline as counterion in simple fatty acid soaps, not only the water solubility is considerably enhanced but also the melting points are substantially reduced, hence facilitating thermotropic mesomorphism at temperatures between  $35$  and  $95^\circ\text{C}$ . Thus, simple choline soaps with  $m=12-18$  may be classified as ionic liquids.

## V.1. Introduction

Choline represents a promising source for the design of sustainable biocompatible compounds. Although choline derivatives such as lecithin have been characterized physico-chemically,<sup>1-4</sup> the application of choline as simple counterion has for long been neglected. As shown chapter II and IV, choline is effective in reducing the Krafft point of fatty acid surfactants.<sup>5-7</sup> Its use permits also to decrease the melting points of salts below 100°C, either as additive in deep eutectic solvents,<sup>8,9</sup> or as counterion in ionic liquids with anions such as lactate,<sup>10</sup> saccharinate,<sup>11</sup> derivatives of phosphate<sup>12</sup> or acesulfamates.<sup>13</sup> Likewise, short-chain alkanooates were found to form ionic liquids with choline.<sup>14,15</sup> However, up to date, only the melting temperatures to an isotropic liquid phase were reported and no thermotropic mesomorphism has been detected.

It is well known that common soaps such as sodium and potassium salts of fatty acids are featured by a rich and complex thermotropic phase behavior.<sup>16-18</sup> For instance, anhydrous sodium soaps with alkyl chain lengths of  $m= 12-18$  exhibit at least five liquid-crystalline allotropic phases at temperatures ranging from 100-320°C.<sup>19-21</sup> Even short-chain sodium alkanooates (with less than seven carbon atoms) were found to form mesophases, but at temperatures approximately 100°C higher than the long-chain alkanooates.<sup>16,22,23</sup> Generally, Krafft and melting temperatures correlate.<sup>24</sup> In the alkali soap series, Krafft points shift to lower temperatures as the size of the cation increases.<sup>25,26</sup> The bulky choline ion simply continues this trend, enabling the use of long-chain derivatives with up to  $m= 16$  at ambient temperature.<sup>5</sup> In the case of melting to either liquid crystals or isotropic liquids, alkali soaps exhibit transition temperatures which are the higher the larger the cation (with  $\text{Li}^+$  being a partial exception).<sup>18,27-29</sup> The question now arises if long-chain choline alkanooates follow the tendency of the alkali homologues or whether they have lower melting points in line with the observed formation of ionic liquids with choline. Since choline soaps show at least five different liquid-crystalline structures in aqueous mixtures, the neat soaps are expected to display thermotropic mesomorphism.

Therefore, the thermotropic phase behavior of anhydrous  $\text{ChC}_m$  surfactants for alkyl chain lengths ranging from  $m= 12-18$  has been studied. To that end, thermal stabilities were evaluated by thermogravimetric measurements, while transition temperatures and enthalpies were determined by differential scanning calorimetry (DSC) between -20°C

and 95°C. The detected phases were characterized by optical polarizing microscopy, NMR spin-spin relaxation and small- (SAXS) as well as wide-angle X-ray scattering (WAXS) measurements.

## V.2. Results and Discussion

### V.2.1. Decomposition Temperatures

Table V.1 lists decomposition temperatures of the studied choline soaps, which were obtained from the onset of mass loss. Since ChC*m* surfactants consist exclusively of organic material, the thermal stability is limited up to about 200°C. Thereby,  $T_{dec}$  values increase linearly by 1.9°C per additional CH<sub>2</sub> group. Common alkali soaps are thermally more stable (over 350°C),<sup>21,30-33</sup> whilst other mono-anionic surfactants such as sodium dodecyl sulfate ( $T_{dec}=222^{\circ}\text{C}$ )<sup>34</sup> are in the same order of magnitude as choline soaps. The decomposition temperatures of short-chain choline carboxylates ( $m=2-10$ ) have been determined recently by Petkovic *et al.* They vary in a non-linear manner from 169°C to 166°C, and are therewith somehow slightly lower than expected on the basis of our experiments. Discrepancies might originate from different heating rates.<sup>14</sup>

**Table V.1** Decomposition temperatures ( $T_{dec}$ ) of ChC*m* surfactants for  $m=12-18$  as determined by thermogravimetric measurements.

$m$	$T_{dec} / ^{\circ}\text{C}$
12	191
14	195
16	199
18	202

### V.2.2. Differential Scanning Calorimetry

Visual observations of neat choline soaps in flame-sealed test tubes showed that all the compounds melt into an isotropic liquid phase between 120-150°C. This is accompanied by a strong dark-brown coloration. Obviously, choline soaps undergo an internal decomposition when heated over 100°C. Therefore, in order to exclude the influence of decomposed byproducts, we limited the temperature range in the following studies to below 95-100°C.

It is well known that melting temperatures and enthalpies of freshly melted samples can differ from reheated ones due to the formation of polymorphic metastable phases.<sup>35</sup> Indeed, the first cycle may differ from the subsequent ones, whereas the second and third cycle should be equal within the experimental error, demonstrating reproducibility and validity of the measurements (tight specimen holder and non-degraded substance). Therefore, three DSC cycles for each compound were recorded and Fig. V.1 displays as an example those of neat ChC12 and ChC16 (those of ChC14 and ChC18 are given in Appendix C.2).

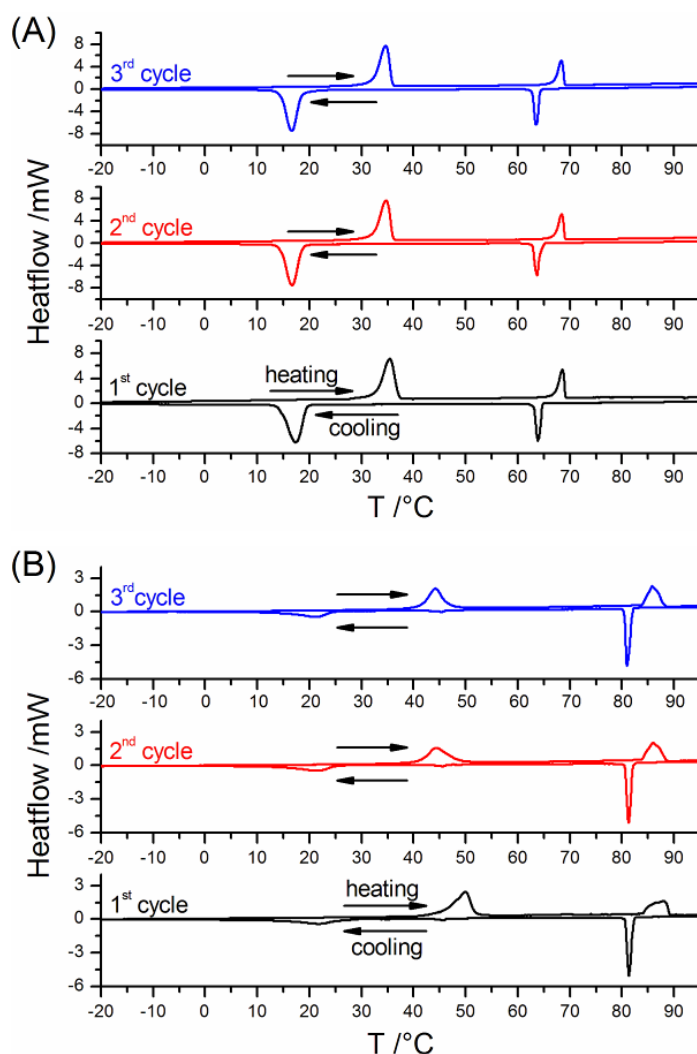


**Fig. V.1** DSC curves of neat ChC12 (A) and ChC16 (B) between  $-20^{\circ}\text{C}$  and  $95^{\circ}\text{C}$ , showing three heating and cooling cycles in comparison, each exhibiting two prominent phase transitions. The transition temperatures and enthalpies of the freshly melted compound (first cycle) are slightly different from the re-heated ones, while the second and third heating-cooling cycles are identical.

For ChC12, differences between freshly melted and reheated samples are rather small ( $\Delta T \leq 0.7^\circ\text{C}$ ), while deviations are evident in the case of ChC16 ( $\Delta T = 5.6^\circ\text{C}$ ). These mainly concern the first peak occurring on heating, indicating that it represents a transition from a different crystalline polymorph. In turn, the second and third heating and cooling cycles of all investigated compounds agree among each other within less than  $0.5^\circ\text{C}$ . For interpreting and comparing the thermograms of the different chain-lengths homologues, the second heating and cooling cycle of each compound is considered in the following.

Fig. V.2 gives a comparison of the thermograms of re-heated ChC $m$  surfactants for  $m=12-18$ . All investigated choline soaps show two reproducible and relatively sharp first-order transitions between  $10^\circ\text{C}$  and  $94^\circ\text{C}$ , both being associated with a considerable enthalpy change. Transitions on cooling often occur with a certain hysteresis due to slow nucleation.<sup>36</sup> In the present case, super-cooling is much more pronounced for the low-temperature ( $\Delta T = 18-23^\circ\text{C}$ ) than for the high-temperature ( $\Delta T = 5-7^\circ\text{C}$ ) transition.

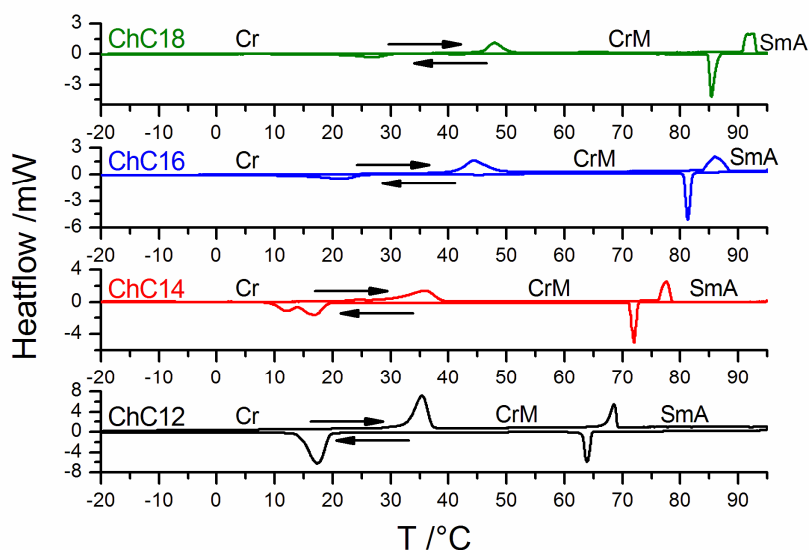


**Fig. V.2** The second heating and cooling DSC cycles of ChC $m$  surfactants for  $m=12-18$ , illustrating that all studied choline surfactants undergo two phase transitions between  $-20^\circ\text{C}$  and  $95^\circ\text{C}$ .

Since a large hysteresis is typical for crystalline materials and a small one is observed for liquid crystalline compounds,<sup>36,37</sup> the different extents of super-cooling already indicate the basic nature of the occurring phases. Taking into account all collected data, the phases observed with increasing temperature can be classified as crystalline (Cr), semi-crystalline (CrM) and liquid-crystalline (smectic-A (SmA)). The measured

thermograms indeed show some systematic tendencies depending on the chain length, but overall they look similar and hence suggest an equal general phase behavior. Only ChC14 differs slightly from the other homologues in that a double peak is discerned on cooling for the CrM to Cr transition. Given that only a single peak is observed on heating, this can most probably be attributed to the formation of a metastable crystalline phase, which is subsequently converted to a more stable form.

The transition temperatures are displayed as a function of the alkyl chain length  $m$  in Fig. V.3. Temperatures of both transitions, Cr to CrM and CrM to SmA, increase linearly with growing alkyl chain length, on heating as well as on cooling. The formation of SmA appears to be affected more strongly by the addition of a CH<sub>2</sub> group (increase by  $\sim 4^\circ\text{C}$ , ranging from  $68.4^\circ\text{C}$  for  $m=12$  up  $92.6^\circ\text{C}$  for  $m=18$ ) than that of CrM ( $\sim 2^\circ\text{C}$ , ranging from  $34.7^\circ\text{C}$  to  $52.6^\circ\text{C}$  for  $m=12-18$ ).

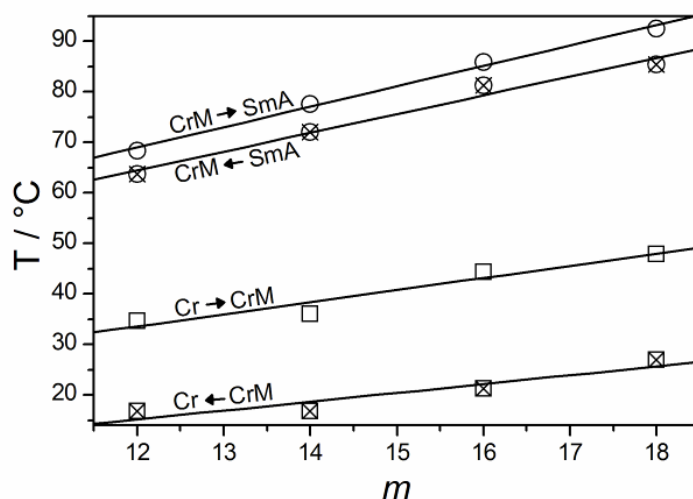


**Fig. V.3** Phase transition temperatures of ChC $m$  surfactants as a function of chain length  $m$  (taken from the second DSC cycle). Empty symbols mark transition temperatures determined on heating (( $\square$ ) crystal (Cr)  $\rightarrow$  semi-crystalline (CrM) and ( $\circ$ ) CrM  $\rightarrow$  liquid crystal (smecticA (SmA))), while crossed symbols represent those detected on cooling.

The variation of the transitions temperatures with alkyl chain length suggests that in both processes the interactions of paraffinic chains are the dominant forces.<sup>36, 37</sup> In the case of alkali soaps, melting temperatures within the various polymorphic crystalline states increase with the chain length, whereas they decrease (with some exceptions) for the conversion to liquid crystals or isotropic liquid.<sup>26, 38</sup> The melting process or mechanism of choline soaps seems therewith to be somewhat distinct from that of their

alkali counterparts. A more detailed discussion of these data including the transition enthalpies is given after the sections describing microscopy, X-ray and NMR data.

### V.2.3. Polarizing Optical Microscopy

By means of polarizing microscopy, a first identification of the phases formed by choline soaps between  $-20$  and  $95^{\circ}\text{C}$  can be achieved. Generally, phase transitions can be traced more easily on cooling where crystallization occurs quickly, while on heating the exact temperature range of crystal “melting” is more difficult to determine. Fig. V.4 shows a series of micrographs of ChC12 at different temperatures, obtained from the first cooling cycle. The high-temperature phase can readily be identified as a lamellar liquid-crystalline phase (smectic-A) by its characteristic oily streak texture and its relatively low viscosity.

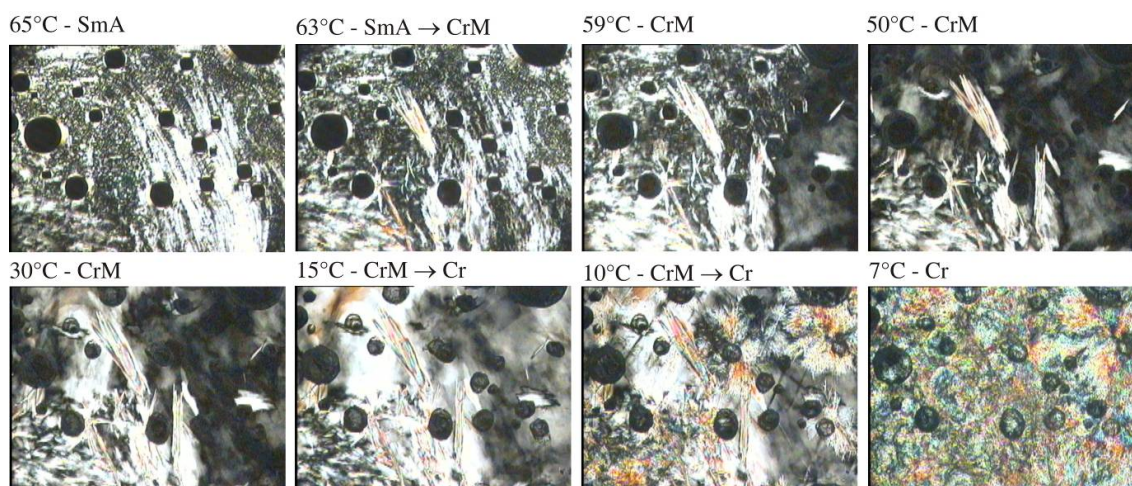


**Fig. V.4** Optical polarizing microscopy images of neat ChC12 at different temperatures with 100x magnification. Micrographs were taken from the same spot in the sample during the first cooling cycle (cooling rate  $10^{\circ}\text{C min}^{-1}$ ) and visualize the three phases formed between  $-20^{\circ}\text{C}$  and  $100^{\circ}\text{C}$ . At high temperatures ( $\geq 65^{\circ}\text{C}$ ), oily streak focal conic textures of low viscosity are observed, typical for a liquid-crystalline lamellar phase (smectic A). At  $64\text{--}63^{\circ}\text{C}$ , birefringent crystallites start to grow, accompanied by a sudden increase of viscosity. The virtual phase transition of SmA to CrM takes place within approximately  $2^{\circ}\text{C}$ . On further cooling, the appearance of the sample changes gradually over a wide range of temperature, first becoming darker and then birefringent. At  $15$  to  $7^{\circ}\text{C}$ , the whole sample crystallizes forming a birefringent solid material.

The other studied homologues also show a liquid-crystalline lamellar phase at high temperatures (see Appendix C.5 for corresponding images). The first phase transition

discerned on cooling (SmA to CrM) occurs for all investigated  $m$  values quickly (within 1-3°C), which fits well to the sharp peaks observed in the DSC curves (cf. Fig. V.2). Moreover, microscopy analyses of ChC12 confirm the DSC transition temperature of SmA to CrM. For  $m=14-18$ , the conversion from SmA to CrM takes place under the microscope at slightly higher temperatures than detected by DSC on cooling, approximating rather the transition temperatures obtained from DSC heating curves. The cooling rate chosen in the microscopy study (10°C min<sup>-1</sup>) was faster than that in the DSC measurements (1°C min<sup>-1</sup>) and would be expected to give a larger super-cooling effect. However, the contact surface of the sample between the microscopy slides is considerably larger than in the DSC vessels. A probable explanation for disagreements between DSC and microscopy analyses is that the larger surface acts as a nucleation site for the crystals and thereby attenuates the super-cooling effect.

Nevertheless, the SmA to CrM transition can be easily recognized under the microscope by a sudden increase of viscosity and change of texture. ChC12 additionally forms some birefringent crystallites with sharp edges. These crystallites were not observed in all experiments (or maybe they were simply not obvious), which might be ascribed to varying sample thicknesses. Mostly, it seems as if the basic structure of the lamellar phase is conserved in the CrM phase, but now being rigid. For all investigated chain lengths, it was reproducibly found that the birefringent, highly viscous texture of CrM changes gradually over a broad temperature range and that the material shrinks, meaning that the density of the substances increases continuously. This is exactly the behaviour expected for a surfactant gel ( $L_{\beta}$ ) phase with rigid and (mainly) all-trans alkyl chains.<sup>39</sup> On further cooling, ChC12 crystallizes entirely and forms a birefringent solid material with distinct texture (see Figure 5). This transition (CrM to Cr) extends over a relatively large temperature interval (approximately 8°C). Once the formation of Cr is complete, the texture does no longer change down to -20°C. The other soaps studied behave similarly in terms of the broad transition of CrM to Cr and the temperature insensitivity of Cr. In turn, while the transition temperatures are well reproducible, the texture of Cr looks different from time to time, which might indicate differing crystalline structures. Nevertheless, it can be concluded that the low-temperature phase of all studied ChC $m$  surfactants is solid crystalline.

#### V.2.4. NMR Spin-Spin Relaxation Time $T_{2eff}$

Proton ( $^1\text{H}$ ) NMR is little used to study crystalline and liquid crystalline phases because the non-averaged dipole-dipole couplings between all the hydrogens in the molecule result in the observation of broad spectra with few well-defined features.<sup>40-42</sup> However, the characteristic time constant ( $T_{2eff}$ ) for the decay of the NMR signal from the broad line feature (the free induction decay, FID) does reflect some “average” degree of molecular order. The more ordered the system, the lower the value of  $T_{2eff}$ . The intensity of the signal is directly proportional to the number of hydrogen atoms present in the system. Thus for two groups of hydrogens with different degrees of order there are two decays, each with a different  $T_{2eff}$  value and having intensities proportional to their concentration.<sup>42</sup> The  $T_{2eff}$  values can be derived from the time at which the normalized signal has decayed to  $1/e$  of the initial value. In previous studies on conventional surfactants the values of  $T_{2eff}$  have been found to be very different for different phase states. For crystalline surfactants, gel phases and lamellar phases the values were  $< 10 \mu\text{s}$ ,  $20\text{-}30 \mu\text{s}$ , and ca.  $100 \mu\text{s}$  respectively.<sup>42-44</sup> Normal liquids give values  $> 1 \text{ms}$ ; thus it is possible to distinguish between different phases, particularly when there is other information available on the phases present.

Principally, all curves follow a single decay which can be described as arising from a mixture of Gaussian and Lorentzian line shapes.<sup>40, 41</sup> Single decays are observed for most of the curves. But close to the phase boundaries some of the spectra show two different decays (see Appendix C.6 for details). Thus, it can be concluded that all three phases of neat choline carboxylate surfactants occurring between  $-20^\circ\text{C}$  and  $95^\circ\text{C}$  are truly mono-phasic, also the middle-temperature one (CrM). Fig. V.5 displays the  $T_{2eff}$  values determined for neat choline soaps at different temperatures on heating as well as on cooling.

In the low-temperature phase, the  $T_{2eff}$  relaxation rate is for all choline soaps studied rather fast ( $3\text{-}5 \mu\text{s}$ ), similar to values for other crystalline surfactants. In turn, this means that the molecular motion is almost completely restricted such as in well-ordered solid crystalline materials. Moreover, similar  $T_{2eff}$  relaxation times have been reported for crystalline polyethylenes.<sup>45</sup> Thus, the NMR measurements confirm the crystalline nature of the low-temperature phase. Further, with rising temperature, the  $T_{2eff}$  values increase suddenly by a factor of 4.5-6, in agreement with the transition temperatures obtained by DSC. The higher  $T_{2eff}$  times reflect a reduction of the molecular ordering and an

increment of the molecular motion. However, for liquid-crystalline materials, where the paraffinic chains possess the dynamics of liquid alkanes, the relaxation rates are too fast.

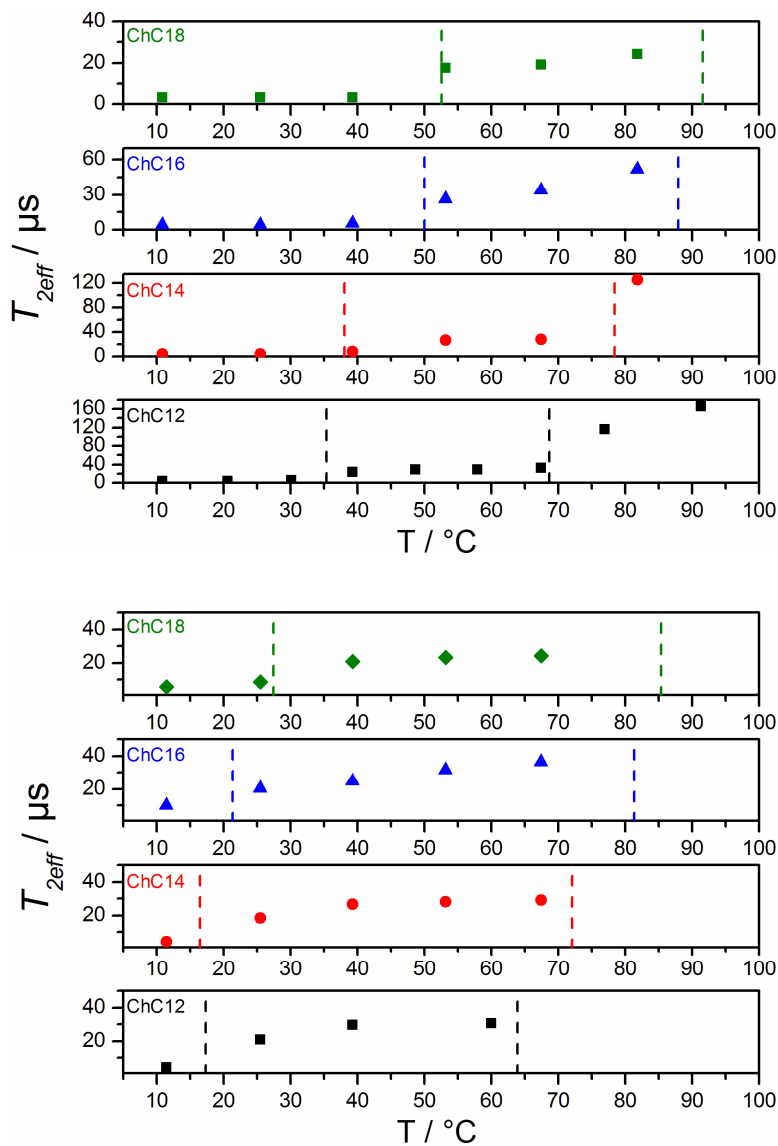


**Fig. V.5** Variation of the decay constant  $T_{2eff}$  of ChC $m$  surfactants ( $m=12-18$ ) with temperature. Data were obtained by heating (top) and cooling (bottom) freshly melted samples. The vertical lines indicate the transition temperatures as detected by DSC. The fast relaxation constants at low temperatures are typical for solid crystalline phases (Cr), while the slow ones at high temperatures are characteristic for liquid-crystalline compounds (SmA). The  $T_{2eff}$  values (20–30  $\mu$ s) of the middle-temperature phase (CrM) reflect an increased molecular motion as compared to solid crystalline materials, but still with a high degree of order and restricted molecular mobility (similar to the values for gel ( $L_\beta$ ) phases).

Obviously, the middle-temperature phase is featured by some degree of chain freedom and mobility, as seen for gel phases of other surfactants.<sup>43,44</sup> The  $T_{2eff}$  times of CrM range from 20-30  $\mu$ s for different  $m$  values and temperatures. No simple variation of  $T_{2eff}$  with varying alkyl chain length is obvious, as expected if a gel phase is formed. On further raising the temperature, the  $T_{2eff}$  values rise steeply to 100-200  $\mu$ s for ChC12 and ChC14, according to the phase transition temperatures measured by DSC. The longer  $T_{2eff}$  values of ChC12 and ChC14 in SmA and their temperature sensibility indicate a substantial increase of molecular dynamics. Generally, the order of magnitude of  $T_{2eff}$  in SmA is consistent with that of liquid-crystalline phases.<sup>45,46</sup>

### **V.2.5. X-ray Scattering as a Function of Temperature and Chain Length**

X-ray scattering provides a powerful method to elucidate structural details. Thereby, peaks at low angles reflect the superior packing of the molecules, i.e. lamellar, hexagonal, etc., whereas reflections at higher angles give evidence on the molecular level, i.e. on the packing and state of the hydrocarbon chains. Therefore, X-ray spectra covering a large  $q$  region were recorded for choline soaps as a function of temperature, on heating as well as on cooling. Fig. V.6 shows the small- and wide-angle X-ray scattering curves of ChC18 at various temperatures for two heating and cooling cycles. At low temperatures, all spectra display sharp reflections in the wide-angle regime, confirming the crystalline nature of the low-temperature phase. Upon increasing the temperature, the peaks at high angles gradually disappear and a bump arises at  $q \approx 15 \text{ nm}^{-1}$ , which indicates increasing disorder and fluidity of the hydrocarbon chains. At 90°C, the alkyl chains are finally molten and a lamellar liquid-crystalline phase is formed. On subsequent cooling, high-angle reflections reappear, proving the reproducibility of the phase transitions. Re-heating and re-cooling the sample generally leads to the same X-ray scattering profile as obtained for freshly-melted samples, with only slight deviations in some instances.

The thermotropic phase behavior is basically similar for the different  $m$  values (the temperature-dependent X-ray spectra of the other homologues ( $m=12-16$ ) can be found in Appendix C.7). All studied choline soaps are crystalline at low temperatures and melt gradually when increasing the temperature before eventually transforming to a lamellar liquid-crystalline phase.

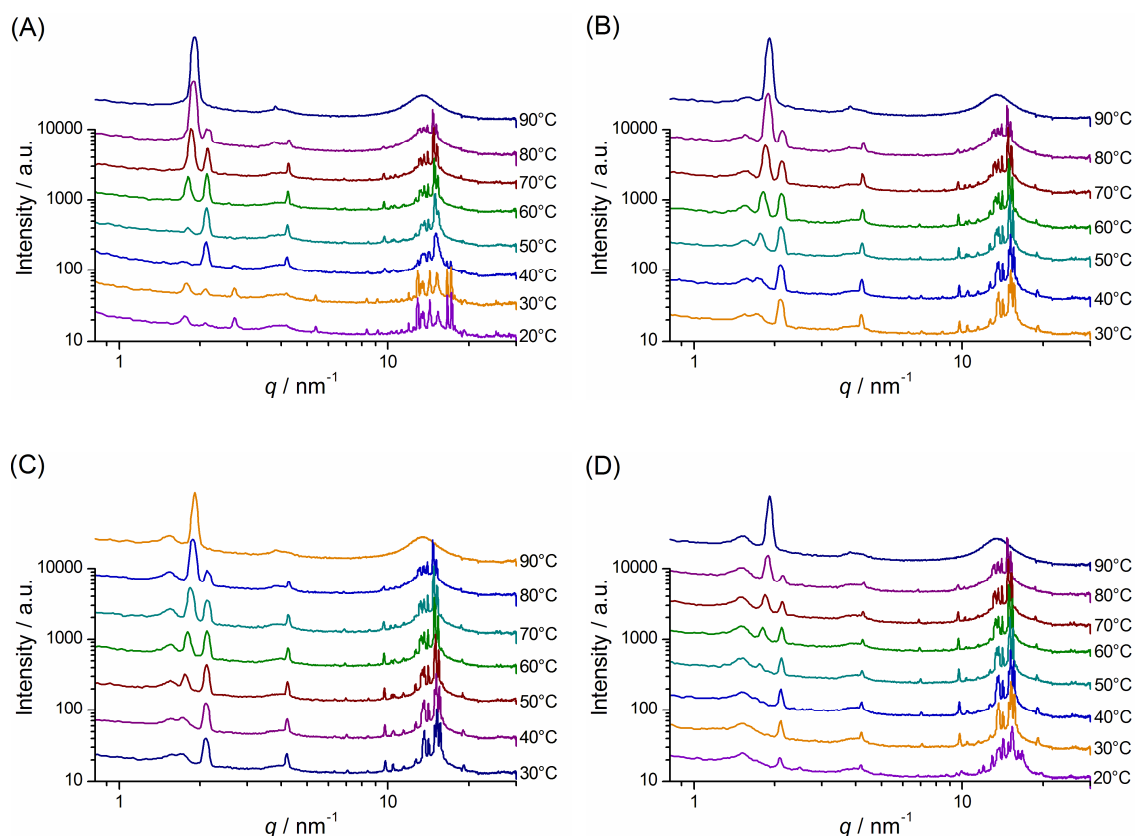


**Fig. V.6** X-ray spectra of neat ChC18 as a function of temperature, determined for two heating and cooling cycles: (A) first heating (freshly melted sample), (B) first cooling, (C) second heating and (D) second cooling. At low temperatures, several sharp high-angle reflections are present, which are typical for crystalline paraffinic chains. When raising the temperature, wide-angle peaks disappear stepwise, accompanied by the occurrence of a bump at around  $q = 15 \text{ nm}^{-1}$ . This indicates a gradual rather than a sharp melting of the hydrocarbon chains. At  $90^\circ\text{C}$ , the alkyl chains are finally molten as evidenced by the characteristic diffuse peak at  $q = 13.4 \text{ nm}^{-1}$ , and a lamellar liquid-crystalline phase is formed. The diverse heating and cooling cycles confirm the reproducibility of the phase transitions. Note that the bump at around  $q = 4 \text{ nm}^{-1}$  stems from the Kapton foil.

However, the distinct phase transition to SmA is in the X-ray spectra shifted to lower temperatures compared to the DSC investigation. For instance, the DSC yields a transition temperature of  $92.6^\circ\text{C}$  for ChC18, whereas the X-ray spectra show the liquid-crystalline lamellar phase already at  $90^\circ\text{C}$ . At this point, it has to be mentioned that the preparation of the samples for X-ray scattering experiments was, in contrast to the other experimental techniques, not carried out under inert atmosphere and that the specimen holder was sealed by Kapton foil. Attempts to measure in flame-sealed glass capillaries gave the problem of insufficient temperature control inside the sample due to

inhomogeneities of the powdery material. Thus, the present set of X-ray data suffers from partial hydration of the substances, which shifts the phase transitions to lower temperatures.

Although the present X-ray investigations need further refinement and should be considered rather as a starting point, the following conclusions on anhydrous ChC*m* soaps can already be drawn assuming that the presence of very small amounts of water does not alter the overall phase behavior:

1. At low temperatures, ChC*m* surfactants with  $m= 12-18$  are crystalline. Even though the details of the crystalline structure (whether it is monoclinic, orthorhombic, etc.) are not yet solved, the presence of one simple lamellar crystalline phase consisting of hydrocarbon chain bilayers sandwiched between the ionic layers, which is commonly observed for long-chain aliphatic compounds,<sup>47</sup> can be ruled out due to the presence of 3-4 small-angle reflections and their order of magnitude. The highest  $d$ -values range from 29.8 Å to 35.9 Å for  $m= 12-18$  at 20°C. Assuming a length of approximately 16.5 Å for a fully extended C<sub>11</sub>H<sub>23</sub>COO<sup>-</sup> molecule and about 14 Å for two choline ions, the crystalline structure likely consists of interdigitated monolayers rather than bilayers.
2. The existence of a conventional rotator or gel (L<sub>β</sub>) phase in the middle-temperature region (which occurs starting from 35-48°C, depending on  $m$ ) of anhydrous ChC*m* soaps can be excluded due to persistent presence of several sharp high-angle reflections. Conventional L<sub>β</sub> phases give only a single reflection in this region and are formed at higher water contents as evidenced by penetration scans of ChC*m* surfactants.<sup>7</sup> Small-angle reflections still indicate the presence of interdigitated monolayers.
3. At high-temperatures (above 68-93°C, depending on  $m$ ), a lamellar liquid-crystalline phase is formed, which agrees with the results gathered by the other experimental techniques.

Considering the two sharp phase transitions monitored by DSC, the temperature-dependent X-ray profiles confirm the melting at high temperatures to liquid crystals, however at more or less shifted temperatures. In contrast, the sharp phase transition identified in the DSC curves at low temperatures is not obvious at first glance in the diffraction pattern. Reflections at low as well as at high angles vanish upon heating, but in a stepwise rather than abrupt manner between one of the 10°C steps. The persistence

of the wide-angle peaks in the temperature range of CrM agrees well with the limited molecular mobility deduced from the spin-spin relaxation constants and the high viscosity suggested by the microscopy investigations. Consequently, the middle-temperature phase CrM is probably characterized by a certain degree of chain flexibility, although maybe the paraffinic chains and also the polar layer are still arranged in a crystalline lattice.

Going into detail on the high-temperature lamellar liquid-crystalline phase, Fig. V.7 shows that the interlayer spacing  $d$  increases with growing number of carbon atoms in the alkyl chains according to Equation (V.1) (determined at 90°C by a least square linear fit ( $R=0.9957$ )).

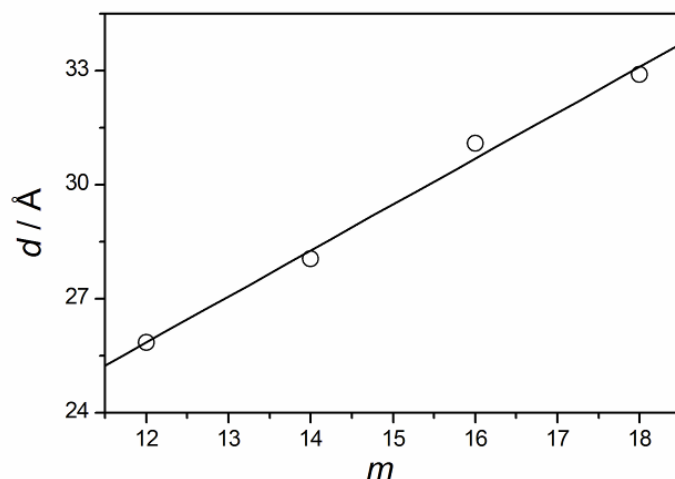


**Fig. V.7** Lamellar interlayer spacing  $d$  of neat choline soaps as a function of alkyl chain length  $m$  at 90°C.

$$d / \text{Å} = (11 \pm 1) + (1.21 \pm 0.08) m \quad (\text{IV.1})$$

Per additional  $\text{CH}_2$  group the bilayer grows by 1.21 Å, which is in good agreement to values reported in literature for the length of one “liquid”  $\text{CH}_2$  group (1.26 Å).<sup>48</sup> Extrapolation to  $m=0$  yields the thickness of the polar layer  $d_0$  (choline and carboxylate headgroup). The obtained value of  $d_0=11$  Å appears reasonable when considering the length of a fully extended choline ion ( $\approx 7\text{-}9$  Å). Using as an approximation the molecular volumes of choline soaps in the aqueous phase region (see Chapter IV),<sup>7</sup> the thickness of the lipophilic bilayer  $d_L$  and the cross-sectional area  $a_S$  at the polar-nonpolar interface can be estimated.<sup>7</sup> Results are listed in Table V.2.

**Table V.2** Thickness of the lipophilic ( $d_L$ ) bilayer and polar ( $d - d_L$ ) layer and the cross-sectional area ( $a_S$ ) at the polar-nonpolar interface of lamellar liquid crystalline phase formed by neat ChC*m* soaps ( $m= 12-18$ ) at 90°C.

$m$	$d_L / \text{Å}$	$d - d_L / \text{Å}$	$a_S / \text{Å}^2$
12	16.2	9.6	39.8
14	18.6	9.4	40.5
16	21.5	9.6	40.2
18	23.5	9.4	41.3

The paraffinic chains adapt 51-52% of the length of the respective fully extended alkyl chain,<sup>48</sup> indicating a highly disordered state.<sup>39</sup> The cross-sectional area  $a_S$  varies in a non-linear manner for different  $m$  values between 39.8 Å<sup>2</sup> and 41.3 Å<sup>2</sup>. The  $a_S$  values seem to be in the same order of magnitude as those of sodium and potassium soaps, which range from 35.7 Å<sup>2</sup> to 42 Å<sup>2</sup> but were determined at much higher temperatures (271-310°C).<sup>26, 49</sup> Thus, the cross-sectional areas of choline soaps in SmA at 90°C are judged to be rather large, most probably due to the bulkiness of the choline ion. The calculation of the polar layer leads to values around 9.5 Å and deviates therewith slightly to that obtained by the linear regression of the interlayer spacing. This can most probably be ascribed to the error resulting from the approximation of the molecular volumes.

### V.2.6. Transition Enthalpies and Entropies

Plots of the transition enthalpies and entropies obtained by DSC are shown in Fig. V.8 as a function of the alkyl chain length  $m$ . For both transitions, the enthalpies and entropies vary linearly with  $m$  (listed  $\Delta H$  values can be found in Appendix C.4). The transition enthalpy of Cr to CrM decreases with growing paraffinic chain length by 1.5 kJ mol<sup>-1</sup> per CH<sub>2</sub> group from 28.1 kJ mol<sup>-1</sup> for  $m= 12$  down to 19.2 kJ mol<sup>-1</sup> for  $m= 18$ . In contrast, enthalpies of CrM to SmA increase by 1.3 kJ mol<sup>-1</sup> per CH<sub>2</sub> group from 9.0 kJ mol<sup>-1</sup> for  $m= 12$  to 16.8 kJ mol<sup>-1</sup> for  $m= 18$ . An increase of  $\Delta H$  with growing alkyl chain length can be likely deduced to increasing Van-der-Waals interactions. However, a decrease of  $\Delta H$  with larger  $m$  values, as observed for the conversion from Cr to CrM, has not been reported to the best of our knowledge for mono-ionic surfactants.

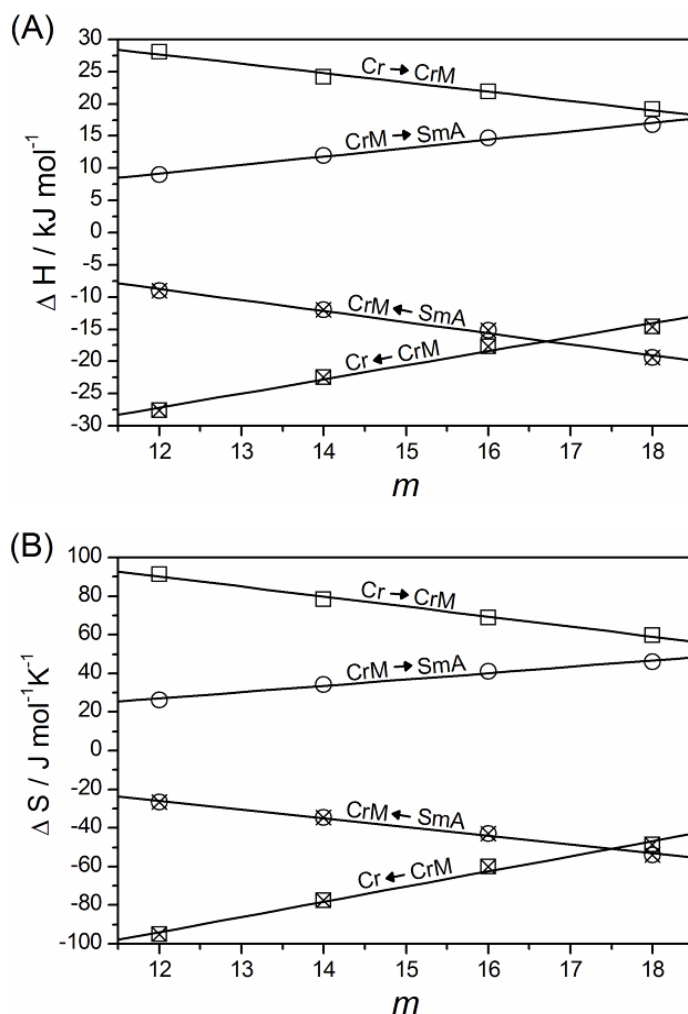


**Fig. V.8** Transition enthalpies (A) and entropies (B) of choline soaps as a function of the alkyl chain length  $m$ . Data were obtained from DSC scans between  $-20^\circ\text{C}$  and  $95^\circ\text{C}$  for re-heated samples. Empty symbols mark enthalpies and entropies on heating ( $(\square)$  crystal (Cr)  $\rightarrow$  semi-crystalline (CrM) and  $(\circ)$  CrM  $\rightarrow$  liquid crystal (smecticA (SmA)), and crossed symbols those on cooling ( $(\boxplus)$  CrM  $\rightarrow$  Cr,  $(\boxtimes)$  SmA  $\rightarrow$  CrM).

The comparatively large transition enthalpies of Cr to CrM (76%-53% of the total enthalpy change) indicate that the paraffinic chains are considerably disordered and partially molten in CrM. Only from that, one may conclude that the middle-temperature phase corresponds to a conventional  $L_\beta$  phase,<sup>39,50</sup> in which specific chain-chain interactions are lost and individual carbon atoms are able to rotate a few degrees within a hexagonal or quasi-hexagonal lattice.<sup>50</sup> The assignment would also agree with the magnitude of  $\Delta H$  (CrM  $\rightarrow$  SmA) and the conversion to liquid crystals. However, the X-ray profiles of CrM still show several sharp high-angle reflections instead of one at  $4.2 \text{ \AA}$  and thus suggest a certain degree of crystallinity. This must involve the ionic groups, the major source of anisotropy. Neither the carboxylate headgroup nor the

choline ion possesses circular symmetry. Most probably, the hydroxyl group of choline is connected by a hydrogen bond to the COO<sup>-</sup> headgroup. Consequently, there will be differing arrangements of head groups in the plane perpendicular to the director – i.e. the crystalline phase is biaxial. Some of this structure could be carried over into the CrM phase, meaning that the CrM phase is also biaxial, and giving additional X-ray reflections in the high-angle region.

When comparing the sum of the enthalpies (see Table V.3) with those of linear paraffins, the total enthalpy change of ChC12 (37.1 kJ mol<sup>-1</sup>) equals approximately that of dodecane fusion (36.8 kJ mol<sup>-1</sup>).<sup>26</sup> Also, the total entropy change of ChC12 (117.3 J K<sup>-1</sup>mol<sup>-1</sup>) complies well with a liquid-like state of the alkyl chains at high temperatures, being in the order of magnitude of dodecane or dodecanoic acid melting.<sup>26</sup> It is worth noting that the enthalpy variation on cooling is slightly lower than on heating (cf. Table V.3), similarly as observed by Amorim Da Costa *et al.*,<sup>35</sup> although changes are probably within the experimental error.

**Table V.3** Sum of the enthalpies of ChC $m$  surfactants ( $m= 12-18$ ) obtained for re-heated samples from DSC scans between -20 and 95°C.

	$\sum\Delta H_{\text{heat}} /$ $\text{kJ mol}^{-1}$	$\sum\Delta H_{\text{cool}} /$ $\text{kJ mol}^{-1}$	$\sum\Delta S_{\text{heat}} /$ $\text{J K}^{-1} \text{mol}^{-1}$	$\sum\Delta S_{\text{cool}} /$ $\text{J K}^{-1} \text{mol}^{-1}$
<b>ChC12</b>	37.1	-36.6	117.6	-121.9
<b>ChC14</b>	36.2	-34.5	112.5	-112.3
<b>ChC16</b>	36.6	-32.9	109.9	-103.0
<b>ChC18</b>	36.0	-34.0	105.7	-102.8

Surprisingly, the total enthalpy change (Table V.3) does not increase with growing alkyl chain length as actually would have been expected.<sup>21</sup> There are several feasible scenarios potentially explaining this discrepancy.

Either, choline carboxylates with  $m > 12$  are not in a liquid-crystalline state at high temperatures. However, this can likely be ruled out in light of the results obtained by other techniques.

Alternatively, choline soaps with longer alkyl chains could possess another crystalline phase at temperatures lower than -20°C. This is also considered to be unlikely with

regard to the complete melting of ChC12 and the linear relationship between the transition temperatures and enthalpies and the alkyl chain length.

Another possible reason refers to the nature of the crystalline phase. In the low-temperature crystalline phases of alkali soaps, the paraffinic chains commonly adopt the minimum-energy *all-trans* configuration.<sup>51-53</sup> Since with increasing alkyl chain length the probability of an *all-trans* configuration decreases, not all CH<sub>2</sub> groups are probably in the low-energy *all-trans* state for larger *m* values, which seems particularly possible with choline as counterion due the large cross-sectional area at the polar-nonpolar interface (compared to alkali soaps).<sup>7</sup> The partial “kinked” alkyl chain conformation allows a less efficient regular crystalline packing. Thus, the crystal lattice energy is lower for the longer-chain homologues, which is consistent with the decrease of  $\Delta H$  (Cr  $\rightarrow$  CrM) and the more or less constant total enthalpy change with increasing alkyl chain length. This hypothesis would also fit to the approximately constant total enthalpy change described for the different chain-length homologues of potassium soaps.<sup>54</sup> The two to three different polymorphic crystalline phases of potassium alkanates mainly differ by their number of hydrocarbon chain conformations.<sup>18</sup> Unfortunately, only the crystalline phases of KC10 and their respective transitions have been investigated in detail,<sup>51,53</sup> such that a comparison to the longer-chain derivatives cannot be established at the moment.

The uncommon decrease of  $\Delta H$  (Cr  $\rightarrow$  CrM) with growing alkyl chain length could also rely on different degrees of disorder of CrM. In this case, CrM of ChC12 would be featured by a higher hydrocarbon chain flexibility than ChC18, possibly resulting from enhanced van-der-Waals interactions. However, such a scenario would not explain the constant total enthalpy change, which supports the above hypothesis of different energy contents in the crystalline state.

### **V.2.7. Comparison to Alkali Soaps**

Generally, the thermotropic phase behavior of alkali soaps is complex and does not follow a simple trend with growing cation size. For instance, sodium alkanates start forming diverse ribbon phases at around 100-117°C and melt not into a lamellar phase until 255-257°C.<sup>19-21,32,38</sup> On the other hand, cesium alkanates melt from a polymorphic crystalline directly into a lamellar liquid-crystalline phase.<sup>28</sup> One rough property of the thermal mesomorphism of alkali soaps is that with increasing cation size

the lamellar arrangement becomes the major upper-temperature mesophase.<sup>26</sup> In that context, choline can be considered as a continuation of this trend. Like cesium soaps, anhydrous choline carboxylates show only one mesophase (lamellar) upon heating, but at substantially lower temperatures. ChC12, for instance, melts at 68.4°C into a lamellar liquid-crystalline phase, whereas CsC12 requires 278°C.<sup>28</sup> Actually, all investigated choline surfactants transform to a lamellar mesophase below 100°C and may thus be regarded as ionic liquids. This is generally consistent with the recent study of Petkovic *et al.* who found that short-chain choline alkanoates ( $m= 2-10$ ) are ionic liquids with melting temperatures ranging from 26°C to 80°C.<sup>14</sup> However, the reported melting temperatures correspond to the formation of an isotropic liquid phase. Since it has not been the focus of their study, the authors did not report thermotropic mesophases, which are supposed to be formed at least by ChC10 or ChC8.

### V.3. Conclusion

Choline soaps with chain lengths of  $m= 12-18$  were shown to exhibit three distinct phases between -20 and 95°C. Both phase transitions involve major enthalpy changes. At low temperatures, a crystalline phase (Cr) was identified, consisting probably of interdigitated monolayers with biaxial arrangement due to a feasible hydrogen bond between the choline ion and the carboxylate headgroup, both having non circular symmetry. The formation of the middle-temperature phase (CrM) occurs at 35°C for  $m= 12$  and shifts linearly to higher temperatures up to 48°C for  $m= 18$ . The corresponding transition enthalpies decrease linearly in an uncommon fashion with growing hydrocarbon chain length, from 28.1 kJ mol<sup>-1</sup> for  $m= 12$  down to 19.2 kJ mol<sup>-1</sup> for  $m= 18$ . This decrease is may originate from different degrees of molecular ordering or packing in Cr when varying the alkyl chain length, which however remains to be proven. NMR investigations revealed an enhanced but still limited molecular mobility of CrM, which was found to be slightly sensitive to temperature. Optical polarizing microscopy images of CrM showed highly viscous birefringent textures (partially containing crystallites), which change gradually with temperature. The collected X-ray spectra indicate a gradual melting of the alkyl chains on heating over a large range of temperature, and rule out the presence of a conventional rotator phase ( $L_{\beta}$ ). We suppose that CrM is a biaxial semi-crystalline phase consisting of interdigitated monolayers with properties similar but not equal to a common gel phase. Probably the polar layer still

retains some order in CrM and the paraffinic chains are in view of the considerable enthalpy changes partially molten (the more the higher the temperature).

The second phase transition occurs at 68°C for  $m=12$  and shifts linearly with increasing  $m$  towards higher temperatures up to 93°C for  $m=18$ , with enthalpy values of 9.0-16.8 kJ mol<sup>-1</sup>. Optical polarizing microscopy, spin-spin relaxation constants  $T_{2eff}$  and X-ray spectra confirms that this transition corresponds to the complete melting of paraffinic chains and the formation of a lamellar liquid-crystalline phase (smectic A).

Consequently, with regard to the size of the choline ion, choline soaps are in line with the trend of the alkali soap series, where the number of mesophases diminishes with growing cation size and mainly a lamellar liquid-crystalline phase is formed. However, the melting to liquid crystals is considerably shifted to lower temperatures with choline as counterion in fatty acid soaps. The traced thermotropic mesomorphism thus confirms the low melting temperatures of short-chain choline alkanoates and shows that even choline alkanoates with chain lengths of  $m=12-18$  may be classified as ionic liquids.

## V.4. Experimental

### V.4.1. Materials

ChCm surfactants with  $m=12-18$  were synthesized and purified as described in Chapter II. The salts were obtained as white crystalline, hygroscopic powders and were subsequently stored in a nitrogen glove box.

### V.4.2. Methods

#### V.4.2.1. Decomposition Temperatures ( $T_{dec}$ )

Decomposition temperatures ( $T_{dec}$ ) were measured using a thermogravimetric analyzer from Perkin-Elmer (TGA 7). Data were collected under a constant nitrogen flow with a heating rate of 10 K min<sup>-1</sup>.  $T_{dec}$  was taken as the onset of the mass loss and has been determined by the intersection of the baseline before decomposition and the tangent to the mass loss versus temperature in the following. The experimental curves are shown in Appendix C.1.

#### **V.4.2.2. Differential Scanning Calorimetry (DSC)**

Differential scanning calorimetry (DSC) data were recorded on a Perkin-Elmer DSC 7. Approximately 10-20 mg sample were filled in aluminum pans and sealed in a nitrogen glove box. Scans were conducted in a temperature interval ranging from -20 to 95°C with a heating and cooling rate of 1°C min<sup>-1</sup>. At least three cycles were recorded for each compound. Temperature and enthalpy calibration was performed by measuring indium as a standard. Raw data were corrected for the empty aluminum pan in order to achieve a flat baseline. The position of the peak maximum was taken as transition temperature. Transition enthalpies were obtained by integrating over the whole peak area and calculated taking into account the known heating and cooling rate, the employed sample mass and the molar mass of the substance.

#### **V.4.2.3. Polarizing Optical Microscopy**

Optical microscopy was carried out on a Leitz Orthoplan microscope (Wetzlar, Germany) equipped with a JVC digital camera (TK-C130) and a Linkham hot stage operated with a TMS90 temperature controller ( $\pm 0.5^\circ\text{C}$ ) and a CS196 cooling system. The heating and cooling rate was 10°C min<sup>-1</sup> in all experiments. Small amounts of the crystalline choline salts were trapped between microscopy slides under a nitrogen atmosphere. Measurements were conducted under a continuous nitrogen flow in order to prevent contact with air humidity. At least two heating and cooling cycles were recorded for each sample.

#### **V.4.2.4. NMR Spectroscopy**

NMR measurements were performed on a bench-top Maran Ultra NMR Spectrometer, which can be operated with either a proton or deuterium probe (10 mm diameter, 23.3 MHz and 3.66 MHz respectively). The spectrometer was equipped with a centrifugal and membrane dryer to allow temperature cooling to 5°C ( $\pm 0.5^\circ\text{C}$ ). Powdered anhydrous choline salts were filled under a nitrogen atmosphere into high-precision NMR tubes from Wilmad Glass (10 mm diameter, 8 cm height), which were immediately flame sealed. The optimum sample depth was determined to be 8 mm. The number of scans for each spectrum was 32 with 1024 data points and a spectrum width of 2 MHz.

#### V.4.2.5. X-ray Scattering

X-ray scattering measurements were conducted with X-ray radiation provided by a sealed molybdenum tube (wavelength  $\lambda = 0.71 \text{ \AA}$ ) on a bench built by XENOCES. The scattered beam was detected by a large two-dimensional automatic image plate system (MAR 345, MAR Research, diameter: 345 mm), having a resolution of  $150 \times 150 \text{ \mu m}$ . Given a sample-to-detector distance of 750 mm and due to an off-centered detection, the accessible  $q$ -region was  $0.2\text{-}30 \text{ nm}^{-1}$  with an experimental resolution of  $\Delta q/q = 0.05$ . The used collimation system was a  $12:\infty$  multilayer XENOCES mirror coupled to two sets of FORVIS scatterless slits,<sup>55</sup> which reduces the beam area to  $0.8 \times 0.8 \text{ mm}^2$ . Samples were mounted in aluminum cells of 3 mm thickness sealed with Kapton foil. The acquisition time varied between 900-3600 s. Data are shown without empty cell subtraction since the investigated samples were of crystalline or liquid crystalline nature and only peak positions were important to determine. Two-dimensional spectra were integrated using the FIT2D software in order to obtain the scattered intensity as a function of the scattering vector  $q$ , which is defined as  $q = 4\pi/\lambda \cdot \sin(\theta/2)$  with  $\theta$  being the scattering angle. Temperature control was achieved by a home-built apparatus equipped with a heater resistance coupled to a Pelletier cooling base, allowing a temperature range of  $-10^\circ\text{C}$  up to  $120^\circ\text{C}$  with  $\Delta T = \pm 5^\circ\text{C}$ .

### V.5. References

1. J. L. Ranck, L. Mateu, D. M. Sadler, A. Tardieu, T. Gulik-Krzywicki, V. Luzzati, *J. Mol. Biol.*, 1974, **85**, 249.
2. A. Tardieu, V. Luzzati, F. C. Reman, *J. Mol. Biol.*, 1973, **75**, 711.
3. T. Gulik-Krzywicki, A. Tardieu, V. Luzzati, *Mol. Cryst. Liquid Cryst.*, 1969, **8**, 285.
4. V. Luzzati, T. Gulik-Krzywicki, A. Tardieu, *Nature*, 1968, **218**, 1031.
5. R. Klein, D. Touraud, W. Kunz, *Green Chem.*, 2008, **10**, 433.
6. R. Klein, M. Kellermeier, M. Drechsler, D. Touraud, W. Kunz, *Colloids Surf. A*, 2009, **338**, 129.

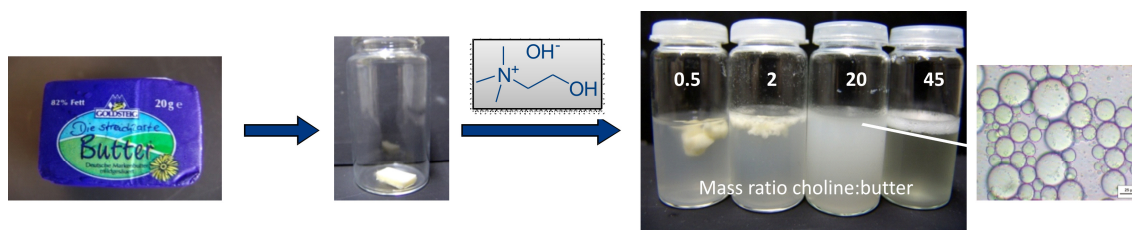
7. R. Klein, G. J. T. Tiddy, E. Maurer, D. Touraud, J. Esquena, O. Tache, W. Kunz, *Aqueous Phase Behavior of Choline Carboxylate Surfactants - Exceptional Variety and Extent of Cubic Phases*, accepted by *Soft Matter*.
8. A. P. Abbott, D. Boothby, G. Capper, D. L. Davies, R. K. Rasheed, *J. Am. Chem. Soc.*, 2004, **126**, 9142.
9. A. P. Abbott, G. Capper, D. L. Davies, R. K. Rasheed, V. Tambyrajah, *Chem. Commun.*, 2003, 70.
10. D. Constantinescu, K. Schaber, F. Agel, M. H. Klingele, T. J. S. Schubert, *J. Chem. Eng. Data*, 2007, **52**, 1280.
11. P. Nockemann, B. Thijs, K. Driesen, C. R. Janssen, K. Van Hecke, L. Van Meervelt, S. Kossmann, B. Kirchner, K. Binnemans, *J. Phys. Chem. B*, 2007, **111**, 5254.
12. K. D. Weaver, H. J. Kim, J. Sun, D. R. MacFarlane, G. D. Elliott, *Green Chem.*, 2010, **12**, 507.
13. J. Pernak, A. Syguda, I. Mirska, A. Pernak, J. Nawrot, A. Pradzynska, S. Griffin, R. Rogers, *Chem. Eur. J.*, 2007, **13**, 6817.
14. M. Petkovic, J. L. Ferguson, H. Q. N. Gunaratne, R. Ferreira, M. C. Leitao, K. R. Seddon, L. P. N. Rebelo, C. S. Pereira, *Green Chem.*, 2010, **12**, 643.
15. Y. Fukaya, Y. Iizuka, K. Sekikawa, H. Ohno, *Green Chem.*, 2007, **9**, 1155.
16. K. Binnemans, *Chem. Rev.*, 2005, **105**, 4148.
17. B. Gallot, A. Skoulios, *Compt. Rend.*, 1965, **260**, 3033.
18. B. Gallot, A. Skoulios, *Kolloid Z. Z. Polym.*, 1966, **210**, 143.
19. A. Skoulios, V. Luzzati, *Nature*, 1959, **183**, 1310.
20. R. D. Vold, *J. Am. Chem. Soc.*, 1941, **63**, 2915.
21. P. Pacor, H. L. Spier, *J. Amer. Oil Chem. Soc.*, 1968, **45**, 338.
22. A. R. Ubbelohde, H. J. Michels, J. J. Duruz, *Nature*, 1970, **228**, 50.
23. T. A. Mirnaya, V. D. Prisyazhnyi, V. A. Shcherbakov, *Usp. Khim.*, 1989, **58**, 1429.
24. K. Shinoda, Y. Minegishi, H. Arai, *J. Phys. Chem.*, 1976, **80**, 1987.

25. M. J. Vold, *J. Am. Chem. Soc.*, 1943, **65**, 465.
26. D. M. Small, *Handbook of Lipid Research 4: The Physical Chemistry of Lipids*, Plenum Press, New York, 1986, pp. 285-343.
27. B. Gallot, A. Skoulios, *Kolloid Z. Z. Polym.*, 1966, **209**, 164.
28. B. Gallot, A. Skoulios, *Kolloid Z. Z. Polym.*, 1966, **213**, 143.
29. B. Gallot, A. Skoulios, *Mol. Cryst.*, 1966, **1**, 263.
30. J. W. McBain, W. W. Lee, *Oil Soap*, 1943, **20**, 17.
31. J. W. McBain, W. C. Sierichs, *J. Am. Oil Chem. Soc.*, 1948, **25**, 221.
32. C. Madelmont, R. Perron, *Colloid Polym. Sci.*, 1976, **254**, 581.
33. K. N. Mehrotra, M. S. Rajpurohit, V. K. Godara, *J. Macromol. Sci., Chem.*, 1983, **A19**, 181.
34. R. Klein and W. Kunz, *unpublished results*.
35. A. M. Amorim da Costa, H. D. Burrows, C. F. G. C. Geraldès, J. J. C. Teixeira-Dias, C. G. Bazuin, D. Guillon, A. Skoulios, E. Blackmore, G. J. T. Tiddy, D. L. Turner, *Liq. Cryst.*, 1986, **1**, 215.
36. F. Mathevet, P. Masson, J.-F. Nicoud, A. Skoulios, *J. Am. Chem. Soc.*, 2005, **127**, 9053.
37. C. G. Bazuin, D. Guillon, A. Skoulios, A. M. Amorim da Costa, H. D. Burrows, C. F. G. C. Geraldès, J. J. C. Teixeira-Dias, E. Blackmore, G. J. T. Tiddy, *Liq. Cryst.*, 1988, **3**, 1655.
38. M. J. Vold, M. Macomber, R. D. Vold, *J. Am. Chem. Soc.*, 1941, **63**, 168.
39. S. Hassan, W. Rowe, G. J. T. Tiddy, in *Handbook of Applied Surface and Colloid Chemistry*, Ed. K. Holmberg, John Wiley & Sons Ltd., Chichester 2002, pp. 465-508.
40. H. Wennerstrom, *Chem. Phys. Lett.*, 1973, **18**, 41.
41. M. Bloom, E. E. Burnell, S. B. W. Roeder, M. I. Valic, *J. Chem. Phys.*, 1977, **66**, 3012.
42. C. D. Adam, J. A. Durrant, M. R. Lowry, G. J. T. Tiddy, *J. Chem. Soc., Faraday Trans. 1*, 1984, **80**, 789.

43. E. S. Blackmore, G. J. T. Tiddy, *Liq. Cryst.*, 1990, **8**, 131.
44. K. Rendall, G. J. T. Tiddy, M. A. Trevethan, *J. Chem. Soc., Faraday Trans. 1*, 1983, **79**, 637.
45. I. Kamel, A. Charlesby, *J. Polym. Sci., Polym. Phys. Ed.*, 1981, **19**, 803.
46. R. Y. Dong, M. Wiszniewska, E. Tomchuk, E. Bock, *J. Chem. Phys.*, 1973, **59**, 6266.
47. A. I. Kitaigorodskii, *Organic Chemical Crystallography*, Consultant Bureau, New York, 1961, p. 180.
48. C. Tanford, *J. Phys. Chem.*, 1972, **76**, 3020.
49. A. Skoulios, V. Luzzati, *Acta Crystallogr.*, 1961, **14**, 278.
50. D. M. Small, *J. Lipid Res.*, 1984, **25**, 1490.
51. D. M. Glover, *Acta Crystallogr., Sect. A*, 1981, **A37**, 251.
52. T. R. Lomer, *Acta Crystallogr.*, 1952, **5**, 11.
53. T. Ishioka, H. Wakisaka, T. Saito, I. Kanesaka, *J. Phys. Chem. B*, 1998, **102**, 5239.
54. D. M. Glover, T. R. Lomer, *Mol. Cryst. Liq. Cryst.*, 1979, **53**, 181.
55. Y. Li, R. Beck, T. Huang, M. C. Choi, M. Divinagracia, *J. Appl. Crystallogr.*, 2008, **41**, 1134.



## Chapter VI Solubilization of Stearic Acid by the Organic Base Choline



As shown in Chapter I, the substitution of alkali ions in common fatty acid soaps by choline as counterion of biological origin increases the solubility of the respective soaps without lowering the biocompatibility. Nevertheless, while choline dodecanoate (ChC12), myristate (ChC14), and palmitate (ChC16) have Krafft points below room temperature or even under  $0^\circ\text{C}$ , choline stearate (ChC18) was not soluble below  $40^\circ\text{C}$ . In this chapter it will be shown that an excess of choline hydroxide is able to solubilize choline stearate at temperatures as low as  $14^\circ\text{C}$ . The results are compared to those obtained for the sodium and potassium salts of fatty acids with molar ratios of base to acid higher than 1:1. In order to elucidate the solubilization process with regard to specific counterion binding to the carboxylic headgroup, the effect of different chloride salts on the solubility of choline stearate was investigated. The findings indicate that the cation affinity to the carboxylate headgroup follows the trend  $\text{Na}^+ > \text{K}^+ \gg \text{Ch}^+$ . The results are discussed in terms of hydrolysis of the fatty acids in combination with Collins' concept of "matching water affinities". As a feasible application of choline base, the saponification and simultaneous solubilization of butter as an example of a hardly soluble triglyceride is presented.

## VI.1. Introduction

As shown in Chapter I, choline carboxylate (ChC $m$ ) surfactants are highly soluble in water with Krafft temperatures below room temperature up to  $m = 16$  and partly even below 0°C.<sup>1</sup> However, the Krafft point of choline stearate (ChC18) is still above room temperature ( $T_{Kr}(\text{ChC18}) = 40^\circ\text{C}$ ). McBain and Sierichs have shown that by addition of small amounts of potassium hydroxide to potassium carboxylate solutions, the protonation of the fatty acid ion (“hydrolysis reaction”) is completely suppressed.<sup>2</sup> As a consequence, the solubility temperature of, for example, potassium stearate (KC18) decreases from around 60°C to 47.5°C. Furthermore, a similar but less pronounced effect was observed when substituting potassium hydroxide by potassium chloride. On the other hand, if sodium hydroxide is added in minor fractions to sodium carboxylate soaps, the protonation is also suppressed, but the solubility temperature of the respective surfactants is not influenced noticeably.<sup>2,3</sup> Moreover, for instance, Lin *et al.* showed that the addition of sodium chloride to sodium myristate (NaC14) worsens the solubility of the soap.<sup>4</sup>

Considering the different behavior of sodium and potassium hydroxide with respect to soap solubility, likely two effects are operating. One is the suppression of carboxylate protonation. The other is most probably a “salting-in” or “salting-out” effect of the respective cation.

Based on these observations, the solubility of choline stearate as a function of choline hydroxide addition has been studied. In order to shed light on the solubilization process and to distinguish between hydrolysis and specific ion-ion interactions, the choline base was replaced in a second set of experiments by the different chloride salts of sodium, potassium and choline. Furthermore, the results are compared with those of the corresponding sodium and potassium soaps. As a potential application of choline base, the saponification and simultaneous solubilization of butter as an example of a hardly soluble triglyceride is presented.

## VI.2. Results and Discussion

### VI.2.1. Influences of Different Hydroxides on Soap Solubility

In Fig. VI.1, the solubility temperatures of stearic and lauric acid are displayed as a function of added choline, sodium and potassium hydroxide. For studying the effect of sodium hydroxide, lauric acid was considered as more suitable than stearic acid, since the Krafft temperatures reach more than 90°C upon addition of NaOH in the latter case. Such high transition temperatures are hard to determine accurately in aqueous solutions. Nevertheless, the observed tendencies are the same for both fatty acids. Addition of the different hydroxides in excess to the respective soap systems obviously leads to considerably differing results, as visualized by Fig. VI.1.

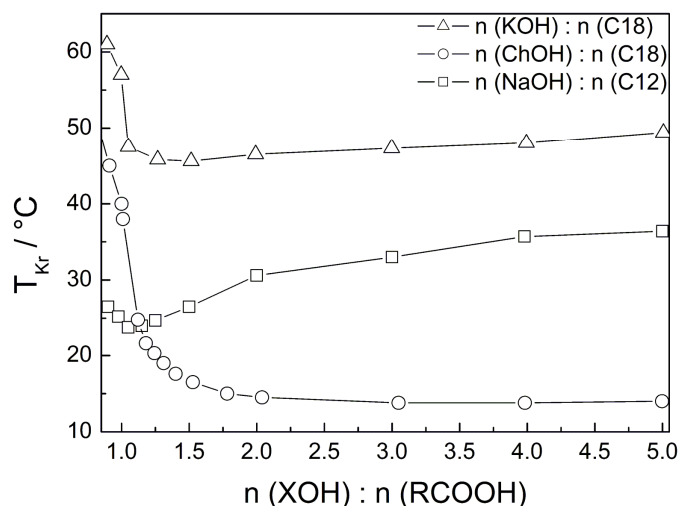


**Fig. VI.1** Krafft temperature  $T_{Kr}$  as a function of the molar ratio of NaOH ( $\square$ ), KOH ( $\Delta$ ) and ChOH ( $\circ$ ) to stearic and lauric acid, respectively (fatty acid concentration fixed at 1 wt%).

In the case of the NaC12 system, a small excess of NaOH does not reduce the solubility temperature of the surfactant by more than 1°C, from 25°C to 24°C. These findings agree well with those of McBain *et al.*<sup>2</sup> Continued addition of NaOH results in a re-increase of the system's clearing temperature, first rapidly and then moderately. If samples with more than 50 mol% excess of NaOH are left to stand for 24 h at ambient temperature, solutions turn into solid white masses, indicating that the volume fraction increases quickly upon addition of sodium hydroxide. For KC18, we observed, in analogy to McBain *et al.*, that a small excess (~ 5 mol%) of potassium hydroxide is able to reduce the solubility temperature from 57°C to 47.5°C. Further addition of KOH

produces initially a decrease to even lower Krafft temperatures (down to 45.5°C), followed by a gradual increase again up to 49.5°C. Solutions of KC18 remain liquid upon addition of KOH and storage for 24 h at ambient temperatures, unlike the viscosity increment observed for the studied sodium system. In the case of ChC18, the presence of excess choline hydroxide exerts a strongly pronounced effect on the respective soap solubility. At 11 mol% excess of choline base, choline stearate becomes soluble already at 25°C. Continued choline base addition leads to solubility temperatures of ChC18 of as low as 14°C that remain more or less constant also at very high ChOH fractions. Consequently, it is possible to observe choline stearate micelles at or below 25°C, if the molar ratio of base to acid is chosen higher than 1:1. Cryo-transmission electron micrographs indicate that in aqueous solutions of ChC18 with a 200 mol% excess of choline base, spherical micelles of an approximate radius of 2 nm are present, as shown by Fig. VI.2.

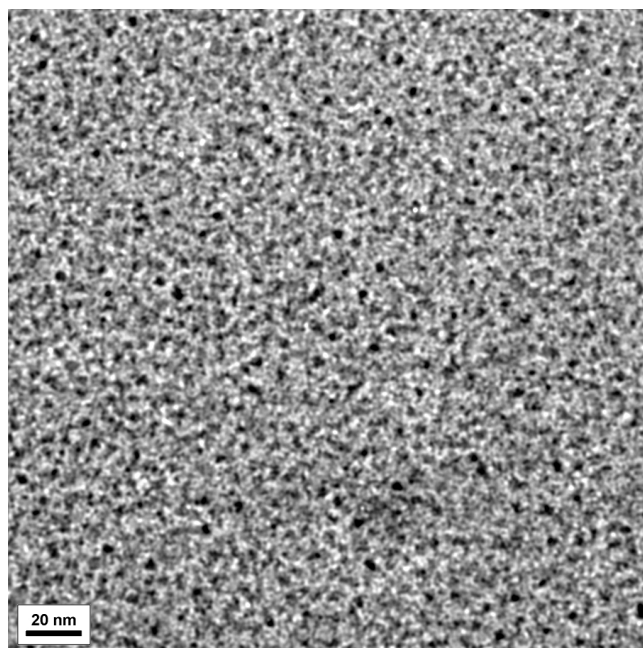


**Fig. VI.2** Cryo-TEM image of an aqueous solution of 1 wt% C18 with  $n(\text{ChOH}) : n(\text{C18}) = 2.00$  at 25°C; showing spherical micelles with an approximate radius of 2 nm.

Obviously, a minor excess of the corresponding hydroxides results in all three systems in an improved solubility of the respective soap. Indeed, this effect is least pronounced in the case of NaOH/C12. These findings, which are consistent with the data of other groups,<sup>2,3,5,6</sup> can be interpreted in terms of a suppression of the fatty acid hydrolysis according to reaction (VI.1):



All investigated hydroxides are strong bases. Hence, each base should be capable of a complete deprotonation of the fatty acid, at least at a small excess. Nevertheless, essential divergences could be discerned among the studied systems. A 5 mol% excess of base enhances the corresponding soap solubility to different extents ( $\Delta T = 1^\circ\text{C}$  for NaOH/C12,  $9.5^\circ\text{C}$  for KOH/C18 and  $7^\circ\text{C}$  for ChOH/C18). In the case of the NaOH/C12 system, this excess value is commensurate to the minimum of the solubility curve, whereas in the other two investigated systems maximum soap solubility can be achieved by addition of still higher amounts of base. 25-50 mol% and 200-300 mol% excess of potassium and choline hydroxide, respectively, are necessary to reach the lowest possible clearing temperatures for the surfactants. Apparently, the amount of hydroxide required to achieve maximum solubility of the corresponding soaps follows the order NaOH < KOH < ChOH. Further addition of alkali hydroxide leads in both cases to a re-increase of the Krafft temperature, indeed to unequal degrees for NaOH and KOH. On the other hand, the clearing temperatures of ChOH/C18 remain more or less constant up to high molar ratios of ChOH:C18.

These observations indicate that the solubilization of fatty acid soaps by hydroxides is also affected by processes other than the hydrolysis, such as “salting-in” and “salting-out” effects. In order to distinguish between the hydrolysis and the salt effect, we conducted a further experiment series in which we added different chloride salts instead of excess choline base to ChC18 solutions.

At this point, the most outstanding result of these studies is the fact that it is possible to obtain ChC18 micelles at temperatures as low as  $14^\circ\text{C}$  by addition of choline hydroxide, in contrast to the homologous alkali stearates.

### **VI.2.2. Influences of Different Chloride Salts on the Solubility of Choline Stearate**

In Fig. VI.3, Krafft temperatures for 1 wt% ChC18 systems are plotted as a function of the addition of sodium, potassium and choline chloride. Obviously, the solubility of choline stearate deteriorates upon addition of alkali chlorides in all cases. At a molar ratio of 1:4 of chloride salt to ChC18, NaCl increases the surfactant's clearing temperature ( $46.9^\circ\text{C}$ ) somewhat less than KCl ( $48.5^\circ\text{C}$ ). In turn, at higher chloride salt

fractions the solubility temperatures of ChC18 rise much more steeply when adding NaCl (up to 69°C in the studied concentration regime) than when adding KCl.

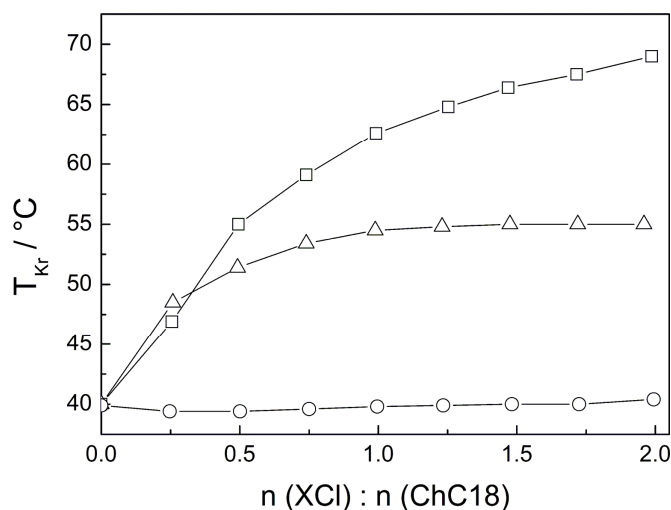


**Fig. VI.3** The Krafft temperature  $T_{Kr}$  of ChC18 soap solutions as a function of added NaCl (□), KCl (△) and ChCl (○) (ChC18 concentration fixed at 1 wt%).

Considering the Krafft temperature of NaC18 ( $T_{Kr}(\text{NaC18}) = 71^\circ\text{C}$ ), it may be concluded that choline as the initial counterion of the soap is completely substituted by sodium.<sup>4,7</sup> However, one has to be careful to interpret such solubility curves simply based on counterion exchange processes, since it is well known that NaCl exerts a “salting-out” influence on sodium carboxylate solutions, leading to decreased soap solubility.<sup>3,4</sup> Hence, this effect could increase the solubility temperatures of ChC18 in the same manner as the replacement of choline by sodium would do.<sup>4</sup>

Solubility temperatures of choline stearate solutions reach 55°C and subsequently remain more or less constant at molar ratios of KCl to ChC18 higher than 1:1. Regarding the Krafft temperature of KC18 ( $T_{Kr}(\text{KC18}) = 57^\circ\text{C}$ ), it is again possible to argue that choline is fully replaced by potassium as the counterion of the soap.<sup>1</sup> Furthermore, in contrast to the salting-out effect of NaCl, McBain *et al.* reported an increase of the soap solubility temperature by 2°C when small amounts of KCl are added to aqueous KC18 solutions.<sup>2</sup> This finding suggests that KCl can indeed exert a slight salting-in effect on alkali carboxylate soap solutions at low concentrations. However, larger amounts of KCl were found to induce salting-out of potassium laurate.<sup>8</sup> Whether a counterion exchange of choline by the alkali ions takes place or not will be discussed in the following section.

The addition of choline chloride to ChC18 solutions appears to have no significant influence on the solubility. Initially, a small decrease of the clearing temperature from 40°C to 39.4°C is observed, followed by a subsequent increase to 40.4°C. It was shown by other groups that TAA ions exhibit a salting-in effect on alkali carboxylate solutions.<sup>4</sup> However, the present set of data does not indicate such an effect of choline chloride on choline carboxylate surfactants.

### **VI.2.3. Specific Ion Effects in Aqueous Alkylcarboxylate Surfactant Solutions**

When discussing solubilities or Krafft points of surfactants, two competing thermodynamic forces have to be considered. These are the free energy of the micellar solution on the one hand, and that of the solid crystalline state on the other. The latter contribution is often considered as the main driving force. However, it is well known that the Krafft points of alkali carboxylate surfactants follow the trend  $\text{Li} > \text{Na} > \text{K} > \text{Cs}$ , which is opposite to that observed for alkylsulfates.<sup>2,9-12</sup> This reversed order cannot be explained simply based on different degrees of hindrance in the crystalline packing. With regard to this fact and the present experiments, specific ion interactions will be addressed in the following.

Previously, the Hofmeister series with respect to the influences of ions on macromolecular properties was interpreted mainly in terms of “making” or “breaking” the bulk water structure.<sup>13</sup> However, several groups have shown that short-range ion-macromolecule interactions are the dominant forces instead of the long-range electrostatic fields generated by simple ions in water, which appeared to be weak relative to the strength of water-water interactions.<sup>14-19</sup> According to this, simple monovalent ions do not alter the hydrogen bonding network of the bulk water outside their direct vicinity.<sup>14</sup>

Collins’ “concept of matching water affinities” provides a straightforward model of specific ion-ion interactions, wherein ion pair formation is controlled by hydration-dehydration processes.<sup>17-19</sup> Essentially, his model divides ions into two classes. Thereby, ions of high hydration and high surface charge density, such as  $\text{Li}^+$  and  $\text{F}^-$ , are referred to as “kosmotropes”, while large ions of weak hydrations and low surface charge density, such as  $\text{Cs}^+$  and  $\text{I}^-$ , are termed “chaotropes”.<sup>17-19</sup> In this context, water is regarded as a medium-size zwitterion. Matching congeneric cations and anions results

in a breakdown of the hydration shell and in the spontaneous formation of an inner-sphere ion pair.<sup>19</sup> In turn, when ions are mismatched (kosmotrope-chaotrope or vice versa), they will not dehydrate spontaneously, since their affinities to (medium-size) water are higher than to each other. Consequently, these ions remain separated by water. The dissolution of salts is accompanied by either the formation of ion pairs or a complete dissociation of the salt, the latter promoting solubility.<sup>9,18</sup>

In the realm of this model, sodium is classified as a small and highly hydrated ion (kosmotrope), whereas potassium and choline as big and weakly hydrated ions (chaotropes).<sup>19-22</sup> Furthermore, alkylcarboxylates can be considered as kosmotropes.<sup>23</sup> Applying Collins' "law of matching water affinities" onto the present system thus results in the following affinity trend of the cations to the carboxylate anion:  $\text{Na}^+ > \text{K}^+ \gg \text{Ch}^+$ . While the order of the first two cations has been confirmed by several studies,<sup>24-27</sup> there is to our knowledge no work published on the behavior of choline and alkylcarboxylates in this context. Sodium and the carboxylate ion, both being kosmotropes, are supposed to form ion pairs in water. In turn, the chaotropic potassium ion remains separated from the carboxylic headgroup by water. Consequently, the solubilities of sodium carboxylates are expected to be worse than those of the corresponding potassium salts. This prediction is verified by the observed trend of the Krafft points. In this regard, the reversed order reported for alkylsulfates is also easily explained, considering the fact that the sulfate anion is of chaotropic nature.<sup>26,28</sup>

The obtained influence of different chloride salts on the solubility of ChC18 agrees well with the prognosis of Collins' concept. NaCl was found to decrease drastically the solubility of ChC18 solutions. While there is a similar but less pronounced effect observed for KCl, no noticeable influence could be discerned for ChCl. In view of this, it can be assumed that choline as counterion is substituted by the alkali ions. At high chloride salt concentrations, however, additional effects may play a significant role as well.<sup>29</sup> Sodium, for instance, as a highly hydrated ion, could remove free bulk water and hence increase the effective surfactant concentration, resulting in a salting-out of the latter.<sup>4</sup>

The influence of the different hydroxides on the solubility of the corresponding carboxylate surfactants appears to be explicitly more complex. The amount of hydroxide required to reach maximum soap solubility was found to follow the order  $\text{NaOH} < \text{KOH} \ll \text{ChOH}$ , and ranges up to 200 mol% excess for ChOH. Since all of the

investigated hydroxides are strong bases, each should be capable of completely deprotonating the fatty acid. The addition of the choline ion itself is unlikely to increase the solubility of ChC18 to such a great extent (from 40°C down to 13.8°C), as virtually no effect was observed when adding choline chloride.

Taking into account the different cation-anion affinities, two reactions are likely involved according to Equation (IV.2). One is the ionization of the fatty acid and the other is the subsequent formation of ion pairs.



According to this, the carboxylate anion can be removed from the hydrolysis equilibrium by association with the cation. With regard to Collins' concept, sodium should be able to shift the equilibrium to the right side, whereas for choline the association step is negligible. Consequently, less NaOH is necessary compared to ChOH to achieve complete ionization of the fatty acid, while KOH adopts an intermediate position in this order. However, further experiments need to be conducted to confirm this argumentation.

Nevertheless, for higher amounts of added alkali hydroxides, the solubility of the respective surfactants decreases again, similarly as observed for the chloride salts. At higher salt concentrations, the removal of bulk water by ion hydration apparently becomes more significant, resulting in a more concentrated soap solution. As a consequence, the surfactant "salts out".

#### **VI.2.4. Saponification and Solubilization of Butter by Choline Base**

Butter as a biological product underlies certain fluctuations regarding the contents. As such it is of course not appropriate for detailed chemical studies. Nonetheless, we considered it as suitable for demonstrating the principle of the dissolution of water-insoluble triglycerides in aqueous solutions of choline hydroxide. Moreover, butter represents a daily household product and is therefore closer to a feasible application than perhaps a defined chemical would be.

Conventional cow butter typically contains around 82 wt% fat, which in turn is composed of triglycerides that are constituted typically by palmitic (~ 25%), oleic

(~ 25%), stearic (~ 10%) and myristic (~ 9%) acid [46, 47]. Shorter- and middle-chain saturated fatty acids are further present in a non-negligible amount (~ 12%).<sup>30,31</sup> Other appreciable ingredients of the butter are the water-insoluble cholesterol and vitamin E.

In Fig. VI.4, a picture of aqueous butter solutions at 25°C with different mass ratios of choline hydroxide to butter is shown. At small amounts of added ChOH, the butter remains more or less completely insoluble in water. However, continued addition of choline base leads initially to an emulsification and finally to the dissolution of butter. The amount of choline hydroxide required to obtain almost clear and foaming solutions ranges between mass ratios of ChOH to butter of 40-45.

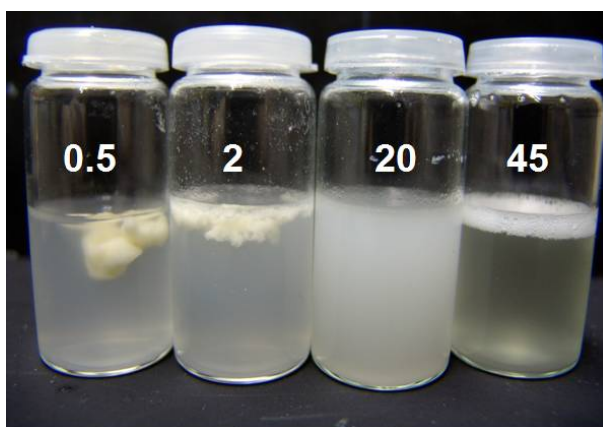


**Fig. VI.4** Attempts to dissolve butter at 25°C in aqueous solutions of choline hydroxide at different mass ratios of choline to butter (butter concentration fixed at 1 wt%).

Although quantitative data regarding the composition of the used butter, such as the number of enclosed ester bridges, cannot be given, the dissolution process is likely as following.

First, the ester bridges of the water-insoluble triglycerides are split by addition of choline base. Then, by neutralization, the released fatty acids become surfactants with choline as counterion. These choline soaps in turn are, as shown above, highly soluble in water, particularly if excessive ChOH is present. Subsequently, the generated surfactants can solubilize other water-insoluble compounds, such as cholesterol and vitamin E, resulting in almost clear and foaming aqueous solutions.

## VI.3. Conclusion

It was shown that adding excess choline hydroxide to choline stearate solutions is effective to reduce the solubility temperature of the soap from 40°C down to 14°C. To explain this considerable increase in solubility, the effect of alkali hydroxide addition to aqueous solutions of sodium laurate and potassium stearate was likewise investigated. The amount of hydroxide required to gain maximum soap solubility follows the order  $\text{NaOH} < \text{KOH} \ll \text{ChOH}$ . Still higher amounts of alkali base induced a re-increase of the respective solubility temperatures, while no further change was found in the case of choline base.

In order to distinguish between the effects of fatty acid hydrolysis and of specific ionic interactions, the influence of sodium, potassium and choline chloride on the solubility of choline stearate were additionally investigated. Both alkali chlorides caused an increase of the Krafft temperature of the surfactant, while the influence of KCl was less pronounced than that of NaCl. By contrast, choline chloride exerted no noticeable effect on the solubility.

The results were discussed in terms of Collins' "law of matching water affinities" based on different cation-anion affinities and association behaviors. Accordingly it is proposed that the affinity of the investigated cations to the alkylcarboxylate anion follows the order  $\text{Na}^+ > \text{K}^+ \gg \text{Ch}^+$ .

## VI.4. Experimental

### VI.4.1. Materials

Dodecanoic acid (Merck, p.a.) and octadecanoic acid (Fluka, puriss.) were used as received. The chloride salts of sodium and potassium were obtained from Merck (p.a.), choline chloride was purchased from Sigma-Aldrich (min. 98%). Sodium and potassium hydroxide were employed in the form of 1N titer solutions (Merck). Choline hydroxide was obtained as a clear (APHA < 300) 46 wt% aqueous solution from the company Taminco. The solution was stored under nitrogen at -18°C and protected against light in order to avoid decomposition. For experiments, small samples were taken and converted immediately. The concentration of the choline base stock was determined precisely to 46.6 wt% by threefold titration with 0.1M HCl (Merck). For the butter experiments, a

conventional mildly acidic butter (“Die streichzarte Butter”, Goldsteig, Bayerwald GmbH) was used, containing typically 82 wt% fat.

## **VI.4.2. Methods**

### **VI.4.2.1. Sample Preparation**

Samples for the determination of the influence of excess hydroxide on different soap solutions were prepared as follows. Appropriate amounts of the fatty acid were weighed separately for each investigated molar ratio of base to acid. Then the respective hydroxides were added, yielding solutions containing 1 wt% fatty acid with different molar ratios of base to acid.

For studying the influence of different chloride salts on the solubility behavior of choline stearate, stock solutions of the soap and the chloride salts were prepared first. For the surfactant stock, twofold recrystallized ChC18 was used (for details on preparation see Chapter I). Afterwards, stock solutions were mixed and diluted correspondingly in order to obtain 1 wt% ChC18 solutions with different molar ratios of the chloride salts to soap.

Regarding the butter experiments, small amounts of the frozen butter (1 wt%) were weighed separately and treated with different amounts of choline hydroxide.

Each sample was stirred for 12 hours and, if necessary, heated in order to obtain homogenous solutions. In all cases, Millipore water was used as solvent.

### **VI.4.2.2. Determination of the Solubility Temperature**

Krafft or solubility temperatures were first determined by direct visual observation, spotting the temperature at which the solutions turned completely clear and isotropic. For this purpose, small amounts (~3 mL) of the respective samples were flame-sealed in glass vials and subsequently heated with about 1°C per hour. Solutions, which were already clear at ambient temperature, were slowly cooled until turbidity was discernible, prior to experiment start.

Precise solubility temperatures were gained from turbidity measurements using an automated home-built apparatus.<sup>32</sup> Specimen holders were placed in a computer-controlled thermostat. Light emitted by a LED crosses the samples and the transmitted

light is detected by a light-dependent resistor (LDR). Samples were cooled if necessary until precipitation occurred and then heated with 1°C per hour.

### **VI.4.2.3. Cryogenic Transmission Electron Microscopy (Cryo-TEM)**

For cryo-TEM studies, a 2 $\mu$ l drop of the sample was placed on an hydrophilized lacey carbon filmed copper TEM grid (200 mesh, Science Services, Muenchen, Germany). Most of the liquid was removed with blotting paper, leaving a thin film stretched over the carbon lace holes. The specimens were vitrified by rapid immersion into liquid ethane cooled to approximately 90 K by liquid nitrogen in a temperature controlled freezing unit (Zeiss Cryobox, Zeiss NTS GmbH, Oberkochen, Germany). The temperature was monitored and kept constant in the chamber during all of the sample preparation steps. After freezing the specimens, the remaining ethane was removed using blotting paper. The specimen was inserted into a cryo-transfer holder (CT3500, Gatan, Muenchen, Germany) and transferred to a Zeiss EM922 EFTEM instrument. Examinations were carried out at temperatures around 90 K. The transmission electron microscope was operated at an acceleration voltage of 200 kV. Zero-loss filtered images ( $\Delta E = 0$  eV) were taken under reduced dose conditions (100-1000 e/nm<sup>2</sup>). All images were registered digitally by a bottom mounted CCD camera system (Ultrascan 1000, Gatan, Muenchen, Germany) combined and processed with a digital imaging processing system (Gatan Digital Micrograph 3.10 for GMS 1.5).

## **VI.5. References**

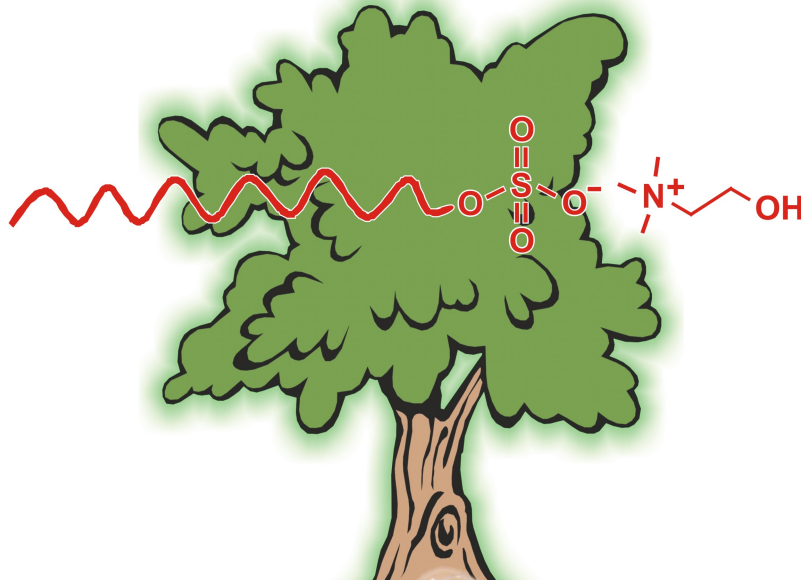
1. R. Klein, D. Touraud, W. Kunz, *Green Chem.*, 2008, **10**, 433.
2. J. W. McBain, W. C. Sierichs, *J. Am. Oil Chem. Soc.* 1948, **25**, 221.
3. X. Wen, E. I. Franses, *J. Colloid and Interface Sci.* 2000, **231**, 42.
4. B. Lin, A. V. McCormick, H. T. Davis, R. Strey, *J. Colloid Interface Sci.* 2005, **291**, 543.
5. J. Lucassen, *J. Phys. Chem.* 1966, **70**, 1824.
6. M. N. G. de Mul, H. T. Davis, D. F. Evans, A. V. Bhave, J. R. Wagner, *Langmuir* 2000, **16**, 8276.
7. J. W. McBain, W. W. Lee, *Oil Soap* 1943, **20**, 17.

8. J. W. McBain, M.C. Field, *J. Phys. Chem.* 1926, **30**, 1545.
9. M. J. Vold, *J. Am. Chem. Soc.* 1943, **65**, 465.
10. H. Demarcq, *Inds. corps gras* 1946, 2, 341-352, 370.
11. K. Shinoda, M. Hato, T. Hayashi, *J. Phys. Chem.* 1972, **76**, 909.
12. M. J. Rosen, *Surfactants and Interfacial Phenomena*, John Wiley & Sons Ltd, USA, 2nd Ed., 1989, pp. 216-217.
13. K. D. Collins, M. W. Washabaugh, *Q. Rev. Biophys.* 1985, **18**, 323.
14. Y. Zhang, P. S. Cremer, *Curr. Opin. Chem. Biol.* 2006, **10**, 658.
15. A. W. Omta, M. F. Kropman, S. Woutersen, H. J. Bakker, *Science* 2003, **301**, 347.
16. J. D. Batchelor, A. Olteanu, A. Tripathy, G. J. Pielak, *J. Am. Chem. Soc.* 2004, **126**, 1958.
17. K. D. Collins, *Biophys. Chem.* 2006, **119**, 271.
18. K. D. Collins, G. W. Neilson, J. E. Enderby, *Biophys. Chem.* 2007, **128**, 95.
19. K. D. Collins, *Methods* 2004, **34**, 300.
20. K. Fujita, D. R. MacFarlane, M. Forsyth, M. Yoshizawa-Fujita, K. Murata, N. Nakamura, H. Ohno, *Biomacromolecules* 2007, **8**, 2080.
21. K. Lohner, A. F. Esser, *Biochemistry* 1991, **30**, 6620.
22. M. C. Pinna, P. Bauduin, D. Touraud, M. Monduzzi, B. W. Ninham, W. Kunz, *J. Phys. Chem. B* 2005, **109**, 16511.
23. N. Vlachy, M. Drechsler, J. M. Verbavatz, D. Touraud, W. Kunz, *J. Colloid Interface Sci.* 2008, **319**, 542.
24. H. I. Rosano, A. P. Christodoulou, M. E. Feinstein, *J. Colloid Interface Sci.* 1969, **29**, 335.
25. L. Vrbka, J. Vondrasek, B. Jagoda-Cwiklik, R. Vacha, P. Jungwirth, *Proc. Nat. Acad. Sci. U.S.A.* 2006, **103**, 15440.
26. B. Jagoda-Cwiklik, R. Vacha, M. Lund, M. Srebro, P. Jungwirth, *J. Phys. Chem. B* 2007, **111**, 14077.
27. R.A. Curtis, J. Ulrich, A. Montaser, J. M. Prausnitz, H. W. Blanch, *Biotechnol. Bioeng.* 2002, **79**, 367.

28. A. Renoncourt, N. Vlachy, P. Bauduin, M. Drechsler, D. Touraud, J. M. Verbavatz, M. Dubois, W. Kunz, B. W. Ninham, *Langmuir* 2007, **23**, 2376.
29. L. Vrbka, P. Jungwirth, P. Bauduin, D. Touraud, W. Kunz, *J. Phys. Chem. B* 2006, **110**, 7036.
30. H. D. Belitz, W. Grosch, P. Schieberle, *Lehrbuch der Lebensmittelchemie*, Springer, 5th Ed., 2001.
31. Butter specification sheet, Universtiy of Weihenstephan, 2008.
32. S. Schroedle, R. Buchner, W. Kunz, *Fluid Phase Equilib.* 2004, **216**, 175



## Chapter VII Choline Alkyl Sulfates



As demonstrated in the preceding chapters, choline soaps exhibit high counterion-headgroup dissociation. This facilitates on the one hand the superior water solubility of the surfactants but, on the other, is accompanied by a fundamental susceptibility to the addition of simple salts such as sodium chloride. The latter undesirable feature may simply be overcome by combining the “soft” choline ion with a “soft” surfactant headgroup such as sulfate. Accordingly, this chapter introduces choline dodecyl sulfate (ChDS) exemplarily as a representative of choline alkyl sulfates – a new group of promising biocompatible anionic surfactants.

In this context, the *cmc* and Krafft point of ChDS were determined and a rough aqueous phase diagram is presented. Beyond that, cytotoxicity measurements on HeLa and SK-Mel 28 cells were conducted. The enhanced counterion-headgroup binding relative to choline carboxylate soaps is confirmed by the value of the *cmc* and the traced self-assembly behavior of ChDS in water, while the Krafft point of ChDS is maintained at temperatures as low as 0°C. Cytotoxicity studies reveal that ChDS is similarly harmless as the widely applied sodium dodecyl sulfate (SDS). Finally, the effect of different mono- and divalent salts on the solubility of ChDS is discussed and compared to its alkali and alkyl carboxylate homologues.

## VII.1. Introduction

Soaps (i.e. salts of fatty acids) are still nowadays a very important surfactant type due to their biocompatibility and relatively low costs. However, their limited water solubility, relatively high pH and substantial sensitivity to water hardness cause serious problems in the formulation of skin-friendly home- and personal-care products.<sup>1-3</sup> As shown in Chapters II-VI, choline carboxylates provide an effective alternative to classical soaps due to their improved water solubility, while sustaining biocompatibility. However, they still bear the other common drawbacks related to fatty acid surfactants, that is, strong alkalinity and reduced performance in the presence of hard water or simple alkali salts.

The high pH of soaps can be avoided by using a headgroup of reinforced acidity such as sulfate. Sodium alkyl sulfate surfactants were furthermore shown to be less sensitive to water hardness, while still being readily biodegradable and allowing synthesis from renewable raw materials.<sup>4,5</sup> The most prominent and intensively studied example of this class of surfactants is sodium dodecyl sulfate (SDS), which finds broad application as an active agent for instance in products like shampoos or shower gels.<sup>4</sup> Pure SDS typically becomes well-soluble at temperatures ranging from 12 to 20°C.<sup>6-8</sup> However, although being less sensitive to salts than carboxylate detergents, the solubility temperature of SDS soon exceeds 25°C when other salts are present.<sup>9,10</sup> The use of the more surface-active longer-chain homologues of SDS, such as sodium tetradecyl sulfate, is moreover restricted due to poor solubility in water.<sup>4,7,11</sup>

According to Collins' concept of "matching water affinities" (as described in Chapter VI),<sup>12,13</sup> sodium is supposed to bind only weakly to the alkyl sulfate anion. Further, in contrast to carboxylate soaps, the degree of counterion-headgroup association in alkyl sulfate surfactants should increase with the size of the cation ( $\text{Li}^+ < \text{Na}^+ < \text{K}^+ < \text{Rb}^+ < \text{Cs}^+$ ). This has been confirmed in several previous studies, for example by combined small-angle X-ray and neutron scattering (SAXS and SANS) measurements.<sup>14-17</sup> Usually, the gain in the strength of counterion-headgroup binding brings about an increment in the Krafft point ( $T_{Kr}$ ) of the surfactants. Accordingly, the Krafft temperatures of alkali alkyl sulfates increase with growing size of the cations,<sup>6</sup> whereas those of alkyl carboxylates decrease.<sup>2,18,19</sup>

Interestingly, when bulky tetraalkylammonium (TAA) ions are employed as counterions in alkyl sulfate surfactants, the water solubility is extended towards low temperatures, in

line with what has been reported for fatty acid soaps but as opposed to the above-mentioned trend for alkyl sulfates.<sup>20-25</sup> Nevertheless, an important difference between TAA alkyl sulfate and TAA carboxylate surfactants is obvious in the case of tetrabutylammonium (TBA). With increasing temperature, TBA alkyl sulfates show a clouding phenomenon as it is otherwise only observed for non-ionic surfactants, while such an effect does not occur for TBA alkyl carboxylates.<sup>11,23,24,26,27</sup> Whether TAA ions are more associated to the alkyl sulfate anion than for instance sodium has been the object of some debates. Several studies confirmed that the degree of counterion dissociation  $\alpha$  is less pronounced for TAA ions than for sodium.<sup>14,17,26,28,29</sup> In turn, aggregation numbers of TAA alkyl sulfate surfactants were found to be lower and micellar sizes smaller than expected on the basis of the critical micellization concentration (*cmc*) and the value of  $\alpha$ .<sup>25,26,30-32</sup> Zana *et al.* proposed that, due to sterical hindrance, TAA ions are condensed in two layers over the surface of the micelle, with a first layer being rather compact and a second appearing largely incomplete.<sup>25,26</sup> Unfortunately, information on the influence of alkali chlorides on the Krafft temperatures of corresponding surfactants is not available to date.

In this regard, alkyl sulfate surfactants can be considered effective alternatives to carboxylate soaps, and TAA ions as counterions seem to be suitable for an enhancement of the surfactants' solubility also in this case. However, whether their salt sensitivity is reduced as compared to common soaps remains to be proven. Since simple TAA ions do not meet the requirements for most application fields of surfactants due to their toxic impact,<sup>33-35</sup> choline as a natural human metabolite was chosen as counterion of dodecyl sulfate (DS<sup>-</sup>) in this work. Choline dodecyl sulfate (ChDS) (outlined in Fig. VII.1) has been synthesized and its Krafft point and *cmc* value were determined. Further, a rough aqueous phase diagram has been constructed for ChDS and first cytotoxicity studies on two human cell lines were carried out. Finally, the influence of various chloride salts on the Krafft temperature of ChDS has been examined and a comparison to values reported for SDS and potassium dodecyl sulfate (KDS) is established. The results are further related to those obtained for alkyl carboxylate surfactants.

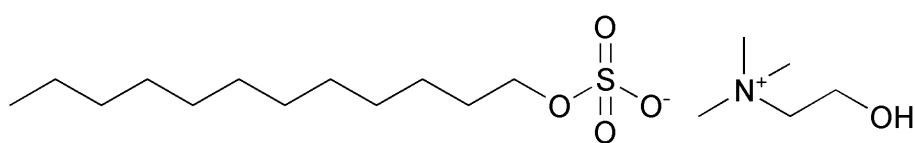


**Fig. VII.1** Molecular structure of choline dodecyl sulfate (ChDS).

## VII.2. Results and Discussion

### VII.2.1. Krafft Point and *cmc*

According to the common convention, the solubility temperature of a 1 wt% ChDS solution was taken as the Krafft point.<sup>2</sup> For comparison, the Krafft temperatures of SDS and KDS were determined with the same procedure as applied for ChDS and were found to be in a good agreement with the literature (Table VII.1).<sup>5-7,36</sup> In line with the reported tendency of TAA ions to decrease  $T_{Kr}$ , ChDS was confirmed to be soluble down to 0°C, which is a considerable improvement regarding the water solubility as compared to the sodium and potassium counterparts (cf. Table VII.1). Notably, no clouding phenomenon could be discerned for ChDS upon heating, in contrast to what was observed for instance for TBADS.<sup>11,23,27</sup>

**Table VII.1** Physicochemical properties of ChDS in comparison to other dodecyl sulfate surfactants: Krafft temperatures ( $T_{Kr}$ ), critical micellization concentrations (*cmc*'s) determined by conductivity<sup>a</sup> and surface tension<sup>b</sup> measurements, the degree of counterion condensation  $\alpha$  (derived from conductivity data), the surface excess concentration ( $\Gamma$ ) and the area per molecule ( $A_s$ ) calculated from the concentration-dependent surface tension plots.

	$T_{Kr} / ^\circ\text{C}$	$cmc^a / \text{mM}$	$cmc^b / \text{mM}$	$\alpha^a$	$A_s^b / \text{\AA}^2$	$\Gamma / \text{mol m}^{-2}$
<b>ChDS</b>	0	$5.99 \pm 0.06$	$4.26 \pm 0.04$	0.25	36	$4.62 \cdot 10^{-6}$
<b>SDS</b>	14.1	$8.65^{38}$	$5.54 \pm 0.29$	$0.26^{38}$	28	$5.94 \cdot 10^{-6}$
<b>KDS</b>	37.3	$7.8^{39}$	-	-	-	-
<b>TMADS</b>	$< 0^\circ\text{C}^{26}$	$5.56^{17}$	-	$0.20^{26}$	-	-

The *cmc* of ChDS has been determined by means of two techniques, namely surface tension and conductivity measurements. Results are compiled in Table VII.1. Both methods yielded somewhat different *cmc* values, which is a well-known phenomenon originating from distinct sensitivities of the techniques to different physical properties.<sup>37</sup> However, as clearly shown by the values in Table 1, the *cmc*'s of alkyl sulfate surfactants decrease with growing size of the cations, which usually reflects an increasing counterion-headgroup association. The reported *cmc* of tetramethylammonium dodecyl sulfate (TMADS) is slightly lower than that of ChDS. This deviation may yet be well within the experimental inaccuracy associated with the use of two distinct experimental setups.<sup>17</sup> A comparison of the *cmc* of ChDS and ChC12 (*cmc*

= 25.5 mM, see Section II.2.1.) evidently supports the notion that counterion-headgroup binding is greatly enhanced when substituting the carboxylate by a sulfate headgroup.<sup>12</sup> This becomes further manifest in the degrees of micelle ionization  $\alpha$  estimated for ChDS ( $\alpha = 0.25$ ) and ChC12 ( $\alpha = 0.33$ , see Section II.4.2.). In turn, the  $\alpha$  values of ChDS and SDS differ only slightly,<sup>38</sup> while that of TMADS is significantly lower ( $\alpha = 0.20$ ).<sup>26</sup> This is clearly in contrast to the traced variations of the *cmc*. The deviation between  $\alpha$  of TMADS and ChDS might indicate that choline is less efficiently bound to the micelle surface than TMA due to the hydroxyl group of choline. Thereby it should be noted that no marked differences between TMA and choline could be detected for alkyl carboxylate surfactants in the dilute aqueous phase region. Whether ChDS micelles have a similar charge as SDS micelles, as indicated by the  $\alpha$  values but controverted by the magnitude of the *cmc*, remains to be proven.

Surface tension measurements furthermore allow for the determination of the surface excess concentration ( $\Gamma$ ) and the area per surfactant molecule ( $A_s$ ) at the surface. As obvious from Table VII.1, the area per surfactant molecule is distinctly larger for ChDS than for SDS, which can likely be ascribed to the bulkiness of the choline counterion. This results in a lower surface excess concentration for ChDS relative to SDS.

Thus, ChDS shows increased water solubility as compared to its sodium and potassium homologues, in analogy to what has been found when choline was employed as counterion in fatty acid soaps. However, the *cmc* and  $\alpha$  values suggest that ChDS exhibits considerably stronger counterion-headgroup binding than the highly dissociated choline carboxylates. Whether this feature factually accounts for a reduced salt sensitivity of the surfactant will be examined below. In this context, two other advantages of choline alkyl sulfate surfactants over choline carboxylate soaps should be emphasized, which concern the handling of the compounds. Neat ChDS turned out to be much less hygroscopic than ChC*m* surfactants. In the presence of small amounts of water ( $\approx 1$  wt% H<sub>2</sub>O), the latter form a glutinous mass (liquid crystals), which complicates their further processing. By contrast, powdery ChDS samples can readily be applied under ambient conditions without protection against air humidity. Moreover, ChDS is thermally more stable (see Section VII.4.3.5) than ChC*m* salts and even outrivals SDS in this respect, exhibiting a decomposition temperature which exceeds those of the counterparts by up to 50-60°C and  $\sim 30^\circ\text{C}$ , respectively.

### VII.2.2. Aqueous Self-Assembly Behavior

The size and shape of ChDS micelles in aqueous solution were investigated by cryo-TEM exemplarily for concentrations of 1 wt% and 5 wt%. A representative image for 5 wt% ChDS is displayed in Fig. VII.2, disclosing spherical micelles with a radius of about 2 nm. This value agrees well with the micellar size of TMADS determined by SANS ( $r = 2$  nm),<sup>31</sup> and generally falls in the order of magnitude of micellar radii typically detected for alkali dodecyl sulfates by SAXS and SANS.<sup>15,16</sup>

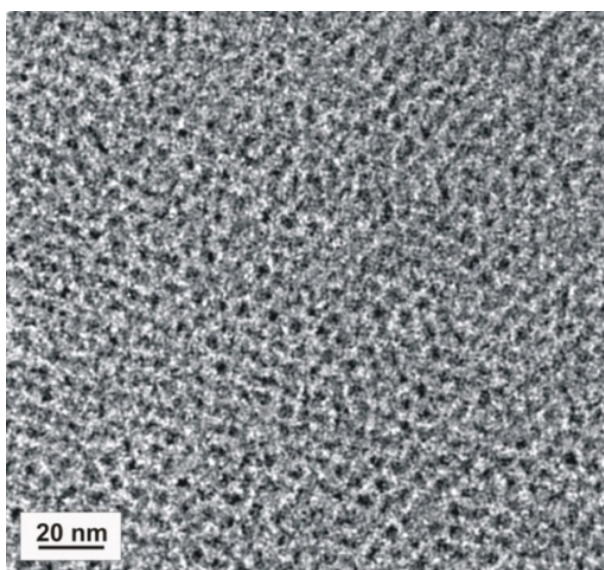


**Fig. VII.2** Cryo-TEM micrograph of a 5 wt% ChDS solution, revealing spherical micelles with an approximate radius of 2 nm.

The more concentrated surfactant region of ChDS was studied by the penetration scan technique and the establishment of a preliminary aqueous phase diagram (see Chapter IV for details on procedures). The penetration scan study showed that the first liquid-crystalline phase formed by ChDS is a hexagonal ( $H_1$ ) phase, which persists down to 0°C (Fig. VII.3).

At a temperature of 45-46°C, a bicontinuous cubic phase ( $V_1$ ) occurred (Fig. VII.4), while a lamellar phase ( $L_a$ ) could not be detected up to 100°C (actually not up to 130°C). Instead, a highly viscous birefringent region was observed, which displays sharp etches and hence probably is of crystalline nature. Though not addressed in detail in this work, the thermotropic phase behavior of neat ChDS proved to be rather complex, with up to 4-5 distinct phases being detected between 0°C and 150°C.

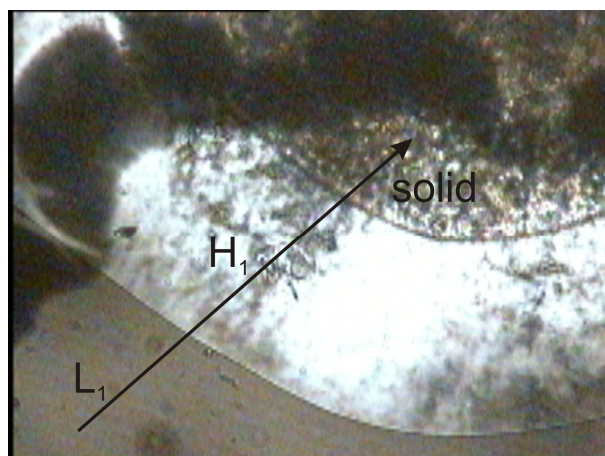


**Fig. VII.3** Penetration scan image of ChDS at 0°C acquired at 100x magnification between half-crossed polarizers. With increasing surfactant concentration (indicated by the arrow), a micellar solution  $L_1$ , a hexagonal phase  $H_1$  and a partially birefringent solid region can be identified.

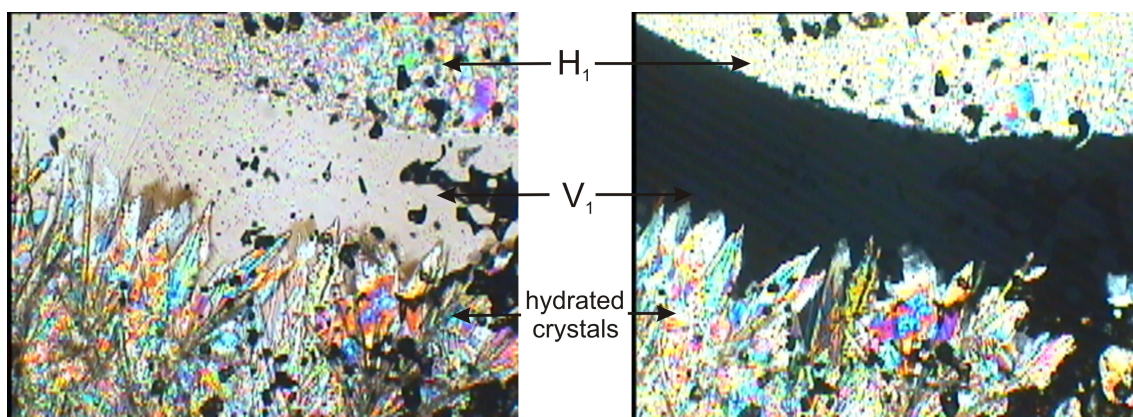


**Fig. VII.4** Penetration scan (100x magnification) of ChDS at 48°C with non-crossed (left) and crossed polarizers (right), showing the following phases towards higher surfactant concentrations: hexagonal  $H_1$ , bicontinuous cubic  $V_1$ , and a birefringent crystalline region.

By preparing liquid-crystalline samples in concentration steps of 5 wt% and spotting their development on raising the temperature between crossed polarizers, the binary phase diagram of ChDS shown in Fig. VII.5 was constructed. In line with other common anionic surfactants<sup>40,41</sup> but opposed to choline carboxylate soaps, the first liquid-crystalline phase formed by ChDS at a concentration of ~38 wt% is  $H_1$ . This phase actually dominates the overall appearance of the phase diagram since it extends up 80-85 wt%. The only other type of mesophase distinguished in the studied temperature range was the bicontinuous cubic  $V_1$  phase. It should be kept in mind that Fig. VII.5 represents a first rough sketch of the phase diagram of ChDS and that small

regions of intermediate phases, potentially located between  $H_1$ ,  $V_1$  and solid, may have been missed in the present work. However, a prominent feature of ChDS already obvious is its low Krafft boundary, which remains at or below  $0^\circ\text{C}$  up to  $\sim 65$  wt%. By contrast, SDS requires around  $45^\circ\text{C}$  at 65 wt% to form a mesophase.<sup>40,42</sup> An overall comparison of the phase diagrams of SDS<sup>40</sup> and ChDS reveal that the regions of  $H_1$  and  $V_1$  are substantially expanded in the case of ChDS. Moreover, SDS forms a  $L_\alpha$  phase at around 70 wt% surfactant,<sup>40</sup> which is absent for ChDS. Apparently, SDS favors phases of lower curvatures than ChDS, which is reasonable when considering packing constraints<sup>43</sup> and the large headgroup area of ChDS caused by the bulky choline ion. The latter is further confirmed by the surface tension measurements (see Table VII.1)

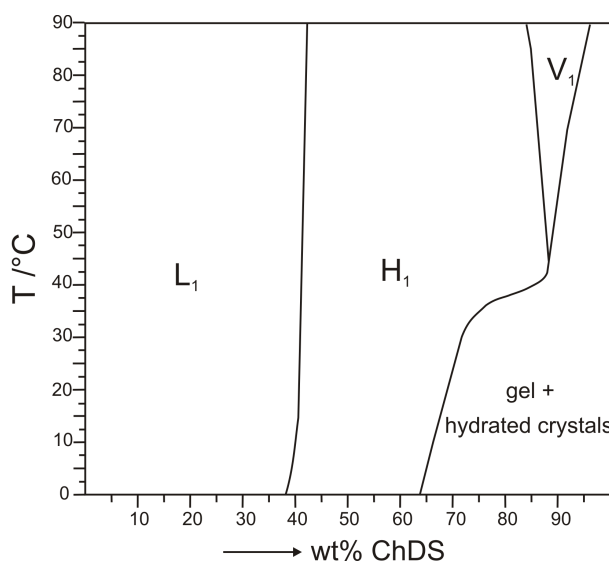


**Fig. VII.5** Rough binary aqueous phase diagram of ChDS between  $0^\circ\text{C}$  and  $90^\circ\text{C}$ .

The phase diagram established for ChDS corroborates the idea that the extent of counterion-headgroup binding is appreciably higher for ChDS than for choline fatty acid soaps. The broad discontinuous cubic phase region ( $I_1$ ) detected for ChCm surfactants is missing for ChDS, and the  $V_1$  region of ChDS is considerably smaller than that of ChC12 (see Chapter IV). Consequently, ChDS prefers less curved mesophases as compared to ChC12. This can be deduced to stronger cation-anion interactions between the “soft” choline and the “soft” alkyl sulfate ion,<sup>44</sup> which in turn lead to a smaller headgroup area of ChDS relative to the highly dissociated choline soaps.

### VII.2.3. Cytotoxicity of ChDS

In order to derive first information on the biocompatibility of ChDS, its cytotoxicity on cervix carcinoma cells (HeLa) as well as on keratinocytes (SK-Mel-28) has been examined. As outlined in Chapter III, studies with HeLa cells serve as a reasonable alternative to frequently performed *in vivo* eye-irritancy tests on rabbits, while analyses with SK-Mel-28 cells permit first conclusions on the skin irritancy power. To be able to assess the toxic impact of ChDS on a relative scale, SDS and ChC12 were investigated in parallel under identical experimental conditions. Cytotoxicities of ChDS, SDS and ChC12 (expressed as  $IC_{50}$  values – the higher the less toxic) are depicted in Fig. VII.6.

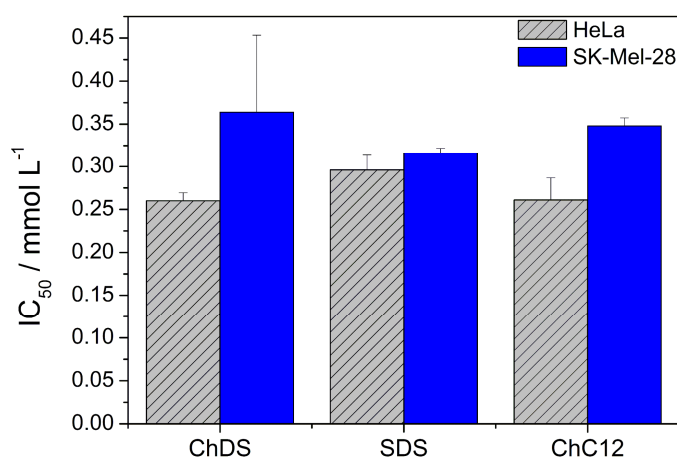


**Fig. VII.6** Comparison of the cytotoxicity of ChDS, SDS and ChC12 on two human cell lines (HeLa and SK-Mel-28).

On both cell lines,  $IC_{50}$  values obtained for ChDS are more or less similar to those determined for SDS and Ch12. Apparent differences between the compounds and the two cell lines are judged to be rather small. A more important finding is that the measured  $IC_{50}$  values range between 0.25-0.40 mM. Thus, ChDS can be considered as toxicologically harmless under the given circumstances.

### VII.2.4. Influence of Salts on the Krafft Points of Alkyl Sulfate and Alkyl Carboxylate Surfactants

Collins' concept implicates that counterion condensation around the “soft” alkyl sulfate micelles is more pronounced for large “soft” cations, such as choline, than for small “hard” cations like sodium.<sup>12,13,45</sup> The results presented in the preceding sections led to ambiguous conclusions in this respect. Therefore, the influence of added lithium,

sodium, potassium and choline chloride on the Krafft temperature of SDS, KDS and ChDS was studied so as to shed more light on specific ion effects in these systems. Moreover, the corresponding alkyl carboxylate homologues (i.e. NaC12, KC12 and ChC12) were also included in these investigations in order to verify the postulated reversed trends of “hard” carboxylic and “soft” sulfate headgroups in terms of ion association and its impact on the Krafft temperature. Obtained progressions of the Krafft points with growing salt content are depicted in Fig. VII.7.

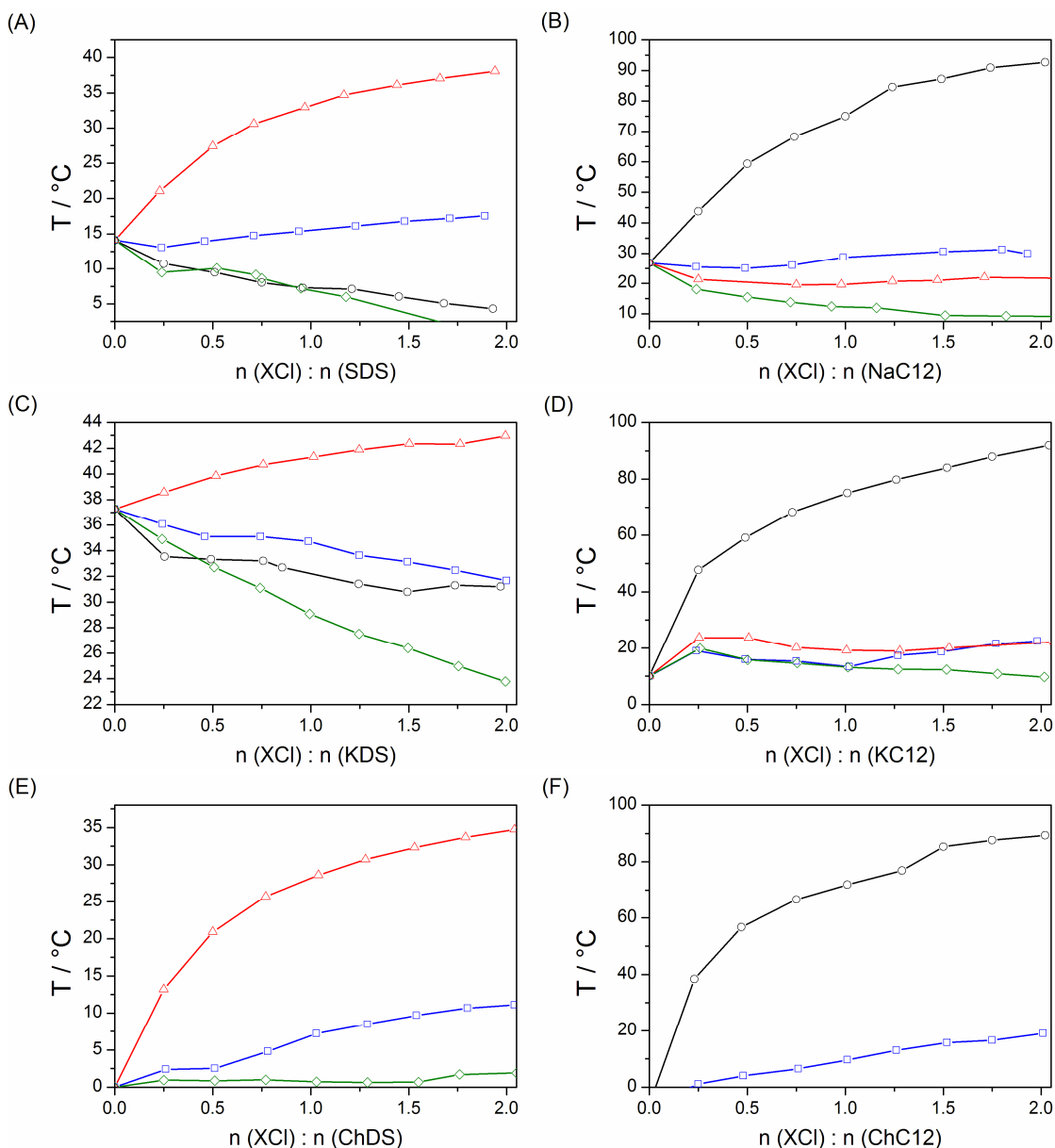


**Fig. VII.7** The effect of varying amounts of alkali chlorides (LiCl ( $\circ$ ), NaCl ( $\square$ ), KCl ( $\triangle$ )) and choline chloride (ChCl ( $\diamond$ )) on the Krafft temperature of dodecylsulfate surfactants (SDS (A), KDS (C), ChDS (D)) and, for comparison, dodecanoate soaps (NaC12 (B), KC12 (D), ChC12 (F)). The curves of LiCl in (E) and those of KCl and ChCl in (F) are not shown, since the

measured values were below 0°C. The surfactant concentration was kept constant at 1 wt% in the experiments.

It is evident that addition of KCl generally causes a distinct increase of  $T_{Kr}$  in case of alkyl sulfate surfactants, whereas its influence is moderate or even mitigating with regard to the water solubility for alkyl carboxylates. In turn, the presence of LiCl was found to lower the Krafft point of SDS and KDS, in contrast to alkanooates soaps for which a sharp rise in  $T_{Kr}$  up to 90-100°C was observed in all instances. A relative ordering of the salts according to their ability to increase the Krafft temperature of the different surfactants is given in Table VII.2.

**Table VII.2** Specific effects of distinct alkali salts and choline chloride on the Krafft temperatures of dodecyl sulfate (SDS, KDS, ChDS) and dodecanoate (NaC12, KC12, ChC12) surfactants. Salts are ordered with respect to their potential to increase  $T_{Kr}$ . The effect of the alkali chlorides is reversed when the sulfate headgroup is replaced by carboxylate. In turn, added choline chloride generally tends to decrease the Krafft point, regardless of the type of surfactant headgroup.

<b>SDS</b> KCl >> NaCl > LiCl ≈ ChCl	<b>NaC12</b> LiCl >> NaCl > KCl > ChCl
<b>KDS</b> KCl >> NaCl > LiCl > ChCl	<b>KC12</b> LiCl >> NaCl > KCl > ChCl
<b>ChDS</b> KCl >> NaCl > ChCl > LiCl	<b>ChC12</b> LiCl >> NaCl > KCl, ChCl

The fact that pure alkali alkyl sulfate and alkyl carboxylate surfactants exhibit opposite trends in their Krafft temperatures with growing size of the cations has been reported previously.<sup>5,37</sup> Table VII.2 highlights that this behavior applies also for the influence of added alkali chloride salts on the Krafft points of the different surfactants investigated,<sup>46</sup> that is, the sequence of the alkali ions is reversed when exchanging the headgroups. In this sense, Collins' concept of "matching water affinities" accounts for the observed tendencies. However, choline chloride breaks the trend, as it factually lowers the Krafft point of both surfactant types. In the case of alkyl sulfates, the large choline cation surprisingly exerts an effect which is similar to that of the small lithium ion. Possible

reasons for this finding remain unknown. How can a salt decrease the Krafft point of a surfactant when it neither changes the bulk water structure and nor interacts significantly with the surfactant headgroup? Further, Fig. VII.7 shows that addition of NaCl noticeably elevates the solubility temperature of ChDS. Thus, it must be doubted that the degree of counterion-headgroup binding is really stronger in ChDS than in SDS, as it would be suggested by Collins' concept. In turn, it appears quite certain that the affinity of choline to the alkyl sulfate moiety is higher than to the carboxylate anion, given that the presence of NaCl in a molar excess of 2:1 raises the Krafft temperature of ChDS by only 10°C, whereas an increase by up to 20°C can be discerned in the same situation for ChC12.

Finally, the influence of calcium chloride on the solubility of ChDS and, for comparison, SDS was examined in order to mimic conditions prevailing in hard water. Corresponding results are outlined in Fig. VII.8. Since calcium is a divalent cation, it replaces both sodium and choline as counterions of alkyl sulfate micelles. Accordingly, the Krafft temperatures of ChDS and SDS increase steeply and in a similar fashion upon addition of CaCl<sub>2</sub>, soon approaching the  $T_{Kr}$  value of pure aqueous calcium dodecylsulfate ( $T_{Kr}(\text{Ca}(\text{DS})_2) = 50^\circ\text{-}55^\circ\text{C}$ )<sup>47</sup>. Indeed, the Krafft point of ChDS + CaCl<sub>2</sub> falls below that of SDS + CaCl<sub>2</sub> by about 2-3°C. However, this cannot be judged as a considerable improvement. Apart from that, an important advantage of alkyl sulfate surfactants relative to fatty acid soaps is evident from Fig. VII.8: the temperature needed to solubilize Ca(DS)<sub>2</sub> amounts only up to about 55-56°C – in contrast to the water-insoluble lime soaps formed by carboxylate surfactants.

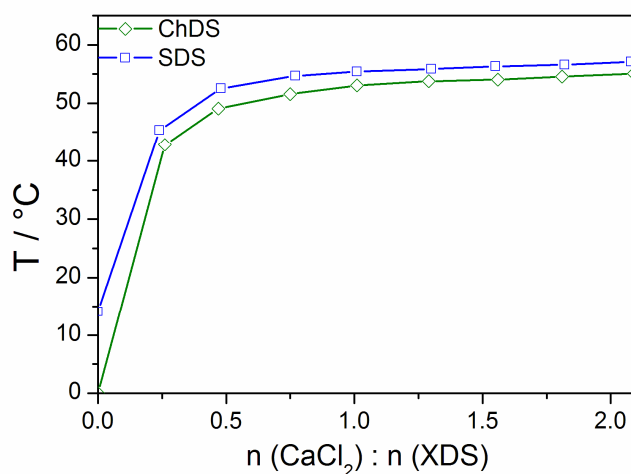


**Fig. VII.8** Influence of calcium chloride on the Krafft temperatures of ChDS and SDS, at a surfactant concentration of 1 wt% in both cases.

## VII.3. Conclusion

The data presented in this chapter have evidenced that choline dodecyl sulfate is soluble down to 0°C up to a concentration of ~65 wt% in water, which represents a considerable improvement of the water solubility with regard to its sodium and potassium homologues. The *cmc*, the degree of micelle ionization  $\alpha$  and the mesophases detected for ChDS suggest that counterion-headgroup binding is substantially stronger than in case of the highly dissociated choline fatty acid soaps. Analyses of its cytotoxicity revealed that ChDS is virtually harmless and exhibits  $IC_{50}$  values comparable to those of SDS. Studies on the effect of added alkali and choline chlorides on the Krafft point of alkyl sulfate and carboxylate surfactants confirmed a reversed tendency of the alkali salts in terms of their influence on the solubility temperature of the two distinct types of headgroups. Interestingly, choline did not follow this trend and was found to generally decrease the value of  $T_{Kr}$ . The present findings suggest that the binding of choline to the sulfate headgroup is not stronger than for sodium as proposed by Collins' concept. However, the degree of association in ChDS is in fact higher than in choline carboxylate soaps. Investigations on the influence of added calcium chloride on the solubility of ChDS and SDS revealed that the Krafft temperature indeed rises sharply in both cases, but only to levels around 50-55°C. This feature is expected to permit an application of the surfactants in "regular" hard water at moderately elevated temperatures without the requirement of water softeners.

Certainly, the present study should be regarded as the starting point for further investigations on choline alkyl sulfate surfactants. Nevertheless, the low Krafft temperature determined for ChDS suggests that also its longer-chain derivatives will exhibit enhanced water solubility as compared to its alkali homologues. Thus, due to their high water solubility, low toxic impact and reduced sensitivity relative to the soap counterparts to the presence of both alkali and alkaline-earth chlorides, choline alkyl sulfates depict a new promising class of anionic surfactants.

## VII.4. Experimental

### VII.4.1. Chemicals

SDS (Merck,  $\geq 99\%$ ), NaC12 (Sigma-Aldrich, 99-100%), lithium chloride (Merck, p.a.), sodium chloride (Merck, p.a.), potassium chloride (Merck, p.a.), choline chloride

(Sigma,  $\geq 99\%$ ) and calcium chloride-2-hydrate (Riedel-de Haën,  $\geq 99\%$ ) were used as received. Titer solutions of potassium hydroxide (0.1 N and 1 N) were purchased from Merck, while choline base (ChOH) was provided by Taminco as a clear (APHA  $< 300$ ) 46 wt% aqueous solution. ChC12 was prepared and purified according to the procedure described in Section II.4.1. KC12 was obtained by direct neutralization of dodecanoic acid (Merck,  $\geq 99\%$ ) with 0.1 N KOH. The stock solution of choline hydroxide was stored at  $-18^{\circ}\text{C}$  under nitrogen and protected from light in order to prevent decomposition. The exact concentration of ChOH was determined by a threefold titration with 0.1 M HCl (Merck).

### **VII.4.2. Synthesis of ChDS and KDS**

ChDS as well as KDS were prepared by ion exchange of SDS using a strong cation exchanger (type I, Merck, p.a.). First, the column material was washed successively with 1 M HCl (Merck) and a large amount of Millipore water such that a near-neutral pH was achieved. Afterwards, the ion exchanger was loaded with the chloride salts, which were available in high purity. For this purpose, 1 M aqueous salt solutions were passed over the resin until the resulting pH value was around 4-5 (corresponding to 4 times the maximum cation exchange capacity). In order to ensure completeness of the exchange process, the column was subsequently treated with 0.1 M solutions of the respective hydroxides (effluent pH  $\approx 10$ ). The resin was then rinsed with Millipore water until quantitative removal of any excess base was accomplished (final pH  $\approx 7$ ). SDS was employed as a 0.1 M solution in an amount lower than 1/3 of the minimum resin capacity. After generously discarding forerunnings, the solid surfactants were obtained by lyophilization of the effluent. The resulting white powders were dried subsequently in a desiccator at a pressure of  $10^{-2}$  mbar for about 2-3 days.

The purity of ChDS and KDS was ascertained by  $^1\text{H}$  NMR ( $\text{CDCl}_3$ ),  $^{13}\text{C}$  NMR ( $\text{CDCl}_3$ ) and ES-MS (electro-spray mass) spectroscopy. NMR spectra were recorded on a Bruker Avance 300 spectrometer at 300 MHz with tetramethylsilane (TMS) as internal standard. Mass spectrometry was performed on a ThermoQuest Finnigan TSQ 7000 instrument.

**ChDS:**

$\delta_{\text{H}}$  (300 MHz;  $\text{CDCl}_3$ ) 0.86 (3 H, t, ,  $J_{1,2} = 6.31$  Hz,  $J_{2,3} = 6.86$  Hz,  $\text{CH}_3\text{CH}_2$ ), 1.24 (18 H, m,  $\text{CH}_2$  (DS)), 1.62 (2 H, quintett,  $J_{1,2} = 6.86$  Hz,  $J_{2,3} = 7.14$  Hz,  $J_{3,4} = 7.41$  Hz,  $J_{4,5} = 6.86$  Hz,  $\text{CH}_2\text{CH}_2\text{OSO}_3^-$ ), 3.29 (9 H, s,  $(\text{CH}_3)_3\text{N}$ ), 3.64 (2 H, m,  $\text{NCH}_2$ ), 3.95 (2 H, t,  $J_{1,2} = 6.86$  Hz,  $J_{2,3} = 7.14$  Hz,  $\text{CH}_2\text{OSO}_3^-$ ), 4.05 (2H, s,  $\text{NCH}_2\text{CH}_2\text{OH}$ ), 4.90 (1 H, s, OH).

$\delta_{\text{C}}$  (300 MHz;  $\text{CDCl}_3$ ) 14.14, 22.70, 25.88, 29.38 – 29.70, 31.93, 54.29, 56.46, 67.76, 68.01.

$m/z$  343 ( $\text{M}^+$ , 100%), 148 (11), 473.3 (13,  $2\text{M}^+ + \text{M}^-$ ), 265 ( $\text{M}^-$ , 100%), 634 (9,  $2\text{M}^- + \text{M}^+$ ).

**KDS:**

$\delta_{\text{H}}$  (300 MHz;  $(\text{CD}_3)_2\text{SO}$ ) 0.85 (3 H, t, ,  $J_{1,2} = 6.59$  Hz,  $J_{2,3} = 6.86$  Hz,  $\text{CH}_3\text{CH}_2$ ), 1.24 (18 H, m,  $\text{CH}_2$  (DS)), 1.47 (2 H, quintett,  $J_{2,3} = 6.59$  Hz,  $J_{3,4} = 6.59$  Hz,  $\text{CH}_2\text{CH}_2\text{OSO}_3^-$ ), 2.5 (2 H, s, quintett,  $J_{1,2} = 1.65$  Hz,  $J_{2,3} = 1.92$  Hz,  $J_{3,4} = 1.65$  Hz,  $J_{4,5} = 1.92$  Hz), 3.67 (2 H, t,  $J_{1,2} = 6.86$  Hz,  $J_{2,3} = 6.59$  Hz,  $\text{CH}_2\text{OSO}_3^-$ ).

$\delta_{\text{C}}$  (300 MHz;  $(\text{CD}_3)_2\text{SO}$ ) 13.86, 22.00, 25.43, 28.69 – 28.97, 31.20, 65.36.

$m/z$  343 ( $2\text{K}^+ - \text{M}^-$ , 100%), 647 (73,  $3\text{K}^+ - 2\text{M}^-$ ), 956 (35,  $4\text{K}^+ - 3\text{M}^-$ ), 1256 (27,  $5\text{K}^+ - 4\text{M}^-$ ), 265 ( $\text{M}^-$ , 100%), 569 (11,  $2\text{M}^- + \text{K}^+$ ).

**VII.4.3. Methods****VII.4.3.1. Determination of Krafft Temperatures**

For the sake of simplicity, the common convention of the Krafft point being the solubility temperature of a 1 wt% surfactant solution (which is typically far above the *cmc*) was applied. The influence of various salts on  $T_{Kr}$  of the distinct surfactants was assessed in a similar fashion. The surfactant concentration was fixed to 1 wt% and the salts were introduced by adding different amounts of stock solutions.

Precise solubility temperatures were determined by turbidity measurements using an automated home-built apparatus, which was equipped with a computer-controlled thermostat.<sup>48</sup> Turbidity was detected by monitoring the transmission of light emitted by a LED with the aid of a light-dependent resistor (LDR). If necessary, samples were

cooled until precipitation occurred, followed by subsequent heating with a rate of 1°C per hour.

### VII.4.3.2. Density Measurements

Densities,  $\rho$ , were required in order to evaluate exact concentrations of the samples investigated by surface tension and conductivity measurements. They were determined at 25°C using a vibrating tube densimeter (Anton Paar DMA 60), which was calibrated by measuring purified dry nitrogen and degassed water. The resulting experimental values are compiled in Table VII.3.

**Table VII.3** Density data of ChDS solutions at 25°C.

wt% ChDS	$\rho / \text{g L}^{-3}$
0.99	997.57
2.51	998.31
4.96	999.59
9.97	1002.09
14.99	1004.69
19.96	1007.24

The obtained density values were found to increase linearly in the concerned concentration regime. Linear regression of the experimental data gave an equation for the calculation of density values, according to  $\rho / \text{g L}^{-1} = 0.51 \cdot \text{wt}\%_{\text{ChDS}} + 997.05 / \text{g L}^{-1}$ . The collected data also allow for a determination of the molar volume,  $V_m$ , of the surfactant, following the procedure described in Appendix B.1 ( $V_m$  (ChDS) = 0.522 L mol<sup>-1</sup>).

### VII.4.3.3. Surface Tension Measurements

The surface tension,  $\sigma$ , was measured with a platinum-iridium ring using a Krüss tensiometer (model K100 MK2), which was equipped with a double-dosing system (Methrom Liquino 711). This setup permits automated data acquisition as a function of the surfactant concentration (reversed *cmc* determination). The temperature was monitored on-line and kept constant at 25°C ± 0.1°C. Measured values were corrected according to a procedure introduced by Harkins and Jordan.<sup>49</sup> The resulting progression

of the surface tension as a function of the surfactant concentration is shown in Fig. VII.9.

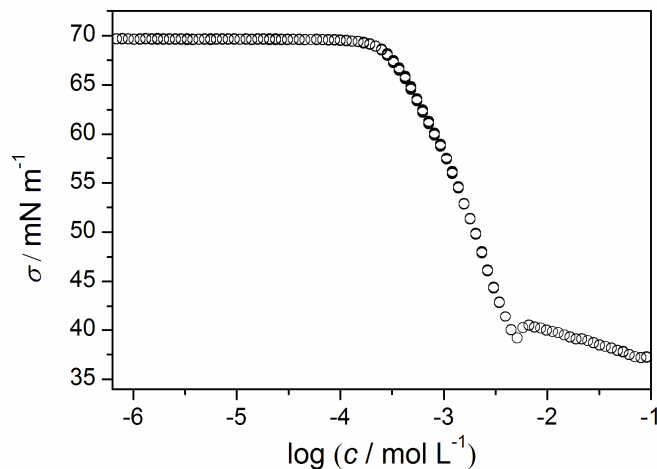


**Fig. VII.9** Surface tension of ChDS as a function of the surfactant concentration at 25°C.

The *cmc* corresponds to the surfactant concentration at the onset of the pronounced increase in  $\sigma$ , which is given by the intersection of linear fits to the curve segments before and after the *cmc*. Further, the excess surfactant concentration,  $\Gamma$ , and the area per molecule,  $A_S$ , were calculated on the basis of the recorded data (obtained values are listed in Table VII.1). To facilitate proper comparison, the surface tension of SDS was measured in an identical manner (cf. Table VII.1).

#### VII.4.3.4. Conductivity Measurements

Conductivities,  $\kappa$ , of aqueous ChDS solutions were measured at 25°C by means of an autobalance conductivity bridge (Konduktometer 702, Knick), equipped with a Consort SK41T electrode cell. The cell constant was determined by measuring 0.01 m, 0.1 m and 1 m potassium chloride solutions at 25°C.<sup>50</sup> The *cmc* value was obtained from the breakpoint in the concentration-dependent plot of the conductivity (Fig. VII.10). The degree of micelle ionization,  $\alpha$ , can be derived by the expression of Evans<sup>38</sup> as outlined in Section II.4.2. This requires the aggregation number  $N_{agg}$  at the *cmc*, which can be estimated to  $N_{agg} = 56$  for ChDS when assuming spherical micelles with fully extended hydrocarbon chains and using the expressions of Tanford.<sup>51</sup>

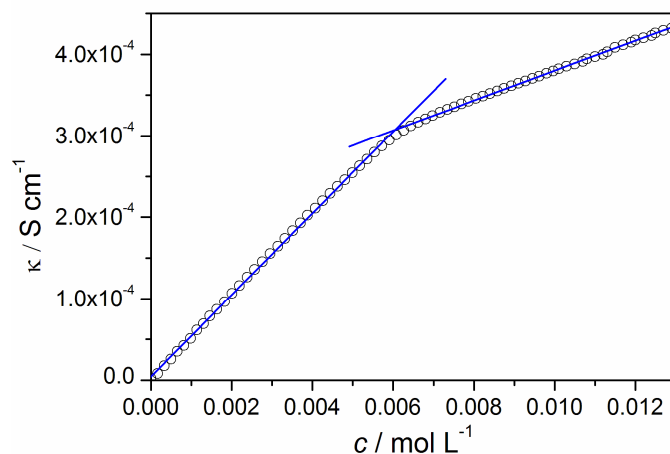


Fig. VII.10 Plot of the specific conductivity  $\kappa$  versus the concentration of ChDS at 25°C.

#### VII.4.3.5. Decomposition Temperatures

The thermal stability of ChDS was studied by determining the decomposition temperature,  $T_{dec}$ , on a thermogravimetric analyzer of Perkin-Elmer (TGA 7). Measurements were conducted under a constant nitrogen flow with a heating rate of  $10 \text{ K min}^{-1}$ . The onset of mass loss, defined by the intercept of the baseline before decomposition and the tangent to the curve afterwards, was taken as  $T_{dec}$ . Resulting data for ChDS and SDS are outlined in Fig. VII.11.

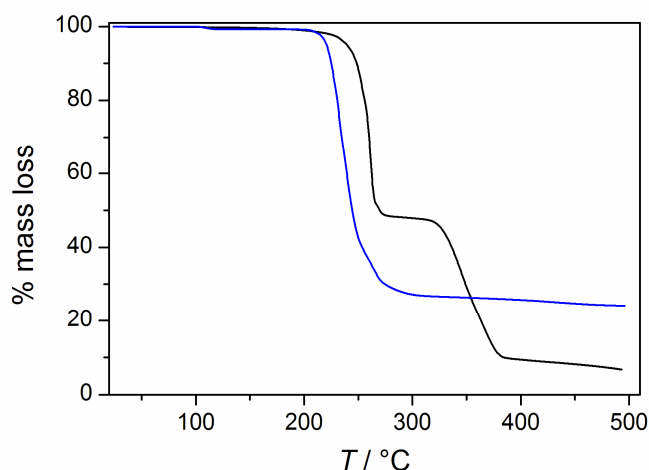


Fig. VII.11 TGA curves of ChDS (black) and SDS (blue).

Obviously, ChDS is decomposed by a two-step mechanism, while SDS degrades in a single step. However, the latter reaches a degree of decomposition of only about 26% up to 500°C ( $T_{dec}(\text{SDS}) = 221^\circ\text{C}$ ). A possible scenario explaining the behavior traced for ChDS is that, in a first step, the alkyl sulfate part is decomposed, whereas the choline

cation disintegrates at higher temperatures (starting from about 330°C). This is supported by the fact that the onset temperature of mass loss found for ChDS ( $T_{dec}$  (ChDS) = 252°C) is close to that of SDS. However, the most surprising result is that ChDS appears to be thermally even more stable than SDS and much more stable than choline fatty acid soaps ( $T_{dec}$  (ChC*m*) = 190-202°C, see Section V.2.1).

#### **VII.4.3.6. Cryo-Transmission Electron Microscopy (Cryo-TEM)**

For cryo-TEM, aliquots of sample were loaded onto holey carbon grids and blotted with a piece of filter paper to give a thin liquid film. The latter was vitrified by quickly immersing the grid in liquid ethane and transferred to a Zeiss EM922 EF transmission electron microscope. Analyses were performed at 90 K and an acceleration voltage of 200 kV. A Gatan Ultrascan 1000 CCD camera was used for imaging. Recording and processing of images was accomplished with the aid of the Digital Micrograph software package (version 3.9).

#### **VII.4.3.7. Penetration Scan Studies**

Penetration scans were performed as described in Chapter IV.4.2. A JVC digital camera (TK-C130) mounted on a Leitz Orthoplan microscope (Wetzlar, Germany) was used for imaging. Temperature control was realized by a Linkham hot stage (TMS90) equipped with a CS196 cooling system. A rate of 10°C min<sup>-1</sup> was chosen for heating and cooling in all cases.

#### **VII.4.3.8. Establishment of the Phase Diagram**

Liquid-crystalline samples were prepared as described in Chapter IV.4.2. As for the choline soaps, a first concentration-dependent mapping of the aqueous phase behavior of ChDS was achieved by visual inspection of the samples between crossed polarizers at different temperatures. Samples were prepared in concentration steps of 5 wt% concentration steps. The temperature interval studied ranged from 0°C to 90°C and was monitored with a heating rate of about 5°C per hour. Samples were checked initially after 2 days and after ageing for 1 month. Phase boundaries were thereby determined based on the latter results.

### VII.4.3.9. Cytotoxicity Tests

The cytotoxicity of ChDS, SDS and ChC12 was assessed on two distinct human cell lines, namely HeLa (cervix carcinoma, ATCC CCL17) and SK-Mel-28 (keratinocytes, CLS 300337) by using the MTT assay.<sup>52,53</sup> This procedure is based on the reduction of the yellow MTT salt (3-(4,5-dimethylthiazol-2-yl)-2,5-diphenyl tetrazolium bromide) to a blue formazan dye by mitochondrial dehydrogenase in viable cells. Details on the measurements are given in Chapter III.4.3. The IC<sub>50</sub> value, which represents the surfactant concentration that induces 50% loss of the viable cells (relative to the untreated control cells), was derived from concentration-dependent response curves (8 different concentrations). Experiments were carried out in triplicate over several weeks while, on one day, IC<sub>50</sub> values were determined in four independent measurements, each being the average of two analyses of a given sample.

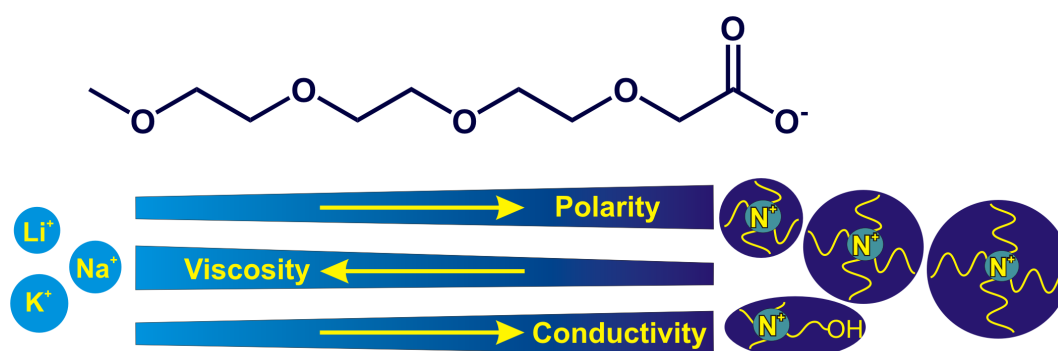
## VII.5. References

1. R. Klein, D. Touraud, W. Kunz, *Green Chem.*, 2008, **10**, 433.
2. R. G. Laughlin, *The Aqueous Phase Behavior of Surfactants*, Academic Press, San Diego, 1994, p. 108.
3. J. W. McBain, W. W. Lee, *Oil Soap*, 1943, **20**, 17.
4. A. Schmalstieg, G. W. Wasov, in *Handbook of Applied Surface and Colloid Chemistry*, Ed. K. Holmberg, John Wiley & Sons Ltd., 2002, pp. 271-293.
5. H. W. Stache, *Surfactant Science Series - Anionic Surfactants*, Marcel Dekker, New York, 1996.
6. M. J. Schwuger, *Kolloid-Z. Z. Polym.*, 1969, **233**, 979.
7. H. Lange, M. J. Schwuger, *Kolloid-Z. Z. Polym.*, 1968, **223**, 145.
8. J. K. Weil, F. D. Smith, A. J. Stirton, R. G. Bistline, Jr., *J. Am. Oil Chem. Soc.*, 1963, **40**, 538.
9. H. Nakayama, K. Shinoda, *Bull. Chem. Soc. Jpn.*, 1967, **40**, 1797.
10. A. Renoncourt, *Study of Supra-Aggregates in Catanionic Surfactant Systems*, PhD thesis, University of Regensburg, 2005.
11. Z. Yu, X. Zhang, G. Xu, G. Zhao, *J. Phys. Chem.*, 1990, **94**, 3675.

12. K. D. Collins, *Methods*, 2004, **34**, 300.
13. K. D. Collins, G. W. Neilson, J. E. Enderby, *Biophys. Chem.*, 2007, **128**, 95.
14. J. B. S. Bonilha, R. M. Z. Georgetto, E. Abuin, E. Lissi, F. Quina, *J. Colloid Interface Sci.*, 1990, **135**, 238.
15. J. V. Joshi, V. K. Aswal, P. Bahadur, P. S. Goyal, *Curr. Sci.*, 2002, **83**, 47.
16. J. V. Joshi, V. K. Aswal, P. S. Goyal, *J. Phys.: Condens. Matter*, 2007, **19**, 196219/1-196219/9.
17. S. J. Froehner, A. Belarmino, D. Zanette, *Colloids Surf. A*, 1998, **137**, 131.
18. R. Klein, M. Kellermeier, M. Drechsler, D. Touraud, W. Kunz, *Colloids Surf. A*, 2009, **338**, 129.
19. B. L. Bales, M. Benrraou, R. Zana, *J. Phys. Chem. B*, 2002, **106**, 9033.
20. P. Mukerjee, *Adv. Colloid Interface Sci.*, 1967, **1**, 241.
21. R. Zana, *Langmuir*, 2004, **20**, 5666.
22. R. Zana, J. Schmidt, Y. Talmon, *Langmuir*, 2005, **21**, 11628.
23. Z. J. Yu, G. Xu, *J. Phys. Chem.*, 1989, **93**, 7441.
24. B. L. Bales, R. Zana, *Langmuir*, 2004, **20**, 1579.
25. R. Zana, M. Benrraou, B. L. Bales, *J. Phys. Chem. B*, 2004, **108**, 18195.
26. M. Benrraou, B. L. Bales, R. Zana, *J. Phys. Chem. B*, 2003, **107**, 13432.
27. Z. J. Yu, Z. Zhou, G. Xu, *J. Phys. Chem.*, 1989, **93**, 7446.
28. V. Pradines, D. Lavabre, J.-C. Micheau, V. Pimienta, *Langmuir*, 2005, **21**, 11167.
29. M. Benrraou, B. Bales, R. Zana, *J. Colloid Interface Sci.*, 2003, **267**, 519.
30. B. L. Bales, K. Tiguida, R. Zana, *J. Phys. Chem. B*, 2004, **108**, 14948.
31. A. Paul, P. C. Griffiths, E. Pettersson, P. Stilbs, B. L. Bales, R. Zana, R. K. Heenan, *J. Phys. Chem. B*, 2005, **109**, 15775.
32. C. M. Tcacenco, R. Zana, B. L. Bales, *J. Phys. Chem. B*, 2005, **109**, 15997.
33. R. Moberg, F. Boekman, O. Bohman, H. O. G. Siegbahn, *J. Am. Chem. Soc.*, 1991, **113**, 3663.
34. M. E. O'Leary, R. Horn, *J. Gen. Physiol.*, 1994, **104**, 507.

35. M. E. O'Leary, R. G. Kallen, R. Horn, *J. Gen. Physiol.*, 1994, **104**, 523.
36. C. Vautier-Giongo, B. L. Bales, *J. Phys. Chem. B*, 2003, **107**, 5398.
37. B. Lindman, in *Handb. Appl. Surf. Colloid Chem.*, Ed. K. Holmberg, John Wiley & Sons Ltd., Chichester 2002, pp. 421-443.
38. H. C. Evans, *J. Chem. Soc.*, 1956, 579.
39. P. Mukerjee, K. J. Mysels, *Critical Micelle Concentrations of Aqueous Surfactant Systems*, NSRDS-NBS 36, Washington D.C., 1971.
40. P. Kekicheff, C. Grabielle-Madelmont, M. Ollivon, *J. Colloid Interface Sci.*, 1989, **131**, 112.
41. S. Hassan, W. Rowe, G. J. T. Tiddy, in *Handbook of Applied Surface and Colloid Chemistry.*, Ed. K. Holmberg, John Wiley & Sons Ltd., Chichester 2002, pp. 465.
42. P. Kekicheff, *J. Colloid Interface Sci.*, 1989, **131**, 133.
43. J. N. Israelachvili, D. J. Mitchell, B. W. Ninham, *J. Chem. Soc., Faraday Trans. 2*, 1976, **72**, 1525.
44. N. Vlachy, B. Jagoda-Cwiklik, R. Vácha, D. Touraud, P. Jungwirth, W. Kunz, *Adv. Colloid Interface Sci.*, 2009, **146**, 42.
45. K. D. Collins, *Biophys. Chem.*, 2006, **119**, 271.
46. H. V. Tartar, R. D. Cadle, *J. Phys. Chem.*, 1939, **43**, 1173.
47. S. Miyamoto, *Bull. Chem. Soc. Jpn.*, 1960, **33**, 371.
48. S. Schroedle, R. Buchner, W. Kunz, *Fluid Phase Equilib.*, 2004, **216**, 175.
49. W. D. Harkins, H. F. Jordan, *J. Am. Chem. Soc.*, 1930, **52**, 1751.
50. D. R. Lide, *CRC - Handbook of Chemistry and Physics*, CRC Press, Boca Raton, USA, 2004.
51. C. Tanford, *J. Phys. Chem.*, 1972, **76**, 3020.
52. T. Mosmann, *J. Immunol. Methods*, 1983, **65**, 55.
53. N. Vlachy, D. Touraud, J. Heilmann, W. Kunz, *Colloids Surf. B*, 2009, **70**, 278.

## Chapter VIII Oligoether Carboxylates – Task-Specific Room-Temperature Ionic Liquids



Recently, a new family of ionic liquids based on oligoether carboxylates was introduced. 2,5,8,11-Tetraoxatridecan-13-oate (TOTO) was shown to form room-temperature ionic liquids (RTILs) even with small alkali ions such as lithium and sodium. However, the alkali TOTO salts suffer from their extremely high viscosities and relatively low conductivities. Therefore, in this study the alkali cations have been replaced by tetraalkylammonium (TAA) ions (tetraethyl- (TEA), tetrapropyl- (TPA), and tetrabutylammonium (TBA). In addition, the environmentally benign quaternary ammonium ion choline (Ch) was included in the series. All salts were found to be ionic liquids at ambient temperatures with a glass transition typically at around  $-60^{\circ}\text{C}$ . Viscosities, conductivities, solvent polarities and Kamlet-Taft parameters were determined as a function of temperature. When using quaternary ammonium ions, the viscosities of the resulting TOTO ionic liquids are more than 600 times lower while conductivities increase by a factor of up to 1000 compared to their alkali counterparts. Solvent polarities further reveal that choline and TAA cations yield TOTO ionic liquids which are more polar than those obtained with the, *per se*, highly polar sodium ion. Results are discussed in terms of ion-pairing and structure-breaking concepts with regard to a possible complexation ability of the TOTO anion.

## VIII.1. Introduction

In the past two decades, ionic liquids (ILs) – being defined as salts with melting points below 100°C – have attracted an enormous deal of attention due to their potential as green alternatives to common organic solvents.<sup>1</sup> Since ILs consist entirely of ions, their vapor pressure is, in contrast to molecular liquids, almost non-detectable. Beyond that, solvent properties such as viscosity, conductivity, polarity and thermal stability can be tuned by combining adequate pairs of cations and anions.

The reduced melting points of ILs can usually be obtained by hindering a regular crystalline packing of the ions.<sup>2</sup> An efficient means to achieve this is the use of large and preferably non-symmetrical ions, which have high conformational flexibility and delocalized charge distribution.<sup>2</sup> Therefore, previous work has widely been focused on cations such as imidazolium, pyridinium, or pyrrolidinium and halogenated anions like hexafluorophosphate ( $\text{PF}_6^-$ ), tetrafluoroborate ( $\text{BF}_4^-$ ) or triflate ( $\text{SO}_3\text{CF}_3^-$ ).<sup>3</sup>

However, the non-volatility and the low vapor pressure of ILs do not *a priori* imply that these substances are biocompatible. Several studies disclosed the potential toxic impact of imidazolium and pyridinium derivatives.<sup>4-8</sup> Large cations, particularly those with a certain hydrophobicity, exhibit intrinsic toxicity due to their capability to adsorb on natural surfaces and interact with DNA.<sup>9</sup> In turn, knowledge about ILs based on small cations and larger anions, especially concerning salts which are liquid at room temperature (RTILs), is still strongly limited.

Recently, alkali metal oligoether carboxylates were reported as a new class of ILs.<sup>10-12</sup> Using 2,5,8,11-tetraoxatridecan-13-oate (TOTO, shown in see Fig. VIII.1) as anion and small alkali ions such as lithium and sodium, RTILs of high electrochemical and thermal stability are gained.<sup>10</sup> The observed low melting points can thereby be ascribed mainly to the introduction of ethylene oxide (EO) units, which increase the chain flexibility of the anion. Dielectric relaxation and polarity measurements showed that Na-TOTO forms a cross-linked structure with strong  $-\text{COO}^- \cdots \text{Na}^+$  interactions rather than a crown ether-like complex.<sup>12</sup> However, these strong ionic interactions cause low ionicities of the alkali TOTO salts and viscosities as high as for example ~164 000 mPa s with sodium as cation, which is comparable to polymer melts or syrup. It is well-known that the binding strength between carboxylates and alkali ions decreases with growing size of the cation ( $\text{Li}^+ > \text{Na}^+ > \text{K}^+ > \text{Cs}^+$ ).<sup>13,14</sup> Further, the

fluidity and ion mobility of ILs is commonly expected to increase when ion association is weakened.<sup>15,16</sup> On this account, the alkali cations in TOTO ILs were substituted by bulky tetraalkylammonium (TAA) ions, namely tetraethyl- (TEA), tetrapropyl- (TPA) and tetrabutylammonium (TBA) (see Fig. VIII.1). In addition, choline (Ch) as a benign quaternary ammonium ion of biological origin has been investigated.<sup>17-19</sup>

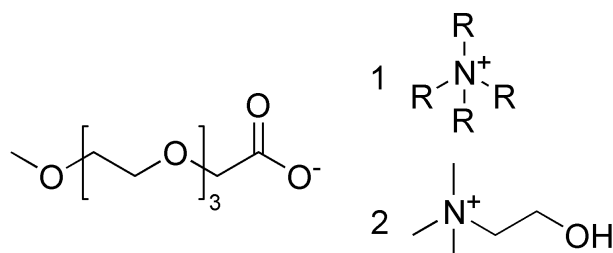


**Fig. VIII.1** Molecular structure of the investigated ionic liquids, which consist of the TOTO anion and various cations: (1) quaternary ammonium ions with R=  $\text{CH}_2\text{CH}_3$  (TEA),  $\text{CH}_2\text{CH}_2\text{CH}_3$  (TPA),  $\text{CH}_2\text{CH}_2\text{CH}_2\text{CH}_3$  (TBA), and (2) choline (Ch).

Ionic liquids based on saturated ammonium ions have been described in the literature and were found to be featured by satisfactory electrochemical stability as compared to 1,3-dialkylimidazolium cations, which renders them promising candidates for electrolytes in high-energy devices.<sup>20-23</sup> However, most of these TAA ILs comprise halogenated anions, among which bis(trifluoromethanesulfonyl)imide (TFSI) and hydrophobic perfluoroalkyltrifluoroborates proved to be most efficient in terms of low viscosity and high conductivity.<sup>23</sup> Very recently, also choline was employed for the design of novel, truly green ionic liquids with anions such as short- and middle-chain alkanoates,<sup>24</sup> lactate,<sup>25</sup> saccharinate,<sup>26</sup> acesulfamates,<sup>26, 27</sup> derivatives of phosphate<sup>28</sup> or naphthenic acid.<sup>29</sup>

In the present work, TAA- and Ch-TOTO ILs were synthesized and characterized with respect to basic physical solvent properties such as glass or melting temperatures, decomposition temperatures, as well as temperature-dependent viscosities and conductivities. The studied ILs were moreover classified according to a Walden plot in analogy to the work by Xu *et al.*<sup>16,30</sup> Finally, empirical solvent polarities by means of  $E_T^N$ -values and Kamlet-Taft parameters were determined at various temperatures.

## VIII.2. Results and Discussion

### VIII.2.1. Decomposition and Glass Temperatures

The  $T_{dec}$  and  $T_g$  values obtained for the studied compounds are listed in Table VIII.1. The thermal stability of TAA- and Ch-TOTO is limited to (189-218)°C, which is (139-195)°C lower than for the alkali derivatives.<sup>10</sup> This finding can likely be ascribed to the organic nature of the cations and the well-known poor thermal stability of tetraalkylammonium ions.<sup>31,32</sup>

**Table VIII.1** Decomposition ( $T_{dec}$ ) and glass ( $T_g$ ) temperatures and molar volumes ( $V_m$ ) at 25°C of TAA- and Ch-TOTO ionic liquids.

Cation	$T_{dec}$ / °C	$T_g$ / °C	$V_m$ /cm <sup>3</sup> mol <sup>-1</sup> (25°C)
Ch	218	-58	288
TEA	196	-62	328
TPA	189	-57	397
TBA	190	-61	464

It is further evident from Table VIII.1 that all investigated TOTO salts are liquid at room temperature and exhibit a glass transition at around -60°C. Comparing these results to the lithium and sodium TOTO salts, which show glass points at -53°C and -57°C, respectively,<sup>10</sup> suggests that the liquid range of TOTO ILs towards low temperatures is almost not affected when changing the cations. This is remarkably when noting that the molecular volume,  $V_m$ , increases by a factor of 2.6 from Na- to TBA-TOTO (Table VIII.1). Actually, Xu *et al.* identified a minimum in the relationship between  $T_g$  values (which are representative for the cohesion energy) and molar volumes (which characterize the interionic spacing) for a variety of quaternary ammonium RTILs with distinct halogenated anions.<sup>16,33</sup> Thus, it has been proposed that the origin of the large liquid range observed for TOTO salts of small alkali and large quaternary ammonium differs. Alkali TOTO ILs were shown to exhibit strong ion-pairing,<sup>10,12</sup> similarly as the phosphonium ILs reported by MacFarlane and coworkers.<sup>34</sup> Accordingly, they can be considered more as an “intermediate” solvent between true molecular solvents and true ionic liquids. The formed “liquid ion pairs” are featured by attenuated intermolecular Coulomb interactions, which leads to low  $T_g$  values. By

contrast, TAA- and Ch-TOTO ILs indeed are dissociated salts, as will be demonstrated in the following. Generally, quaternary ammonium compounds are known to melt at much lower temperatures than inorganic salts.<sup>35,36</sup> Thereby, TOTO appears to be a very efficient anion to enhance their liquid range even further.

Earlier studies on quaternary ammonium RTILs reported an increase of  $T_g$  when alkyl ether groups were inserted in the alkyl side chain of the cation,<sup>33</sup> while others observed a decrease.<sup>23</sup> These diverging results may rest upon two opposing effects of the alkyl ether groups. On the one hand, the introduction of ether functionalities renders the system more polar relative to simple alkyl chains, which would result in higher  $T_g$  values. On the other hand, it also increases the chain flexibility, which causes lower  $T_g$  values. In the present case, the enhanced chain flexibility seems to outbalance the higher polarity. This becomes further manifest when comparing the glass temperature of Ch-TOTO, for instance, to the melting points ( $T_m$ ) of choline alkanoates, which have recently been discovered to be ionic liquids.<sup>24,32,37</sup> Choline octanoate, for example, melts at 26°C.<sup>24</sup> This means that the four additional oxygen atoms present in Ch-TOTO suppress the melting point by 84°C to a glass transition. Choline dodecanoate forms lamellar liquid crystals at 68°C and melts into an isotropic liquid phase at about (120-150)°C.<sup>37</sup> Thus, substitution of four CH<sub>2</sub> groups by four oxygens in the alkyl chain provokes a melting to glass point reduction of more than 178°C. In this context, it should be emphasized that the studied TOTO ILs do not display thermotropic mesomorphism.

Further, it should be noted that glass temperatures commonly provide a measure for the ion mobility or the fluidity of RTILs at ambient temperature.<sup>16,33</sup> The  $T_g$  values detected for TOTO ILs vary within less than 4°C even when replacing the small sodium by the big TBA ion. Nevertheless, the fluidities of the ILs differ considerably, as discussed below.

### **VIII.2.2. Viscosity and Conductivity Measurements**

Fig. VIII.2 shows the plots of the viscosity and conductivity of the different RTILs as a function of temperature. The experimental data can in both cases be well described by the empirical Vogel-Fulcher-Tamman (VFT) equation (see Equations (VIII.1) and (VIII.2)).<sup>38</sup> It contains three adjustable parameters, namely the pre-exponential factor  $\eta_0$

or  $\kappa_0$ , the pseudo-activation energy  $E_\eta$  or  $E_\kappa$ , and the so-called VFT temperature  $T_{0\eta}$  or  $T_{0\kappa}$ .<sup>38</sup>

$$\ln \eta = \ln \eta_0 + E_\eta / R (T - T_{0\eta}) \quad (\text{VIII.1})$$

$$\ln \kappa = \ln \kappa_0 - E_\kappa / R (T - T_{0\kappa}) \quad (\text{VIII.2})$$

The results of the corresponding fits are summarized in Table VIII.2 and Table VIII.3.  $T_{0\eta}$  and  $T_{0\kappa}$  can be regarded as ideal glass transition temperatures. Their values are about (27-86) °C lower than those determined experimentally for  $T_g$ , which is in line with previous work.<sup>38</sup>

**Table VIII.2** VFT parameters obtained from fits of temperature-dependent viscosity data according to Eqn. (VIII.1) for TAA- and Ch-TOTO ionic liquids.

Cation	$\ln \eta_0$ (P)	$E_\eta$ / eV	$T_{0\eta}$ / K
Ch	$-11 \pm 3$	$0.18 \pm 0.09$	$129 \pm 46$
TEA	$-6.8 \pm 0.3$	$0.076 \pm 0.007$	$184 \pm 6$
TPA	$-11 \pm 1$	$0.17 \pm 0.03$	$144 \pm 14$
TBA	$-11 \pm 1$	$0.18 \pm 0.03$	$137 \pm 16$

**Table VIII.3** VFT parameters obtained from fits of temperature-dependent conductivity data according to Eqn. (VIII.2) for TAA- and Ch-TOTO ionic liquids.

Cation	$\ln \kappa_0$ (S m <sup>-1</sup> )	$E_\kappa$ / eV	$T_{0\kappa}$ / K
Ch	$62.31 \pm 1.63$	$0.090 \pm 0.001$	$178.3 \pm 0.4$
TEA	$61.7 \pm 2.46$	$0.071 \pm 0.001$	$182.4 \pm 0.8$
TPA	$87.25 \pm 7.62$	$0.093 \pm 0.002$	$179.2 \pm 1.4$
TBA	$72.16 \pm 3.50$	$0.106 \pm 0.001$	$168.5 \pm 0.8$

As evident from Fig. VIII.2 a, the viscosities of the investigated TOTO ILs increase with the size of the TAA cation, while an inverse trend is observed for their conductivities (Fig. VIII.2 b). This behavior is a common phenomenon. The reinforced van der Waals interactions provoke higher viscosities, while a lower charge density per unit volume accounts for the decrease of the specific conductivity.<sup>16,23,31,33</sup> Ch-TOTO

shows  $\eta$  and  $\kappa$  values close to those of TPA-TOTO. The non-symmetrical structure and smaller size of the choline cation is actually expected to promote a lower viscosity as compared to TEA-TOTO.<sup>15,30</sup> Probably, the terminal hydroxyl group of choline gives rise to inter-molecular hydrogen bonding, which increases the viscosity.

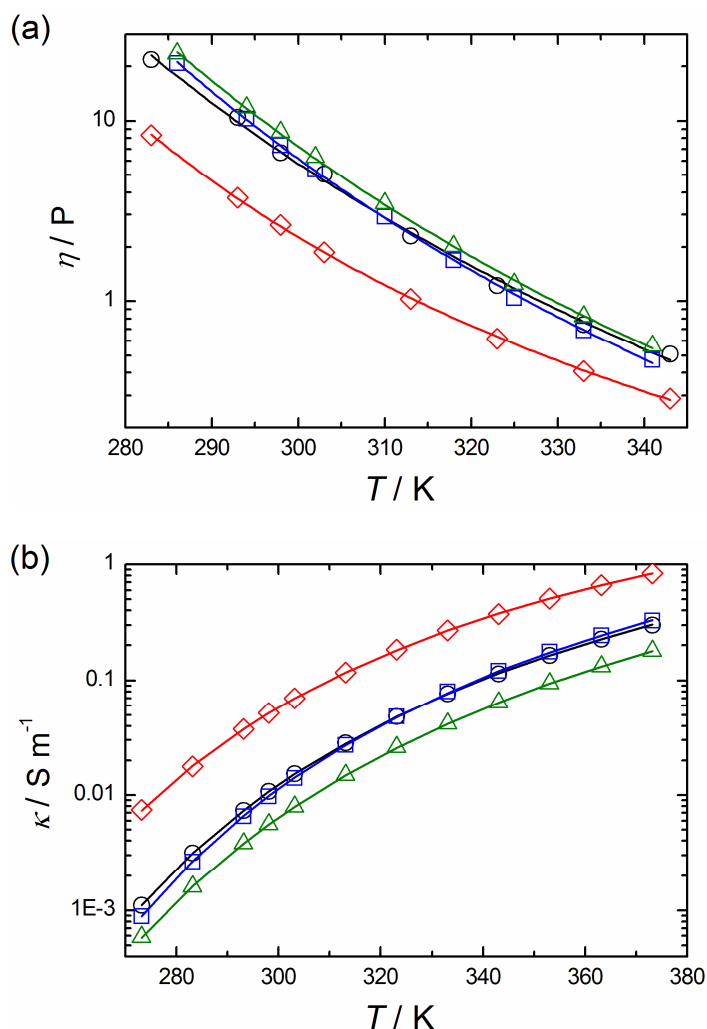


**Fig. VIII.2** (a) Viscosities and (b) specific conductivities of TAA- and Ch-TOTO ionic liquids as a function of temperature (( $\diamond$ ) TEA, ( $\square$ ) TPA, ( $\triangle$ ) TBA), ( $\circ$ ) Ch). Full lines represent fits according to the empirical Vogel-Fulcher-Tamman equation. Corresponding fit parameters are given in Table VIII.2 and Table VIII.3.

The  $\eta$  and  $\kappa$  values at 25°C are further listed in Table VIII.4. The viscosities of TAA- and Ch-TOTO ILs vary between 264 mPa s and 841 mPa s, and the conductivities between 11  $\mu S\ cm^{-1}$  and 517  $\mu S\ cm^{-1}$ . The magnitudes of both,  $\eta$  and  $\kappa$ , are comparable to those of common 1-butyl-3-methylimidazolium ionic liquids with anions such as  $PF_6^-$  or  $TFSI^-$ .<sup>39-41</sup> It has previously been pointed out that small quaternary ammonium ions are suitable for the design of low viscous RTILs.<sup>20,21,23,42,43</sup> For instance, Yu *et al.*

demonstrated that the combination of small tetraalkylammonium ions with certain amino acids yields RTILs with viscosities as low as 81 mPa s (TEA and  $\alpha$ -alanine).<sup>42</sup> Choline has also been shown to form moderately viscous RTILs, for example with naphthenic<sup>29</sup> or carboxylic acid<sup>32</sup> derivatives. Reported viscosities<sup>29,32</sup> and conductivities<sup>29</sup> are in a similar range as those of Ch-TOTO.

**Table VIII.4** Viscosities and specific as well as molar conductivities of TAA- and Ch-TOTO ionic liquids at 25°C in comparison to values reported for Na-TOTO.<sup>10</sup>

Cation	$\eta$ / mPas	$\kappa$ / $\mu\text{S cm}^{-1}$	$10^4 A_m$ / $\text{S m}^2 \text{mol}^{-1}$
Ch	665	10.8	0.031
TEA	264	516.6	0.170
TPA	720	97.6	0.039
TBA	841	55.5	0.026
Na	164 000	0.5	$9.1 \cdot 10^{-5}$

However, the peculiarity of the present data lies in the TOTO anion and its ability to form RTILs with different simple and commercially available cations, which cover a wide range of accessible viscosity and conductivity values. Essentially, by exchanging Na for TEA (Table VIII.4), the viscosity of the resulting TOTO IL is depressed by a factor of beyond 600, while the conductivity increases more than 1000 times. In the light of these findings, we suspect that the cross-linked structure characterizing Na-TOTO<sup>12</sup> is broken up and interactions between the cation and the carboxylate group are weakened when replacing sodium by TAA ions or choline. This notion is corroborated by the Walden plot (see below).

### VIII.2.3. Walden Plot

The association of cations with anions, i.e. the ionicity of ILs, can be assessed by the use of a Walden plot as suggested by Angell and coworkers.<sup>15,16,44</sup> The Walden rule relates the ionic mobilities (represented by the molar conductivity  $A_m$ ) to the fluidity ( $1/\eta$ ) of the medium.<sup>15</sup> If the ions can move independently from their surrounding neighbors, i.e. the salt is fully dissociated, the plot gives a line of unit slope such as for dilute aqueous KCl solutions.<sup>15,16</sup> In turn, if ion pairs are formed, the movement of the distinct ions will be correlated leading to a negative deviation from the ideal line.<sup>15</sup>

Angell and coworkers quantified this vertical deviation ( $\Delta W$ ) and classified ILs according to it.<sup>15,16</sup> ILs close the KCl line ( $\Delta W < 1$ ) combine high fluidities with high conductivities and are therefore referred to as “good” ionic liquids.<sup>15,16</sup> Such ILs are in addition usually featured by very low vapor pressures and are hence suitable as solvents for green syntheses.<sup>15,16,45</sup> In turn, ILs with  $\Delta W > 1$  (“poor” ionic liquids) exhibit less than 10% of the ionic conductivity as would have been expected on the basis of fluidity and a full dissociation of the salt.<sup>46</sup>

As evidenced by the Walden plot (Fig. VIII.3) and the  $\Delta W$  values (Table VIII.5), TAA- and Ch-TOTO ILs are located close to the ideal line ( $\Delta W < 1$ ) and thus belong to the class of “good” ionic liquids. In line with the trend indicated by the viscosity and conductivity data,  $\Delta W$  increases in the order TEA < TPA < TBA, while Ch-TOTO is located between TPA- and TBA-TOTO. As mentioned above, intermolecular hydrogen bonding of the hydroxyl group of choline likely prevails over the effect of its smaller non-symmetrical structure.

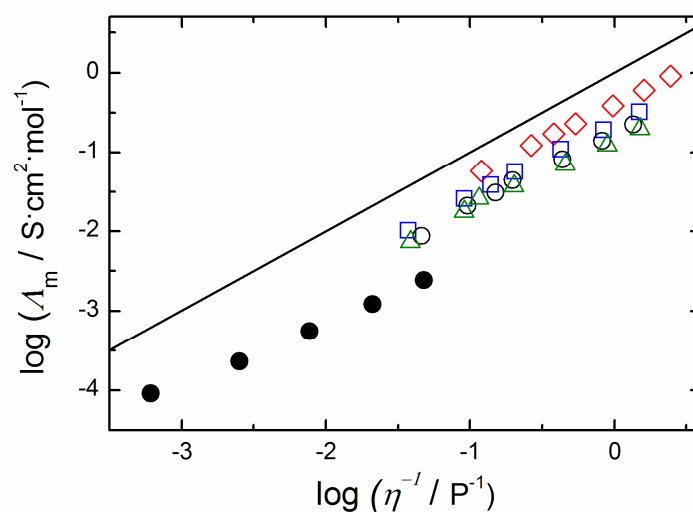


**Fig. VIII.3** Walden plot of TAA- and Ch-TOTO ionic liquids (( $\diamond$ ) TEA, ( $\square$ ) TPA, ( $\triangle$ ) TBA), ( $\circ$ ) Ch) for temperatures ranging from 10°C to 60°C (from the left to the right), as compared to the ideal KCl line (full line) and Na-TOTO ( $\bullet$ ) (values taken from Ref.10).

Interestingly, the TOTO salt of the considerably smaller sodium ion has previously been assigned to the class of “poor” RTILs (cf. Fig. VIII.3).<sup>10</sup> In view of the proposed cross-linked structure of Na-TOTO,<sup>12</sup> the differing positions of TAA- or Ch-TOTO ILs in the Walden plot can probably be ascribed to a more “loose” three-dimensional organization, simply due to the larger cation sizes. In addition, the higher ionicity of TAA- and Ch-TOTO ILs is likely to be caused by weakened ionic interactions between cations and

anions as compared to alkali-TOTO RTILs, which is in agreement with the literature.<sup>14</sup> However, simply increasing the cation radius does not necessarily improve the performance of TOTO RTILs in terms of low  $\Delta W$  values, since the highest ionicity has been detected for the smallest TAA ion, namely TEA. Insertion of functional groups such as -OH in the ammonium ions further promotes larger  $\Delta W$  values of the ionic liquids.

**Table VIII.5** Deviation  $\Delta W$  of TAA- and Ch-TOTO ionic liquids from the ideal KCl line in the Walden plot at different temperatures.

T / °C	10	20	25	30	40	50	60
<b>Ch</b>	0.7	0.7	0.7	0.7	0.7	0.8	0.8
<b>TEA</b>	0.3	0.3	0.3	0.4	0.4	0.4	0.4
<b>TPA</b>	0.6	0.5	0.6	0.6	0.6	0.6	0.7
<b>TBA</b>	0.7	0.7	0.7	0.7	0.8	0.9	0.9

The observed minimum in the relationship between cation radius and ionicity of TOTO ILs can be interpreted in terms of a balance between attractive and repulsive forces: the inter-ionic cohesive coulomb energy decreases with growing cation size, while the van der Waals energy increases.<sup>16</sup>

The present results suggest that the fluidity and ion mobility of TOTO salts should be further enhanced when applying small, non-symmetrical saturated ammonium ions without functional groups. Indeed, such effects have been verified by Yu *et al.* in combination with amino acid anions.<sup>31</sup> Also, primary amines were shown to be suitable cations for the design of low viscous and highly conductive RTILs with a variety of anions.<sup>15,30,43</sup> This trend should be valid as well for ILs based on the TOTO anion. Work addressing this question is currently in progress and preliminary results confirm the latter hypothesis. Alternatively, lower viscosities and higher conductivities could be achieved by modifying the structure of the TOTO anion, for example, by introducing additional EO groups or longer alkyl chains, as indicated by the studies of Watanabe and coworkers.<sup>47,48</sup> However, a particular advantage of the TOTO anion is that the corresponding acid can be obtained in high purity by distillation, which is not possible for longer-chain derivatives containing more EO units.

### VIII.2.4. Polarity Parameters

In 1994, the IUPAC committee verified the definition of solvent polarity as the *solvent's overall solvation capability* (or solvation power).<sup>49,50</sup> A comprehensive scale for the solvent polarity, including most organic solvents as well as many ionic liquids, has been developed empirically on the basis of  $E_T(30)$  or normalized  $E_T^N$  values. These are derived from the solvatochromic shift of Reichardt's dye No. 30 (**1**) (cf. Fig. VIII.6).<sup>50,51</sup> The temperature dependence of the polarity of a solvent, i.e. its thermo-solvatochromism, can also be traced by dye **1**.<sup>52</sup> Typically, the solvation capability of molecular solvents is higher at low temperatures.<sup>52</sup> Several studies confirmed this trend to be also valid for common ILs.<sup>53-56</sup> However, a reversed tendency, i.e. an increase of polarity towards higher temperatures, has recently been identified by Khupse *et al.* for phosphonium-based ILs,<sup>57</sup> which are known to exhibit low ionicities due to strong ion-pairing.<sup>34</sup>  $E_T^N$  values determined for TAA- and Ch-TOTO ILs are outlined in Fig. VIII.4 A as a function of temperature.

The thermo-solvatochromism of the studied compounds is rather weakly pronounced and proceeds as commonly expected, that is, the polarity decreases when the temperature is raised.<sup>56</sup> Within the series of cations investigated, the  $E_T^N$  values increase in the order TBA < TPA < TEA << Ch. The decrease of polarity with growing alkyl chain length is a well-known phenomenon,<sup>54,58,59</sup> accounting for the trend observed for the different TAA ions. Further, the high polarity of Ch-TOTO is reasonable in view of the small alkyl substituents and the polar terminal OH group of choline. Nevertheless, it has to be kept in mind that the  $E_T^N$  value is strongly influenced by the hydrogen-bond donor (HBD) ability of choline, which give rise to specific hydrogen-bond interactions with the phenoxide oxygen of dye **1**.<sup>51,55,60,61</sup> As illustrated by Equation (VIII.6), the magnitude of  $E_T^N$  reflects in case of non-HBD solvents, such as the TAA-TOTO ILs, mainly the dipolarity and the polarizability of the medium, while for HBD solvents the hydrogen-bond acidity can be the  $E_T^N$ -determining solvent property.<sup>56</sup> This is supported by the Kamlet-Taft parameters and will be discussed further in the following

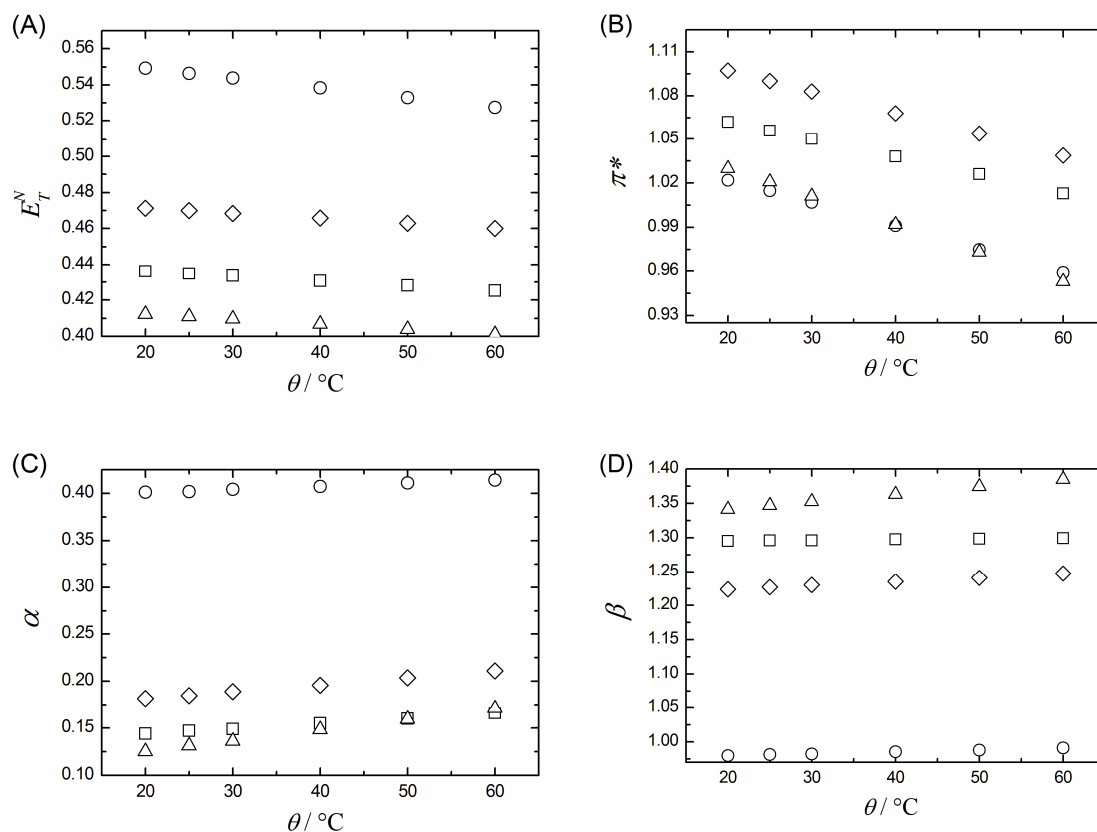


**Fig. VIII.4** Polarity and Kamlet-Taft parameters of TAA- and Ch- TOTO ionic liquids (◇) TEA, (□) TPA, (△) TBA, (○) Ch) as a function of temperature: (A) polarity  $E_T^N$ , (B) dipolarity/polarizability ratio  $\pi^*$ , (C) hydrogen-bond acidity  $\alpha$  and (D) hydrogen-bond basicity  $\beta$ .

A comparison of the  $E_T^N$  parameters of TOTO ionic liquids to common molecular solvents as well as to conventional imidazolium ILs is given in Fig. VIII.5. Apparently, TAA-TOTO salts ( $E_T^N = 0.41$ - $0.47$ ) belong to the class of dipolar non-HBD (“aprotic”) solvents such as acetonitrile.<sup>58</sup> Other quaternary ammonium melts, as for instance tetra-*n*-hexylammonium benzoate ( $E_T^N = 0.41$ ),<sup>58</sup> show very similar polarities. In turn, Ch-TOTO can be considered as a dipolar HBD (“protic”) solvent like for example short-chain primary and secondary alcohols.<sup>51</sup> Its polarity is comparable to that of tetra-*n*-ethylammonium acetate ( $E_T^N = 0.55$ )<sup>58</sup> or to those of common 1,3-dialkyl-imidazolium ionic liquids.<sup>56</sup> Interestingly, the  $E_T^N$  value of Na-TOTO is significantly lower than those of TOTO ILs with quaternary ammonium cations, despite the high charge density of the sodium ion. This is well in line with the results of the Walden plot and further underlines that  $\text{Na}^+$  is strongly bound to the TOTO anion, whereas TAA- and Ch-TOTO ILs are much more dissociated salts. Moreover, it is worth pointing out that the combination of the TOTO anion with different conventional cations gives room-

temperature ionic liquids showing a broad variety of  $E_T^N$  values ( $E_T^N = 0.34$ - $0.55$ ),<sup>12</sup> which meets the demands of task-specific solvent design.

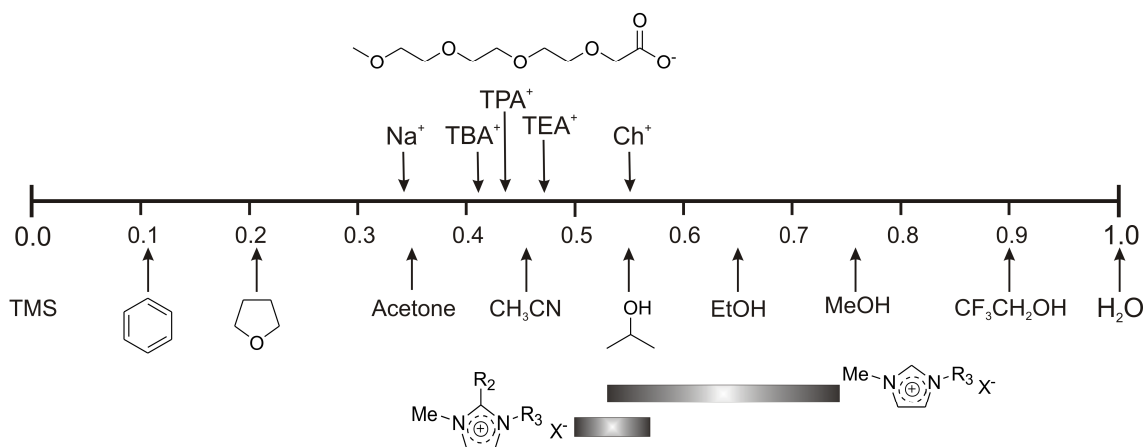


**Fig. VIII.5** Classification of TOTO RTILs in the normalized  $E_T^N$  scale (25°C) as compared to various molecular solvents and conventional ionic liquids. The scheme and the  $E_T^N$  range of imidazolium-typed ILs are partly based on a drawing by Reichardt in 2005.<sup>56</sup> Values for the molecular solvents and Na-TOTO were adapted from refs. <sup>36</sup> and <sup>12</sup>, respectively.

A more detailed insight to solute-solvent interaction can be gained by the three solvent parameters introduced by Kamlet, Abboud and Taft (KAT).<sup>56,62,63</sup> These are the dipolarity / polarizability ratio  $\pi^*$ , the hydrogen-bond donor (HBD) ability (or acidity)  $\alpha$ , and the hydrogen-bond acceptor (HBA) ability (or basicity)  $\beta$ .<sup>51</sup> Fig. VIII.4 B-D shows the distinct Kamlet-Taft parameters of TAA- and Ch-TOTO ILs and their variation with temperature. The observed decrease of  $\pi^*$  with rising temperature agrees well with previous work.<sup>12,53,54,64</sup> Interestingly,  $\alpha$  and  $\beta$  exhibit an inverse trend, i.e. their values increase with temperature. Similar observations have recently been made for pyridinium,<sup>54</sup> pyrrolidinium<sup>57</sup> and phosphonium<sup>57</sup>-based ILs. Lee *et al.* suggested that the hydrogen-bond donor and acceptor capabilities are influenced by steric effects, which are less pronounced at higher temperature.<sup>54</sup> Such steric effects are likely to operate also in TAA- and Ch-TOTO ILs. Thus, the proposed mechanism may account also for the present data. To facilitate the following comparison of the data, the values of the polarity parameters at 25°C are listed in Table VIII.6.

The  $\pi^*$  scale was designed to be free from specific solvent-solute interactions such as hydrogen bonding and ranges for molecular solvents typically from  $\pi^* = 0$  for cyclohexane to  $\pi^* = 1.09$  for water.<sup>55,56,65</sup> The present experiments yielded  $\pi^*$  values

between 1.09 and 1.02 for TAA- and Ch-TOTO ILs, hence rendering them comparable to water (which has the highest  $\pi^*$  among all molecular solvents) or other ionic liquids such as choline propionate ( $\pi^* = 1.05$ )<sup>32</sup> or 1-ethyl-3-methylimidazolium acetate ( $\pi^* = 1.09$ ).<sup>60</sup> Further, the dipolarity / polarizability ratio  $\pi^*$  of TOTO ILs increases with the cation according to  $\text{Na}^{12} \ll \text{Ch} \leq \text{TBA} < \text{TPA} < \text{TEA}$ . A possible scenario explaining this trend is as follows.

**Table VIII.6** Polarity parameters of TAA- and Ch-TOTO ILs at 25°C, in comparison to values reported for Na-TOTO.<sup>12</sup>

Cation	$E_T(30) / \text{kcal mol}^{-1}$	$E_T^N$	$\pi^*$	$\alpha$	$\beta$
Ch	48.41	0.547	1.015	0.403	0.981
TEA	45.92	0.470	1.090	0.185	1.227
TPA	44.79	0.435	1.056	0.147	1.296
TBA	44.01	0.411	1.021	0.131	1.347
Na	41.81	0.342	0.800	0.191	1.027

Generally, the dipolarity of a compound is determined by its permanent dipole moment  $p$ , which is given by the product of the magnitude of charges  $q$  and their distance  $r$  ( $p = q \cdot r$ ). TAA cations do not have a permanent dipole moment. However, their combination with the TOTO anion gives rise to a considerable dipolarity of the salt as a consequence of the relatively “separated” charges. The magnitude of the corresponding dipole moment is expected to increase (although probably not linear due to bending of the alkyl side chains)<sup>66</sup> with the size of the cation ( $\text{TEA} < \text{TPA} < \text{TBA}$ ) due to a growing distance between the positive and negative charge. However, exactly the opposite trend is found for the  $\pi^*$  values. Therefore, the polarizability of TAA cations must have a predominant influence. In general, the polarizability of a molecule or ion increases with the number of valence electrons and thus, usually, with its size. For the different TAA ions, it should scale with the chain length of the alkyl moieties according to  $\text{TBA} > \text{TPA} > \text{TEA}$ . This agrees with the observed trend in  $\pi^*$ . Apparently, for TAA-TOTO ILs the contribution of the polarizability prevails over that of the dipolarity, which is in line with the results of Tokuda *et al.*, who also reported a decrease in  $\pi^*$  with growing alkyl chain length.<sup>59</sup> The choline ion is supposed to be featured by an even lower polarizability than TEA in view of its short alkyl substituents. Consequently, Ch-

TOTO should have the highest  $\pi^*$  in the series. However, this is not observed as  $\pi^*$  values determined for Ch-TOTO equal nearly exactly those of TBA-TOTO (or are even lower). This implies that the dipolarity of Ch-TOTO must be significantly lower than that of TAA-TOTO salts. This is reasonable when considering that in Ch-TOTO opposed "intramolecular" dipole moments exist, since the choline itself has a permanent dipole moment due to its non-symmetrical structure and, in particular, due to its terminal OH group. Therefore, the overall dipolarity of the salt is reduced relative to TAA-TOTO ILs, effecting a "lowered"  $\pi^*$  value. This might be an alternative explanation (instead of hydrogen bonding) for the localization of Ch-TOTO in the Walden diagram as compared to TAA-TOTO ILs.

The proposed scenario would also rationalize the much lower  $\pi^*$  values reported for Na-TOTO.<sup>12</sup> The strong cation-anion interactions in the cross-linked structure of Na-TOTO result in a short distance between  $\text{Na}^+$  and  $\text{COO}^-$ , and hence an overall considerably reduced dipolarity of the salt, which is in line with the  $E_T^N$  scale (cf. Fig. VIII.5).

The  $\alpha$  values of TAA-TOTO ILs vary from 0.13 to 0.19 and are rather low as expected for non-HBD solvents, ranging between those of acetone ( $\alpha = 0.20$ ) and dichloromethane ( $\alpha = 0.04$ ).<sup>67</sup> The acidity of the hydroxyl group of choline becomes manifest in the 2-3 times larger  $\alpha$  measured for Ch-TOTO ( $\alpha = 0.40$ ). This confirms that the detected high  $E_T^N$  value is strongly affected by the hydrogen acidity of the IL. The HBD ability of Ch-TOTO coincides with that of 1-ethyl-3-methylimidazolium acetate ( $\alpha = 0.40$ )<sup>60</sup> and is slightly lower than that of choline propionate ( $\alpha = 0.52$ ).<sup>32</sup>

The  $\beta$  values traced for TAA-TOTO ILs range between 1.23 and 1.35, which is considerably higher than what was found for molecular solvents and most ionic liquids,<sup>53,68-70</sup> including for example imidazolium- and pyridinium-type salts ( $\beta = 0.28-0.33$ ).<sup>54</sup> Very recently, Doherty *et al.* demonstrated that the  $\beta$  parameter provides a measure for the efficiency of ILs to serve as a solvent in lignocellulosic biomass pretreatment.<sup>71</sup> The extraction power for lignin and yields of fermentable sugar were reported to increase with the  $\beta$  value. Thereby, 1-butyl-3-methylimidazolium acetate ( $\beta = 1.18$ ) was most efficient among the ILs investigated in the study.<sup>71</sup> Since the  $\beta$  values of TAA-TOTO ILs are even higher, they might be promising candidates for such applications.

When considering that the hydrogen-bond acceptor or, in other words, the electron-pair donor (EBD) ability of an ionic solvent originates mainly from the anion,<sup>59,68</sup> the  $\beta$

parameter should be representative for the strength of cation-anion interactions. For the present case, this implies that strong binding of the  $\text{COO}^-$  group to a given cation would suppress its electron-pair donor ability, which results in low  $\beta$  values. In this context, the observed order  $\beta$  (Na-TOTO)  $\ll$   $\beta$  (TEA-TOTO)  $<$   $\beta$  (TPA-TOTO)  $<$   $\beta$  (TBA-TOTO) would very well match the known association tendency of carboxylates.<sup>13, 14</sup> However, the choline cation breaks the trend as it exhibits even smaller  $\beta$  values than Na-TOTO. This can most probably be attributed to a feasible HBA ability of the hydroxyl group of choline. As observed likewise for the magnitudes of  $\pi^*$  and  $\alpha$ , Ch-TOTO ( $\beta = 0.98$ ) is, in terms of its  $\beta$  value, comparable to 1-ethyl-3-methylimidazolium acetate ( $\beta = 0.95$ )<sup>60</sup> and choline propionate ( $\beta = 0.98$ )<sup>32</sup> ILs.

### VIII.3. Conclusion

Tetraalkylammonium and choline salts of 2,5,8,11-tetraoxatridecan-13-oic acid (TOTOA) were found to be room-temperature ionic liquids with glass transitions at around  $-60^\circ\text{C}$ . The introduction of EO units in the TOTO anion and the concomitant gain in chain flexibility is apparently very effective in reducing melting or glass points of salts. Viscosities increased in the order TEA  $<$  TPA  $\approx$  Ch  $<$  TBA ( $\eta$  ( $25^\circ\text{C}$ ) = (240 – 860) mPa s) and were accompanied by a decrease in conductivity ( $\kappa$  ( $25^\circ\text{C}$ ) = (517 – 11)  $\mu\text{S cm}^{-1}$ ). Thus, relative to alkali TOTO ILs, both properties could be considerably improved by applying quaternary ammonium cations ( $\eta$  lowered by a factor of  $\sim 600$ ,  $\kappa$  increased by a factor of  $\sim 1000$ ). The Walden plot further revealed that TAA- and Ch-TOTO are, in contrast to Na-TOTO, featured by high ionicity and belong to the class of “good” ionic liquids. With respect to solvent polarity,  $E_T^N$  values obtained for TAA-TOTO ILs show that they can be considered as dipolar aprotic solvents, while Ch-TOTO is a dipolar protic solvent. Remarkably, ionic liquids formed by TOTO and the *per se* highly polar sodium ion are in fact less polar than those comprising quaternary ammonium ions. Taken this and the Walden plot into account, the strong cation-anion interactions of small alkali ions and TOTO appear to be substantially weakened when using quaternary ammonium species as cations. This is supported by the measured Kamlet-Taft parameters, in particular by the values of  $\pi^*$  and  $\beta$ . Thereby, it should be stressed that the magnitude of  $\beta$  found for the studied salts is extraordinarily high as compared to common molecular solvents or ionic liquids.

The TOTO anion is obviously capable of forming RTILs with a variety of cations and therefore depicts a new promising class of ILs. The obtained results demonstrate that the viscosity, conductivity and solvent polarity of TOTO ILs can be effectively tuned over a large range by varying the cation, thus permitting truly task-specific design.

## VIII.4. Experimental

### VIII.4.1. Materials and Syntheses

2,5,8,11-Tetraoxatridecan-13-oic acid (TOTOA) was synthesized according to a procedure described previously.<sup>10</sup> The purity of TOTOA (99.4%) was verified by GC-analysis. Ionic liquids were obtained by direct neutralization of the free TOTO acid and the respective quaternary ammonium hydroxide. Since TOTOA is a weak acid ( $pK_a$  similar to acetic acid) and the applied hydroxides are strong bases, the neutralization reaction is considered to be quantitative, which is confirmed by the recorded NMR spectra. The following bases were used as received: choline hydroxide (purum, 44.6 wt% in methanol, Sigma-Aldrich), tetraethylammonium hydroxide (purum, 25.8 wt% in methanol, Fluka), tetrapropylammonium hydroxide (purum, 1.02 M in water, Fluka), tetrabutylammonium hydroxide (puriss., 1.00 M in water, Fluka). After stirring the neutralized mixtures for about 12 h, the solvent was removed either by a rotary evaporator or via lyophilization. Subsequently, the salts were dried for about 3 days at 40°C in high vacuum ( $p < 10^{-8}$  bar), yielding colorless or slightly yellow liquids. Initially, tetramethylammonium (TMA) was also included in the cation series. However, NMR data revealed a non-sufficient purity of the TMA-TOTO salt, which probably arises from the TMA base being liable to decomposition. Since it was not possible to ensure an adequate quality of TMA-TOTO, it was not considered in the present study.

### VIII.4.2. Methods

#### VIII.4.2.1. Analytics

The purity of the as-prepared ionic liquids was confirmed by  $^1\text{H}$  NMR ( $\text{CDCl}_3$ ),  $^{13}\text{C}$  NMR ( $\text{CDCl}_3$ ) and ES-MS (electro-spray mass spectroscopy). NMR spectra were recorded on a Bruker Avance 300 spectrometer at 300 MHz with tetramethylsilane (TMS) as internal standard. Mass spectrometry was performed a ThermoQuest Finnigan TSQ 7000 instrument. The water content of the ionic liquids was determined by a

coulometric Karl-Fischer titration with the aid of an Abimed MCI analyzer (Model CA-02). Gas chromatography (GC) was carried out on a HP-5 column with high-purity helium as carrier gas, using a HP 6890 chromatograph equipped with an autosampler and a FID detector.

**Choline 2,5,8,11-tetraoxatridecan-13-oate (Ch-TOTO):**

$\delta_{\text{H}}$  (300 MHz;  $\text{CDCl}_3$ ): 3.1 (m, 12 H;  $(\text{CH}_3)_3\text{N}$ ,  $\text{CH}_3\text{O}$ ), 3.4 (m, 14 H;  $\text{CH}_2$ ), 3.7 (s, 2 H;  $\text{CH}_2\text{COO}^-$ ), 3.9 (s, 2 H,  $\text{CH}_2\text{OH}$ ), 7.2 (s, 1 H,  $\text{CH}_2\text{OH}$ );

$\delta_{\text{C}}$  (300 MHz;  $\text{CDCl}_3$ ): 54.5 ( $(\text{CH}_3)_3\text{N}$ ), 56.1 ( $\text{CH}_2\text{OH}$ ), 58.9 ( $\text{CH}_3\text{O}$ ), 68.4 ( $\text{CH}_2\text{CH}_2\text{OH}$ ), 69.8 ( $\text{CH}_2\text{COO}^-$ ), 70.3 – 70.6 ( $\text{CH}_2$ ), 71.5 ( $\text{CH}_2$ ), 71.9 ( $\text{CH}_3\text{OCH}_2$ ), 175.2 ( $\text{COO}^-$ );

**ES-MS** ( $\text{H}_2\text{O}$  /  $\text{MeOH}$  /  $\text{MeCN}$ ):  $m/z$  (%) (+p): 103.9 (100) [ $\text{M}^+$ ], 147.8 (11), 429.2 (18) [ $2\text{M}^+ + \text{M}^-$ ];  $m/z$  (%) (-p): 220.9 (100) [ $\text{M}^-$ ], 546.3 (7) [ $2\text{M}^- + \text{M}^+$ ];

Water content (Karl-Fischer titration):  $(148 \pm 45)$  ppm

**Tetraethylammonium 2,5,8,11-tetraoxatridecan-13-oate (TEA-TOTO):**

$\delta_{\text{H}}$  (300 MHz;  $\text{CDCl}_3$ ): 1.3 (t,  $^3J(\text{H,H}) = 7.4$  Hz, 12 H;  $\text{CH}_3\text{CH}_2$ ), 3.3 (s, 3 H;  $\text{CH}_3\text{O}$ ), 3.6 (m, 20 H;  $\text{CH}_2$ ), 3.8 (s, 2 H;  $\text{CH}_2\text{COO}^-$ );

$\delta_{\text{C}}$  (300 MHz;  $\text{CDCl}_3$ ): 7.6 ( $\text{CH}_3\text{CH}_2$ ), 52.5 ( $\text{CH}_3\text{CH}_2$ ), 59.0 ( $\text{CH}_3\text{O}$ ), 69.6 ( $\text{CH}_2\text{COOH}$ ), 70.3 – 70.7 ( $\text{CH}_2$ ), 71.6 ( $\text{CH}_2$ ), 71.9 ( $\text{CH}_3\text{OCH}_2$ ), 174.6 ( $\text{COO}^-$ );

**ES-MS** ( $\text{H}_2\text{O}$  /  $\text{MeCN}$ ):  $m/z$  (%) (+p): 130.2 (100) [ $\text{M}^+$ ], 481.3 (10) [ $2\text{M}^+ + \text{M}^-$ ];  $m/z$  (%) (-p): 221.0 (100) [ $\text{M}^-$ ], 572.3 (8) [ $2\text{M}^- + \text{M}^+$ ];

Water content (Karl-Fischer titration):  $(161 \pm 20)$  ppm

**Tetrapropylammonium 2,5,8,11-tetraoxatridecan-13-oate (TPA-TOTO):**

$\delta_{\text{H}}$  (300 MHz;  $\text{CDCl}_3$ ): 1.0 (t,  $^3J(\text{H,H}) = 7.1$  Hz, 7.4 Hz, 12 H;  $\text{CH}_3\text{CH}_2$ ), 1.7 (m, 8 H;  $\text{CH}_3\text{CH}_2$ ), 3.3 (m, 11 H;  $\text{CH}_3\text{CH}_2\text{CH}_2$ ,  $\text{CH}_3\text{O}$ ), 3.5 (m, 2 H;  $\text{CH}_2$ ), 3.6 (m, 10 H;  $\text{CH}_2$ ), 3.9 (s, 2 H;  $\text{CH}_2\text{COO}^-$ );

$\delta_C$  (300 MHz;  $CDCl_3$ ): 10.9 ( $CH_3CH_2$ ), 15.7 ( $CH_3CH_2$ ), 59.0 ( $CH_3O$ ), 60.5 ( $CH_3CH_2CH_2$ ), 69.6 ( $CH_2COO^-$ ), 70.3 – 70.7 ( $CH_2$ ), 71.6 ( $CH_2$ ), 71.9 ( $CH_3OCH_2$ ), 174.6 ( $COO^-$ );

**ES-MS** ( $H_2O$  / MeCN): m/z (%) (+p): 186.1 (100) [ $M^+$ ], 593.4 (11) [ $2M^+ + M^-$ ]; m/z (%) (-p): 221.0 (100) [ $M^-$ ], 628.4 (5) [ $2M^- + M^+$ ];

Water content (Karl-Fischer titration): ( $158 \pm 70$ ) ppm

#### **Tetrabutylammonium 2,5,8,11-tetraoxatridecan-13-oate (TBA-TOTO):**

$\delta_H$  (300 MHz;  $CDCl_3$ ): 0.9 (t,  $^3J(H,H) = 7.1$  Hz, 7.4 Hz, 12 H;  $CH_3CH_2$ ), 1.4 (sextet,  $^3J(H,H) = 7.4$  Hz, 7.1 Hz, 8 H;  $CH_3CH_2$ ), 1.6 (m, 8 H;  $CH_3CH_2CH_2$ ), 3.3 (m, 11 H;  $CH_3CH_2CH_2CH_2$ ,  $CH_3O$ ), 3.5 (m, 2 H;  $CH_2$ ), 3.6 (m, 10 H;  $CH_2$ ), 3.9 (s, 2 H;  $CH_2COO^-$ );

$\delta_C$  (300 MHz;  $CDCl_3$ ): 13.7 ( $CH_3CH_2$ ), 19.7 ( $CH_3CH_2$ ), 24.0 ( $CH_3CH_2CH_2$ ), 58.7 ( $CH_3CH_2CH_2CH_2$ ), 59.0 ( $CH_3O$ ), 69.5 ( $CH_2COO^-$ ), 70.4 – 70.7 ( $CH_2$ ), 71.6 ( $CH_2$ ), 71.9 ( $CH_3OCH_2$ ), 174.6 ( $COO^-$ );

**ES-MS** ( $H_2O$  / MeCN): m/z (%) (+p): 242.2 (100) [ $M^+$ ], 705.6 (12) [ $2M^+ + M^-$ ]; m/z (%) (-p): 221.0 (100) [ $M^-$ ], 684.4 (15) [ $2M^- + M^+$ ];

Water content (Karl-Fischer titration): ( $181 \pm 35$ ) ppm

#### **VIII.4.2.2. Densities**

Densities,  $\rho$ , required for the calculation of molar volumes,  $V_m$ , and molar conductivities,  $\Lambda_m$ , were measured at room temperature (298 K) and over a temperature range of (283-333) K in steps of 10 K, utilizing a vibrating tube densimeter (Anton Paar DMA 60). Calibration of the instrument was achieved by measuring purified dry nitrogen and degassed water, for which precise density values are available in literature.<sup>72</sup> The uncertainty of  $\rho$  values is estimated to be less than  $0.1 \text{ kg m}^{-3}$ . Experimental data of  $\rho$  are listed in Table VIII.7. Linear regressions of the  $\rho(T)$  data eventually yielded equations expressing the density as a function of temperature, which are compiled in Table VIII.8. In order to calculate  $\Lambda_m$ ,  $\rho$  and therewith also  $V_m$  data were interpolated to exactly the same temperatures as applied for the determination of specific conductivities,  $\kappa$ . The respective results can be found in Appendix D.

**Table VIII.7** Densities,  $\rho$ , of the investigated ILs at various temperatures.

<b>TEA-TOTO</b>		<b>TPA-TOTO</b>		<b>TBA-TOTO</b>		<b>Ch-TOTO</b>	
<i>T</i> / K	$\rho$ / kg m <sup>-3</sup>	<i>T</i> / K	$\rho$ / kg m <sup>-3</sup>	<i>T</i> / K	$\rho$ / kg m <sup>-3</sup>	<i>T</i> / K	$\rho$ / kg m <sup>-3</sup>
283.22	1081.1	283.51	1037.2	283.07	1010.3	283.18	1142.4
293.16	1074.8	293.16	1031.4	293.09	1004.0	293.15	1135.5
298.09	1071.1	298.17	1027.8	298.17	1000.3	298.18	1131.5
303.14	1068.0	303.17	1024.8	303.15	997.2	303.24	1128.3
313.02	1062.0	313.15	1019.0	313.15	990.9	313.15	1122.1
323.46	1057.4	323.15	1014.6	323.15	986.5	323.24	1117.7
333.24	1054.6	333.13	1011.6	333.15	983.1	333.18	1114.6

**Table VIII.8** Equations for the temperature-dependent densities of TAA- and Ch-TOTO ionic liquids, obtained from linear regressions of the experimental data.

<b>Ch-TOTO</b>	$\rho / \text{kg m}^{-3} = 1300.1 / \text{kg m}^{-3} - 0.56 T / \text{K}$
<b>TEA-TOTO</b>	$\rho / \text{kg m}^{-3} = 1232.6 / \text{kg m}^{-3} - 0.54 T / \text{K}$
<b>TPA-TOTO</b>	$\rho / \text{kg m}^{-3} = 1185.2 / \text{kg m}^{-3} - 0.53 T / \text{K}$
<b>TBA-TOTO</b>	$\rho / \text{kg m}^{-3} = 1165.7 / \text{kg m}^{-3} - 0.54 T / \text{K}$

### VIII.4.2.3. Decomposition Temperatures

Decomposition temperatures,  $T_{dec}$ , were determined by a thermogravimetric analyzer of Perkin-Elmer (TGA 7). Data were recorded under a constant nitrogen flow with a heating rate of 10 K min<sup>-1</sup>.  $T_{dec}$  values were obtained from onset analysis by evaluating the intersection of the baseline before decomposition and the tangent to the mass loss versus the temperature in the following.

### VIII.4.2.4. Differential Scanning Calorimetry

Differential scanning calorimetry (DSC) was performed on a Mettler DSC 30 which was gently flooded with N<sub>2</sub>. Samples were sealed in aluminum pans in a nitrogen glove box and subsequently measured over a temperature range of (203-298) K at a heating rate of 10 K min<sup>-1</sup>. The half-step transition temperature of the heating curve was taken as the glass point ( $T_g$ ).

### VIII.4.2.5. Viscosities

Viscosities,  $\eta$ , were measured under argon atmosphere on a Bohlin rheometer (CVO 120 High Resolution) with cone / plate geometry (CP 40/4°), which was equipped with a temperature control unit. The investigated temperature range was (283-353) K, while the shear rates were varied between (10 - 500) s<sup>-1</sup>. All studied ionic liquids revealed constant shear stress-to-shear ratios at a given temperature (i.e. they exhibit Newtonian behavior). The uncertainty of  $\eta$  values was estimated to be about 1%. Corresponding experimental data are listed in Table VIII.9. In order to be able to construct a Walden plot,  $\eta$  values at exactly the same temperatures as those prevailing in the conductivity measurements are required. As there were slight deviations in the temperatures between the two techniques,  $\eta$  values were interpolated by a best-fit procedure as described in Appendix D.

**Table VIII.9** Dynamic viscosities,  $\eta$ , of the investigated ILs at temperatures ranging from 10°C to 68°C.

TEA-TOTO		TPA-TOTO		TBA-TOTO		Ch-TOTO	
<i>T</i> / K	$\eta$ / mPas						
283	830	286	2072	286	2350	283	2180
293	375	294	1023	294	1178	293	1045
298	264	298	727	298	862	298	665
303	186	302	536	302	626	303	506
313	103	310	293	310	346	313	230
323	62	318	168	318	200	323	122
333	41	325	104	325	124	333	74
343	29	333	68	333	82	343	51
		341	47	341	57		

### VIII.4.2.6. Conductivities

Conductivities,  $\kappa$ , were determined at ambient temperature (298 K) as well as in steps of 10 K over a range of (273 - 373) K. Measurements were carried out with an custom-designed apparatus built in-house.<sup>73,74</sup> It consists of a precision thermostat, a symmetrical Wheatstone bridge with Wagner earth, a sine generator and a resistance decade. Temperature accuracy is estimated to  $\pm 0.01$  K (NIST traceable platinum

sensor, ASL). Three capillary cells, each containing a three-electrode setup, with cell constants,  $a$ , of  $(224 - 1161) \text{ m}^{-1}$  were utilized. Cell constants were derived by measuring aqueous KCl solutions according to a procedure described by Barthel *et al.*<sup>75</sup> Resistance measurements were performed at frequencies,  $\nu$ , between 480 Hz and 10 kHz. To eliminate electrode polarization effects resistances,  $R$ , were extrapolated to  $R_\infty = \lim_{\nu \rightarrow \infty} R(\nu)$ .<sup>75</sup> The relative uncertainty of the obtained electrical conductivities,  $\kappa = a/R_\infty$ , was estimated to be  $< 0.5 \%$ . The reported temperature dependence of cell constants  $a(T)$ <sup>73,76</sup> was confirmed to be negligible for the present measurements. The experimental data of  $\kappa$  are compiled in Table VIII.10.

**Table VIII.10** Conductivities,  $\kappa$ , of the investigated ILs between 0°C and 100°C.

$T / \text{K}$	$\kappa / \text{S} \cdot \text{m}^{-1}$			
	TEA-TOTO	TPA-TOTO	TBA-TOTO	Ch-TOTO
273.15	0.00742	0.000891	0.000586	0.00110
283.15	0.01788	0.00264	0.001606	0.00312
293.15	0.0374	0.00653	0.00380	0.00736
298.15	0.0517	0.00976	0.00555	0.01076
303.15	0.0695	0.01414	0.00792	0.01525
313.15	0.1173	0.0273	0.01496	0.0283
323.15	0.1837	0.0482	0.0260	0.0482
333.15	0.271	0.0796	0.0417	0.0765
343.15	0.375	0.1211	0.0641	0.1142
353.15	0.509	0.1752	0.0942	0.1650
363.15	0.662	0.243	0.1318	0.227
373.15	0.835	0.325	0.1776	0.300

#### VIII.4.2.7. Absorbance

Absorbance values,  $A$ , of dyes upon solubilization in the synthesized ILs were recorded on a Cary 3E spectrophotometer between 200 nm and 900 nm in steps of 0.1 nm and at temperatures ranging from (20 to 60) °C. Samples were measured in sealed 1 mm Quartz cuvettes (Helma). The temperature was monitored by NTC resistance thermometers with a precision of  $\pm 0.2^\circ\text{C}$ . The dyes used for the determination of

solvent polarity,  $E_T(30)$ , and Kamlet-Taft parameters were Reichardt's dye 30 (Aldrich,  $\geq 90\%$  dye), *N,N*-diethyl-4-nitroaniline (Fluorochem,  $\geq 99\%$ ) and 4-nitroaniline (Fluka,  $\geq 99\%$ ). Their molecular structures are shown in Fig. VIII.6.

First, stock solutions of all three dyes in  $\text{CH}_2\text{Cl}_2$  were prepared. An appropriate amount (adjusted such that  $0.5 \leq A \leq 1$ ) was then filled into vials and the solvent was removed in an exsiccator under vacuum. ILs were added in a nitrogen atmosphere so as to prevent contact with air. The resulting mixtures were filled into cuvettes under  $\text{N}_2$  and sealed. After preparation, solutions were measured within one day to ensure comparability of the data. The wavelength of the desired absorption maximum,  $\lambda_{max}$ , was determined by fitting the corresponding peak with a Gaussian profile. The accuracy of the applied procedure was evaluated by measuring the  $E_T$  values of several organic solvents ( $\text{CH}_2\text{Cl}_2$ ,  $\text{CH}_3\text{OH}$ , EtOH, Aceton) for which the polarity is documented in literature.<sup>56</sup>  $\Delta E_T = |(E_T - E_T^{Lit}) / \overline{E_T}|$  was found to be  $\leq 2.4\%$ . No evidence for dye aggregation could be discerned at the given solute concentrations.

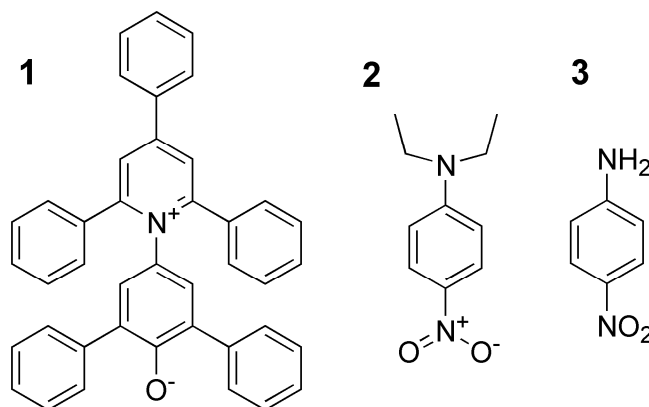


**Fig. VIII.6** Molecular structures of the dyes employed for the characterization of solvent polarity and Kamlet-Taft parameters: **1** – Reichardt's Dye 30, **2** – *N,N*-diethyl-4-nitroaniline, **3** – 4-nitroaniline.

#### VIII.4.2.8. Calculation of Solvent Polarity and Kamlet-Taft Parameters

The empirical solvent parameter  $E_T(30)$  is defined as the molar transition energy of Reichardt's betaine dye (**1**).<sup>51,58</sup> Its determination is based on the solvatochromic shift of the  $\pi$ - $\pi^*$  absorption band of dissolved dye **1**. According to Equation (VIII.3), the  $E_T(30)$

value can be derived by measuring the wavelength  $\lambda_{max}$ , or respectively the wave number,  $\tilde{\nu}_{max}$ , of the long-wave absorption maximum of dye **1**.<sup>58</sup>

$$E_T(30) / (\text{kcal} \cdot \text{mol}^{-1}) = hc \tilde{\nu}_{max,1} N_A = 28591 / (\lambda_{max,1} / \text{nm}) \quad (\text{VIII.3})$$

Alternatively, the dimensionless  $E_T^N$  scale can be used, which varies between 1 and 0 with water as most polar ( $E_T^N = 1.00$ ) and tetramethylsilane (TMS) as least polar ( $E_T^N = 0.00$ ) reference solvents.<sup>58</sup>  $E_T^N$  values can be calculated by Equation (VIII.4).

$$E_T^N = [E_T(\text{solvent}) - 30.7] / 32.4 \quad (\text{VIII.4})$$

In a similar manner, the Kamlet-Taft parameters  $\pi^*$ ,  $\alpha$ , and  $\beta$  are obtained by measuring the wave numbers corresponding to the absorption maxima of the solvatochromic dyes *N,N*-diethyl-4-nitroaniline (**2**) and 4-nitroaniline (**3**) (molecular structures outlined in Chart 2).<sup>62,63</sup> The dipolarity / polarizability ratio,  $\pi^*$ , of the solvent can be gained from  $\tilde{\nu}_{max}$  of dye **2** using Equation (VIII.5).<sup>62,63</sup>

$$\pi^* = \frac{(\tilde{\nu}_{max,2} / 10^{-3} \text{cm}^{-1}) - (27.52 / 10^{-3} \text{cm}^{-1})}{-3.182} \quad (\text{VIII.5})$$

The definitions for the hydrogen-bond donor (HBD) ability or acidity,  $\alpha$ , and those for the hydrogen-bond acceptor (HBA) ability or basicity,  $\beta$ , are given by Equations (VIII.6) and (VIII.7).<sup>54,62,63,65</sup>

$$\alpha = \frac{(E_T(30) - 14.6 \cdot (\pi^* - 0.23) - 30.31)}{16.5} \quad (\text{VIII.6})$$

$$\beta = \frac{((1.035 \cdot \tilde{\nu}_{max,2} / 10^{-3} \text{cm}^{-1}) - (\tilde{\nu}_{max,3} / 10^{-3} \text{cm}^{-1}) + 2.64)}{2.8} \quad (\text{VIII.7})$$

## VIII.5. References

1. P. Wasserscheid, W. Keim, *Angew. Chem. Int. Ed.*, 2000, **39**, 3772.
2. I. Krossing, J. M. Slattery, C. Daguinet, P. J. Dyson, A. Oleinikova, H. Weingaertner, *J. Am. Chem. Soc.*, 2006, **128**, 13427.

3. T. L. Greaves, C. J. Drummond, *Chem. Soc. Rev.*, 2008, **37**, 1709.
4. S. Stolte, J. Arning, U. Bottin-Weber, M. Matzke, F. Stock, K. Thiele, M. Uerdingen, U. Welz-Biermann, B. Jastorff, J. Ranke, *Green Chem.*, 2006, **8**, 621.
5. S. Stolte, M. Matzke, J. Arning, A. Bösch, W.-R. Pitner, U. Welz-Biermann, B. Jastorff, J. Ranke, *Green Chem.*, 2007, **9**, 1170.
6. M. Matzke, S. Stolte, K. Thiele, T. Juffernholz, J. Arning, J. Ranke, U. Welz-Biermann, B. Jastorff, *Green Chem.*, 2007, **9**, 1198.
7. J. Ranke, K. Moelter, F. Stock, U. Bottin-Weber, J. Poczobutt, J. Hoffmann, B. Ondruschka, J. Filser, B. Jastorff, *Ecotoxicol. Environ. Saf.*, 2004, **58**, 396.
8. X. Wang, C. A. Ohlin, Q. Lu, Z. Fei, J. Hu, P. J. Dyson, *Green Chem.*, 2007, **9**, 1191.
9. J. Cross, E. J. Singer, *Cationic Surfactants - Analytical and Biological Evaluation*, Dekker, New York, 1994.
10. O. Zech, M. Kellermeier, S. Thomaier, E. Maurer, R. Klein, C. Schreiner, W. Kunz, *Chem. Eur. J.*, 2009, **15**, 1341.
11. W. Kunz, S. Thomaier, E. Maurer, O. Zech, M. Kellermeier, R. Klein, WO 2008 135 482, BASF SE (Germany), 2008.
12. O. Zech, J. Hunger, J. R. Sangoro, C. Iacob, F. Kremer, W. Kunz, R. Buchner, *Phys. Chem. Chem. Phys.*, 2010, **12**, 14341.
13. W. Kunz, *Curr. Opin. Colloid Interface Sci.*, 2010, **15**, 34.
14. R. Klein, M. Kellermeier, M. Drechsler, D. Touraud, W. Kunz, *Colloids Surf., A*, 2009, **338**, 129.
15. M. Yoshizawa, W. Xu, C. A. Angell, *J. Am. Chem. Soc.*, 2003, **125**, 15411.
16. W. Xu, E. I. Cooper, C. A. Angell, *J. Phys. Chem. B*, 2003, **107**, 6170.
17. J. K. Blusztajn, *Science*, 1998, **281**, 794.
18. J. K. Blusztajn, R. J. Wurtman, *Science*, 1983, **221**, 614.
19. R. Klein, D. Touraud, W. Kunz, *Green Chem.*, 2008, **10**, 433.
20. H. Matsumoto, H. Kageyama, Y. Miyazaki, *Chem. Lett.*, 2001, 182.
21. H. Matsumoto, H. Kageyama, Y. Miyazaki, *Chem. Commun.*, 2002, 1726.

22. H. Matsumoto, T. Matsuda, T. Tsuda, R. Hagiwara, Y. Ito, Y. Miyazaki, *Chem. Lett.*, 2001, 26.
23. Z.-B. Zhou, H. Matsumoto, K. Tatsumi, *Chem. Eur. J.*, 2005, **11**, 752.
24. M. Petkovic, J. L. Ferguson, H. Q. N. Gunaratne, R. Ferreira, M. C. Leitao, K. R. Seddon, L. P. N. Rebelo, C. S. Pereira, *Green Chem.*, 2010, **12**, 643.
25. D. Constantinescu, K. Schaber, F. Agel, M. H. Klingele, T. J. S. Schubert, *J. Chem. Eng. Data*, 2007, **52**, 1280.
26. P. Nockemann, B. Thijs, K. Driesen, C. R. Janssen, K. Van Hecke, L. Van Meervelt, S. Kossmann, B. Kirchner, K. Binnemans, *J. Phys. Chem. B*, 2007, **111**, 5254.
27. J. Pernak, A. Syguda, I. Mirska, A. Pernak, J. Nawrot, A. Pradzynska, S. Griffin, R. Rogers, *Chem. Eur. J.*, 2007, **13**, 6817-6827.
28. K. D. Weaver, H. J. Kim, J. Sun, D. R. MacFarlane, G. D. Elliott, *Green Chem.*, 2010, **12**, 507.
29. Y. Yu, X. Lu, Q. Zhou, K. Dong, H. Yao, S. Zhang, *Chem. Eur. J.*, 2008, **14**, 11174.
30. W. Xu, C. A. Angell, *Science*, 2003, **302**, 422.
31. H. Yu, Y.-T. Wu, Y.-Y. Jiang, Z. Zhou, Z.-B. Zhang, *New J. Chem.*, 2009, **33**, 2385.
32. Y. Fukaya, Y. Iizuka, K. Sekikawa, H. Ohno, *Green Chem.*, 2007, **9**, 1155.
33. W. Xu, L.-M. Wang, R. A. Nieman, C. A. Angell, *J. Phys. Chem. B*, 2003, **107**, 11749.
34. K. J. Fraser, E. I. Izgorodina, M. Forsyth, J. L. Scott, D. R. MacFarlane, *Chem. Commun.*, 2007, 3817.
35. R. M. Pagni, in *Advances in Molten Salt Chemistry*, Eds. G. Mamantov and J. Braunstein, Elsevier, Amsterdam, 1988, pp. 41-128.
36. G. P. Smith, R. M. Pagni, in *NATO ASI Series*, Eds. G. Mamantov and R. Marassi, Reidel, Dordrecht, 1987, pp. 383-404.
37. R. Klein, H. Dutton, O. Diat, G. J. T. Tiddy, W. Kunz, *Thermotropic Phase Behavior of Choline Soaps*, in press by J. Phys. Chem B.

38. A. Grandjean, M. Malki, C. Simonnet, D. Manara, B. Penelon, *Phys. Rev. B: Condens. Matter Mater. Phys.*, 2007, **75**, 054112/1-054112/7.
39. F. M. Kerton, in *Alternative Solvents for Green Chemistry*, Royal Society of Chemistry, Cambridge, 2009, pp. 118-142.
40. D. J. Adams, P. J. Dyson, S. J. Taverner, *Chemistry in Alternative Reaction Media*, John Wiley & Sons Ltd., Chichester, 2004.
41. O. Zech, A. Stoppa, R. Buchner, W. Kunz, *J. Chem. Eng. Data*, 2010, **55**, 1774.
42. Y.-Y. Jiang, G.-N. Wang, Z. Zhou, Y.-T. Wu, J. Geng, Z.-B. Zhang, *Chem. Commun.*, 2008, 505.
43. J. Stoimenovski, E. I. Izgorodina, D. R. MacFarlane, *Phys. Chem. Chem. Phys.*, 2010, **12**, 10341.
44. P. Walden, *Z. Phys. Chem., Stoichiom. Verwandtschaftsl.*, 1906, **55**, 207.
45. T. Welton, *Chem. Rev.*, 1999, **99**, 2071.
46. D. R. MacFarlane, M. Forsyth, E. I. Izgorodina, A. P. Abbott, G. Annat, K. Fraser, *Phys. Chem. Chem. Phys.*, 2009, **11**, 4962.
47. H. Shobukawa, H. Tokuda, M. A. B. H. Susan, M. Watanabe, *Electrochim. Acta*, 2005, **50**, 3872.
48. H. Shobukawa, H. Tokuda, S.-I. Tabata, M. Watanabe, *Electrochim. Acta*, 2004, **50**, 305.
49. P. Müller, *Pure Appl. Chem.*, 1994, **66**, 1077.
50. C. Reichardt, *Org. Process Res. Dev.*, 2007, **11**, 105.
51. C. Reichardt, *Pure Appl. Chem.*, 2004, **76**, 1903.
52. C. Reichardt, *Pure Appl. Chem.*, 2008, **80**, 1415.
53. S. N. Baker, G. A. Baker, F. V. Bright, *Green Chem.*, 2002, **4**, 165.
54. J.-M. Lee, S. Ruckes, J. M. Prausnitz, *J. Phys. Chem. B*, 2008, **112**, 1473.
55. W. B. Harrod, N. J. Pienta, *J. Phys. Org. Chem.*, 1990, **3**, 534.
56. C. Reichardt, *Green Chem.*, 2005, **7**, 339.
57. N. D. Khupse, A. Kumar, *J. Phys. Chem. B*, 2010, **114**, 376.
58. C. Reichardt, *Chem. Rev.*, 1994, **94**, 2319.

59. H. Tokuda, K. Ishii, M. A. B. H. Susan, S. Tsuzuki, K. Hayamizu, M. Watanabe, *J. Phys. Chem. B*, 2006, **110**, 2833.
60. S. Zhang, X. Qi, X. Ma, L. Lu, Y. Deng, *J. Phys. Chem. B*, 2010, **114**, 3912.
61. H. Jin, B. O'Hare, J. Dong, S. Arzhantsev, G. A. Baker, J. F. Wishart, A. J. Benesi, M. Maroncelli, *J. Phys. Chem. B*, 2008, **112**, 81.
62. M. J. Kamlet, R. W. Taft, *J. Am. Chem. Soc.*, 1976, **98**, 377.
63. R. W. Taft, M. J. Kamlet, *J. Am. Chem. Soc.*, 1976, **98**, 2886.
64. S. Trivedi, N. I. Malek, K. Behera, S. Pandey, *J. Phys. Chem. B*, 2010, **114**, 8118.
65. Y. Marcus, *Chem. Soc. Rev.*, 1993, **22**, 409.
66. W. Kunz, P. Calmettes, P. Turq, *J. Chem. Phys.*, 1990, **92**, 2367.
67. I. Persson, *Pure Appl. Chem.*, 1986, **58**, 1153.
68. L. Crowhurst, P. R. Mawdsley, J. M. Perez-Arlandis, P. A. Salter, T. Welton, *Phys. Chem. Chem. Phys.*, 2003, **5**, 2790.
69. R. Lungwitz, S. Spange, *New J. Chem.*, 2008, **32**, 392.
70. A. Oehlke, K. Hofmann, S. Spange, *New J. Chem.*, 2006, **30**, 533.
71. T. V. Doherty, M. Mora-Pale, S. E. Foley, R. J. Linhardt, J. S. Dordick, *Green Chem.*, 2010, **12**, 1967.
72. D. R. Lide, *CRC - Handbook of Chemistry and Physics*, CRC Press, Boca Raton, USA, 2004.
73. J. Barthel, R. Wachter, H. J. Gores, *Mod. Aspects Electrochem.*, 1979, **13**, 1.
74. R. Wachter, J. Barthel, *Ber. Bunsenges. Phys. Chem.*, 1979, **83**, 634.
75. J. Barthel, F. Feuerlein, R. Neueder, R. Wachter, *J. Solution Chem.*, 1980, **9**, 209.
76. R. A. Robinson, R. H. Stokes, *Electrolyte Solutions*, Butterworth, London, 1959.

## Chapter IX Summary

Choline soaps (ChC $m$ ) with alkyl chain lengths ranging from  $m= 12-18$  have been synthesized, purified and characterized in various aspects. In contrast to their alkali homologues – the classical soaps – choline fatty acid surfactants are highly soluble in water, which allows for an application of the desirable long-chain derivatives up to a hydrocarbon chain length of  $m= 16$  under ambient conditions. In addition, these surfactants can be prepared from natural components by a straightforward synthesis without the requirement of heat, thus minimizing energy costs in a potential large-scale industrial production. Biodegradability and cytotoxicity studies on two human cell lines demonstrated that choline soaps can be considered as readily biodegradable according to the European norm, and are virtually harmless at least for the investigated cell lines. Indeed, further sets of analyses such as on ecotoxicity, mutagenicity or acute toxicity (oral, dermal, inhalation) are needed for a complete and reasonable assessment of environmental and human risks. Nonetheless, the results of the present work already strongly suggest high biocompatibility for choline carboxylate surfactants. In combination with the demonstrated superior water solubility and economic advantages, these properties allow for the conclusion that choline soaps are promising green alternatives to classical soaps.

Moreover, the aqueous phase diagrams of ChC $m$  surfactants have been established, disclosing a rich and complex self-assembly behavior in water. For instance, a broad range of discontinuous cubic phases could be detected, which has so far not been reported for mono-anionic surfactants and is rather typical for divalent, zwitter-ionic, or cationic amphiphiles. Such mesophases could for example serve as templates for the design of mesoporous materials. The obtained phase diagrams further highlight the very low Krafft boundary of choline soaps up to very high concentrations (0°C for 93 wt% ChC12!). The reason for this beneficial feature can likely be ascribed to two contributing factors. On the one hand, the bulkiness of the choline ion hinders effectively a regular crystalline packing of the surfactant molecules. On the other hand, choline alkyl carboxylates can be considered as salts with a high degree of dissociation, which promotes their dissolution. With respect to *packing* constraints, these aspects also explain why ChC $m$  surfactants prefer mesophases of high curvatures (i.e. cubic phases): the bulky and highly dissociated choline counterion causes a large headgroup area.

Investigations on the thermotropic phase behavior of neat choline soaps showed that the mentioned two factors induce in a similar manner low melting points. Accordingly, it has been demonstrated that ChC $m$  surfactants with  $m= 12-18$  pass through three different phases when the temperature is increased from  $-20^{\circ}\text{C}$  to  $100^{\circ}\text{C}$ . The lower-temperature phases were identified to be of crystalline or semi-crystalline nature, respectively, while the upper-temperature phase (occurring between  $68^{\circ}\text{C}$  and  $93^{\circ}\text{C}$ ) could be assigned to a lamellar liquid-crystalline structure. In this regard, choline soaps meet the conventional definition of ionic liquids (salts with mp.  $< 100^{\circ}\text{C}$ ).

The hypothesis of a very loose binding of choline to alkyl carboxylate anions was corroborated by exploring the influence of chloride salts and hydroxides on the Krafft temperature of ChC18. The traced increase in the Krafft point of ChC18 provoked by addition of sodium or potassium chloride supports the proposed low counterion association of choline in fatty acid soaps, and is moreover in agreement with trends discerned in previous studies on specific ion effects and Collins' concept of "matching water affinities". The consequential high sensitivity of ChC $m$  soaps to the presence of simple salts must be regarded as a drawback of this new type of surfactants in view of their applicability in the formulation of distinct products. In turn, an advantage of this high degree of counterion dissociation was recognized when choline base was added in excess to ChC18 solutions. As opposed to the behavior of the alkali homologues, excess choline base leads to a further decrease of the Krafft temperature, such that ChC18 could be dissolved at temperatures as low as  $14^{\circ}\text{C}$ . To illustrate the potential of this feature for applications in the field of grease removal agents, butter was successively solubilized in choline hydroxide solutions at room temperature.

The inherent sensitivity of choline soaps to foreign salts and their relative alkaline pH – caused by the weak acidity of fatty acid anions – were sought to be overcome by using a sulfate headgroup, which is more acidic and, in terms of specific ion effects, "softer" than carboxylates. Therefore, choline dodecyl sulfate (ChDS) was synthesized and investigated concerning its physicochemical properties and its cytotoxicity. As in the case of choline soaps, the substitution of alkali cations as counterions in alkyl sulfate surfactants by choline resulted in enhanced water solubility ( $T_{Kr}$  (ChDS)  $\approx 0^{\circ}\text{C}$ ). Analyses of the aqueous self-assembly behavior of ChDS and the influence of different chloride salts on its Krafft temperature confirmed that the extent of counterion-headgroup association is higher in choline alkyl sulfates as compared to choline fatty

acid soaps and, also, that they are more resistant to salts. Although studies in the field of choline alkyl sulfates have only started yet, it can be anticipated, in light of the low Krafft point found for ChDS, that also the longer-chain derivatives will be more water-soluble than their alkali counterparts. Beyond that, cytotoxicity assays provided evidence that ChDS is toxicologically similarly harmless as the widely applied sodium dodecyl sulfate. Thus, the introduced choline alkyl sulfates represent a new promising family of anionic surfactants – biocompatible and exhibiting beneficial properties such as high water solubility and reduced salt sensitivity.

On the basis of the knowledge achieved about the effects of the molecular structure and specific ion-ion interactions on the macroscopic physicochemical properties of the investigated compounds, various room-temperature ionic liquids could finally be developed. Neat choline soaps were shown to already melt at moderate temperatures. A further reduction of the melting points was realized by substituting methylene groups in the alkyl chain for ethylene oxide units. Due to their considerably increased chain flexibility, the resulting oligoether carboxylates were found to form ionic liquids with a variety of cations, including small alkali ions as well as bulky tetraalkylammonium ions and choline. Most of these salts showed glass transitions at around  $-60^{\circ}\text{C}$ . Moreover, physical properties such as the viscosity, conductivity or solvent polarity could be tuned over a large range by the appropriate choice of the cation. In line with the specific ion effects identified for alkyl carboxylate surfactants, the use of large quaternary ammonium ions led to oligoether carboxylate salts with a high degree of ion dissociation, causing low viscosities and high conductivities. In turn, the corresponding alkali salts are characterized by strong cation-anion interactions and thus were, by orders of magnitude, more viscous and less conductive.

After all, it is evident that the application of choline as a counterion of biological origin gives access to a wide range of novel “green” substances – surfactants as well as ionic liquids. The observed phenomena rely on the hindrance of a regular packing of molecules in a crystalline lattice and the action of specific ion effects. The combination of these two factors is apparently a powerful concept to design surfactants, or salts in general, with tunable features such as water solubilities or melting points. Current studies are focused on the characterization of intermediate-chain choline carboxylates, which proved to be true ionic liquids with surfactant properties. Likewise, investigations on the longer-chain derivatives of choline alkyl sulfates are underway. Finally, further projects are devoted to examining in detail the self-assembly behavior of choline

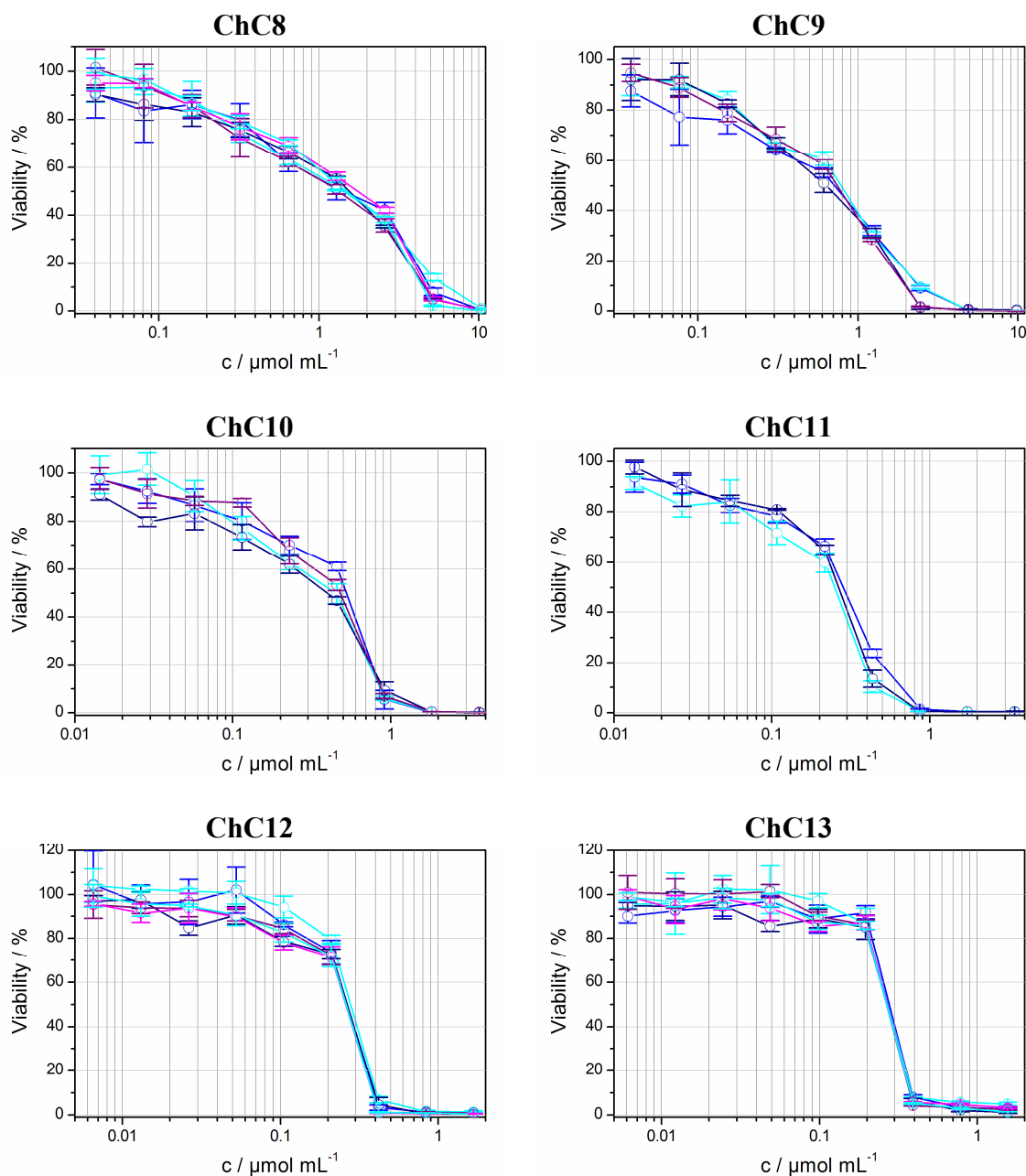
dodecyl sulfate, as well as to a “quantitative” evaluation of the counterion-headgroup binding strengths by means of dielectric relaxation and infrared-visible sum-frequency spectroscopy.

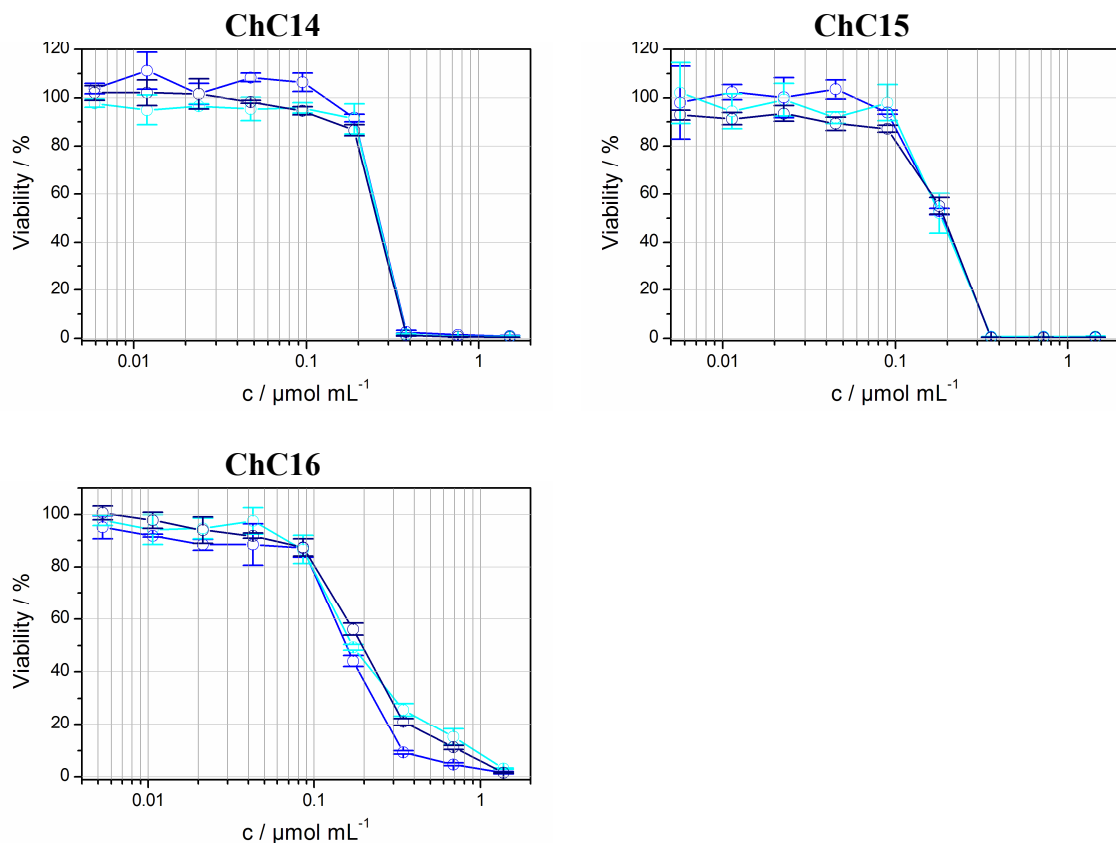
# Appendix A: Biodegradability and Cytotoxicity on Human Cell Lines of Choline Soaps

## A.1 HeLa Dose-Response Curves of ChCm Surfactants for $m=8-16$

Each plot contains three to six dose-response curves, established over several weeks.

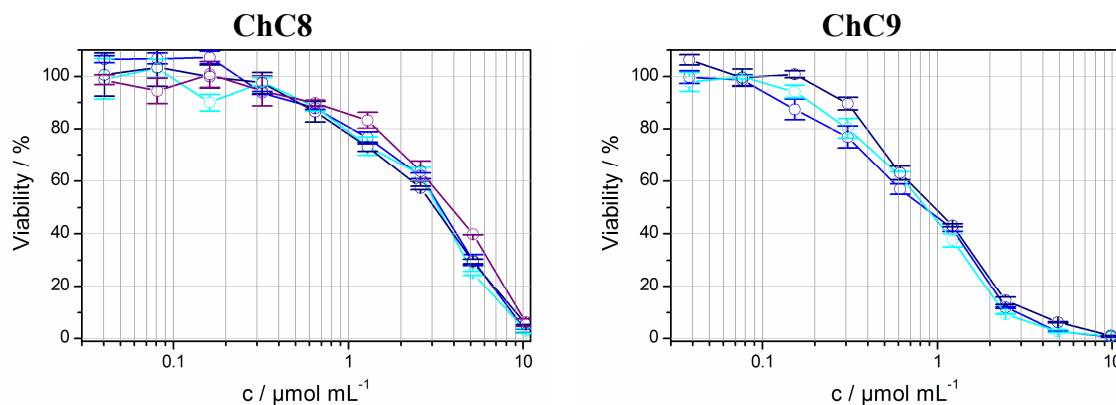
Every data point represents the mean of three parallels.

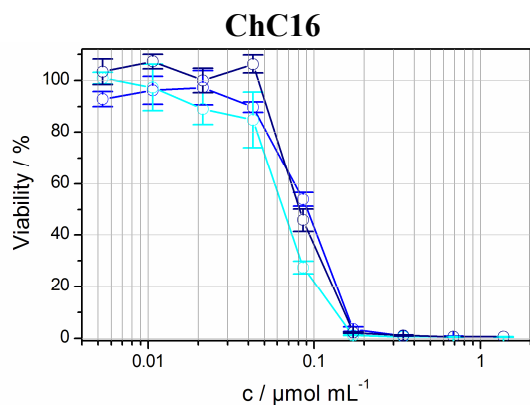
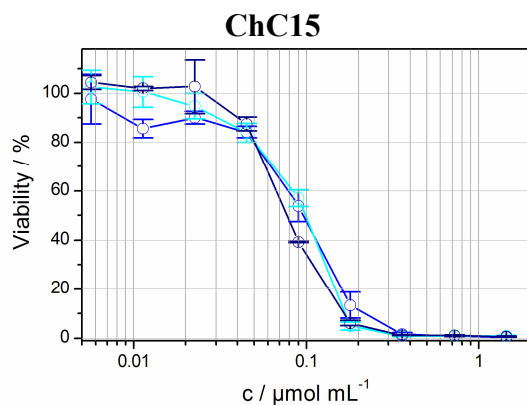
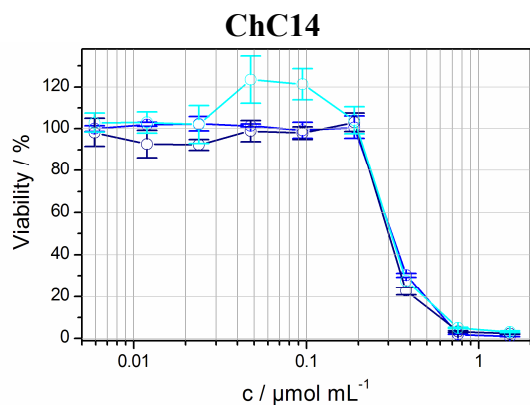
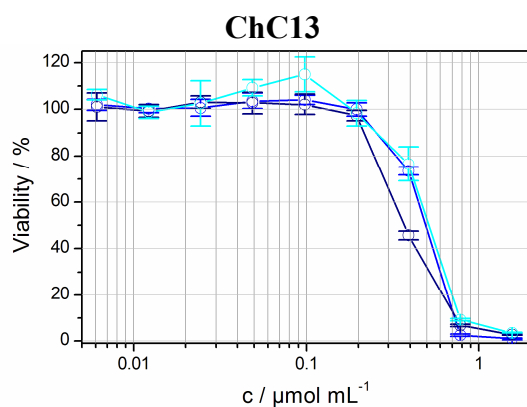
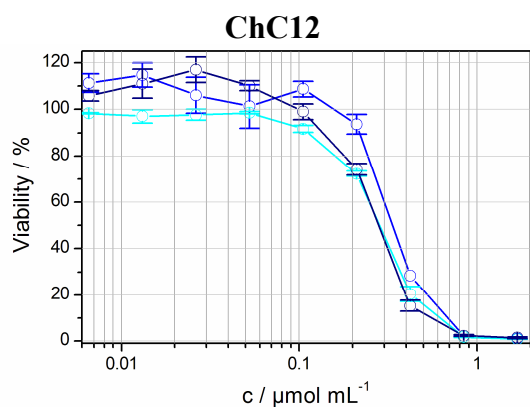
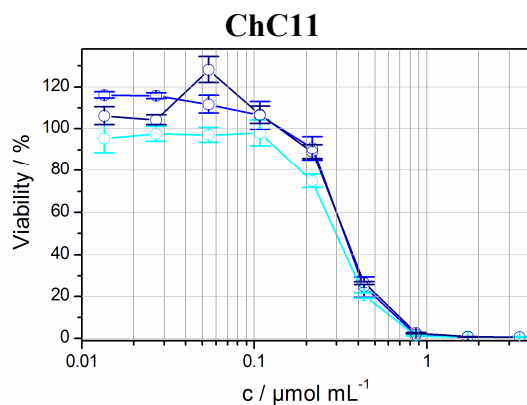
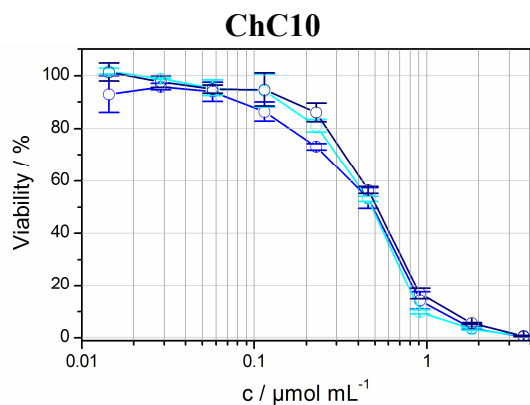




## A.2 SK-Mel-28 Dose-Response Curves of ChCm Surfactants for m= 8-16

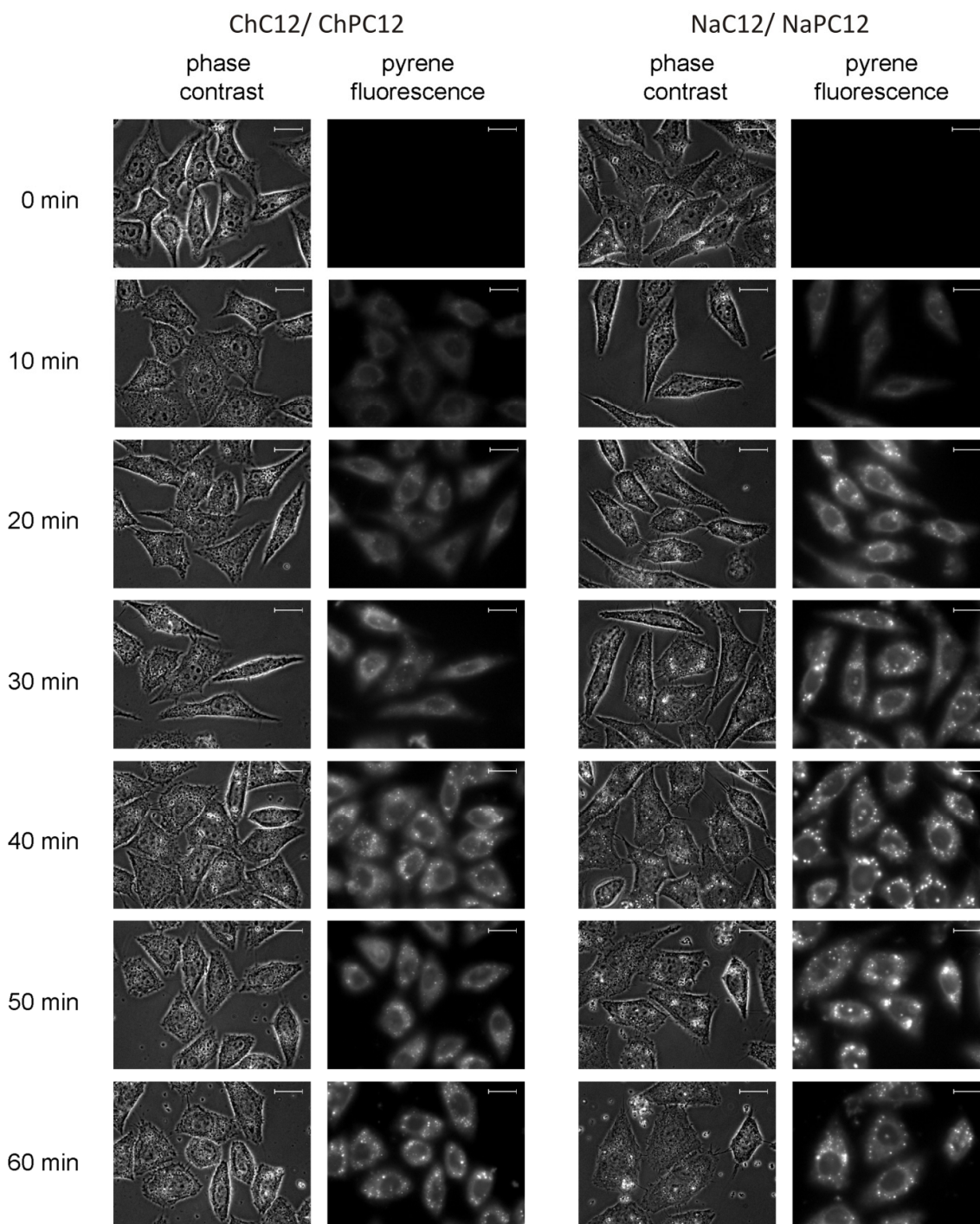
Each plot contains three to six dose-response curves, established over several weeks. Each data point represents the mean of three parallels.





### A.3 Phase Contrast and Fluorescence Images of HeLa Cells Treated with Pyrene-Substituted Choline and Sodium Soaps over Time

HeLa cells were incubated with 2:1 molar mixtures of ChC12/ChPC12 and NaC12/NaPC12, respectively, at concentrations right below the according  $IC_{50}$  values ( $c(\text{ChC12/ChPC12}) = 81 \mu\text{mol L}^{-1}$ ,  $c(\text{NaC12/NaPC12}) = 102 \mu\text{mol L}^{-1}$ ). Pictures were recorded every 10 min after addition of surfactants over 60 min (scale bars: 20  $\mu\text{m}$ ).



## Appendix B: Aqueous Phase Behavior of Choline Carboxylate Surfactants

### B.1 Density and Determination of the Molar Volume of ChC $m$ Surfactants

Densities of aqueous choline carboxylate solutions were determined at 25°C by a vibrating tube densimeter (Anton Paar DMA 60). The experimental derived values are listed in Table B.1.

**Table B.1** Density data of ChC $m$  surfactants at 25°C.

ChC12		ChC14		ChC16		ChC18	
wt%	$\rho / \text{g L}^{-1}$						
1.00	997.09	1.00	996.78	1.00	996.65	1.00	996.62
2.49	996.79	2.49	996.32	2.50	996.00	2.49	995.82
5.00	996.33	4.99	995.44	4.99	995.05	5.00	994.43
7.48	995.89	7.46	994.71	7.50	993.82	7.48	993.13
9.98	995.40	10.00	993.91	10.00	992.95	9.55	992.11
12.50	994.97	12.46	993.14	12.47	991.77	12.49	990.62
14.95	994.45	15.00	992.32	15.00	990.68	14.98	989.47
17.44	994.04	17.46	991.54	17.51	989.78	17.48	988.07
20.00	993.56	20.00	990.87			20.01	986.83

Using the known molar masses of surfactants and water, the total volume ( $V_{total}$ ) of solution with regard to 1 mol H<sub>2</sub>O can be calculated. With  $n_s$  and  $V_S$  as number of moles and molar volume of surfactant,  $V_{total}$  is defined as:

$$V_{total} = n_{\text{H}_2\text{O}} V_{\text{H}_2\text{O}} + n_s V_S \quad (\text{B.1})$$

Consequently,  $V_S$  can be derived by the plot of  $V_{total}$  versus  $n_s$  (Fig. B.1). As obvious from Fig. B.1,  $V_S$  is constant over the investigated concentration region and can thus be obtained by the slope of a linear regression. Thereby, the y-axis interception represents

the molar volume of water, since  $V_{total}$  was calculated for  $n_{H_2O} = 1$  mol. The results of the linear regression are listed in Table B.2.  $V_{H_2O}$  agrees well with literature. Further,  $V_S$  increases in average by a factor of  $0.0165 \text{ L mol}^{-1}$  ( $= 27.4 \text{ \AA}^3$ ) per additional  $\text{CH}_2$  group, which coincides approximately with the value predicted by Tanford ( $26.9 \text{ \AA}^3$ ).<sup>1</sup>

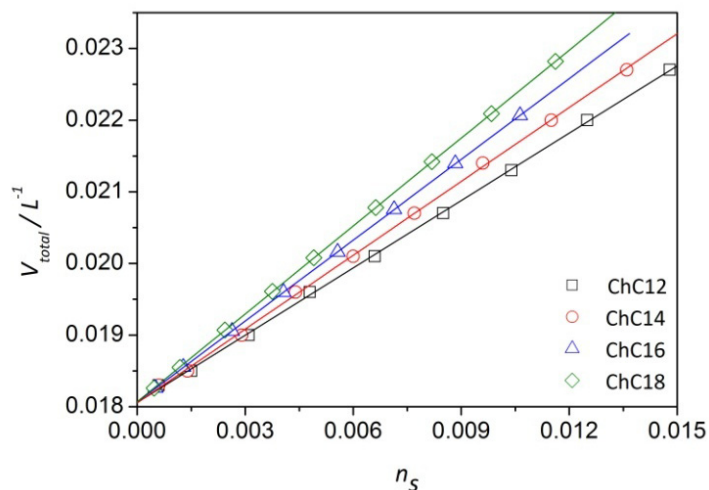


**Fig. B.1** Plot of the total volume  $V_{total}$  at  $25^\circ\text{C}$  versus the number of moles of  $\text{ChC}_m$  surfactants according to Equation (B.1).

**Table B.2** Results of linear regressions according to Fig. B.1, yielding the molar volumes of choline surfactants and water at  $25^\circ\text{C}$ .

	$V_S / \text{L mol}^{-1}$	$V_{H_2O} / \text{L mol}^{-1}$
ChC12	0.310	0.0181
ChC14	0.343	0.0181
ChC16	0.376	0.0181
ChC18	0.409	0.0181

## B.2 Penetration Scan Images of ChCm Surfactants at Various Temperatures

### B.2.1 ChC14

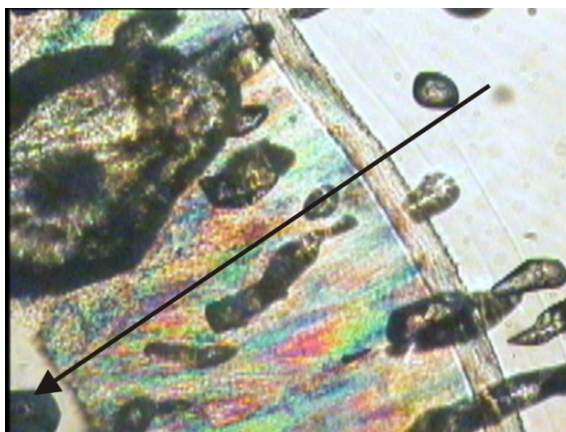


**Fig. B.2** Penetration scan image of ChC14 at 25°C and 100x magnification, showing – towards higher soap concentrations as assigned by the arrow) – the following mesophases:  $L_1$ ,  $I_1'$ ,  $I_1''$ ,  $H_1$ , and  $V_1$ .

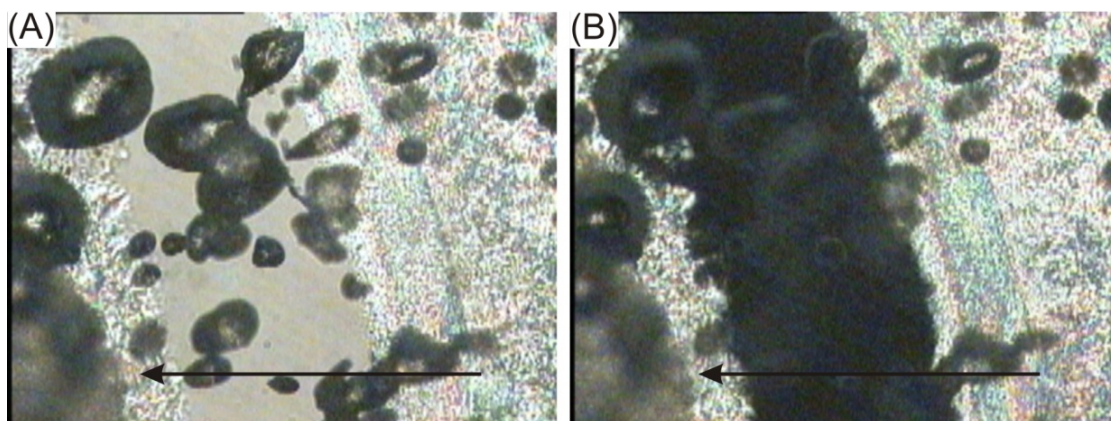


**Fig. B.3** Penetration scan image of ChC14 in the more concentrated surfactant region at 50°C and 100x magnification without (A) and with (B) applied crossed polarizers. From the right to the left (increasing surfactant concentration), an  $H_1$ ,  $V_1$ , and  $L_\alpha$  phase and a solid birefringent region can be identified.

### B.2.2 ChC16

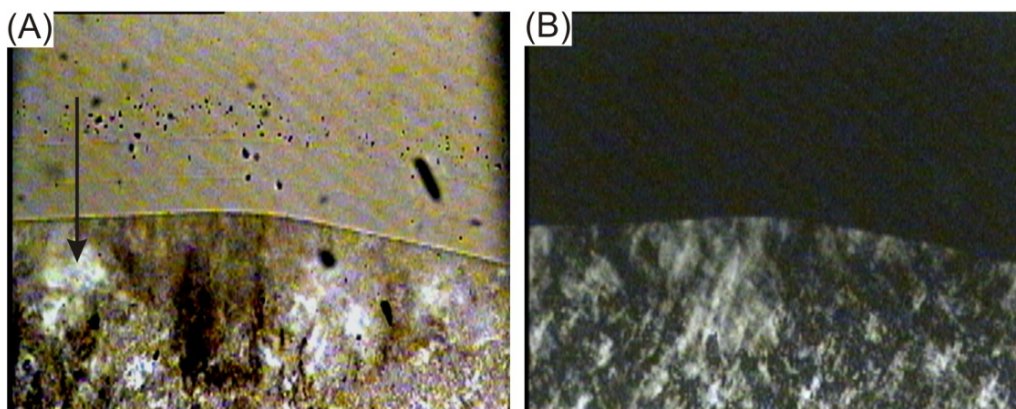


**Fig. B.4** Penetration scan of ChC16 at 25°C and 100x magnification without (A) and with (B) crossed polarizers, showing the following phases from the top to the bottom:  $L_1$ ,  $I_1'$ ,  $I_1''$  and  $H_1$ .

### B.2.3 ChC18

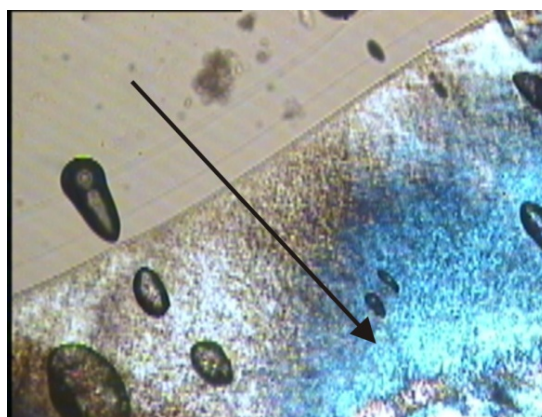


**Fig. B.5** Penetration scan photograph of ChC18 at 40°C and 100x magnification. With increasing soap concentration (as indicated by the arrow) the following mesophases can be recognized:  $L_1$ ,  $I_1'$ ,  $I_1''$  and  $H_1$ .

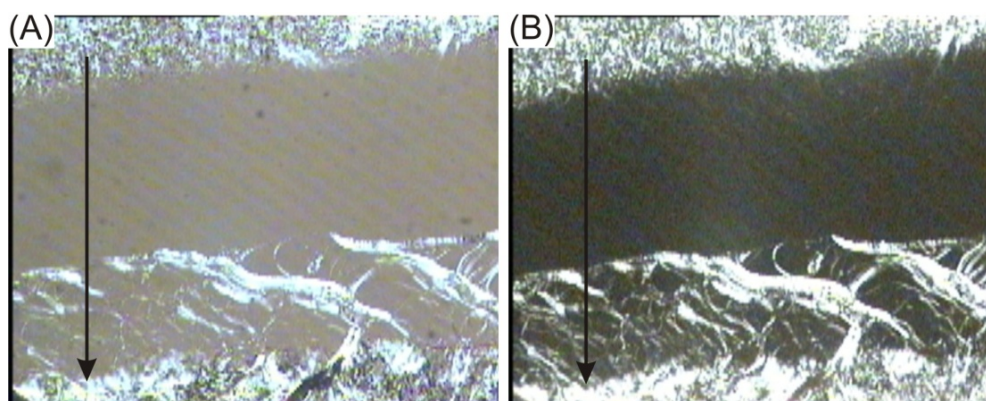


**Fig. B.6** Penetration scan of ChC18 in the more concentrated surfactant region at 59°C and 100x magnification (with (A) and without (B) crossed polarizers), showing from the top to the bottom the following mesophases:  $H_1$ ,  $V_1$ ,  $L_\alpha$  and  $L_\beta$ .

### B.3 SAXS Experimental

SAXS measurements were performed on three different devices of various labs due to limited facilities and different demands such as varying required scattering angles, temperature controlling or the recording of two dimensional X-ray patterns. An assignment of the investigated samples to the respective experimental setups is given in Tables B.3 and B.4.

#### A) SAXS setup at the laboratories of LIONS/CEA, Saclay (France):

X-ray radiation with wavelength  $\lambda = 1.54 \text{ \AA}$  was provided by a copper rotating anode operated at 3 kW equipped with a multilayer Xenocs mirror as monochromator and a three-slit collimation system. The scattered X-rays were detected by a two-dimensional automatic image plate system (Mar300) from Mar Research. Calibrations were done by measuring standards such as octadecanol, iron, water and Lupolen. At a sample-to-detector distance of 122 cm, the accessible  $q$ -range was  $0.3\text{-}6.3 \text{ nm}^{-1}$ . More details regarding the experimental setup can be found in the literature.<sup>2,3</sup> Samples were enclosed between Kapton sheets with sample thicknesses of 1 mm and 1.5 mm. Acquisition times varied between 900-7200 s. Radial averaging was performed with the ImageJ Software. With this setup, ChC12 and ChC16 were fully characterized and ChC18 to a large extent.

#### B) SAXS instrument at the Institute for Advanced Chemistry of Catalonia, Barcelona (Spain):

Small-angle X-ray scattering data were recorded using a S3 MICRO instrument (Hecus X-ray Systems, Graz, Austria) equipped with a sealed copper anode providing Cu-K $\alpha$  radiation with  $\lambda = 1.54 \text{ \AA}$ . The beam was focused using a Genix microfocus X-ray source and a Fox 2D point-focusing element (both from Xenocs, Grenoble), reducing the beam area to approximately  $0.04 \text{ mm}^2$ . The detection system was composed of two linear position sensitive detector (PSD-50M, Hecus, Graz, Austria), which allows the simultaneous determination of small and wide angles, covering  $q$ -values between approximately  $0.2$  and  $5.9 \text{ nm}^{-1}$ , and between  $13$  and  $19 \text{ nm}^{-1}$ , respectively. Exact  $d$  spacing values were achieved by calibration with silver behenate for small angles and  $p$ -bromobenzoic acid for large angles.<sup>4-6</sup> Samples were measured in a paste cell of approximately 1 mm thickness sealed with plastic foil (Kallebrat Folie, Kalle GmbH, Germany). Investigated temperatures ranged from  $0^\circ\text{C}$  until  $90^\circ\text{C}$  with acquisition times of 900-1800 s. Primarily ChC14 was characterized with this setup.

**C) SAXS apparatus at the Max-Planck Institute Potsdam (Germany):**

This homebuilt instrument consists of a rotating anode (Fr591, Bruker-Nonius, Netherlands) with point collimation and a two-dimensional Mar CCD Detector (Mar 165), having a resolution of 2048 x 2048 pixels with a pixel size of 79  $\mu\text{m}$ . Calibration was performed by measuring silverbehenate.<sup>4,6</sup> With a sample to detector distance of 74.1 cm, a  $q$ -range of 0.6-4.6  $\text{nm}^{-1}$  was attained. Primary data were processed with the ImageJ Software.

**Table B.3** Assignment of ChC12 and ChC14 samples, which were investigated by SAXS, to the respective X-ray setup used for measurement.

ChC12			ChC14		
wt%	$T/^\circ\text{C}$	SAXS setup	wt%	$T/^\circ\text{C}$	SAXS setup
30.0	25	A	29.0	25	C
32.9	25	A	34.9	25	C
35.1	25	A	37.4	25	C
37.9	25	A	40.9	25	C
40.1	25	A	45.0	25	B
45.0	25	A	50.6	25	B
47.2	25	A	56.0	25	B
49.7	25	A	61.0	25	B
55.1	25	A	65.0	25	B
60.2	25	A	70.2	25	B
65.5	25	A	75.4	25	B
69.9	25	A	79.8	25	B
74.7	25	A	79.8	60	B
79.9	25	A	83.3	25	B
83.8	25	A	85.5	20	B
86.9	25	A	90.4	25	B
89.5	25	A	93.2	35	B
91.5	25	A	95.1	45	B
94.0	25	A	95.1	80	B
97.5	60	A	97.5	80	B

**Table B.4** Assignment of ChC16 and ChC18 samples to the X-ray setup used for their investigation.

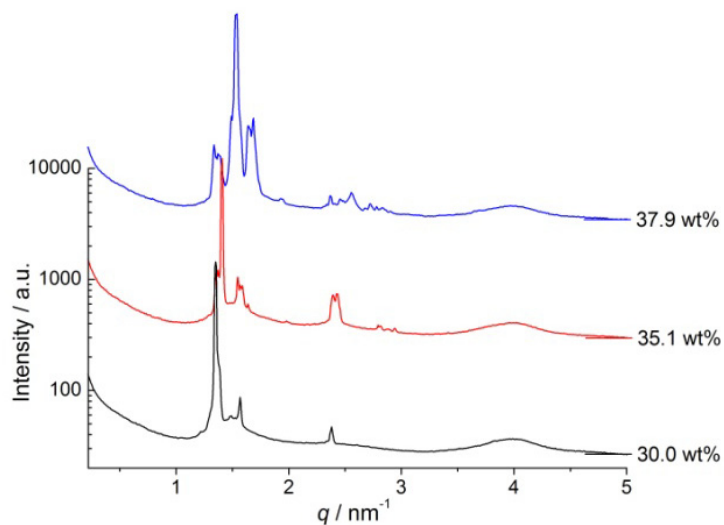
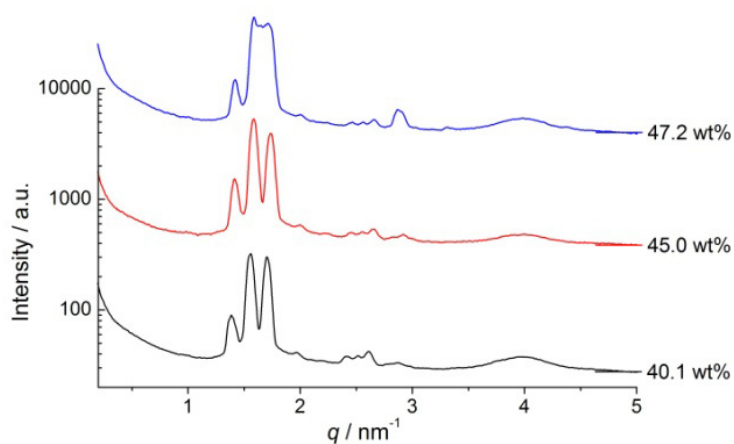
ChC16			ChC18		
wt%	$T/^\circ\text{C}$	SAXS setup	wt%	$T/^\circ\text{C}$	SAXS setup
30.1	25	A	34.7	60	A
34.8	25	A	45.2	60	A
40.1	25	A	50.3	60	A
45.2	25	A	60.0	50	C
49.7	25	A	69.9	50	C
54.7	25	A	75.7	70	C
59.6	25	A	79.8	70	C
64.4	25	A	85.7	70	C
69.7	25	A	90.2	70	C
75.3	50	A	96.0	70	C
79.3	50	A			
85.5	50	A			
89.3	50	A			
92.0	60	A			
94.0	50	A			
95.3	60	A			
97.5	70	C			

## B.4 SAXS spectra

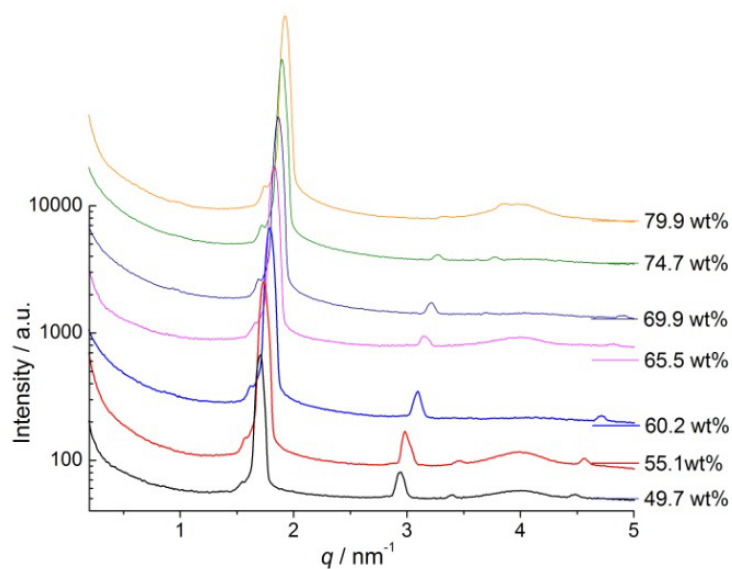
In the following, the SAXS spectra obtained for each compound are presented. Unless indicated otherwise, the temperature is 25°C. The spectra are ordered roughly with respect to corresponding mesophases. Details and an exact assignment of the occurring phases to distinct liquid-crystalline structures are given in Section B5.

### B.4.1 ChC12

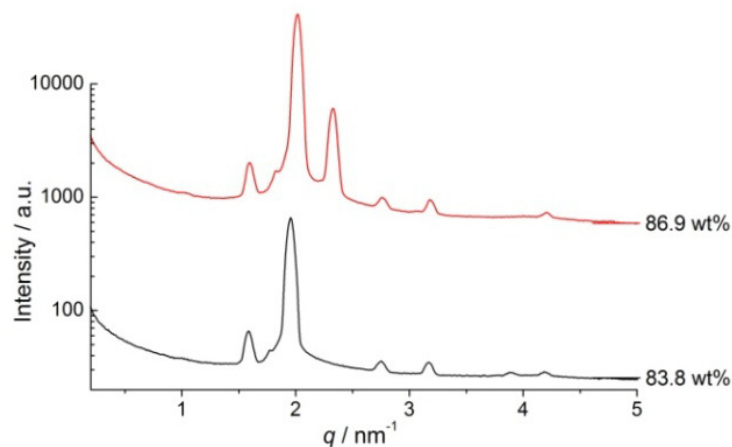
#### A) Discontinuous cubic $I_1'$ and $I_1''$ ( $Pm3n$ )



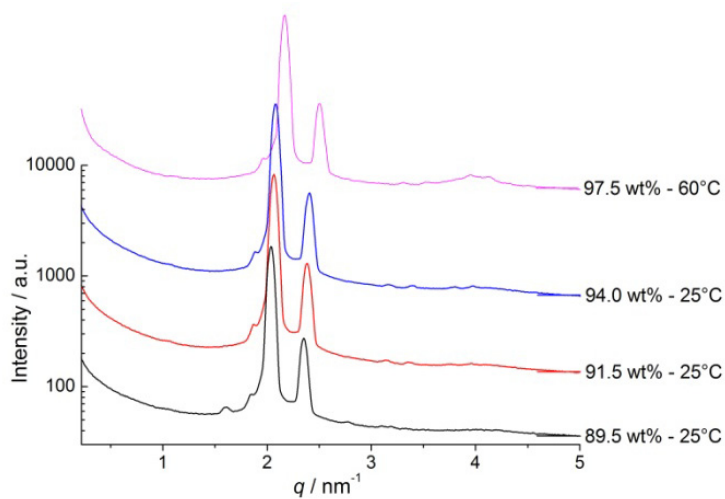
**B) Hexagonal phase  $H_1$**



**C)  $H_1 - V_1$  boundary – intermediate phase?**



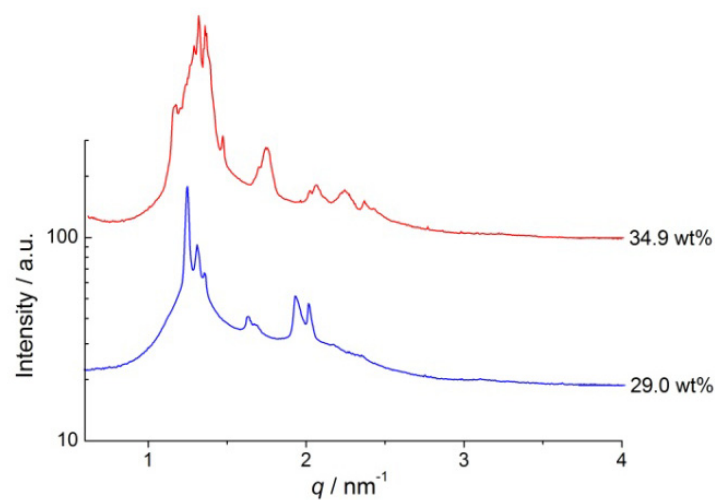
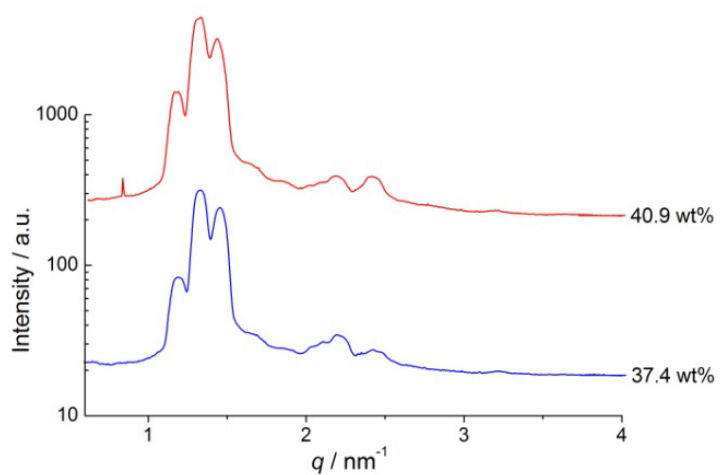
**D) Bicontinuous phase  $V_1$  with  $Ia3d$  structure**



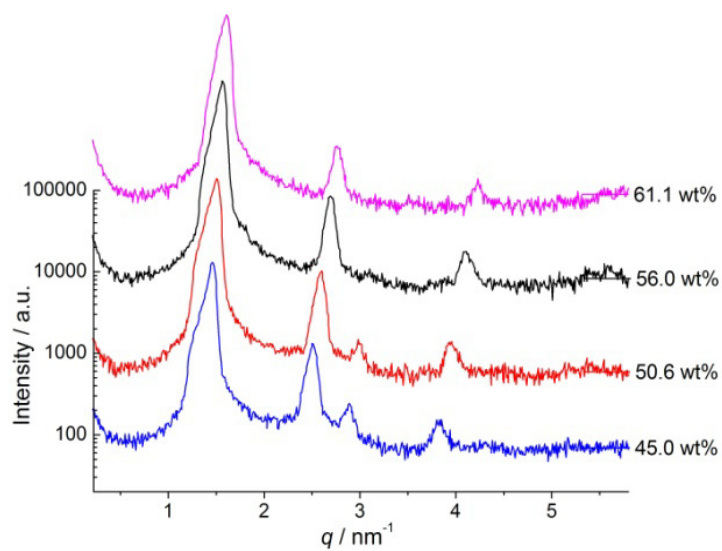
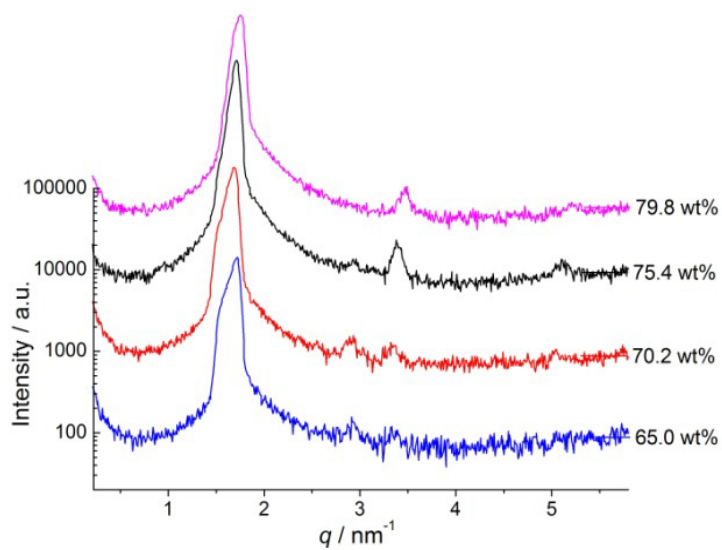
For  $L_\alpha$  of ChC12, no X-ray data are available at the moment owing to the particular narrowness of the phase region in this case and since, in addition, it only occurs at elevated temperatures.

## B.4.2 ChC14

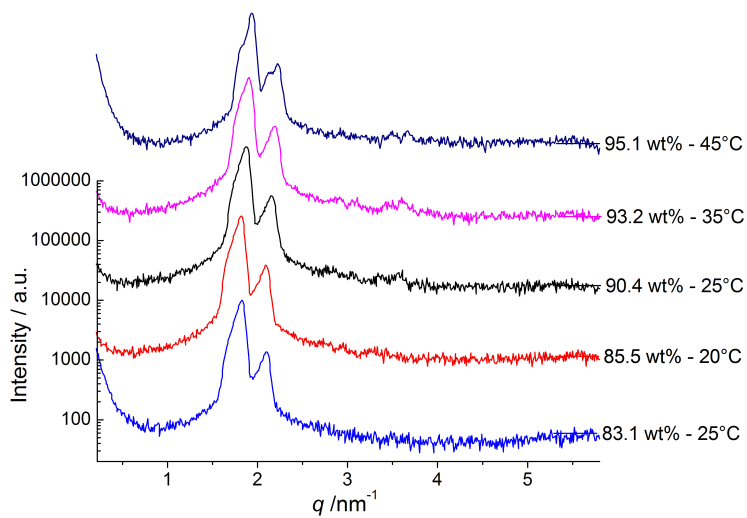
### A) Discontinuous cubic $I_1'$ and $I_1''$ ( $Pm3n$ )



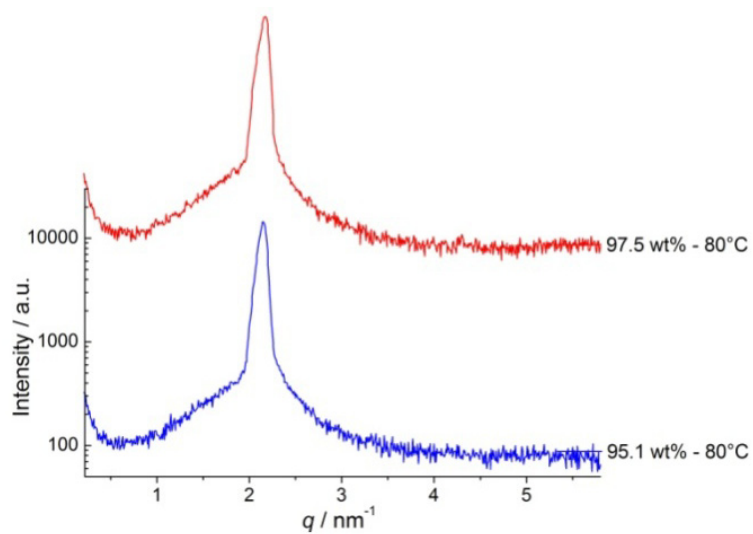
**B) Hexagonal phase  $H_1$**



**C) Bicontinuous phase  $V_1$  with  $Ia3d$  structure**

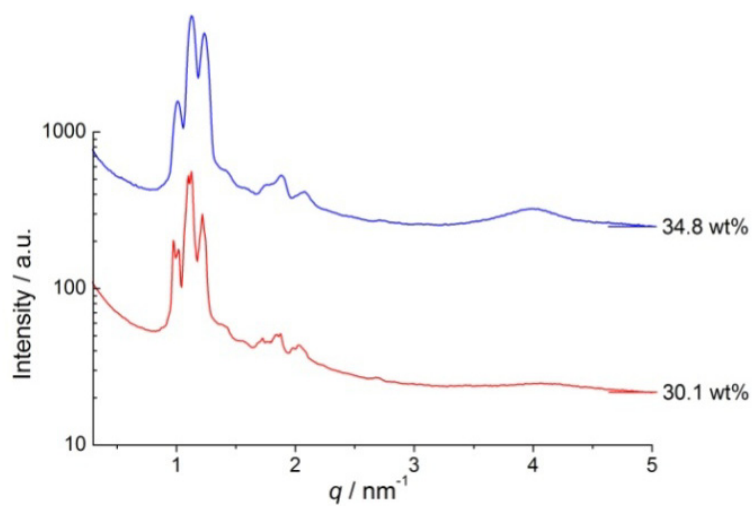


**D) Lamellar phase  $L_\alpha$**

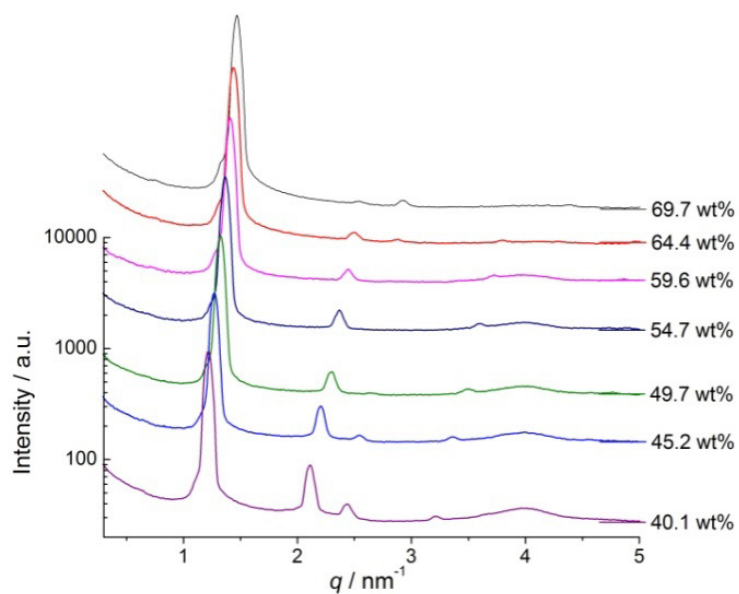


**B.4.3 ChC16**

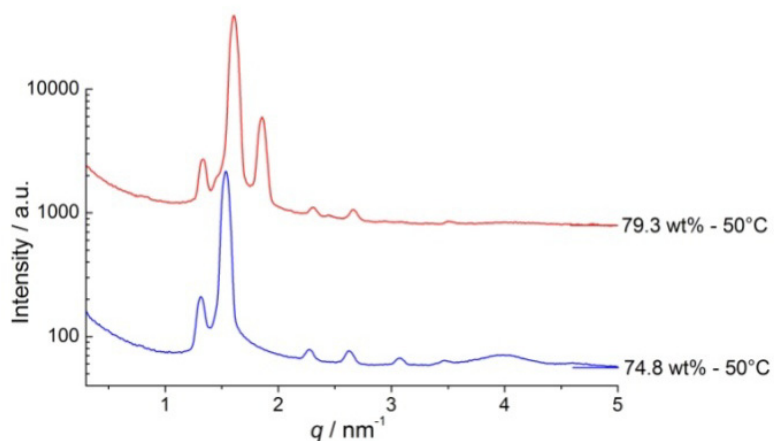
**A) Discontinuous cubic  $I_1'$  and  $I_1''$  ( $Pm3n$ )**



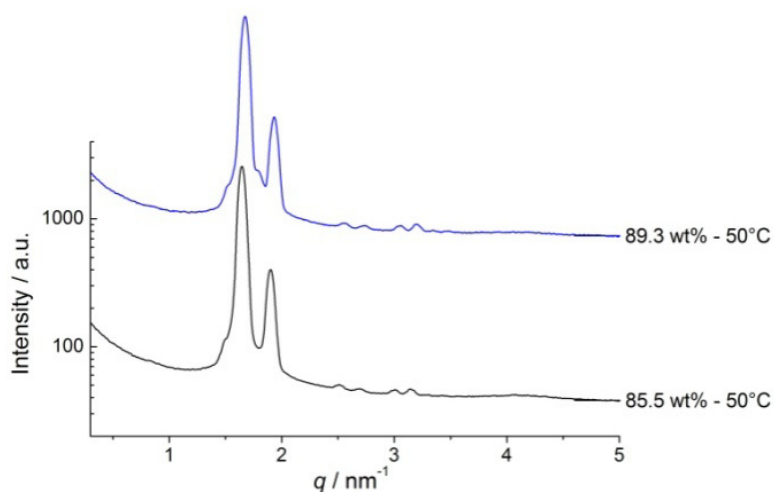
**B) Hexagonal phase  $H_1$**



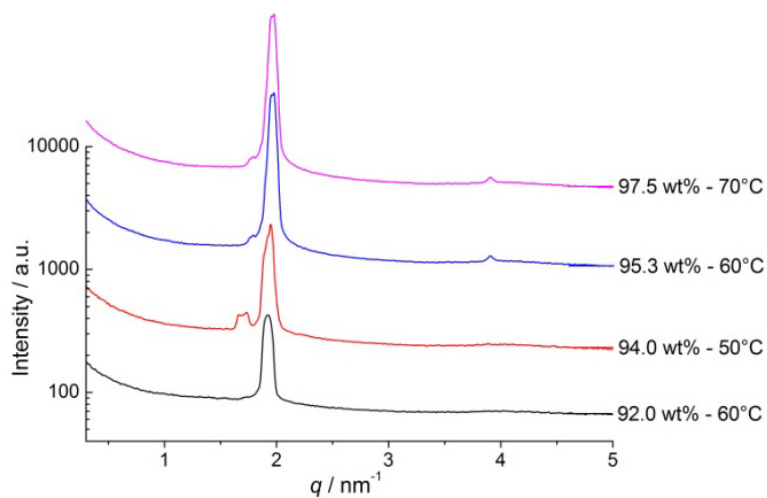
**C)  $H_1 - V_1$  boundary – intermediate phase?**



**D) Bicontinuous phase  $V_1$  with  $Ia3d$  structure**

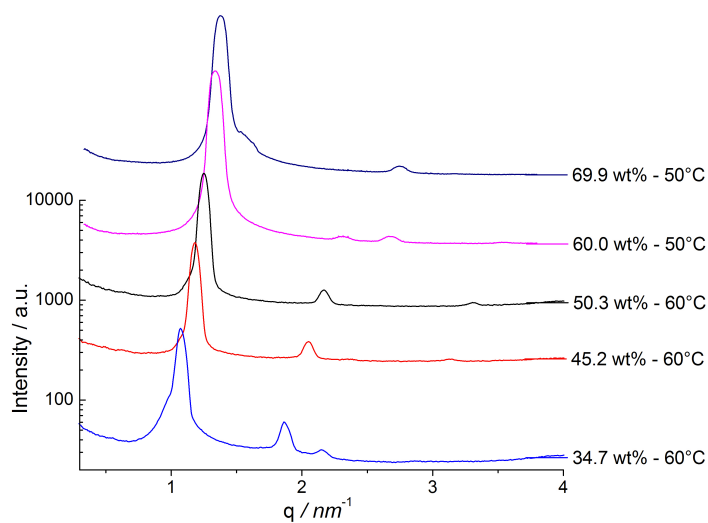


**E) Lamellar phase  $L_\alpha$**

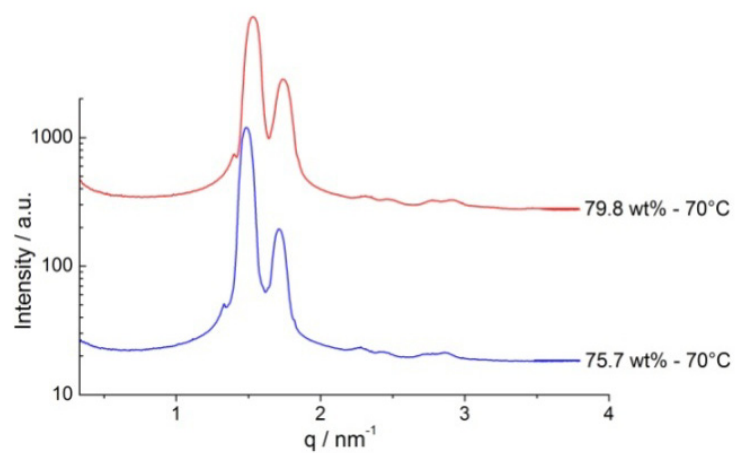


**B.4.4 ChC18**

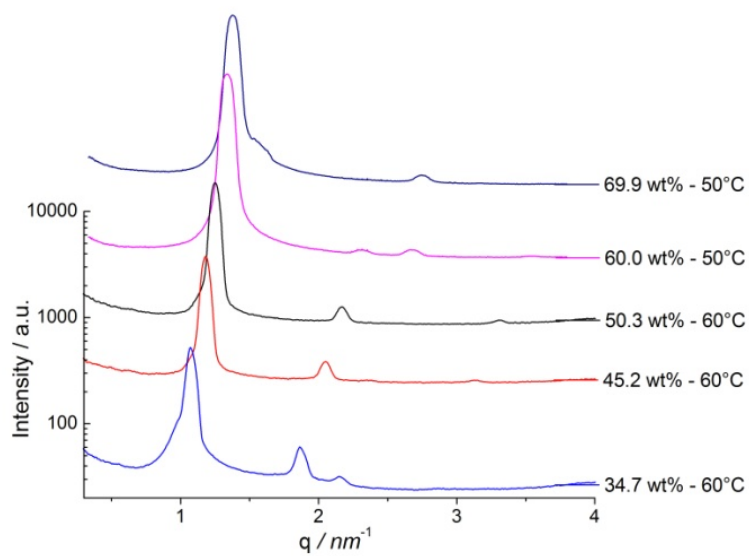
**A) Hexagonal phase  $H_1$**



**B) Bicontinuous phase  $V_1$  with  $Ia3d$  structure**



**C) Lamellar phase  $L_a$**



## B.5 X-ray Data and Phase Assignment

### B.5.1 Attempt of Assigning $I_1'$ to $P6_3/mmc$

Clerc reported in 1996 on a new symmetry for a discontinuous cubic phase, occurring in the non-ionic system  $C_{12}EO_8$ .<sup>7</sup> This phase was located between the micellar solution and an  $I_1$  phase of  $Pm3n$  structure. It consists of two micelles per unit cell arranged in a hexagonal compact structure of space group  $P6_3/mmc$  and is nonetheless of isotropic nature. The ratio  $R = c/a$  of the hexagonal unit cell indicated that the micelles are of quasi-spherical shape. Afterwards, in 2007, Zeng *et al.* confirmed that this isotropic phase is composed of hexagonal close packed (hcp), perfectly spherical micelles.<sup>8</sup>

Assuming that the  $P6_3/mmc$  structure reflects the basic lattice of  $I_1'$ , the unit cell parameter  $a$  is given by:<sup>7</sup>

$$a = d \sqrt{\frac{4}{3}(h^2 + k^2 + hk) + l^2/R^2} \quad (B.2)$$

By trying different values for 35.1 wt% ChC12, for instance, the lowest statistical error was found for  $R = 1.635$ , which is very close to those of a hexagonal close compact packing of spheres ( $R = 1.633$ ). The volume of the hexagonal unit cell is defined as:<sup>7</sup>

$$V_{Unitcell} = \frac{\sqrt{3}}{2} Ra^3 \quad (B.3)$$

As the volume fraction of surfactant  $\Phi_S$  and the volume of one surfactant molecule  $V_S$  are known, the micelle aggregation  $N_{agg}$  with respect to two micelles per unit cell can be calculated according to:

$$N_{agg} = (V_{Unitcell} \cdot \Phi_S / V_S) / 2 \quad (B.4)$$

Based thereon, values of  $a = 51.3 \pm 0.8 \text{ \AA}$  and to  $V_{Unit cell} = 191\,381 \text{ \AA}^3$  were derived for 35.1 wt% ChC12 resulting in an aggregation number of  $N_{agg} = 66.0$ .

## B.5.2 X-ray Data of $I_1''$

Table B.5 lists the X-ray diffraction data obtained on  $I_1''$  for choline soaps of different  $m$  values. Unfortunately data on  $I_1''$  of ChC18 are missing at the moment due to limited measurement time.

**Table B.5** X-ray diffraction data of ChC $m$  salts up to  $m=16$  at 25°C with  $Pm3n$  structure. The table comprises the volume fraction of surfactant  $\Phi_S$ , the experimental  $d$  values (in Å) with the corresponding *Miller* indices, the resulting unit cell parameter  $a$  (in Å) and the aggregation numbers  $N_{agg}$ , which have to be considered as rough approximations. 37.9 wt% ChC12 and 34.9 wt% ChC14 are biphasic samples of  $I_1'$  and  $I_1''$ , while 47.2 wt% ChC12 is located in the two phase region of  $I_1''$  and  $H_1$ .

	$I_1'' - Pm3n$							
	ChC12	ChC12	ChC12	ChC12	ChC14	ChC14	ChC14	ChC16
wt%	37.9	40.1	45.0	47.2	34.9	37.4	40.9	34.8
$\Phi_S$	0.383	0.405	0.455	0.477	0.356	0.381	0.416	0.358
$d_{110}$	-	-	62.8	62.2	-	73.9	74.8	-
$d_{200}$	45.5	45.2	44.6	44.2	53.2	52.8	52.4	62.2
$d_{210}$	40.5	40.0	39.8	39.5	47.6	46.9	46.9	55.6
$d_{211}$	37.2	36.7	36.1	36.6	42.5	43.0	43.6	51.1
$d_{220}$	32.2	31.7	31.6	31.3	37.0	37.2	38.1	44.6
$d_{310}$	-	28.6	28.2	28.0	-	34.0	34.1	39.3
$d_{222}$	26.4	26.0	25.5	25.5	31.0	30.8	31.0	35.7
$d_{320}$	25.5	24.9	24.6	24.5	-	29.8	29.8	34.9
$d_{321}$	24.5	24.0	23.7	23.6	28.2	28.6	28.7	33.4
$d_{400}$	-	22.4	22.2	-	26.5	26.7	-	31.4
$d_{410}$	-	21.8	21.5	-	25.9	25.9	26.0	30.2
$d_{330+411}$	-	21.0	20.9	20.8	-	-	-	-
$a$	91.3 ± 0.5	89.9 ± 0.3	88.8 ± 0.2	88.4 ± 0.4	105.8 ± 1.1	106.1 ± 1.0	106.7 ± 1.2	124.9 ± 0.8
$N_{agg}$	70.9	71.4	77.4	79.8	92.7	100.1	111.1	139.4

### B.5.3 X-ray Data of H<sub>1</sub>

Table B.6 lists the X-ray diffraction data of H<sub>1</sub> obtained for the different alkyl chain lengths of choline soaps. Towards higher surfactant concentrations, some reflections are systematically suppressed. For instance, the intensity of the *110* reflection tends to zero, while that of the *200* reflection passes through a minimum, in analogy to what has been reported by Luzzati and coworkers for alkali soaps.<sup>9</sup>

**Table B.6** X-ray diffraction data for the hexagonal phase H<sub>1</sub> of ChC<sub>m</sub> soaps with *m*= 12-18, including the volume fraction of surfactant  $\Phi_S$ , the temperature *T* (in °C), the experimental *d* values (in Å) with corresponding Miller indices, and the resulting unit cell parameters *a* ((in Å). 83.8 wt% ChC12 is possibly a biphasic sample, as shown in the following section.

	Hexagonal – H <sub>1</sub>									
	wt%	$\Phi_S$	<i>T</i>	<i>d</i> <sub>100</sub>	<i>d</i> <sub>110</sub>	<i>d</i> <sub>200</sub>	<i>d</i> <sub>210</sub>	<i>d</i> <sub>300</sub>	<i>d</i> <sub>220</sub>	<i>a</i>
ChC12	49.7	0.502	25	36.7	21.3	18.5	14.0	-	-	42.6 ± 0.1
	55.1	0.556	25	36.1	21.1	18.1	13.8	-	-	41.9 ± 0.2
	60.2	0.606	25	35.1	20.3	-	13.3	-	10.1	40.6 ± 0.1
	65.5	0.659	25	34.3	19.9	-	13.0	-	-	39.8 ± 0.1
	69.9	0.703	25	33.8	19.5	17.0	12.8	-	-	39.1 ± 0.1
	74.7	0.750	25	33.1	19.2	16.6	-	-	-	38.3 ± 0.1
	79.9	0.802	25	32.6	-	16.3	-	10.9	-	37.7 ± 0.1
	83.8	0.840	25	32.2	-	16.2	-	10.8	-	37.3 ± 0.1
ChC14	45.0	0.457	25	43.3	25.1	21.7	16.3	-	-	50.1 ± 0.2
	50.6	0.513	25	41.9	24.2	21.1	15.9	-	-	48.5 ± 0.2
	56.0	0.567	25	40.3	23.4	20.3	15.3	-	-	46.7 ± 0.1
	61.0	0.618	25	39.0	22.8	-	14.9	-	-	45.3 ± 0.2
	70.2	0.708	25	37.2	21.4	18.6	-	12.4	-	43.0 ± 0.1
	75.4	0.759	25	36.7	21.2	18.5	-	12.3	-	42.6 ± 0.2
	79.8	0.803	25	35.9	-	18.0	-	12.0	-	41.6 ± 0.1
ChC16	40.1	0.411	25	51.5	29.8	25.8	19.5	-	-	59.5 ± 0.1
	45.2	0.463	25	49.5	28.4	24.8	18.7	16.6	-	57.2 ± 0.2
	49.7	0.510	25	47.6	27.3	23.8	17.9	-	13.2	54.8 ± 0.2
	54.7	0.557	25	45.9	26.5	-	17.5	-	13.3	53.1 ± 0.2
	59.6	0.606	25	44.6	25.8	22.4	16.9	-	12.9	51.6 ± 0.2
	64.4	0.654	25	43.6	25.1	21.8	16.5	-	12.7	50.4 ± 0.2
	69.7	0.706	25	42.7	24.7	21.6	-	14.3	12.4	49.5 ± 0.2
ChC18	34.7	0.359	60	58.7	33.8	29.2	-	-	-	67.6 ± 0.2
	45.2	0.465	60	53.2	30.6	26.7	20.1	-	-	61.5 ± 0.2
	50.3	0.516	60	50.3	29.0	-	19.0	-	-	58.0 ± 0.1
	60.0	0.612	50	46.9	27.2	23.4	17.7	-	-	54.2 ± 0.1
	69.9	0.710	50	45.5	-	22.9	-	-	-	52.8 ± 0.3

### B.5.4 $H_1 - V_1$ Boundary: Intermediate Phase?

As mentioned in Chapter IV, additional reflections occur close to the phase boundary of  $H_1/V_1$ . Indeed, these have not been observed for ChC14. However, this can most probably be attributed to the lower resolution of the experimental setup used for the measurement of corresponding samples.

Table B.7 shows the attempt of assigning the additional reflections to an intermediate phase of complex hexagonal structure (ribbon phase with  $cm\bar{m}$  symmetry). Compared to the other liquid crystalline phases, the peak positions are much less sensitive to concentration variations, but are still shifted to lower scattering angles when elongating the alkyl chain.

**Table B.7** X-ray diffraction data of choline soaps near the phase boundary  $H_1 / V_1$ . Each sample represents a biphasic system of possibly an intermediate phase with complex hexagonal structure and  $H_1$  (83.8 wt% ChC12 and 74.8 wt% ChC16) or  $V_1$  (all other samples), respectively. The table includes the volume fraction of surfactant  $\Phi_S$ , the temperature  $T$  (in °C) the experimental  $d$  values (in Å) with the *Miller* indices for a 2-D hexagonal lattice, and the unit cell parameter  $a$  (in Å).

	$H_1 / V_1$ – complex hexagonal							
	wt%	$\Phi_S$	$T$	$d_{100}$	$d_{110}$	$d_{200}$	$d_{210}$	$a$
ChC12	83.8	0.840	25	39.5	22.8	19.8	15.0	$45.7 \pm 0.1$
	86.9	0.871	25	39.3	22.8	19.7	14.9	$45.5 \pm 0.2$
	89.5	0.897	25	38.8	22.6	-	-	$45.0 \pm 0.3$
ChC16	74.8	0.756	60	47.6	27.6	23.9	18.1	$55.1 \pm 0.1$
	79.3	0.800	50	47.2	27.2	23.6	17.8	$54.5 \pm 0.1$
ChC18	79.8	0.806	70	51.1	29.6	25.8	-	$59.2 \pm 0.2$

Alternatively, the additional peaks can be fitted by a cubic lattice, namely  $I4_132$ , which exhibits Bragg spacing ratios of  $\sqrt{2} : \sqrt{6} : \sqrt{8} : \sqrt{10} : \sqrt{12}$  (see Table B.8). The statistical error of the  $I4_132$  unit cell is only slightly larger as for a 2-D hexagonal lattice, but the  $310$  and  $222$  reflections are missing in all instances.

**Table B.8** X-ray diffraction data of choline soaps near the phase boundary  $H_1 / V_1$ . Each sample represents a biphasic system of possibly a cubic  $I4_132$  structure and  $H_1$  (83.8 wt% ChC12 and 74.8 wt% ChC16) or  $V_1$  (remaining samples), respectively. The table includes the volume fraction of surfactant  $\Phi_S$ , the temperature  $T$  (in °C), the experimental  $d$  values (in Å) with the corresponding *Miller* indices for  $I4_132$ , and the unit cell parameter  $a$  (in Å).

	$H_1 / V_1 - I4_132$									
	wt%	$\Phi_S$	$T$	$d_{110}$	$d_{211}$	$d_{220}$	$d_{310}$	$d_{222}$	$d_{321}$	$a$
ChC12	83.8	0.840	25	39.5	22.8	19.8	-	-	15.0	$56.0 \pm 0.1$
	86.9	0.871	25	39.3	22.8	19.7	-	-	14.9	$55.8 \pm 0.2$
	89.5	0.897	25	38.8	22.6	-	-	-	-	$55.1 \pm 0.4$
ChC16	74.8	0.756	60	47.6	27.6	23.9	-	-	18.1	$67.5 \pm 0.1$
	79.3	0.800	50	47.2	27.2	23.6	-	-	17.8	$66.7 \pm 0.1$
ChC18	79.8	0.806	70	51.1	29.6	25.8	-	-	-	$72.6 \pm 0.3$

### B.5.5 Bicontinuous Cubic Phase $V_1$

**Table B.9** X-ray diffraction data for  $V_1$  of ChC*m* soaps with  $Ia3d$  structure, comprising the volume fraction of surfactant  $\Phi_S$ , the temperature  $T$  (in °C), the experimental  $d$  values (in Å) with the assignment to the corresponding *Miller* indices and the unit cell parameter  $a$  (in Å). Samples of ChC12 up to 89.5 wt%, 79.3 wt% ChC16 and 75.7 wt% ChC18 are potentially biphasic as discussed in the previous section.

	$V_1 - Ia3d$									
	wt%	$\Phi_S$	$T$	$d_{211}$	$d_{220}$	$d_{321}$	$d_{400}$	$d_{420}$	$d_{332}$	$a$
ChC12	86.9	0.871	25	31.1	27.0	-	-	-	-	$76.2 \pm 0.1$
	89.5	0.897	25	30.8	26.7	20.3	-	-	-	$75.6 \pm 0.2$
	91.5	0.916	25	30.4	26.4	20.0	18.7	16.7	15.9	$74.6 \pm 0.2$
	94.0	0.941	25	30.2	26.1	19.9	18.5	16.5	15.8	$74.0 \pm 0.2$
	97.5	0.975	60	29.0	25.0	19.0	17.9	15.9	15.1	$71.1 \pm 0.2$
ChC14	79.8	0.803	60	34.0	29.4	-	-	-	-	$83.1 \pm 0.1$
	83.3	0.837	25	35.1	30.7	-	-	-	-	$86.3 \pm 0.5$
	85.5	0.859	20	34.5	30.1	-	-	-	-	$84.8 \pm 0.3$
	90.4	0.906	25	33.6	29.2	22.1	20.6	18.5	17.6	$82.6 \pm 0.3$
	93.2	0.934	35	32.9	28.7	21.6	20.2	18.0	17.2	$80.7 \pm 0.3$
	95.1	0.952	45	32.4	28.3	21.3	19.9	17.7	17.1	$79.7 \pm 0.4$
ChC16	79.3	0.800	50	39.0	33.9	25.8	-	21.4	20.3	$95.8 \pm 0.4$
	85.5	0.860	50	38.1	33.1	25.0	23.4	20.9	19.9	$93.4 \pm 0.2$
	89.3	0.897	50	37.6	32.6	24.6	23.0	20.5	19.6	$92.1 \pm 0.1$
ChC18	75.7	0.766	70	42.2	36.7	27.6	25.8	23.1	22.0	$103.3 \pm 0.3$
	79.8	0.806	70	41.1	35.9	27.2	25.4	22.7	21.6	$101.4 \pm 0.4$

Fig. B.7 shows that the decrease of the unit cell towards higher soap concentrations.

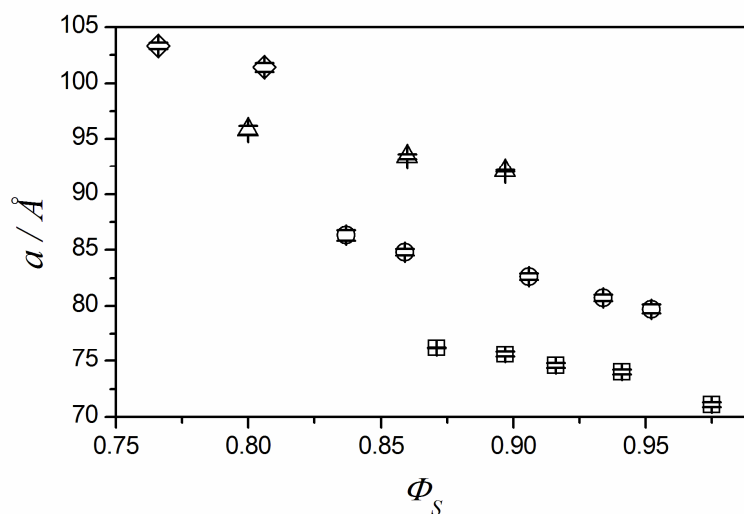


**Fig. B.7**  $V_1$  phase of ChCm salts: plot of the unit cell parameter  $a$  of the  $Ia3d$  structure versus the volume fraction of surfactant  $\Phi_S$ , showing the different alkyl chain lengths in comparison (ChC12 ( $\square$ ), ChC14 ( $\circ$ ), ChC16 ( $\triangle$ ) and ChC18 ( $\diamond$ )). Data correspond to the temperatures given in Table B.9.

## B.6 References

1. C. Tanford, *J. Phys. Chem.*, 1972, **76**, 3020.
2. S. Fouilloux, A. Desert, O. Tache, O. Spalla, J. Daillant, A. Thill, *J. Colloid Interface Sci.*, 2010, **346**, 79.
3. T. Zemb, O. Tache, F. Ne, O. Spalla, *Rev. Sci. Instrum.*, 2003, **74**, 2456.
4. T. C. Huang, H. Toraya, T. N. Blanton, Y. Wu, *J. Appl. Crystallogr.*, 1993, **26**, 180.
5. V. Urban, P. Panine, C. Ponchut, P. Boesecke, T. Narayanan, *J. Appl. Crystallogr.*, 2003, **36**, 809.
6. T. N. Blanton, C. L. Barnes, M. Lelental, *J. Appl. Crystallogr.*, 2000, **33**, 172.
7. M. Clerc, *J. Phys. II*, 1996, **6**, 961.
8. X. Zeng, Y. Liu, M. Imperor-Clerc, *J. Phys. Chem. B*, 2007, **111**, 5174.
9. F. Husson, H. Mustacchi, V. Luzzati, *Acta Crystallogr.*, 1960, **13**, 668.

## Appendix C: Thermotropic Phase Behavior of Choline Soaps

### C.1 Thermogravimetric analyses

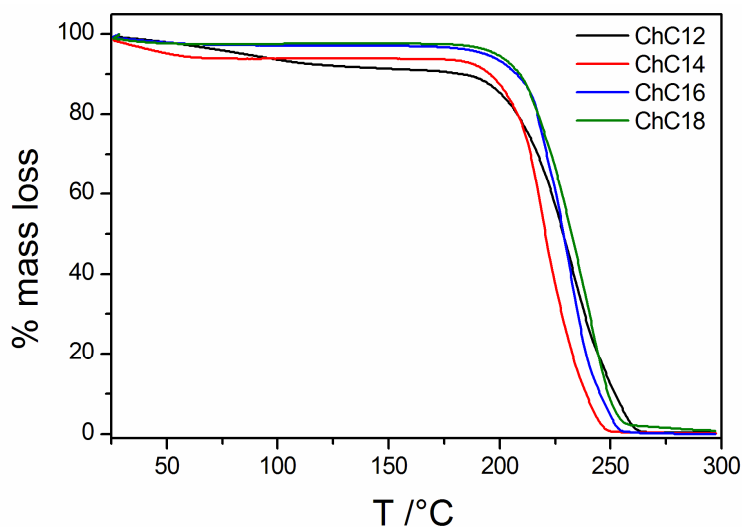
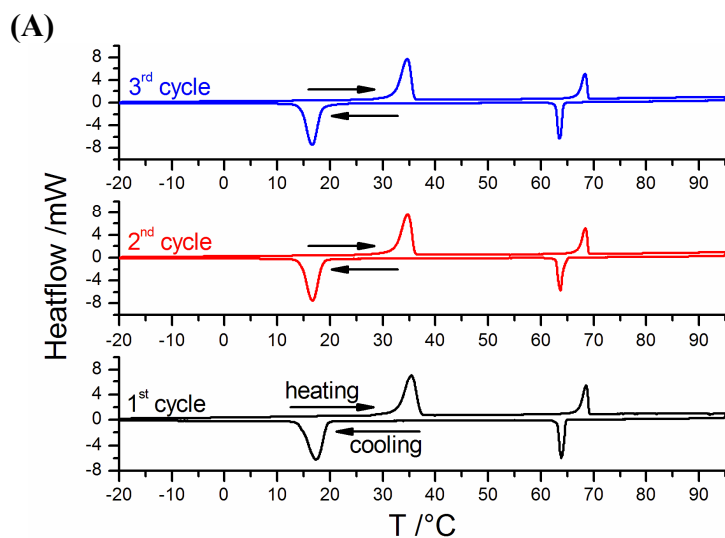
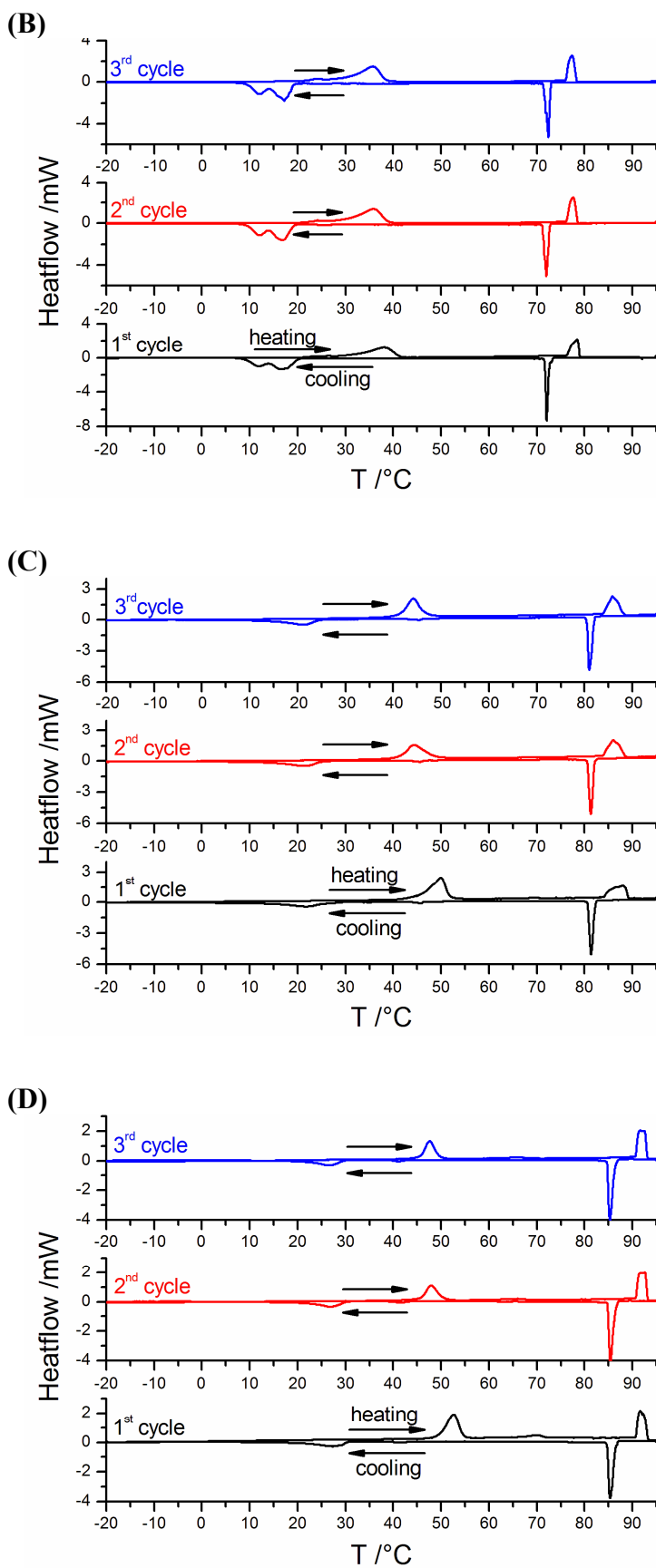


Fig. C.1 TGA curves of  $\text{ChC}_m$  surfactants for  $m=12-18$ .

All investigated choline soaps show a one-step degradation process. The initial decay of ChC12 and ChC14 most probably originates from evaporation of water.

### C.2 DSC diagrams





**Fig. C.2** Three DSC cycles of ChCm surfactants between -20°C and 95°C:  $m= 12$  (A),  $m= 14$  (B),  $m= 16$  (C) and  $m= 18$  (D).

### C.3 Transition Temperatures

In the following, the indices “1” and “2” signify low- and high-temperature transitions, respectively.

**Table C.1** Transition temperatures on heating and cooling of ChC*m* surfactants for *m*= 12-18, as determined by DSC for three cycles between -20°C and 95°C.

	ChC12		ChC14		ChC16		ChC18	
	T <sub>1</sub> / °C	T <sub>2</sub> / °C	T <sub>1</sub> / °C	T <sub>2</sub> / °C	T <sub>1</sub> / °C	T <sub>2</sub> / °C	T <sub>1</sub> / °C	T <sub>2</sub> / °C
1 <sup>st</sup> heating	35.4	68.6	38.1	78.4	50.0	87.9	52.6	91.6
1 <sup>st</sup> cooling	17.3	63.9	16.5	72.1	21.4	81.4	27.4	85.4
2 <sup>nd</sup> heating	34.7	68.4	36.0	77.6	44.4	85.9	47.9	92.6
2 <sup>nd</sup> cooling	16.7	63.7	16.9	72.0	21.2	81.3	26.9	85.4
3 <sup>rd</sup> heating	34.6	68.4	35.7	77.4	44.2	85.8	47.6	92.5
3 <sup>rd</sup> cooling	16.6	63.5	17.2	72.5	21.3	81.0	26.7	85.3

### C.4 Transition Enthalpies

**Table C.2** Transition enthalpies (in kJ mol<sup>-1</sup>) on heating and cooling of ChC*m* surfactants for *m*= 12-18, as determined by DSC for three cycles between -20°C and 95°C.

	ChC12		ChC14		ChC16		ChC18	
	ΔH <sub>1</sub>	ΔH <sub>2</sub>						
1 <sup>st</sup> heating	28.3	9.2	23.4	12.9	26.7	14.2	25.5	15.9
1 <sup>st</sup> cooling	-27.7	-9.1	-22.9	-13.0	-17.9	-15.3	-14.4	-19.5
2 <sup>nd</sup> heating	28.1	9.0	24.2	12.0	21.9	14.7	19.2	16.8
2 <sup>nd</sup> cooling	-27.6	-9.0	-22.5	-12.0	-17.7	-15.2	-14.6	-19.4
3 <sup>rd</sup> heating	27.2	9.1	24.4	12.2	19.7	15.2	21.2	16.8
3 <sup>rd</sup> cooling	-27.9	-9.0	-22.7	-12.3	-17.9	-15.1	-14.3	-19.5

**Table C.3** Sum of the transition enthalpies of ChC $m$  surfactants for  $m= 12-18$  as obtained by DSC for three heating-cooling cycles between  $-20^{\circ}\text{C}$  and  $95^{\circ}\text{C}$ .

	<b>ChC12</b>	<b>ChC14</b>	<b>ChC16</b>	<b>ChC18</b>
	$\sum H / \text{kJ mol}^{-1}$			
1 <sup>st</sup> heating	37.5	36.3	40.9	41.4
1 <sup>st</sup> cooling	-36.8	-35.9	-33.2	-33.9
2 <sup>nd</sup> heating	37.1	36.2	36.6	36.0
2 <sup>nd</sup> cooling	-36.6	-34.5	-32.9	-34
3 <sup>rd</sup> heating	36.3	36.6	34.9	38.0
3 <sup>rd</sup> cooling	-36.9	-35.0	-33.0	-33.8

## C.5 Optical Polarizing Microscopy

All pictures were recorded at 100x magnification with a heating and cooling rate of  $10^{\circ}\text{C min}^{-1}$ . The photographs presented in the following were taken during the first cooling cycle. Light intensity and the sample position were kept constant.

### C.5.1 ChC14

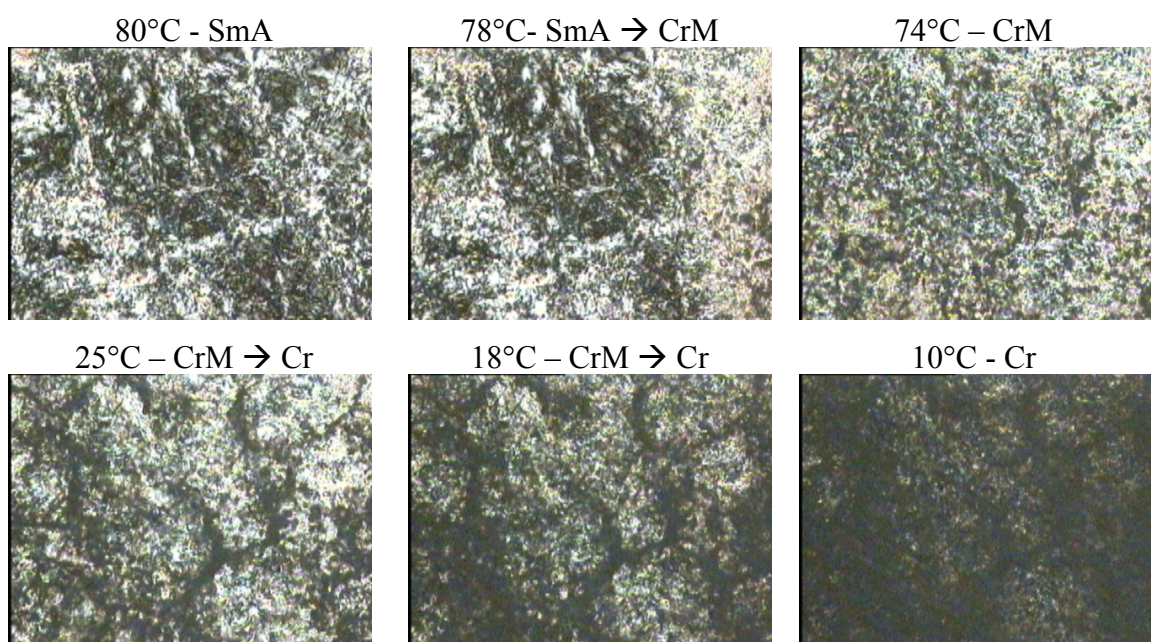


**Fig. C.3** Polarizing microscopy images of ChC14 obtained on the first cooling between  $100^{\circ}\text{C}$  and  $-20^{\circ}\text{C}$ . Above  $78^{\circ}\text{C}$  a low-viscous liquid-crystalline lamellar phase (SmA) is present. At  $78\text{--}75^{\circ}\text{C}$ , the transition from SmA to a semi-crystalline (CrM) phase takes place, which is obvious by a sudden increase of viscosity and change of texture. On further cooling, the appearance of the sample changes gradually and breaks in the texture indicate a stepwise increment of density. Between  $25^{\circ}\text{C}$  and  $10^{\circ}\text{C}$ , the sample turns finally completely dark, indicating a transition from CrM to crystalline (Cr).

## C.5.2 ChC16

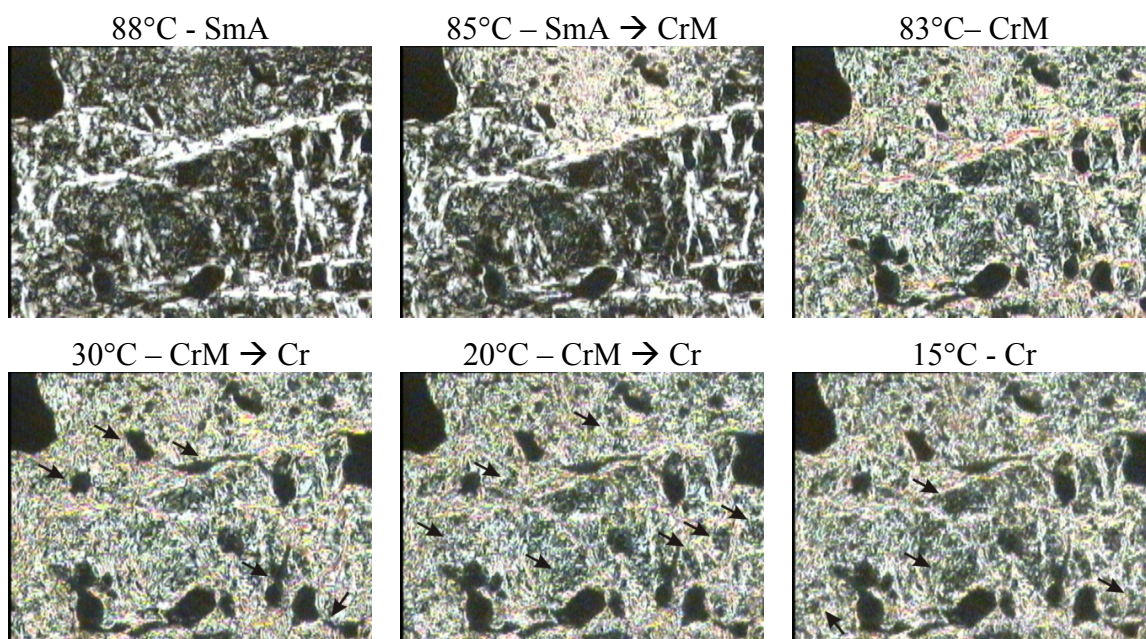


**Fig. C.4** Polarizing microscopy images of ChC16 obtained during the first cooling between 100°C and -20°C. At high temperatures ( $> 86^\circ\text{C}$ ), a liquid-crystalline lamellar phase can be identified by its characteristic oily streak texture and low viscosity. At 85-83°C, the sample becomes abruptly highly viscous and birefringent, which is due to the transition from SmA to a semi-crystalline (CrM) phase. On further cooling, breaks in the texture (as highlighted by the arrows) gradually appear, indicating a growing density. The transition from CrM to crystalline (Cr) between 20°C and 15°C becomes manifest in an attenuation of birefringence and a sudden increment of the breaks in the texture. This texture is maintained down to -20°C.

### C.5.3 ChC18

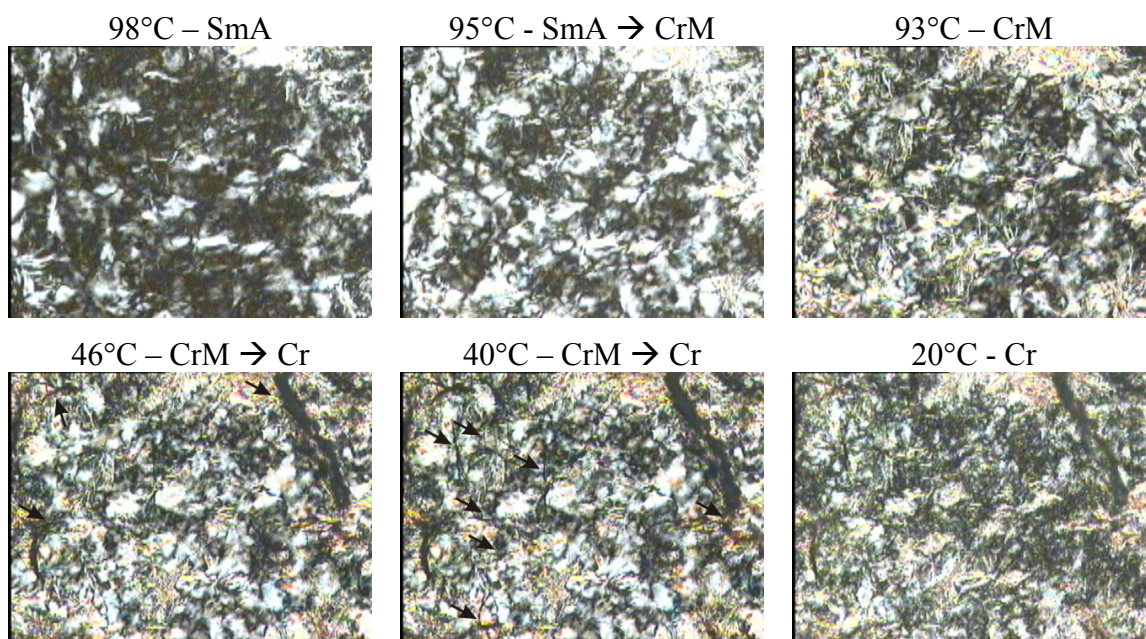
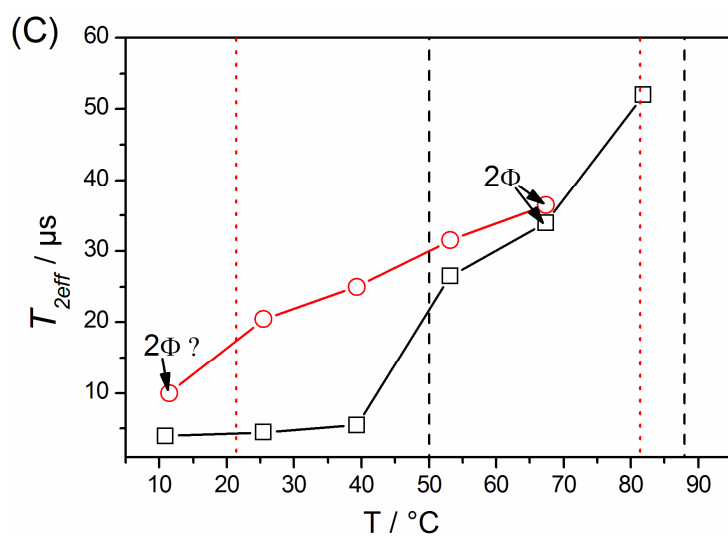
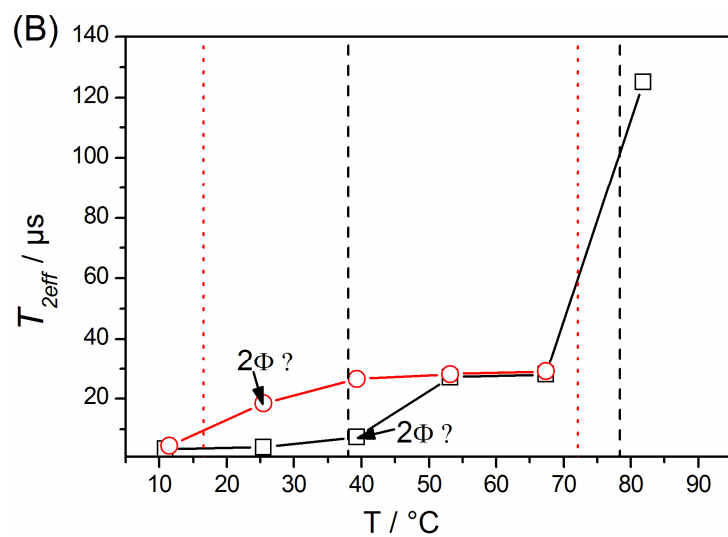
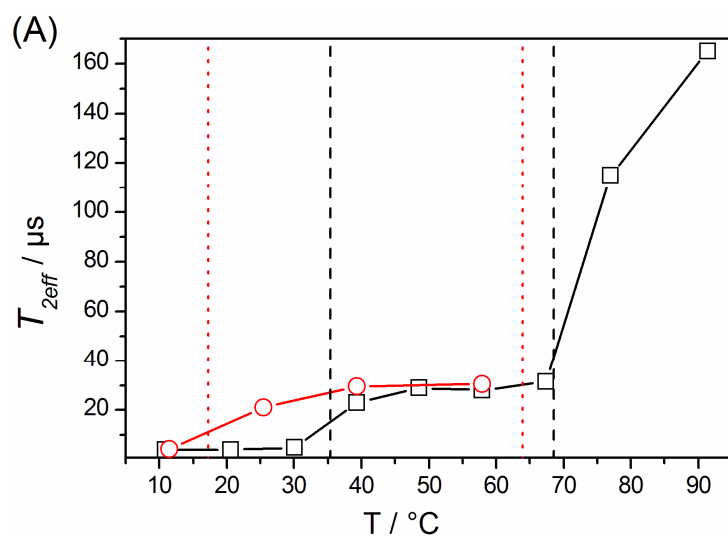


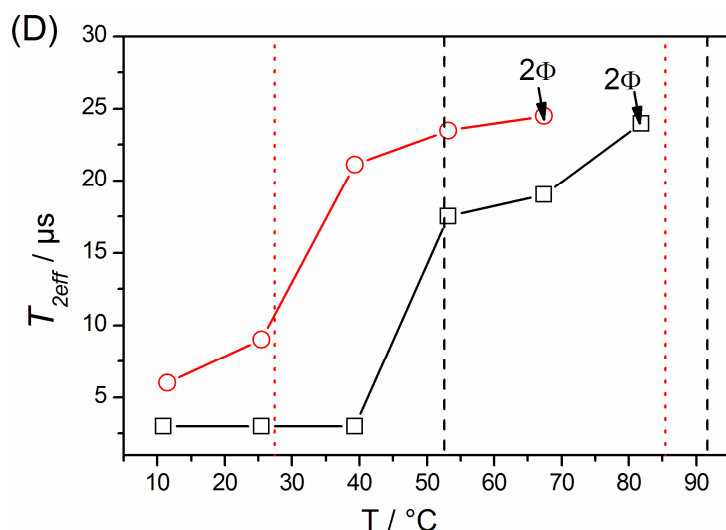
**Fig. C.5** Polarizing microscopy images of ChC18 obtained during the first cooling between 100°C and -20°C. At high temperatures ( $> 96^\circ\text{C}$ ), a liquid-crystalline lamellar phase can be identified its characteristic oily streak texture and low viscosity. At 95-93°C, the sample gets rapidly highly viscous and birefringent, which corresponds to the transition from SmA to semi-crystalline (CrM) phase. On further cooling, the appearance of the sample changes gradually, accompanied with breaks in the texture (as indicated by the arrows). The transition from CrM to crystalline (Cr) between 46°C and 35°C gets obvious from an attenuation of birefringence and a sudden increment of the breaks in the texture. Once Cr is formed, the appearance of the sample does no longer change down to -20°C.

## C.6 NMR Proton Spin-Spin Relaxation Times $T_2$

**Table C.4** NMR proton spin-spin relaxation constants  $T_{2eff}$  of ChCm surfactants ( $m=12-18$ ) as a function of temperature.

		<b>ChC12</b>	<b>ChC14</b>	<b>ChC16</b>	<b>ChC18</b>
	$T/^\circ\text{C}$	$T_{2eff}/\mu\text{s}$	$T_{2eff}/\mu\text{s}$	$T_{2eff}/\mu\text{s}$	$T_{2eff}/\mu\text{s}$
heating	10.9	4	3.5	4	3
	20.6	4	-	-	-
	25.5	-	4	4.5	3
	30.1	5	-	-	-
	39.3	23	7.5 - 2 $\Phi$ (?)	5.5	3
	48.6	29	-	-	-
	53.2	-	27	26.5	17.5
	57.9	28	-	-	-
	67.4	31.5	28	34 - 2 $\Phi$	19
	77.0	115	-	-	-
	81.8	-	125	52	24 - 2 $\Phi$ ( $\approx$ 5%)
91.4	165	-	-	-	
cooling	67.4	-	29	36.5 - 2 $\Phi$	24.5 - 2 $\Phi$ (< 1%)
	57.9	30.5	-	-	-
	53.2	-	28	31.5	23.5
	39.3	29.5	26.5	25	21.1
	25.5	21	18.5 - 2 $\Phi$ (?)	20.5	9
	11.5	4.5	4.5	10 - 2 $\Phi$ (?) -	-
	10.9	-	-	-	6
Intensity at 1/e		3.13	2.68	2.57	2.68

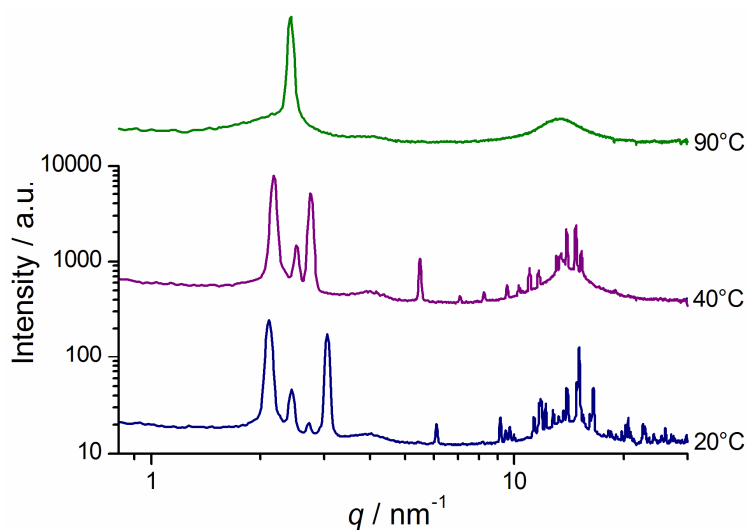




**Fig. C.6** Variation of the decay constant  $T_2$  with temperature (( $\square$ ) heating, ( $\circ$ ) cooling) of ChCm surfactants for  $m=12$  (A),  $m=14$  (B),  $m=16$  (C) and  $m=18$  (D). The black dashed vertical lines mark the transition temperatures on heating as detected by DSC, and the dotted red ones those on cooling (both for the first cycle).

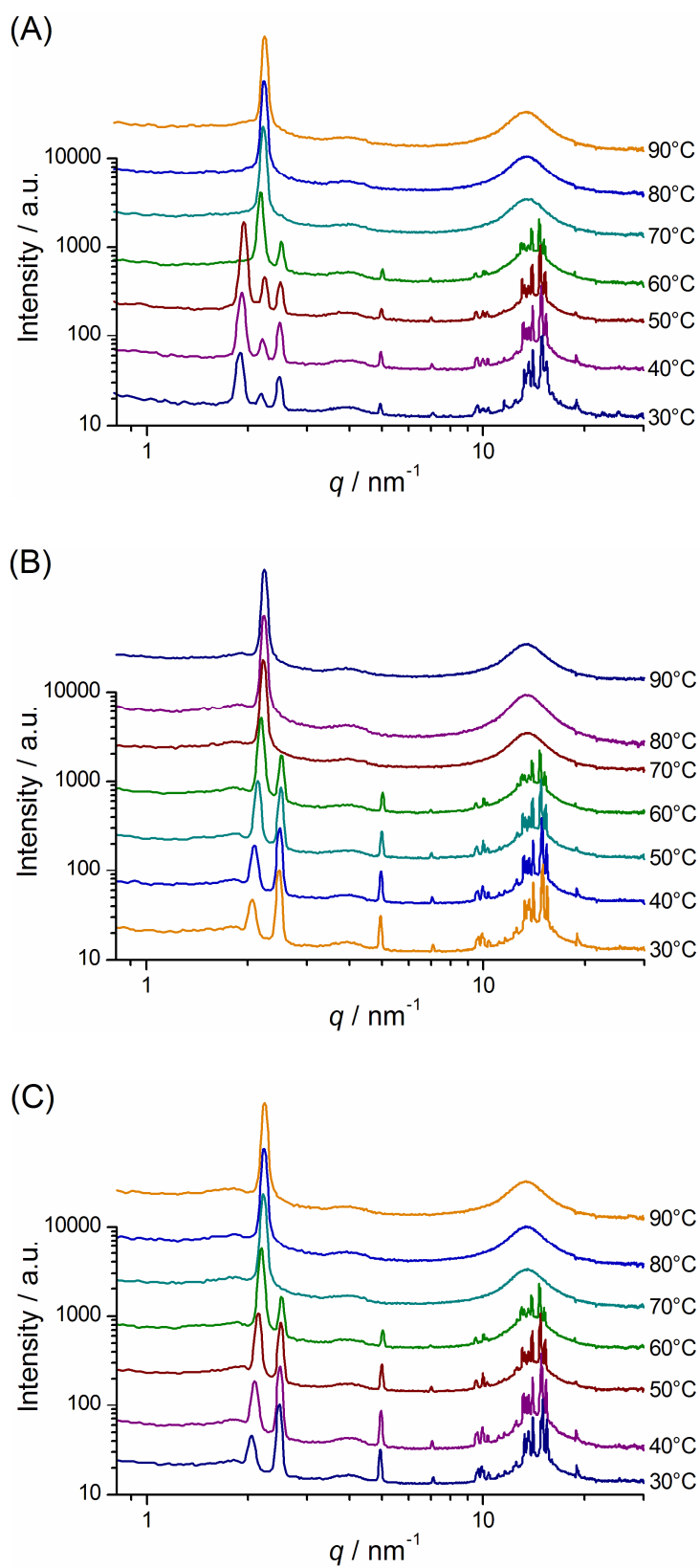
## C.7 X-ray Scattering Curves of ChCm Soaps as a Function of Temperature

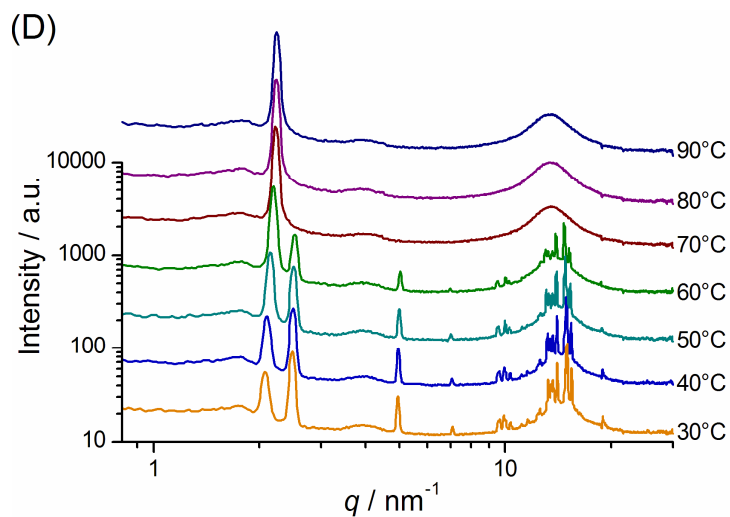
### C.7.1 ChC12



**Fig. C.7** Small- and wide-angle X-ray scattering curves of neat ChC12 with increasing temperature (freshly melted sample).

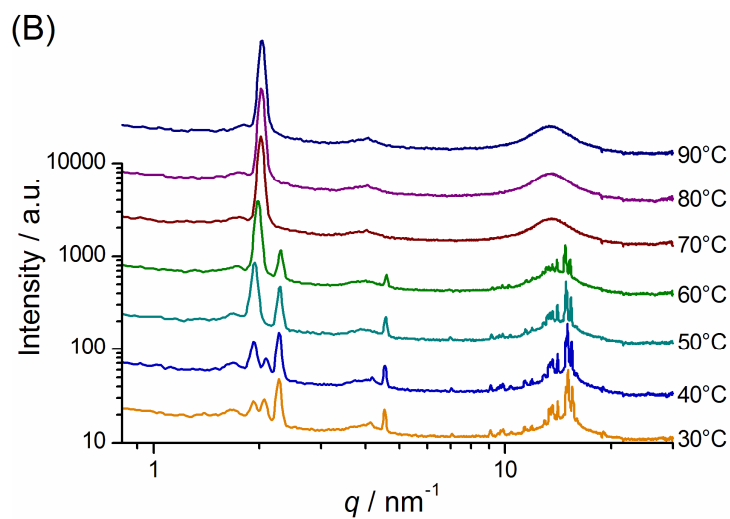
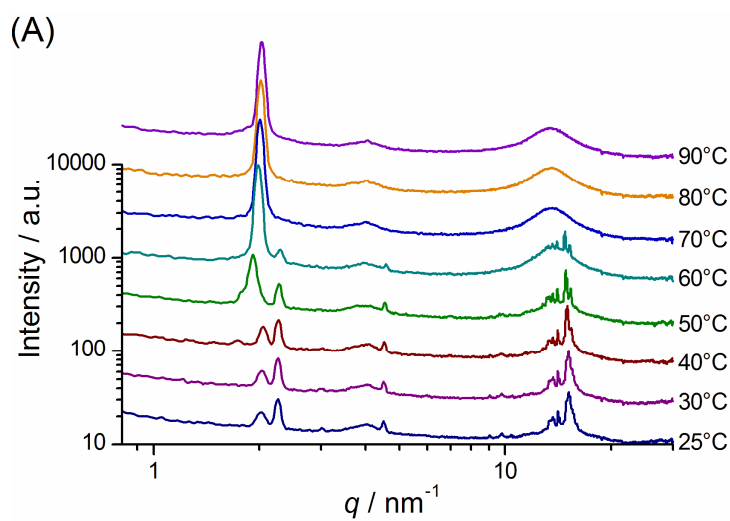
## C.7.2 ChC14

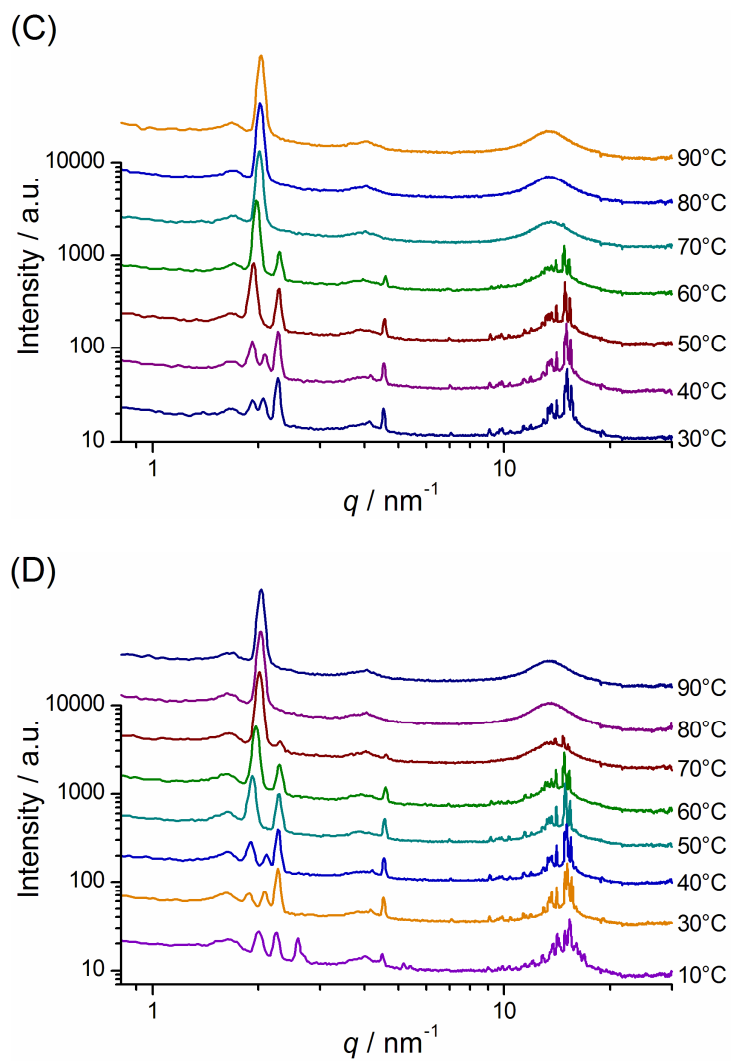




**Fig. C.8** Small- and wide-angle X-ray scattering curves of neat ChC14 at various temperatures and heating-cooling cycles: (A) freshly heated, (B) first cooling, (C) re-heated and (D) second cooling.

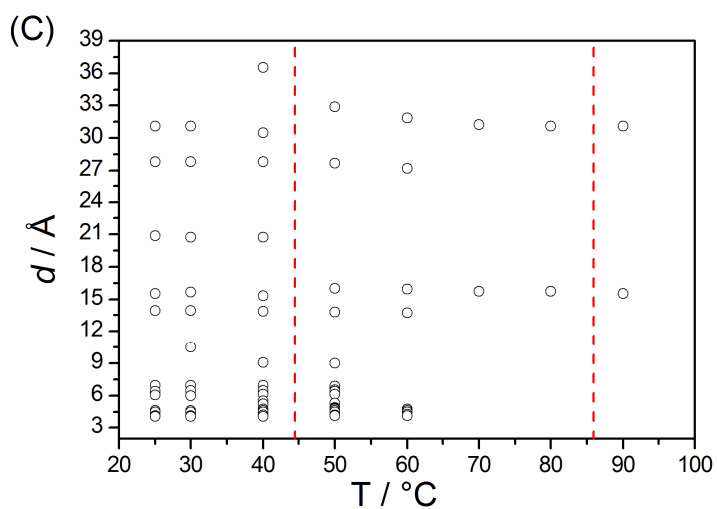
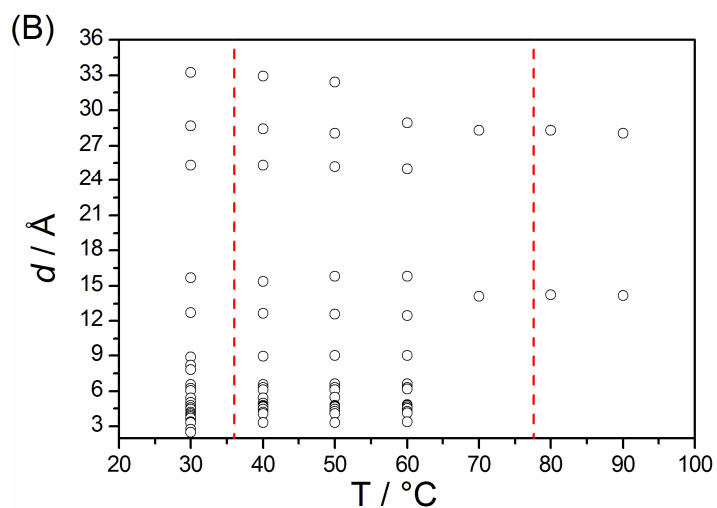
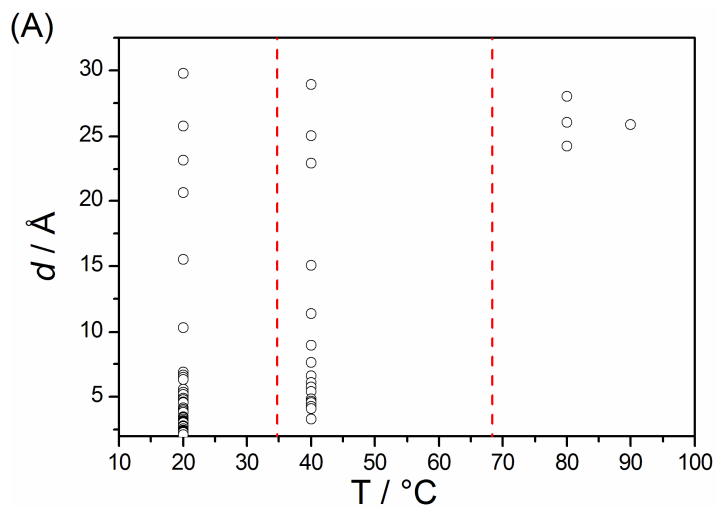
### C.7.3 ChC16





**Fig. C.9** Small- and wide-angle X-ray scattering curves of neat ChC16 at various temperatures and heating-cooling cycles: (A) freshly heated, (B) first cooling, (C) re-heated and (D) second cooling.

### C.7.4 *d*-Spacing of ChCm Surfactants as a Function of Temperature



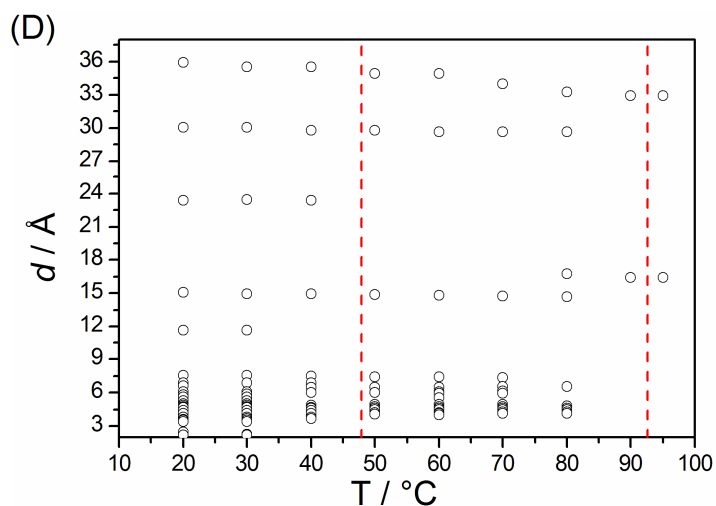


**Fig. C.10** Evolution of  $d$ -spacing values of neat ChC*m* surfactants with increasing temperature (freshly melted samples):  $m=12$  (A),  $m=14$  (B),  $m=16$  (C) and  $m=18$  (D). The vertical dashed red lines mark the transition temperatures determined by DSC.

### C.7.5 $d$ -Spacing of ChC*m* Surfactants as a Function of $m$ at Low Temperatures

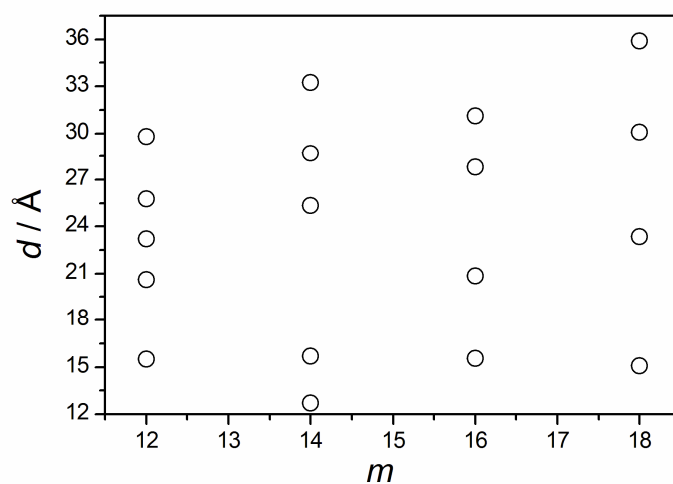


**Fig. C.11** Comparison of the low-angle  $d$ -spacing values (up to  $q=5\text{ nm}^{-1}$ ) for different alkyl chain lengths ( $m=12$ -18) at low temperatures ( $20^\circ\text{C}$  for  $m=12$  and 18,  $25^\circ\text{C}$  for  $m=16$ , and  $30^\circ\text{C}$  for  $m=14$ ).

### C.7.6 *d*-Spacing of ChC*m* Surfactants as a Function of *m* at 40°C

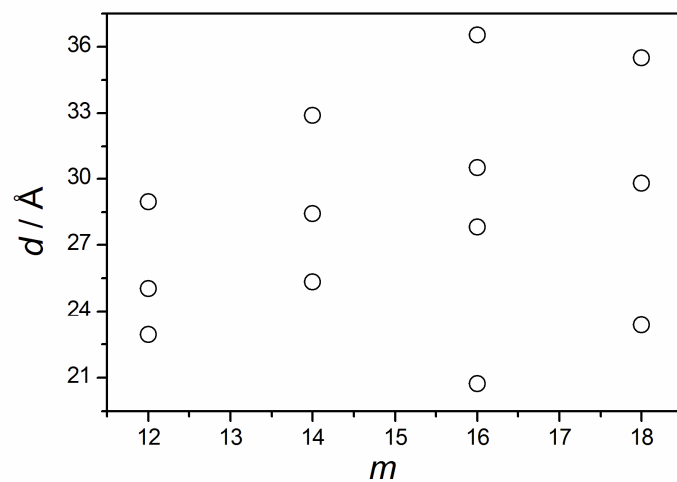


**Fig. C.12** Comparison of the low-angle *d*-spacing values (up to  $q=5\text{ nm}^{-1}$ ) for  $m=12-18$  at 40°C.

## Appendix D: Oligoether Carboxylates – Task-Specific Room-Temperature Ionic Liquids

As mentioned in Chapter VIII, the temperatures at which densities and viscosities were determined differed slightly from those of conductivity measurements. Thus, data were interpolated in order to gain density and viscosity values at exactly the same temperatures. The resulting interpolated  $\rho$  and  $\eta$  values are compiled in Table D.1 together with the molar volumes  $V_m$  and solvent polarity parameters ( $E_T(30)$ ,  $\pi^*$ ,  $\alpha$ ,  $\beta$ ).

**Table D.1** Physicochemical parameters of TAA- and Ch-TOTO salts at various temperatures (with  $\rho$  and  $\eta$  as interpolated values).  $T$ : temperature in K,  $\rho$ : density in  $\text{kg m}^{-3}$ ,  $V_m$ : molar volume in  $\text{cm}^3 \text{mol}^{-1}$ ,  $\kappa$ : specific conductivity in  $\text{S m}^{-1}$ ,  $A_m$ : equivalent conductivity in  $\text{S m}^2 \text{mol}^{-1}$ ,  $\eta$ : viscosity in  $\text{mPa s}$ ,  $E_T(30)$  (in  $\text{kcal mol}^{-1}$ ),  $\pi^*$ ,  $\alpha$ ,  $\beta$ : polarity parameters.

Ch-TOTO									
$T$	$\rho$	$V_m$	$\kappa$	$10^4 \cdot A_m$	$\eta$	$E_T(30)$	$\pi^*$	$\alpha$	$\beta$
283.15	1142.3	285	0.00312	0.00888	2180	-	-	-	-
293.15	1135.5	287	0.00736	0.0211	1045	48.49	1.022	0.401	0.980
298.15	1131.7	288	0.01076	0.0309	665	48.41	1.015	0.403	0.981
303.15	1128.1	288	0.01525	0.0440	506	48.32	1.007	0.404	0.982
313.15	1122.1	290	0.0283	0.0821	230	48.14	0.991	0.407	0.985
323.15	1117.8	291	0.0482	0.1403	122	47.96	0.975	0.411	0.988
333.15	1114.5	292	0.0765	0.223	74	47.79	0.959	0.414	0.991
TEA-TOTO									
$T$	$\rho$	$V_m$	$\kappa$	$10^4 \cdot A_m$	$\eta$	$E_T(30)$	$\pi^*$	$\alpha$	$\beta$
283.15	1081.2	325	0.01788	0.0581	830	-	-	-	-
293.15	1074.6	327	0.0374	0.1224	375	45.97	1.097	0.182	1.224
298.15	1071.2	328	0.0517	0.1695	264	45.92	1.090	0.185	1.227
303.15	1068.0	329	0.0695	0.229	186	45.88	1.083	0.189	1.230
313.15	1062.0	331	0.1173	0.388	103	45.79	1.068	0.196	1.235
323.15	1057.4	332	0.1837	0.611	62	45.70	1.054	0.204	1.241
333.15	1054.7	333	0.271	0.902	41	45.61	1.039	0.211	1.247

<b>TPA-TOTO</b>									
$T$	$\rho$	$V_m$	$\kappa$	$10^4 \cdot A_m$	$\eta$	$E_T(30)$	$\pi^*$	$\alpha$	$\beta$
283.15	1037.3	393	0.00264	0.01039	2668	-	-	-	-
293.15	1031.4	395	0.00653	0.0258	1100	44.83	1.062	0.144	1.295
298.15	1028.0	396	0.00976	0.0387	720	44.79	1.056	0.147	1.296
303.15	1024.7	398	0.01414	0.0563	489	44.74	1.050	0.149	1.296
313.15	1018.9	400	0.0273	0.1094	235	44.66	1.038	0.155	1.297
323.15	1014.7	402	0.0482	0.1934	118	44.57	1.026	0.160	1.298
333.15	1011.5	403	0.0796	0.321	67	44.48	1.013	0.166	1.299
<b>TBA-TOTO</b>									
$T$	$\rho$	$V_m$	$\kappa$	$10^4 \cdot A_m$	$\eta$	$E_T(30)$	$\pi^*$	$\alpha$	$\beta$
283.15	1010.2	459	0.001606	0.00737	2969	-	-	-	-
293.15	1004.1	462	0.00380	0.01756	1283	44.06	1.030	0.125	1.341
298.15	1000.5	463	0.00555	0.0257	841	44.01	1.021	0.131	1.347
303.15	996.9	465	0.00792	0.0368	575	43.97	1.011	0.136	1.352
313.15	990.9	468	0.01496	0.0700	277	43.88	0.992	0.148	1.363
323.15	986.6	470	0.0260	0.1223	142	43.78	0.973	0.159	1.374
333.15	983.0	472	0.0417	0.1965	82	43.69	0.954	0.171	1.385

## List of Figures

<b>Fig. I.1</b>	Molecular structure of the studied choline soaps.....	4
<b>Fig. I.2</b>	Scheme illustrating the self-assembly behavior of choline soaps in water upon increasing the surfactant concentration. At very low concentrations, only monomers are present. Once the <i>cmc</i> is reached, spherical micelles are formed. Their number increases with the surfactant concentration in the following, whereas their size and shape are not affected (i.e. there is no sphere-to-rod transition). The first liquid-crystalline phase observed at a volume fraction of 25-30% is featured by a discontinuous cubic lattice ( $I_1$ ). When further raising the surfactant content, successive transitions into a hexagonal ( $H_1$ ), a bicontinuous cubic ( $V_1$ ) and eventually a lamellar phase ( $L_a$ ) occur.....	6
<b>Fig. I.3</b>	The effect of counterion size and dissociation on the curvature of surfactant aggregates, exemplified for the choline (left) and sodium (right) salts of dodecanoic acid. The bulkiness of the choline cation and its high degree of dissociation cause an increase in the headgroup area $a_0$ relative to sodium and thus a decrease of the packing parameter $N_s$ , since the length and volume of the hydrophobic part are the same in both cases. As a consequence, aggregates of higher curvature are promoted when choline is used as counterion (i.e. spherical micelles are for example favored over rod-like ones).....	8
<b>Fig. I.4</b>	The Hofmeister series – a classification of anions and cations according to their capability of influencing the surface tension of water, solubilizing hydrocarbons and stabilizing protein solutions (drawing based on ref <sup>42</sup> ).....	11
<b>Fig. I.5</b>	Schematic representation of Collins’ law of matching water affinities (drawing based on ref <sup>57</sup> ). Ions are classified concerning their size with respect to the “medium-sized” water molecule as small “hard” ions of high charge density (kosmotropes) and big “soft” ions of low charge density (chaotropes). Collins’ model states that matching of congeneric ions results in the formation of, an inner-sphere ion pair, whereas the combination of ”unlike” ions will lead to enhanced dissociation as each ion prefers to keep its hydration shell. <sup>54</sup> .....	12
<b>Fig. I.6</b>	“Like seeks like” for surfactant systems: small “hard” cations preferably interact with congeneric “hard” surfactant headgroups, and <i>vice versa</i> . Combing hard and soft ions will in turn yield surfactants of high counterion dissociation. <sup>59</sup> .....	13
<b>Fig. I.7</b>	2,5,8,11-Tetraoxatridecan-13-oate – the TOTO anion.....	16
<b>Fig. II.1</b>	Molecular structure of the choline cation.....	23
<b>Fig. II.2</b>	Comparison of the Krafft temperatures $T_{Kr}$ (°C) of (■) $ChCm$ , (□) $TMACm$ , (▲) $KCm$ and (●) $NaCm$ surfactants with increasing number of carbon atoms $m$ (values of $NaCm$ with $m = 12$ taken from [3], with $m = 14, 16, 18$ from [4]).....	26

<b>Fig. III.1</b>	Biodegradation of choline laurate ( $\square$ ), myristate ( $\circ$ ), palmitate ( $\Delta$ ) and stearate ( $\diamond$ ) as a function of time with sodium acetate ( $\boxtimes$ ) as standard. .... 36
<b>Fig. III.2</b>	IC <sub>50</sub> values of choline ( $\square$ ), sodium ( $\circ$ ) and potassium ( $\diamond$ ) carboxylates obtained on HeLa cells as a function of alkyl chain length $m$ . .... 38
<b>Fig. III.3</b>	IC <sub>50</sub> values of choline ( $\square$ ), sodium ( $\circ$ ) and potassium ( $\diamond$ ) carboxylates obtained on SK-Mel-28 cells as a function of alkyl chain length $m$ . .... 39
<b>Fig. III.4</b>	Phase contrast and fluorescence images of HeLa cells incubated with a mixture of ChPC12/ChC12 (molar ratio of 1 : 2), acquired 10, 20 and 60 min after addition of the surfactants. Scale bars: 20 $\mu\text{m}$ . .... 42
<b>Fig. IV.1</b>	Penetration scan of ChC12 at 20°C acquired at 100x magnification between half-crossed polarizers, showing the following sequence of the formed mesophases: L <sub>1</sub> , I <sub>1</sub> ' and I <sub>1</sub> '', H <sub>1</sub> , V <sub>1</sub> and a gel + solid region. The discontinuous cubic phases I <sub>1</sub> ' and I <sub>1</sub> ' can be identified by their isotropy, high viscosity and refractive index discontinuities (dark lines). .... 56
<b>Fig. IV.2</b>	Penetration scan of ChC16 at 61°C with non-crossed (left) and crossed (right) polarizers at 100x magnification, visualizing the formed mesophases in the more concentrated surfactant region. .... 56
<b>Fig. IV.3</b>	Binary aqueous phase diagrams of ChC <sub>m</sub> surfactants between 0°C and 90°C for $m=12$ (A), $m=14$ (B), $m=16$ (C) and $m=18$ (D). Experimental data near the phase boundaries were determined visually between crossed polarizers as isotropic ( $\circ$ ), biphasic ( $\oplus$ ) and anisotropic ( $\times$ ). .... 58
<b>Fig. IV.4</b>	Two-dimensional X-ray patterns of the system ChC12/H <sub>2</sub> O at 25°C at surfactant concentrations ranging from 30.0-49.7 wt% ChC12, showing single and biphasic patterns of the discontinuous cubic phases I <sub>1</sub> ' and I <sub>1</sub> ' and the hexagonal phase H <sub>1</sub> . 60
<b>Fig. IV.5</b>	Radially averaged SAXS profiles of ChC12 at 25°C and surfactant concentrations of (A) 35.1, (B) 40.1, (C) 47.2, and (D) 49.7 wt%. Vertical lines mark the positions and Miller indices of peaks expected for a P6 <sub>3</sub> /mmc (---), Pm3n (--) and H <sub>1</sub> (···) structure. Patterns correspond to (A) a single I <sub>1</sub> ' phase tentatively assigned to a P6 <sub>3</sub> /mmc structure, (B) a single I <sub>1</sub> ' with Pm3n symmetry, (C) a biphasic region of I <sub>1</sub> ' (Pm3n) and H <sub>1</sub> , and (D) a pure H <sub>1</sub> phase. Note that the bump around $q=4\text{ nm}^{-1}$ stems from Kapton foil. .... 61
<b>Fig. IV.6</b>	The interlayer spacing $d$ (A), the radius of the lipophilic part $r_L$ (B) and the cross-sectional area at the polar-nonpolar interface $a_S$ (C) outlined as a function of $\Phi_S$ for the hexagonal phase of ChC <sub>m</sub> soaps (ChC12 ( $\square$ ), ChC14( $\circ$ ), ChC16 ( $\Delta$ ) and ChC18 ( $\diamond$ )) (T= 25°C for $m=12-16$ , and T= 50-60°C (see SI) for $m=18$ ). The error bars were calculated assuming uncertainties of $\Delta q=0.01\text{ nm}^{-1}$ and $\Delta\Phi_L=0.01$ . .... 64

- Fig. IV.7** SAXS spectra of (A) 74.8 wt% ChC16 ( $T= 60^{\circ}\text{C}$ ) and (B) 79.3 wt% ChC16 ( $T= 50^{\circ}\text{C}$ ), representing biphasic samples of a potential intermediate phase and  $H_1$  (A) or, respectively,  $V_1$  (B). Theoretical peak positions are indicated by the vertical lines with the corresponding *Miller* indices outlined above (complex hexagonal (--),  $H_1$  (···) and  $Ia3d$  (-·-)). The bump around  $q= 4 \text{ nm}^{-1}$  is due to the Kapton foil. .... 66
- Fig. IV.8** SAXS spectrum of  $V_1$  of ChC16 (85.5 wt%,  $50^{\circ}\text{C}$ ), revealing  $Ia3d$  symmetry. The vertical lines mark the theoretical peak positions with the corresponding *Miller* indices outlined above. .... 67
- Fig. IV.9** Half-length of the lipophilic bilayer  $r_L$  (A) and cross-sectional area at the polar-nonpolar interface  $a_S$  (B) in the lamellar phase of ChC*m* surfactants plotted as a function of volume fraction surfactant  $\Phi_S$  (ChC14(○), ChC16 (Δ) and ChC18 (◇)). The error bars were calculated assuming uncertainties of  $\Delta q= 0.01 \text{ nm}$  and  $\Delta\Phi_L= 0.01$ . .... 70
- Fig. V.1** DSC curves of neat ChC12 (A) and ChC16 (B) between  $-20^{\circ}\text{C}$  and  $95^{\circ}\text{C}$ , showing three heating and cooling cycles in comparison, each exhibiting two prominent phase transitions. The transition temperatures and enthalpies of the freshly melted compound (first cycle) are slightly different from the re-heated ones, while the second and third heating-cooling cycles are identical. .... 82
- Fig. V.2** The second heating and cooling DSC cycles of ChC*m* surfactants for  $m= 12-18$ , illustrating that all studied choline surfactants undergo two phase transitions between  $-20^{\circ}\text{C}$  and  $95^{\circ}\text{C}$ . .... 83
- Fig. V.3** Phase transition temperatures of ChC*m* surfactants as a function of chain length  $m$  (taken from the second DSC cycle). Empty symbols mark transition temperatures determined on heating ((□) crystal (Cr)  $\rightarrow$  semi-crystalline (CrM) and (○) CrM  $\rightarrow$  liquid crystal (smectic A (SmA))), while crossed symbols represent those detected on cooling. .... 84
- Fig. V.4** Optical polarizing microscopy images of neat ChC12 at different temperatures with 100x magnification. Micrographs were taken from the same spot in the sample during the first cooling cycle (cooling rate  $10^{\circ}\text{C min}^{-1}$ ) and visualize the three phases formed between  $-20^{\circ}\text{C}$  and  $100^{\circ}\text{C}$ . At high temperatures ( $\geq 65^{\circ}\text{C}$ ), oily streak focal conic textures of low viscosity are observed, typical for a liquid-crystalline lamellar phase (smectic A). At  $64-63^{\circ}\text{C}$ , birefringent crystallites start to grow, accompanied by a sudden increase of viscosity. The virtual phase transition of SmA to CrM takes place within approximately  $2^{\circ}\text{C}$ . On further cooling, the appearance of the sample changes gradually over a wide range of temperature, first becoming darker and then birefringent. At  $15$  to  $7^{\circ}\text{C}$ , the whole sample crystallizes forming a birefringent solid material. .... 85
- Fig. V.5** Variation of the decay constant  $T_{2eff}$  of ChC*m* surfactants ( $m= 12-18$ ) with temperature. Data were obtained by heating (top) and cooling (bottom) freshly melted samples. The vertical lines indicate the transition temperatures as detected

	by DSC. The fast relaxation constants at low temperatures are typical for solid crystalline phases (Cr), while the slow ones at high temperatures are characteristic for liquid-crystalline compounds (SmA). The $T_{2eff}$ values (20-30 $\mu$ s) of the middle-temperature phase (CrM) reflect an increased molecular motion as compared to solid crystalline materials, but still with a high degree of order and restricted molecular mobility (similar to the values for gel ( $L_{\beta}$ ) phases). ..... 88
<b>Fig. V.6</b>	X-ray spectra of neat ChC18 as a function of temperature, determined for two heating and cooling cycles: (A) first heating (freshly melted sample), (B) first cooling, (C) second heating and (D) second cooling. At low temperatures, several sharp high-angle reflections are present, which are typical for crystalline paraffinic chains. When raising the temperature, wide-angle peaks disappear stepwise, accompanied by the occurrence of a bump at around $q=15\text{ nm}^{-1}$ . This indicates a gradual rather than a sharp melting of the hydrocarbon chains. At 90°C, the alkyl chains are finally molten as evidenced by the characteristic diffuse peak at $q=13.4\text{ nm}^{-1}$ , and a lamellar liquid-crystalline phase is formed. The diverse heating and cooling cycles confirm the reproducibility of the phase transitions. Note that the bump at around $q=4\text{ nm}^{-1}$ stems from the Kapton foil. 90
<b>Fig. V.7</b>	Lamellar interlayer spacing $d$ of neat choline soaps as a function of alkyl chain length $m$ at 90°C..... 92
<b>Fig. V.8</b>	Transition enthalpies (A) and entropies (B) of choline soaps as a function of the alkyl chain length $m$ . Data were obtained from DSC scans between -20°C and 95°C for re-heated samples. Empty symbols mark enthalpies and entropies on heating (( $\square$ ) crystal (Cr) $\rightarrow$ semi-crystalline (CrM) and ( $\circ$ ) CrM $\rightarrow$ liquid crystal (smecticA (SmA)), and crossed symbols those on cooling (( $\boxplus$ ) CrM $\rightarrow$ Cr, ( $\boxtimes$ ) SmA $\rightarrow$ CrM). ..... 94
<b>Fig. VI.1</b>	Krafft temperature $T_{Kr}$ as a function of the molar ratio of NaOH ( $\square$ ), KOH ( $\Delta$ ) and ChOH ( $\circ$ ) to stearic and lauric acid, respectively (fatty acid concentration fixed at 1 wt%). ..... 107
<b>Fig. VI.2</b>	Cryo-TEM image of an aqueous solution of 1 wt% C18 with $n(\text{ChOH}) : n(\text{C18}) = 2.00$ at 25°C; showing spherical micelles with an approximate radius of 2 nm. .... 108
<b>Fig. VI.3</b>	The Krafft temperature $T_{Kr}$ of ChC18 soap solutions as a function of added NaCl ( $\square$ ), KCl ( $\Delta$ ) and ChCl ( $\circ$ ) (ChC18 concentration fixed at 1 wt%). ..... 110
<b>Fig. VI.4</b>	Attempts to dissolve butter at 25°C in aqueous solutions of choline hydroxide at different mass ratios of choline to butter (butter concentration fixed at 1 wt%). 114
<b>Fig. VII.1</b>	Molecular structure of choline dodecyl sulfate (ChDS). ..... 123
<b>Fig. VII.2</b>	Cryo-TEM micrograph of a 5 wt% ChDS solution, revealing spherical micelles with an approximate radius of 2 nm. .... 126

<b>Fig. VII.3</b>	Penetration scan image of ChDS at 0°C acquired at 100x magnification between half-crossed polarizers. With increasing surfactant concentration (indicated by the arrow), a micellar solution $L_1$ , a hexagonal phase $H_1$ and a partially birefringent solid region can be identified. ....	127
<b>Fig. VII.4</b>	Penetration scan (100x magnification) of ChDS at 48°C with non-crossed (left) and crossed polarizers (right), showing the following phases towards higher surfactant concentrations: hexagonal $H_1$ , bicontinuous cubic $V_1$ , and a birefringent crystalline region. ....	127
<b>Fig. VII.5</b>	Rough binary aqueous phase diagram of ChDS between 0°C and 90°C. ....	128
<b>Fig. VII.6</b>	Comparison of the cytotoxicity of ChDS, SDS and ChC12 on two human cell lines (HeLa and SK-Mel-28). ....	129
<b>Fig. VII.7</b>	The effect of varying amounts of alkali chlorides (LiCl (○), NaCl (□), KCl (△)) and choline chloride (ChCl (◇)) on the Krafft temperature of dodecylsulfate surfactants (SDS (A), KDS (C), ChDS (D)) and, for comparison, dodecanoate soaps (NaC12 (B), KC12 (D), ChC12 (F)). The curves of LiCl in (E) and those of KCl and ChCl in (F) are not shown, since the measured values were below 0°C. The surfactant concentration was kept constant at 1 wt% in the experiments. ...	130
<b>Fig. VII.8</b>	Influence of calcium chloride on the Krafft temperatures of ChDS and SDS, at a surfactant concentration of 1 wt% in both cases. ....	132
<b>Fig. VII.9</b>	Surface tension of ChDS as a function of the surfactant concentration at 25°C. ....	137
<b>Fig. VII.10</b>	Plot of the specific conductivity $\kappa$ versus the concentration of ChDS at 25°C. ....	138
<b>Fig. VII.11</b>	TGA curves of ChDS (black) and SDS (blue). ....	138
<b>Fig. VIII.1</b>	Molecular structure of the investigated ionic liquids, which consist of the TOTO anion and various cations: (1) quaternary ammonium ions with R= $\text{CH}_2\text{CH}_3$ (TEA), $\text{CH}_2\text{CH}_2\text{CH}_3$ (TPA), $\text{CH}_2\text{CH}_2\text{CH}_2\text{CH}_3$ (TBA), and (2) choline (Ch). ....	145
<b>Fig. VIII.2</b>	(a) Viscosities and (b) specific conductivities of TAA- and Ch-TOTO ionic liquids as a function of temperature ((◇) TEA, (□) TPA, (△) TBA), (○) Ch). Full lines represent fits according to the empirical Vogel-Fulcher-Tamman equation. Corresponding fit parameters are given in Table VIII.2 and Table VIII.3. ....	149
<b>Fig. VIII.3</b>	Walden plot of TAA- and Ch-TOTO ionic liquids ((◇) TEA, (□) TPA, (△) TBA), (○) Ch) for temperatures ranging from 10°C to 60°C (from the left to the right), as compared to the ideal KCl line (full line) and Na-TOTO (●) (values taken from Ref.10). ....	151
<b>Fig. VIII.4</b>	Polarity and Kamlet-Taft parameters of TAA- and Ch- TOTO ionic liquids ((◇) TEA, (□) TPA, (△) TBA), (○) Ch) as a function of temperature: (A) polarity $E_T^N$ , (B) dipolarity/polarizability ratio $\pi^*$ , (C) hydrogen-bond acidity $\alpha$ and (D) hydrogen-bond basicity $\beta$ . ....	154

- Fig. VIII.5** Classification of TOTO RTILs in the normalized  $E_T^N$  scale (25°C) as compared to various molecular solvents and conventional ionic liquids. The scheme and the  $E_T^N$  range of imidazolium-typed ILs are partly based on a drawing by Reichardt in 2005.<sup>56</sup> Values for the molecular solvents and Na-TOTO were adapted from refs. <sup>36</sup> and <sup>12</sup>, respectively..... 155
- Fig. VIII.6** Molecular structures of the dyes employed for the characterization of solvent polarity and Kamlet-Taft parameters: **1** – Reichardts Dye 30, **2** – N,N-diethyl-4-nitroaniline, **3** – 4-nitroaniline..... 165

## List of Tables

<b>Table II.1</b>	Comparison of the <i>cmc</i> 's [mM] of choline, sodium and potassium carboxylates at 25°C.....	24
<b>Table II.2</b>	Values of the Slopes of the Conductivity Plots versus the concentration before ( $S_1$ ) and after ( $S_2$ ) the <i>cmc</i> with the resulting $\alpha$ values.....	30
<b>Table IV.1</b>	Unit cell parameters $a$ of the $Pm3n$ structure detected for the $I_1''$ phase of ChC <i>m</i> salts up to $m= 16$ at 25°C, with corresponding estimated aggregation numbers $N_{agg}$ . 37.9 wt% ChC12 and 34.9 wt% ChC14 are biphasic samples of $I_1'$ and $I_1''$ , while 47.2 wt% ChC12 belongs to the two-phase region of $I_1''$ and $H_1$ . .....	63
<b>Table IV.2</b>	Results of SAXS analyses for $V_1$ of ChC <i>m</i> soaps with $Ia3d$ structure, with the volume fraction of surfactant $\Phi_S$ , the temperature $T$ , the experimental $d$ -values of the respective first order reflection and the unit cell parameter $a$ . Samples of ChC12 up to 89.5 wt% as well as 79.3 wt% ChC16 and 75.7 wt% ChC18 are potentially biphasic as discussed in the text. ....	68
<b>Table IV.3</b>	Structural parameters of the lamellar phase formed by ChC <i>m</i> soaps with $m= 14-18$ , comprising the experimental $d$ -values, the ratio of the lipophilic bilayer thickness $d_L$ and the all- <i>trans</i> alkyl chain length $l_{max}$ , the difference of the surfactant length $r_S$ and the lipophilic half-length $r_L$ (representing the headgroup-counterion layer), and the thickness of the water layer $d_W$ . ....	69
<b>Table IV.4</b>	Density $\rho_{surf}$ and volume $V_S$ of one surfactant molecule of ChC <i>m</i> salts with $m= 12-18$ at 25°C. The volume of the lipophilic part $V_L$ and the length of the fully extended alkyl chains $l_{max}$ were calculated according to the expression introduced by Tanford. <sup>60</sup> .....	74
<b>Table V.1</b>	Decomposition temperatures ( $T_{dec}$ ) of ChC <i>m</i> surfactants for $m= 12-18$ as determined by thermogravimetric measurements.....	81
<b>Table V.2</b>	Thickness of the lipophilic ( $d_L$ ) bilayer and polar ( $d - d_L$ ) layer and the cross-sectional area ( $a_S$ ) at the polar-nonpolar interface of lamellar liquid crystalline phase formed by neat ChC <i>m</i> soaps ( $m= 12-18$ ) at 90°C.....	93
<b>Table V.3</b>	Sum of the enthalpies of ChC <i>m</i> surfactants ( $m= 12-18$ ) obtained for re-heated samples from DSC scans between -20 and 95°C. ....	95
<b>Table VII.1</b>	Physicochemical properties of ChDS in comparison to other dodecyl sulfate surfactants: Krafft temperatures ( $T_{Kr}$ ), critical micellization concentrations ( <i>cmc</i> 's) determined by conductivity <sup>a</sup> and surface tension <sup>b</sup> measurements, the degree of counterion condensation $\alpha$ (derived from conductivity data), the surface excess concentration ( $\Gamma$ ) and the area per molecule( $A_s$ ) calculated from the concentration-dependent surface tension plots. ....	124

---

<b>Table VII.2</b>	Specific effects of distinct alkali salts and choline chloride on the Krafft temperatures of dodecyl sulfate (SDS, KDS, ChDS) and dodecanoate (NaC12, KC12, ChC12) surfactants. Salts are ordered with respect to their potential to increase $T_{Kr}$ . The effect of the alkali chlorides is reversed when the sulfate headgroup is replaced by carboxylate. In turn, added choline chloride generally tends to decrease the Krafft point, regardless of the type of surfactant headgroup. ....	131
<b>Table VII.3</b>	Density data of ChDS solutions at 25°C. ....	136
<b>Table VIII.1</b>	Decomposition ( $T_{dec}$ ) and glass ( $T_g$ ) temperatures and molar volumes ( $V_m$ ) at 25°C of TAA- and Ch-TOTO ionic liquids. ....	146
<b>Table VIII.2</b>	VFT parameters obtained from fits of temperature-dependent viscosity data according to Eqn. (VIII.1) for TAA- and Ch-TOTO ionic liquids. ....	148
<b>Table VIII.3</b>	VFT parameters obtained from fits of temperature-dependent conductivity data according to Eqn. (VIII.2) for TAA- and Ch-TOTO ionic liquids. ....	148
<b>Table VIII.4</b>	Viscosities and specific as well as molar conductivities of TAA- and Ch-TOTO ionic liquids at 25°C in comparison to values reported for Na-TOTO. <sup>10</sup> ....	150
<b>Table VIII.5</b>	Deviation $\Delta W$ of TAA- and Ch-TOTO ionic liquids from the ideal KCl line in the Walden plot at different temperatures. ....	152
<b>Table VIII.6</b>	Polarity parameters of TAA- and Ch-TOTO ILs at 25°C, in comparison to values reported for Na-TOTO. <sup>12</sup> ....	156
<b>Table VIII.7</b>	Densities, $\rho$ , of the investigated ILs at various temperatures. ....	162
<b>Table VIII.8</b>	Equations for the temperature-dependent densities of TAA- and Ch-TOTO ionic liquids, obtained from linear regressions of the experimental data. ....	162
<b>Table VIII.9</b>	Dynamic viscosities, $\eta$ , of the investigated ILs at temperatures ranging from 10°C to 68°C. ....	163
<b>Table VIII.10</b>	Conductivities, $\kappa$ , of the investigated ILs between 0°C and 100°C. ....	164

## List of Publications

- (1) Regina Klein, Didier Touraud, Werner Kunz  
“Choline Carboxylate Surfactants: Biocompatible and Highly Soluble in Water“  
*Green Chemistry*, 2008, 10, 433-435. (Chapter II)
  
- (2) Regina Klein, Didier Touraud, Werner Kunz  
“Cholincarboxylatseifen: umweltfreundlich und höchst wasserlöslich“  
Jahrbuch für den Praktiker 2009, Verlag für chemische Industrie, Augsburg, S. 453-459. (Chapter II)
  
- (3) Regina Klein, Eva Maurer, Birgit Kraus, Boris Estrine, Didier Touraud, Jörg Heilmann, Werner Kunz  
“Biodegradability and cytotoxicity on human cell lines of choline soaps: effects of chain length and cation”  
submitted to *Green Chemistry* (Chapter III)
  
- (4) Regina Klein, Gordon J. T. Tiddy, Eva Maurer, Didier Touraud, Jordi Esquena, Olivier Tache, Werner Kunz  
“Aqueous Phase Behavior of Choline Carboxylate Surfactants - Exceptional Variety and Extent of Cubic Phases”  
accepted by *Soft Matter* (Chapter IV)
  
- (5) Regina Klein, Helen Dutton, Olivier Diat, Gordon J. T. Tiddy, Werner Kunz  
“Thermotropic Phase Behavior of Choline Soaps”  
accepted by *Journal of Physical Chemistry B* (Chapter V)

- (6) Regina Klein, Matthias Kellermeier, Markus Drechsler, Didier Touraud, Werner Kunz  
“Solubilisation of Stearic Acid by the Organic Base Choline Hydroxide”  
*Colloids and Surfaces A*, 2009, 338, 129-134. (Chapter VI)
- (7) Regina Klein, Eva Maurer, Matthias Kellermeier, Jörg Heilmann, Werner Kunz  
“Choline Alkyl Sulfates – A New Biocompatible Class of Anionic Surfactants”  
in preparation (Chapter VII)
- (8) Regina Klein, Oliver Zech, Eva Maurer, Matthias Kellermeier, Werner Kunz  
“Oligoether Carboxylates – Task-Specific Room-Temperature Ionic Liquids”  
accepted by *Journal of Physical Chemistry B* (Chapter VIII)
- (9) Werner Kunz, Eva Maurer, Regina Klein, Didier Touraud, Doris Rengstl, Agnes Harrar, Susanne Dengler, Oliver Zech  
“Low Toxic Ionic Liquids, Liquid Catanionics, and Ionic Liquid Microemulsion”  
*Journal of Dispersion Science & Technology*, in press.
- (10) Matthias Kellermeier, Fabian Glaab, Regina Klein, Emilio Melero-García, Markus Drechsler, Reinhard Rachel, Juan-Manuel García-Ruiz, Werner Kunz  
“Stabilization of Amorphous Calcium Carbonate in Inorganic Silica-Rich Environments”  
*Journal of the American Chemical Society*, 2010, 17859-17866.

- (11) Oliver Zech, Matthias Kellermeier, Stefan Thomaier, Eva Maurer, Regina Klein, Christian Schreiner, Werner Kunz  
“Alkali Metal Oligoether Carboxylates: A New Class of Ionic Liquids“  
*Chemistry - A European Journal*, 2009, 15, 1341-1345.
- (12) Matthias Kellermeier, Fabian Glaab, Emilio Melero-García, Regina Klein, Werner Kunz, Juan-Manuel García-Ruiz  
“The Effect of Silica on Calcium Carbonate Polymorphic Precipitation”  
to be submitted to *Angewandte Chemie International Edition*



## List of Patents

05/2009 DE 10 2009 026 598.8-43 (Universität Regensburg)

Regina Klein, Eva Maurer, Matthias Kellermeier, Didier Touraud, Werner Kunz

“Biologisch verträgliche Cholinverbindungen und deren Verwendung als Tenside“

04/2008 WO 2008135482 (BASF SE)

Werner Kunz, Stefan Thomaier, Eva Maurer, Oliver Zech, Matthias Kellermeier, Regina Klein

“Onium Salts of Carboxyalkyl-Terminated Polyoxyalkylenes for Use as High-Polar Solvents and Electrolytes”



## List of Oral and Poster Presentations

- 06/2010 Formula VI, Stockholm, Sweden  
“Biocompatible, Green: From Ionic Liquids to Surfactants” (Poster)  
“Choline Carboxylate Surfactants: Biocompatible and Highly Soluble in Water” (Poster, awarded the “Soft Matter” poster price)
- 09/2009 23<sup>rd</sup> Conference of the Colloid and Interface Society, Antalya, Turkey  
“Liquid Ion Pair Amphiphiles - LIPAs” (Poster)
- 07/2009 42<sup>nd</sup> IUPAC Congress, Glasgow, UK  
“Choline Carboxylate Surfactants: Biocompatible and Highly Soluble in Water” (Poster)
- 06/2009 3<sup>rd</sup> Congress on Ionic Liquids, Cairns, Australia  
“Liquid Ion Pair Amphiphiles - LIPAs” (Poster)
- 05/2009 Gordon Tiddy: A Lifetime in Formulation Science, Manchester, England  
“Choline Carboxylate Soaps: Biocompatible and Highly Soluble in Water” (Poster)
- 04/2009 5<sup>th</sup> Zsigmondy Colloquium, Bayreuth  
“Choline Carboxylate Soaps: Biocompatible and Highly Soluble in Water” (Poster)
- 10/2008 International Symposium on Green Chemistry for Environment and Health, Munich  
“Choline Carboxylate Soaps: Biocompatible and Highly Water Soluble” (Talk)

- 10/2008 4<sup>th</sup> European Detergents Conference, Würzburg  
“Choline Carboxylates: Soaps with Outstanding Solubility and High Environmental Compatibility“ (Talk)
- 09/2008 22<sup>nd</sup> Conference of the European Colloid and Interface Society, Krakau, Poland  
“Choline Carboxylate Surfactants: Biocompatible and Highly Soluble in Water“ (Poster)
- 08/2008 Conference on Molten Salts and Ionic Liquids, Copenhagen, Denmark  
“Alkali Oligoether Carboxylates - A New Class of Ionic Liquids“ (Poster)
- 06/2008 Liquid Matter Conference, Lund, Sweden  
“Choline Carboxylates - Soaps of Outstanding Solubility and Environmental Compatibility“ (Poster)  
“Low Melting Ion Pair Amphiphiles (LIPA)“ (Poster)  
“Cryptoanionic Liquids - A New Type of Ionic Liquids” (Poster)
- 11/2007 Formula V, Potsdam  
“Choline Carboxylates - Soaps of Outstanding Solubility and Environmental Compatibility“ (Talk)  
“From Ionic to Nonionic Characteristics by Complexation” (Poster)
- 10/2007 43<sup>rd</sup> Meeting of the German Colloid Society, Mainz  
“Choline Carboxylates - Soaps of Outstanding Solubility and Environmental Compatibility“ (Talk)  
“Low Melting Ion Pair Amphiphiles (LIPA)“ (Poster)

09/2007 21<sup>st</sup> Conference of the European Colloid and Interface Society, Geneva,  
Switzerland

“From Ionics to Nonionics” (Poster)

03/2007 Jahrestagung der Deutschen Physikalischen Gesellschaft,  
Regensburg

“SAXS Studies of Choline Carboxylate Surfactants: Biocompatible  
Soaps with Outstanding Solubility” (Poster)

“Downsizing of Silica” (Poster)

04/2006 2<sup>nd</sup> Zsigmondy Colloquium, Berlin

“Choline as a Biological Co-Ion of Long-Chain Organic Acids“ (Poster)

05/2005 42<sup>nd</sup> Meeting of the German Colloid Society, Aachen

“Choline as a Biological Co-Ion of Long-Chain Organic Acids“ (Poster)



---

## **Declaration**

Hereby, I declare that I have composed this work on my own and used only the quoted references and resources. Literally or correspondingly adapted material has been marked accordingly.

## **Erklärung**

Hiermit erkläre ich, dass ich die vorliegende Arbeit selbständig und nur mit den angegebenen Quellen und Hilfsmitteln angefertigt habe. Wörtlich oder sinngemäß übernommenes Gedankengut habe ich als solches kenntlich gemacht.

---

Ort, Datum

---

Regina Klein

---